A chronometric investigation of the initial peopling of the Americas

Lorena A. Becerra Valdivia

Merton College

D.Phil.

Michaelmas Term, 2019

University of Oxford



Abstract

A chronometric investigation of the initial peopling of the Americas

Lorena A. Becerra Valdivia (Merton College)
D.Phil.
Michaelmas Term, 2019

The initial peopling of the American continent marks a major event in the expansion of humans across the planet. For most of the 20th century, it was believed that a group of big-game hunters initially entered North America approximately 13,500 years ago, through the now flooded land bridge of Beringia, between modern day Siberia and Alaska. Once across, they would have moved southward through an ice-free corridor formed between the Laurentide and Cordilleran ice sheets, which began their recession after the last Ice Age. This model, however, was effectively refuted in 1997 when archaeologists found evidence in Chile, South America, which was reliably older than the North American record suggested. Today, questions associated with this dispersal are debated in First American research, and remain largely unanswered. These include the antiquity and origin of the initial arrivals, the number of migrational episodes, and the impact of human expansion in the late Quaternary faunal extinctions. In response, considering that timing is fundamental in the study of human dispersals, this investigation employs radiocarbon dating and Bayesian age modelling to build a robust chronological framework with which to elucidate broad spatio-temporal patterns. This is accomplished by obtaining reliable radiocarbon measurements for key archaeological sites across the continent, resolving dating discrepancies using a single-amino-acid isolation method, and building large-scale Bayesian age models to track human presence and frame current evidence. This involved the laboratory processing of dateable material from 18 archaeological sites, the production of 133 radiocarbon dates, and the statistical analysis of archaeo-chronometric data from 41 archaeological sites in North America and Beringia. A widely used method, called '^{14}C-dates-as-data', is assessed from a radiocarbon dating perspective, and the potentially confounding effects introduced by challenges in sample processing in the analysis are demonstrated. This approach is the only other quantitative technique apart from Bayesian age modelling that uses the chronometric record to elucidate large-scale population events. Here, however, it is argued that Bayesian age modelling is the most efficient tool in tackling human dispersals.

Results obtained in this thesis have enabled the creation of a new Bayesian age model for the initial peopling of the Americas. This suggests that the earliest arrivals to mid-latitude North America were humans from eastern Asia, who most likely crossed near the end of the LGM. The synchronous commencement of Beringian, Clovis and Western Stemmed cultural traditions is also identified, and their overlap with the last appearance dates for 18 extinct genera suggests that human expansion was a key driver behind animal extinction events. Notably, these findings overturn the widespread notion that North America was first penetrated only after 16-15,000 years ago.

It is hoped that, in the future, new evidence in First Americans research will increase the resolution of the models here created, and enhance the conclusions drawn. Particular attention should be paid to Central and South America, regions with more limited archaeo-chronometric data and immediate chronometric potential. Improved chronological control in these regions is key in understanding the pattern of American settlement.

Acknowledgements

Respectfully, I dedicate this to the indigenous people of the American continent, whose past and history is the subject of my thesis.

First, I thank Tom Higham and Katerina Douka, my supervisors, for their kindness and mentorship whilst in Oxford. Thomas, your enthusiasm, support and guidance were key drivers behind this work.

I also extend my gratitude to all other members of the Oxford Accelerator Radiocarbon Unit, past and present, for their camaraderie: Christopher Bronk Ramsey, David Chivall, Joseph Graystone, Philip Leach, Pete Ditchfield, Emma Henderson, Diane Baker, Daniel Comeskey, Kathryn Mears, Thibaut Deviese, Barbara Emery, Jane Davies, Angela Bowles, Luke Spindler, Eileen Jacob, Eduardo Queiroz Alves, Rachel Hopkins, Jamie Cameron, and Bethan Linscott. A special thank you to the D.Phil. students—Eileen, Eduardo and Rachel—for your support and useful discussions (academic and otherwise).

To my fellow RLAHA D.Phil. students, particularly Hannah Ryan and Jaime Swift, Jennifer Keute, and Qian Ma. I wish you all success and happiness.

To Julia Lee-Thorp and Christopher Bronk Ramsey, my D.Phil. assessors, for their feedback and help along the way.

To my academic collaborators—Tom Stafford, Mike Waters, Eileen Johnson, David Meltzer, Rafael Suárez Sainz, Ciprian Ardelean, Mikkel Pedersen, Eske Willerslev, Jean-Luc Schwenninger, Charles G. Oviatt, Juan I. Macías-Quintero, Joaquin Arroyo-Cabrales, Yam Zul E. Ocampo-Díaz, Igor I. Rubio-Cisneros, Jennifer G. Watling, Loren Davis, César Méndez Melgar, Eugenio Aspillaga Fontaine, Francisca Santana Sagredo, Andrea Eyquem Reyes, Nicole Barreaux Höpfl, Charles Koenig, Steve Black, Mike Collins, Timothy Rowe, Jordan Pratt, Matt Des Lauriers, Dave Rhode, David Madsen, Spencer Pelton, David Rubilar Rogers, Rodrigo Leal Cervantes and Rachel Wood—who trusted me with their samples, provided access to collections, or worked with me on interdisciplinary aspects of this research.

To the Clarendon Fund, Merton College, Santander, School of Archaeology and NERC Radiocarbon Facility for funding this work.

To my family (Graciela, Gerardo, Katherine, Pamela, Keith, Char and Iker), friends (Tirsa, Karin, Rodrigo and Francisca) and partner (Gorav) for their love and support. I apologise for the stressed energy I inflicted upon you and any time together that was lost because of it.

Contents

I. Introduction **1**

1.1. Research background 2

1.1.1. History of Research 2

1.1.2. Current evidence 7

1.1.2.1. Archaeological 7

1.1.2.2. Genetic 9

1.1.2.3. Cranio-morphological 11

1.2. Research objectives 12

1.3. Thesis structure and outline 14

II. Methods **16**

2.1. Radiocarbon Dating 16

2.1.1. Principles and assumptions 16

2.1.2. Laboratory processing and measurement 18

2.1.2.1. Sampling 18

2.1.2.2. Bone collagen prescreening 18

2.1.2.3. Chemical pretreatment 19

2.1.2.4. Combustion, recycling and graphitisation 21

2.1.2.5. AMS measurement 22

2.1.2.6. Calibration 23

2.2. Bayesian age modelling 24

III. Article 1: Reassessing the chronology of the archaeological site of Anzick **27**

3.1. Main text 28

3.2. Supplementary text 42

IV. Article 2: The timing and impact of the earliest human arrivals in North America **47**

4.1. Main text 48

4.2. Supplementary text 75

V. Article 3: Challenges in sample processing within radiocarbon dating and their impact in 14C-dates-as-data studies **207**

5.1. Main text 208

5.1. Supplementary Text 233

VI. Discussion and conclusion **243**

6.1. Future research 247

6.2. Conclusion 250

Bibliography **251**

Appendices **273**

Appendix A: Chronometric work apart from the articles presented 273

Appendix B: Co-authored publication including work on Spirit Cave, Nevada 357

Appendix C: Co-authored publication including work on Cooper's Ferry, Idaho 370

Appendix D: Co-authored publication on the redating of heavily contaminated bones from kill/butchery sites in North America 378

Author contribution statements **389**

Conventions, abbreviations and notes

Date reporting conventions

b2k	years before AD 2000
BP	years before AD 1950
cal BP	calibrated years before 1950 (at 95.4% confidence unless otherwise specified)
ka	*kilo annum* or thousands of years (ago)
ya	years ago

Abbreviations

ABA	Acid Base Acid (pretreatment)
HPLC	High Pressure Liquid Chromatography
LGM	Last Glacial Maximum
MIS	Marine Isotope Stage
NGRIP	North Greenland Ice Core Project
ORAU	Oxford Radiocarbon Accelerator Unit
OSL	Optically Stimulated Luminescence

ORAU chemical pretreatment codes

AF(*)	ultrafiltered bone collagen (*solvent-washed)
AG(*)	Ezee-filtered bone collagen (*solvent-washed)
HYP	Hydroxyproline isolation from bone collagen
NRC	Non-routine chemistry
OX	acid dissolution for carbonates
RR	mild acid treatment for delicate or small non-bone, non-carbonate materials
SRa	ABA for sediments or soils (humin)
VV/UV	ABA for non-charred, non-carbonised plant remains/with bleach
WW/UW	ABA for wood/with bleach
ZR	ABA for charcoal and charred plant remains

Notes

If used, the terms ‘America’, ‘American’ and ‘Americans’ follow Latin American custom, where the continent is seen as one, ‘America’, with northern (Canada to Mexico), central (Guatemala and Belize to Panama) and southern regions (Colombia to Chile and Argentina).

I. Introduction

After more than 100 years of intense research and debate, the timing of the initial colonisation of the American continent by modern human remains one of the greatest questions in world archaeology. As it stands, evidence suggests that humans first reached the continent from ancient Beringia, some time during the late Pleistocene. For most of the 20th century, questions concerning this event were effectively answered by the 'Clovis-first' model, which held that a group of big-game hunters initially entered North America from Asia ~13,500 years ago (ya) via Beringia, moved southward through an ice-free corridor between the Laurentide and Cordilleran ice sheets, and, once in mid-latitude North America, developed a material culture best recognised by distinctive stone spear points named Clovis. The Clovis-first model has, however, been challenged repeatedly as the archaeological record provides reliable evidence for; i. sites which predate the Clovis period [dated to 11,050-10,800 BP or 13,250-12,800 cal BP by Waters and Stafford (1); often termed 'pre-Clovis' or 'older-than-Clovis' (2, 3), but see (4) for different terminology] and; ii. coeval technological industries that are significantly distinct and found across America (5–14). The initial peopling of America, therefore, currently lacks a well-defined model with which to interpret current evidence, resulting in uncertainty on a number of topics. These include the antiquity and origin of the initial arrivals, the number of migrational episodes entering the continent, the technological ancestry of Clovis, the impact of human colonisation in the disappearance of over 30 genera of large mammals by the Holocene, and the role of climatic changes brought upon the end of the last Ice Age. Considering the variable of *time* to be fundamental in the study of human dispersals, this thesis uses radiocarbon dating and Bayesian age modelling to build a chronological framework with which to elucidate these and other questions in First Americans research.

1.1. Research background

1.1.1. History of Research

The history of First Americans research can be divided into two parts (15, 16). The first, taking place in the 19th and 20th centuries, is concerned with the antiquity and presence of humans in America during the Pleistocene. The second, currently ongoing, involves the rebuttal of the Clovis-first paradigm and the evaluation of pre-Clovis evidence and alternate peopling narratives.

By the early 1900s, a connection between Asia and the first Americans was widely accepted and the colonisation of the continent by Asiatic immigrants proposed (17, 18). The most controversial aspect of the peopling process rather focused on the antiquity of the first Americans;

> while we now possess numerous and, in some instances, great anthropological collections from this continent [...] there is to this day not a single American bone in existence or on record the geological antiquity of which can be demonstrated beyond doubt. It is in fact impossible for us to produce, though they might be reasonably expected, any specimens that can demonstrably compare in antiquity with the remains of, for instance, the predynastic Egyptians (Hrdlička, 1925, page 487) (18).

This statement was in line with contemporary constructs of cultural evolution and historical progression (19). Scholars then reasoned that if Native Americans had indeed originated from an Ice Age ancestor of considerable antiquity and American prehistory followed the progression of Europe's, they would have long ago evolved from their current state of savagery and become civilised like men from the Old World. The Pleistocene presence of humans in America simply could not be. Only two years after Hrdlicka's ideas were published, however, they were contradicted through unequivocal evidence; a lithic point was found embedded in between the ribs of an extinct bison at the site of Folsom, New Mexico (20, 21) (Figs. 1-2). This was a pivotal discovery that

effectively ended the first dispute of First Americans research. Henceforth, as the prehistory of America opened and Hrdlicka's observations became obsolete, archaeologists in the United States raced to find early 'Paleoindian' sites (16). In this way, Edgar B. Howard found the site of Clovis (Blackwater Draw, Locality no. 1), New Mexico (22, 23), in 1933.

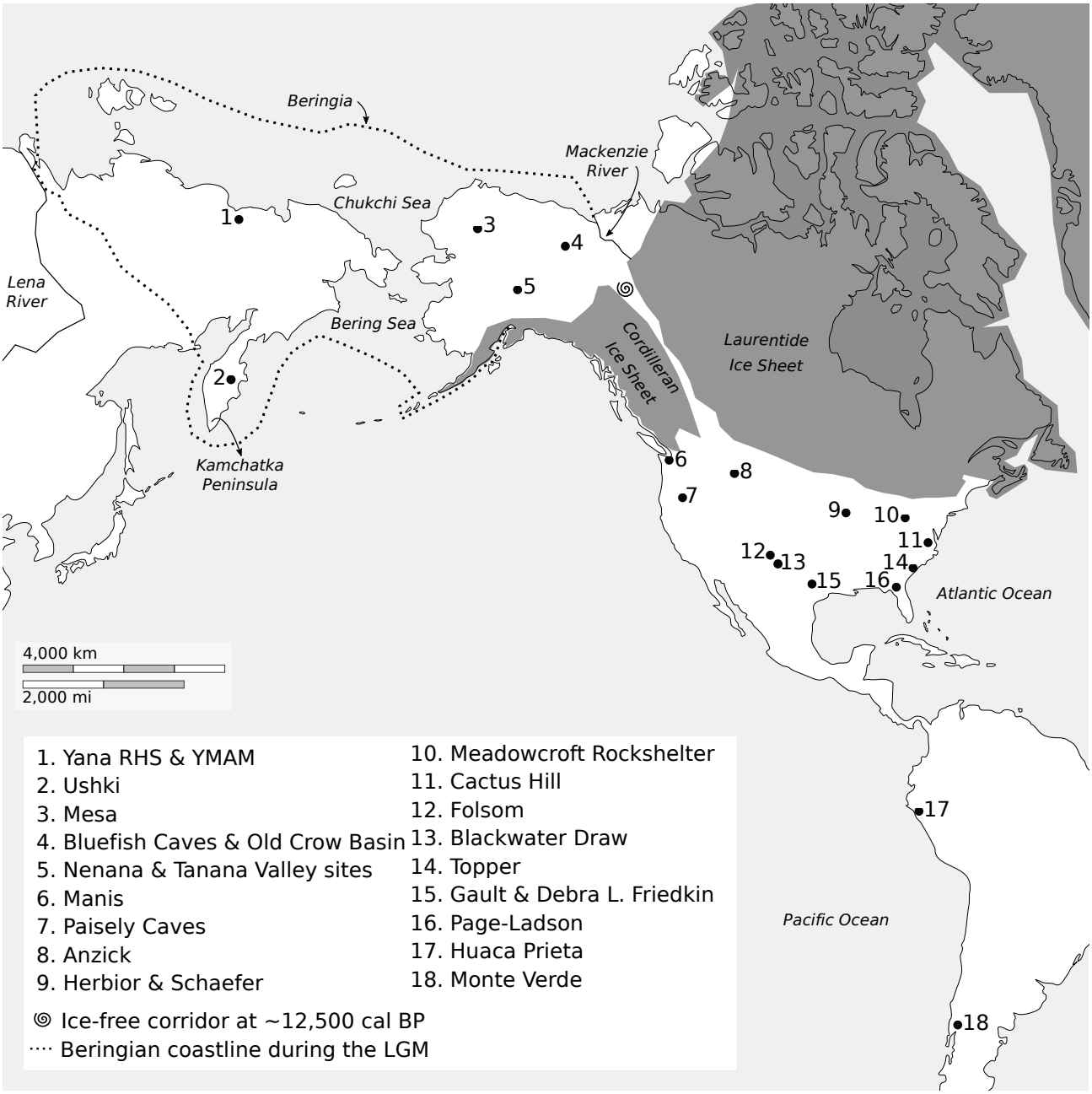


Fig. 1. Map showing the location of archaeological sites mentioned in this and section 1.1.2.1. (archaeological evidence) of Chapter I.



Fig. 2. Lithic point found in between bison ribs at the archaeological site of Folsom, New Mexico, 1926. Image courtesy of the Denver Museum of Nature and Science.

Following Folsom in its degree of importance, the discovery of Clovis prefaces the second phase of First Americans history. Here, lithic artefacts were found in association with skeletal remains of extinct mammoth and bison (22, 23). Like Folsom points, the lithic tools at Clovis contained a distinctive central groove (flute) on both faces (24) (Fig. 3), yet were generally larger, broader, and less finely made (15). Over the years, while the distribution of Folsom sites was limited to the Great Plains region (15), Clovis points were found throughout North America (25, 26). Given that the perceived age of this widespread tradition roughly correlated with the estimated rhythms of glaciation, the opening of the ice-free corridor (27), the large-scale extinction of Pleistocene-aged

megafauna[1], and the inferred "unity of origin of the eastern Asiatics and the American Indians" (18), Clovis was believed to represent the material legacy of the first Americans (16). The Clovis period is traditionally noted to span from 11,500 to 10,900 BP (32, 33). In 2007, this age estimate was updated to 11,050-10,800 BP [or 13,250-12,800 cal BP (1), but see reference 34]. In its updated form, the 'Clovis-first' model stipulates that the initial inhabitants of America came from Asia at around 13,000 ya, traversing Beringia and later North America through an ice-free corridor between Laurentide and Cordilleran ice sheets whilst hunting megafauna. Clovis-first was widely accepted and persisted as the single explanatory model for the colonisation of America for most of the 20th century. This is because it effectively answered every question associated with the peopling process —when, why, by whom, and from where. Exactly sixty years following the discovery at Folsom, however, the Clovis-first model was brought to question when, in 1997, Monte Verde II, Chile (3), was accepted by a group of First Americans researchers as a genuine pre-Clovis site dating to 12,500 BP or ~14,500 cal BP (35). The site showed that humans had penetrated the Southern Cone prior to the earliest evidence from North America. This paradigm break marks the beginning of the second stage in First Americans research. The aftermath is where matters currently stand.

[1] The underlying assumption being that the arrival of humans into America led to the widespread extinction of megafauna through over-hunting. This is known as the 'overkill hypothesis' [(28, 29), but see (30, 31)].



Fig. 4. Clovis lithic points from different archaeological sites across North America. Image courtesy of the Center for the Study of the First Americans, Texas A&M University.

Apart from the important implications of Monte Verde II's antiquity, the site serves to emphasise one of the main issues in First Americans research currently; the reliability of pre-Clovis sites in terms of archaeology, i.e., the strength of the association between the material to human activity, and, to a lesser extent[2], chronological control. Considering that claims of pre-Clovis sites predate the appearance of Monte Verde II in the record—in 1964, a compilation noted over 50 sites which claimed to antedate Clovis (38)—the importance of the site lies, largely, in its acceptance as pre-

[2] In terms of radiocarbon dating, the ages obtained for this time period are generally, at the earliest, late Pleistocene. Since this time period does not near the limit of radiocarbon dating as a technique, i.e., ~50,000 BP (36), issues of modern contamination associated with 'old' samples, e.g., Pleistocene-aged material (37), are less applicable.

Clovis by the academic community. This demands that pre-Clovis sites contain unequivocal evidence of human activity in undisturbed geological contexts and congruent stratigraphic order, accompanied by robust chronometric data (15). Passing this test is not easy. Meadowcroft Rockshelter, Pennsylvania (39–41), for instance, meets the required criteria but has yet to be widely accepted as a genuine pre-Clovis site. For years, it has been criticised and discounted from pre-Clovis compilations (42) as skeptics argue that dates obtained for the pre-Clovis level (Stratum IIa; ~15,000 BP or ~18,000 cal BP) are erroneously overestimated due to old carbon contamination from nearby coal sources and polluted groundwater (43). Micromorphological analysis of sediments have found no evidence of groundwater saturation or coal particles (44), however, and independent radiocarbon laboratories, including the Oxford Radiocarbon Accelerator Unit (ORAU), confirm the integrity of the charcoal (42). This level of scrutiny has resulted in a divided academic community; one where some still champion the Clovis-first model (45, 46) and others do not.

1.1.2. Current evidence

1.1.2.1. Archaeological

Based on current evidence, humans likely began their dispersal into North America in northeast Siberia. Here, the earliest human occupation dates to ~28,000 BP or ~32,000 cal BP, during MIS 3[3], at the Yana Rhinoceros Horn site (RHS)—located ~100 km from the Laptev Sea coast along the lower Yana River (Russia) [(48–50), but see reference 51 for earlier claims] (Fig. 1). Yana RHS and the nearby mass accumulation of mammoth remains (YMAM) preserve lithic and ivory artefacts typical of an Upper Palaeolithic toolkit (48–50). Following Yana RHS, there is a significant gap in the west Beringian record that ends with the bi- and uni-face lithic industry of the Ushki sites, Kamchatka (Russia) (Fig. 1), dated to ~11,000 BP or ~13,000 cal BP (52). Moving into east Beringia, the earliest hint of human presence is found at the Bluefish Caves, Yukon (Canada) (Fig.

[3] MIS 3 is an interstadial phase beginning at 57,000 ya, and ending at the onset of the last glacial period, MIS 2, 30,000 ya (47).

1), at 19,650 ± 130 BP (24,035-23,310 at 95.4% confidence), during the LGM (53, 54). North of Bluefish Caves is the Old Crow Basin (Fig. 1), where radiocarbon dates for purportedly human modified bones range from ~42,000 to 25,000 BP (55, 56). Archaeological evidence from the Old Crow Basin is not deemed reliable, however, as it lacks associated lithic artefacts and natural processes might best explain the bone modifications observed (57). Following the occupation at Bluefish Caves, sites within the Nenana and Tanana valleys of central Alaska (Fig. 1) comprise material traditions containing microblade and bifacial point technologies that likely predate or are coeval with the Clovis culture (58–61). A non-fluted and fluted lanceolate point technology consistent with Paleoindian industries of mid-continental North America, such as Clovis, is also found in Alaska (Mesa complex) (62, 63). Although the relationship between the Arctic Paleoindian and Clovis, in particular, is largely unknown, the presence of Paleoindian points in Alaska might suggest a backward migration from southern latitudes during the late Pleistocene (57, 64). This, coupled with the technological diversity apparent within east Beringia, provides evidence for a dynamic landscape at the Pleistocene-Holocene transition—perhaps the adaptive response of human populations to a fast-changing environment (64).

From Beringia, passage south would have been blocked by the Laurentide and Cordilleran ice sheets (LIS and CIS) during the LGM. These covered most of modern-day Canada, coalescing in the west (65–67). The emergence of an unglaciated corridor between the two began ~15,000-14,000 cal BP, becoming biologically sustainable for humans ~12,500-13,000 cal BP (68, 69). Considering that the Clovis culture dates, at its earliest, to ~13,500 cal BP (32, 33), this time frame is problematic. Matters are further complicated when taking pre-Clovis claims into account, including Monte Verde II (Chile), Meadowcroft Rockshelter (Pennsylvania), Cactus Hill (Virginia) (70, 71), Paisley Caves (Oregon) (72, 73), Manis (Washington) (74), Topper (South Carolina) (75), Page-Ladson (Florida) (76), Debra L. Friedkin (Texas) (77), Gault (Texas) (78–82), Hebior (Wisconsin)

(83, 84), and Schaefer (Wisconsin) (83–85) into account (Fig. 1). Even if all pre-Clovis claims were discounted, multiple Clovis contemporaries showing distinct technologies are present throughout the continent (5–14). This, coupled with the 'late' opening of the internal corridor, has led researchers to suggest that humans probably dispersed southward earlier, following the Pacific coast instead (86–96). Stemmed point technology found across the Pacific margin has been posited as the likely material legacy of these early settlers (87).

In Central and South America, archaeo-chronometric data for the late Pleistocene is more limited (13, 97–105). This is likely influenced by research and funding biases. Moreover, upon assessment, current evidence often requires archaeological-chronometric clarification and/or lacks comprehensive reporting (35, 106–112). As it stands, the earliest, most reputable archaeological sites in these two regions are Monte Verde II (Chile) and Huaca Prieta (Peru) [at ~15,000 cal BP (113, 114)] (Fig. 1)—both with distinct lithic technology (114). These are followed by a small number of archaeological sites with Clovis-coeval dates (5, 11, 12, 14, 115–122) and later appearing technological industries (7, 123–128). Together, these sites suggest that there was a variety of subsistence strategies and adaptations in the region by the late Pleistocene.

1.1.2.2. Genetic

Ancient DNA (aDNA) research suggests that ancestral Native American populations and Siberians/ East Asians diverged 30-22 thousand years ago (ka) (129, 130) with USR1—an ancient individual from Alaska, dated to ~11.5 ka, representing an Ancient Beringian (AB) population—splitting from other Native Americans at around 23.3-21.2 ka (129, 131). Later, at around 17.5-14.6 ka (129–134), it is estimated that the ancestral Native American branch split into two populations—'Northern Native American' (NNA) and 'Southern Native American' (SNA)—likely outside of Eastern Beringia and south of the North American ice sheets (129–131). Anzick-1, from Anzick site

(Montana), is the only Clovis individual yet found that belongs to the SNA population. He shows closer affinity to indigenous Mexican, Central and South American groups, and his genetic legacy is found in ancient individuals from California, Chile, Belize and Brazil (132, 134, 135). At around 16 ka, mitochondrial data shows that a small group entered the Americas following no more than 9,000 years of isolation in Beringia (136). This period is known as the Beringian standstill or Beringian incubation model (130, 136–140). Between 16 and 13 ka, the female population underwent a 60-fold increase (136), coinciding with the rapid retreat of coastal glaciers (141). This led a number of researchers to argue that the initial colonisation likely occurred via the Pacific coast (130, 133), in agreement with some archaeological claims (86–96). Moving southward, an Australasian signal has been detected in South America (129, 130, 139, 142), present by 10.4 ka (129)—although Posth et al. (135) warn this might be a false-positive as it was absent from the ancient Central and South American individuals they analysed. The full expansion to the edge of the continent seemingly took ~1,400 years (139), with data supporting the concomitant arrival of Y-chromosome founding lineages (haplogroups Q-M3 and Q-L54*) to Mesoamerica (143). By ~9 ka, population turnover replaced Anzick and Clovis-associated ancestry in South America (135).

Given its adjacent position to the most likely entry point to America, it is also worth mentioning current research in northeastern Siberia. Here, aDNA results suggest continuity for pre- and post-LGM populations, and the dominance of Eurasian and East Asian lineages. As an outline, the earliest sampled population in the region is that of the ‘Ancient North Siberians’ (ANS), represented by two individuals (Yana1 and Yana2; dated to ~32 ka) discovered at the Yana RHS site. The ANS is distantly related to early West Eurasian hunter-gatherers and is ancestral to the Upper Palaeolithic Mal’ta individual (MA-1; dated to ~24 ka) (144), found near Lake Baikal, south-central Siberia (145). This, in turn, represents an ‘Ancestral North Eurasian’ population that is basal to modern-day western Eurasians and Native Americans. The Mal’ta individual is closely related to later

individuals AG-2 (dated to ~16.9 ka), from the same region at the site of Afontova Gora-2 (145), and Kolyma1 (dated to ~9.8 ka), from western Beringia at the site of Duvanni Yar (144). The latter represents the 'Ancient Palaeo-Siberian' population, which is a mixture of ANS and East Asian ancestry (similar to Native Americans) that formed after ~30 ka, and documents the first genetic shift in the region (144). Data show that for Ancient Palaeo-Siberians and Native Americans, ANS-derived ancestry is more closely related to Mal'ta than the Yana individuals, implying that the ANS lineage did not directly contribute to later Ancient Palaeo-Siberians (Kolyma1) or Native American lineages (144).

1.1.2.3. Cranio-morphological

Human skeletal material dating to the Pleistocene-Holocene transition across the continent is limited (15, 146–150). The highest density of ancient human remains is found in South America, however, within the regions of Lagoa Santa (Brazil) and Sabana de Bogotá (Colombia). Here, cranio-morphological research has shown a strong affinity between both ancient populations and low intra-group variation during the first millennia of the Holocene (148, 151). Results further suggest that these ancient South Americans groups are phenotypically closer to extant Australo-Melanesian groups (152) than modern Native Americans—who, in turn, show greater affinity with late and modern Northern Asians (148, 153, 154). This observed morphological diversity in the record is generally explained by two models: 'Two-Components' and 'Recurrent Gene Flow'. The former maintains that at least two distinct biological groups entered America (148, 153, 155), while the latter contends that the first colonisers likely showed high intra-group variation upon arrival, later fuelled by local microevolutionary processes, and maintained contact with Circum-Arctic groups during the Holocene (140, 156, 157).

1.2. Research objectives

Human dispersals can only fully be understood through the lens of chronology. To this end, my thesis aims to build a robust chronological framework with which to elucidate the broad spatio-temporal pattern of the earliest human dispersals into America, and frame current bio-cultural and climatic evidence. This, in turn, is accomplished via the following underlying objectives;

a) obtaining new radiocarbon measurements for Clovis, Clovis-coeval and/or pre-Clovis archaeological sites across the continent, and resolving the chronological uncertainty of key archaeological sites by producing reliable radiocarbon measurements using rigorous pretreatment methods;

b) using Bayesian age modelling to statistically integrate and assess archaeological and chronometric data (previously published and newly obtained) by building site-specific and large-scale models; and,

c) assessing the reliability of the '^{14}C-dates-as-data' approach in the study of population dynamics in contrast to Bayesian age modelling, one of the main methods used in this thesis.

In collaboration with archaeologists and museum curators, objective (a) involves sampling material from archaeological sites with cultural evidence that places them, either securely or potentially, within one of the temporal categories noted, and which lack chronological control or require improved resolution. This includes the dating of bone samples from human burials or kill/butchery sites that are known or suspected to be contaminated with consolidants used in curation, and for which chronological clarity is important and has not yet been obtained. My thesis aims to take advantage of the recent optimisation of the amino-acid-isolation protocol established at the ORAU (158), and its proven efficiency in the decontamination of heavily contaminated bone samples (159–163). This has the potential to produce accurate radiocarbon measurements, resolve dating discrepancies, and improve the accuracy and reliability of the chronological framework proposed.

The use of Bayesian statistics (underlying objective b) provides a new mechanism through which a chronological framework is built. It moves beyond simple comparisons of dates to each other—often done according to a mean or median, which imposes concurrence and ignores the imprecision of calibrated determinations. Instead, Bayesian statistics provide quantitative estimates to directly or indirectly dated archaeological events. This involves the inclusion of previously published or newly produced chronometric data into site-specific models informed, primarily, by stratigraphic context, and large-scale models based on, for example, technological categories. This approach was previously applied to a continental-scale research question at the ORAU, in a study led by Higham et al. (164), where the spatio-temporal overlap of European Neanderthals and modern humans was quantified using the timeline and spread of their technological traditions. Similarly, this thesis aims to apply the Bayesian approach to address questions in First Americans research that require chronological certainty. These include the initial route taken; the antiquity of the earliest technological traditions, the bio-cultural relationship between pre-Clovis, later Paleoindian, and Asian populations; and the potential links between human arrivals and late Quaternary faunal extinctions.

Objective (c) explores the ^{14}C-dates-as-data method, which uses large sets of radiocarbon dates to reconstruct trends in ancient human populations. Aside from Bayesian age modelling, this is the only other quantitative technique involving the chronometric record that is used to elucidate human dispersals. This, however, relies on a number of assumptions that are explored to varying degrees in the literature and have the potential to misrepresent the magnitude of human activity and misguide interpretation. In particular, biases introduced by challenges in sample processing within radiocarbon dating have gone largely undiscussed. Here, I aim to examine the ^{14}C-dates-as-data method, demonstrating the potentially confounding effects of poor sample preservation and

contamination in the analysis and discussing the comparative efficiency of Bayesian age modelling in the study of human dispersals.

1.3. Thesis structure and outline

The bulk of this thesis comprises three scientific articles (chapters III-V). The first is published (*Proceedings of the National Academy of Sciences of the United States of America*), the second is currently in review (*Nature*), and the third has also been published (*Journal of Archaeological Sciences*). For background, section 1 of this chapter has provided a brief outline of the history of First Americans research and current archaeological, genetic, and cranio-morphological evidence. Chapter II describes the methods of radiocarbon dating and Bayesian age modelling applied in the dissertation. Chapter III (article 1), addresses objective (a) by presenting the results of a comprehensive dating program performed for the archaeological site of Anzick, Montana, the only known Clovis burial in North America. This uses single-amino-acid dating to address a previously identified age discrepancy between the ancient individual ('Anzick-1') and Clovis tools found in the same archaeological context, which led some researchers to reject Anzick-1 as Clovis. Chronological clarity is further required as Anzick-1 shows a closer affinity to Central and South American indigenous groups than northern counterparts, suggesting population structure in Native American populations that predates Anzick-1 and, in turn, Clovis (132). Chapter IV (article 2), addressing research objective (b), tracks the earliest dispersal of humans through North America and Beringia, using Bayesian age modelling and the analysis of chronometric data (n=705) from 39 archaeological sites. This enables the creation of a chronological framework for these regions, and allows the proposal of a new, chronometry-centred model for the peopling of the Americas. Chapter V (article 3), based on research objective (c), considers the suitability of the ^{14}C-dates-as-data approach, which advocates using large datasets of radiocarbon determinations as population proxies. Here, the biases introduced by sample processing within radiocarbon dating are explored and the

viability of the method itself is assessed. Chapter VI summarises the main results of this thesis and discusses future avenues of research.

In addition to the main chapters, I attach a set of appendices related to other relevant work produced during this doctoral research programme. Appendix A describes the chronometric analysis of 17 additional archaeological sites that focused on research objective (a). Materials, results and implications for each are noted. Appendices B and C are co-authored publications in *Science*, which include chronometric work conducted for the archaeological sites of Spirit Cave and Cooper's Ferry, respectively. Appendix D is a co-authored publication in *Quaternary Science Reviews*, which concerns research objective (a) and involves the redating of heavily contaminated bone samples from kill/butchery sites in North America, using single-amino-acid dating. Results obtained were incorporated into the chronological framework built in Chapter IV (article 2).

II. Methods

Although each article has a methods section, radiocarbon dating and Bayesian age modelling are the two main methods used in this thesis and are briefly explained in the following sections. The first is particularly important for assessing the chronometric data presented in Appendix A.

2.1. Radiocarbon Dating

2.1.1. Principles and assumptions

Developed by W. Libby (165, 166), radiocarbon dating is a method that uses ^{14}C to determine the age of carbonaceous material. The element of carbon has three isotopes, i.e., variants of a given chemical element which differ in the number of neutrons contained within the nucleus, which vary in proportion within the atmosphere: ^{12}C (98.89%), ^{13}C (1.1%), and ^{14}C (trace quantities). Unlike ^{12}C and ^{13}C, ^{14}C is radioactive and continuously created in the upper atmosphere by the action of cosmic ray interaction with nitrogen atoms. Once created, ^{14}C quickly oxidises in the atmosphere to form 'heavy' carbon dioxide molecules ($^{14}CO_2$), which enter different carbon reservoirs, e.g., the atmosphere and oceans. From these, ^{14}C is incorporated into the biosphere via photosynthesis. In the atmosphere, the concentration ratio between ^{14}C and ^{12}C is assumed to have remained constant as radiocarbon decay and production are in relative equilibrium. For living organisms, ^{14}C concentration is in near equilibrium with that of their respective carbon reservoirs, e.g., atmosphere or marine, until death, when ^{14}C is no longer replenished and decays back into ^{14}N. The decay of ^{14}C proceeds at a predictive rate of 5,730±40 years, also known as isotopic half-life (167). Therefore, the $^{14}C/^{12}C$ ratio measured in a sample can be used to obtain an estimation of the time elapsed since the organism ceased to uptake carbon from the reservoir in which it lived. The working limit of the method is reached at about 10 half-lives or around 60,000 years. Below, the radiocarbon dating principle is expressed in mathematical terms:

$$R = A \exp(-T/8033) \quad (1)$$

The proportion of radiocarbon to stable carbon reduces according to the exponential decay law, where 'R' is the $^{14}C/^{12}C$ ratio in a given sample, 'A' is the original $^{14}C/^{12}C$ ratio of the living organism, 'T' is the amount of time elapsed since its death, and 8033 is the lifetime or *mean* life of ^{14}C (according to the 'Libby half-life' of 5,568±30 years).

$$T = -8033 \ln(R/A) \quad (2)$$

By measuring the ratio 'R' in a sample, the conventional radiocarbon age can be calculated. This, in turn, incorporates the following conventions (i-iii) and assumptions (iv-vi);

i) 1950 is the present, with radiocarbon ages given in years before 1950 AD;

ii) the use of oxalic acid as a modern standard;

iii) the use of 5568±30 years (166) as the radiocarbon half-life, which is corrected for during calibration for a more accurate estimate of 5730±40 (167);

iv) the amount of radiocarbon or production rate within the atmosphere has remained constant through time;

v) the amount of radiocarbon within an organism is at equilibrium with the atmosphere, being in constant exchange; and

vi) the change in radiocarbon concentration within a sample is due to radioactive decay.

Assumption (iii) does not hold as variations in radiocarbon production have occurred in the past due to a number of factors, including changes in Earth's magnetic field and anthropogenic action, e.g., nuclear bomb testing in the 1960s (168, 169). To account for long- and short-term temporal fluctuations, workers have measured the radiocarbon concentration of known-age materials, determined through alternative chronometric means, and created atmospheric and marine calibration curves—the latest being IntCal13 (170), Marine13 (170), and SHCal13 (171). Their use provides a best age estimate for a radiocarbon measurement, with quantified uncertainties. Assumption (v) is invalidated if an organism obtains its carbon from non-atmospheric reservoirs.

The marine reservoir effect (MRE), for example, applies to organisms that derive their carbon from marine water, which is comparatively depleted in ^{14}C due to slower mixing rates in the ocean. This effect is corrected through the quantification of the parameter ΔR, the local variation from the global average MRE (172). Assumption (vi) negates the possibility of sample contamination with exogenous sources of modern or depleted radiocarbon. This is addressed by the purification of samples following chemical pretreatment methods tailored to sample age, type and perceived levels of contamination.

2.1.2. Laboratory processing and measurement

Samples were processed for radiocarbon dating at the ORAU, using the following methods. Further details on pretreatment protocols and accelerator mass spectrometry (AMS) measurement can be found in references 158, 173 and 174.

2.1.2.1. Sampling

Bone and shell samples were manually cleaned by air abrasion with aluminium oxide powder to remove superficial contaminants. A fragment was then cut manually or using a small diamond disc, and crushed with a pestle and mortar. Bone samples were drilled using a tungsten carbide spherical burr drill bit. The ideal mass required for bone is 600 mg, for shell is 40 mg, for charcoal and plant remains it ranges between 30-100 mg, and for sediment it is 1000 mg. Prior to chemical pretreatment, all samples were placed within 10 or 20 ml glass tubes that were pre-baked in a 500°C oven to remove organic contaminants.

2.1.2.2. Bone collagen prescreening

To assess collagen preservation, bone samples were prescreened for nitrogen content. This is used as a proxy for collagen content in bone since nitrogen is derived solely from the proteinaceous component, the majority of which is collagen (175). Prescreening involves measuring the %N of 1

mg of whole bone powder (placed into a tin capsule) with a CHN elemental analyser (Carlo-Erba NA, 2000), coupled to a gas source isotope ratio mass spectrometer (Sercon 20/20) (176, 177). The cut-off value of 0.76 %N is used in this investigation as routine at the ORAU. This is because at a threshold of 0.76 %N, there is an 84% chance of successfully predicting whether or not a bone sample will yield sufficient collagen for dating [(>1% weight collagen; (176)]. Alanine and L-Glutamic acid standards were used for correction and quality control.

2.1.2.3. Chemical pretreatment

For bones, if consolidants were present or suspected to be, chemical pretreatment was preceded by a series of solvent washes, e.g., acetone/methanol/chloroform. “Collagen” (following the use in references 178–180) was targeted by means of an acid-base-acid (ABA) protocol, gelatinisation (181), Ezee-filtration (ORAU pretreatment code: ‘AG’) and, if yield was sufficient, ultrafiltration (182) (ORAU pretreatment code: ‘AF’). To start, samples were rinsed with 0.5M hydrochloric acid [three or four washes over an ~18 hour period; at room temperature (RT)], 0.1M sodium hydroxide (30 minutes at RT), and 0.5M hydrochloric acid (~1 hour; at RT). Each acid or base wash was followed by three rinses with ultrapure MilliQ™ deionized water. The extracted collagen was then gelatinised in a pH 3 solution at 75°C for 20 hours and filtered using pre-cleaned Ezee-filters™. If ultrafiltered, the gelatin was transferred into previously cleaned ultrafilters [Vivaspin™ 15–30 kD molecular weight cut-off (MWCO)] and centrifuged until 0.5–1.0 mL of the >30 kD gelatin fraction was left. This gelatin was collected using glass pipettes and placed into previously pre-baked glass tubes. Samples were then thoroughly frozen at -18°C and lyophilised using a VaCo 5 freeze-dryer (Zirbus, Germany) for a minimum of 12 hours.

For single-amino-acid dating, if targeting hydroxyproline, 30–50 mg of freeze-dried collagen was placed into pre-baked 11.5 ml screw-top glass test tubes and 6 M HCl was added via micro-pipette

at a ratio of ~1 mL of 6 M HCl per 10 mg of collagen. These were flushed with N_2 gas for 5 min, capped, and heated at 110°C for 24 hours. The hydrolysis solution was then evaporated in a model EZ−2 vacuum evaporator (Genevac Ltd, UK) to eliminate the HCl. Samples were then re-dissolved with 700µL of 0.1 M NaOH and filtered using a 2 ml BP Plastipak™ syringe fitted with a 0.2−µm PTFE syringe filter. Filtered samples were loaded into a 1 ml vial and injected into a high-performance liquid chromatography (HPLC) system, which enabled the separation of underivatised amino acids and the collection of hydroxyproline in MilliQ™ deionised water. The hydroxyproline was then concentrated using a Genevac EZ−2 Plus vacuum evaporator.

Plant remains (charred/carbonised or otherwise) and wood underwent ABA pretreatment (ORAU pretreatment codes: 'VV', 'UV', 'WW', 'UW', and 'ZR'). This involved an initial immersion of ~20-100mg of material in 1M HCl for 20 minutes at 80°C, followed by three rinses with ultrapure water. After rinsing, samples were separated by centrifugation, decanting or glass pipetting. The material was then washed with a 0.2M NaOH solution for 20 minutes at 80°C, and rinsed with ultrapure water in the same manner. Pretreatment was completed by a third wash, an immersion in 1M HCl for 1 hour at 80°C, and three subsequent ultrapure water rinses. For wood and less delicate plant remains, samples were bleached at 80°C using acidified (pH 3) 5% w/v $NaClO_2$ for up to 30 minutes, and rinsed three times with ultrapure water. Small or very delicate materials underwent acid-only and sonication treatment (ORAU code: 'RR'). Following pretreatment, all samples were then thoroughly frozen at -18°C and lyophilised using a VaCo 5 freeze-dryer for a minimum of 12 hours.

For sediments, the humin fraction was targeted following ABA protocol (ORAU code: 'SRa'). This involved an initial immersion in 1M HCl for 1 hour at 80°C, followed by three rinses with ultrapure water. After rinsing, samples were separated by centrifugation and decanting. The material was then

washed with a 0.1-0.5M NaOH solution for 1 hour at 80°C, and rinsed with ultrapure water in the same manner. Pretreatment was completed by a third wash, an immersion in 1M HCl for 1 hour at 80°C, and three subsequent ultrapure water rinses.

Carbonate samples were processed according to an acid dissolution protocol[4] (ORAU pretreatment code: 'OX'). First, a sample was placed in a 10 ml glass tube capped with a septum stopper (Fisherbrand™) and evacuated through a vacuum line with three Ultra-Torr vacuum fittings until pressure (P) was $<10^{-3}$ Torr. This involved injecting through the septum, with a 26G ½" 0.45x13mm needle (BD Microlance™ 3). Reaction was then accomplished by injecting 3ml of concentrated phosphoric acid (H_3PO_4; 85%) with a luer lock glass syringe (Hamilton™). Samples were outgassed in a 50°C water bath for 1 hour or until done effervescing. Later, each sample was connected to a second vacuum line through a 23G ¼" 0.6x0.32mm needle (Terumo Agani™). This line consisted of a water trap (dewar with a propan-2-ol/liquid nitrogen mixture at -65°C) and three ampoule holders. The needle was first evacuated until $P<10^{-3}$ Torr by partial injection (carefully placing the needle inside the septum). Injection was then completed and CO_2 transferred to the water trap three times, each for one minute. Samples were collected into glass ampoules using liquid nitrogen.

Known-age standards accompanied all sample types during pretreatment.

2.1.2.4. Combustion, recycling and graphitisation

Freeze-dried, e.g., bulk collagen and plant remains, and reconstituted hydroxyproline samples (in 25 µl of ultrapure water and loaded by glass pipette onto 12 mg of Chromosorb™) were placed into tin cleaned capsules and combusted in a CF-IRMS system, consisting of a CHN elemental analyser (Carlo-Erba NA, 2000) coupled to a gas source isotope ratio mass spectrometer (Sercon 20/20).

[4] This carbonate protocol was tested and established by Eduardo Queiroz Alves and me, with the help of ORAU members David Chivall, Daniel Comeskey and Joseph Graystone.

This allowed for the measurement of carbon elemental ratios and stable isotopes (173). The CO_2 collected was transferred to pre-outgassed rigs containing a 2.0-2.5mg iron catalyst and H_2 added at a ratio of $2.2H_2$:$1CO_2$ and heated at 560°C for 6 hours. Subsequently, graphite targets were made with approximately 0.5-1.8 mg of carbon, depending on the yield of each sample (183). Isotopic ratios for the samples were calculated relative to the results of alanine standards run in duplicate for every seven unknown-age samples. For the comparison of radiocarbon activity in these samples with that in known-age material, two tin capsules containing oxalic acid II (modern) accompanied the combustion run and final AMS measurement. As an added measure, an empty tin capsule was placed between every other sample in the combustion wheel to purge the system.

Carbon dioxide collected from carbonates following the OX protocol were passed through the same system in a recycling process. Samples were graphitised using the same method described above.

2.1.2.5. AMS measurement

Radiocarbon measurement was done with a High Voltage Engineering Europa (HVEE) AMS system and a Mini Carbon Dating System (MICADAS) AMS. In brief, stable isotope corrected ^{14}C dates are calculated by (i) subtracting AMS/graphitisation and combustion background values through analysis on anthracite (combusted by the CIO Groningen laboratory and graphitised at the ORAU) and nylon standards, correspondingly; (ii) applying background corrections for the chemical pretreatment of bone collagen and hydroxyproline through the analysis of in-house bone standards of background age; (iii) calculating the $\delta^{13}C$ for each target using the $^{13}C/^{12}C$ ratio relative to the average value of oxalic acid targets (done using the AMS-derived $\delta^{13}C$ rather than that from the stable isotope mass spectrometer to correct for any linear mass fractionation); and (iv) calculating the $^{14}C/^{13}C$ ratio of unknown samples relative to the average value from the oxalic acid samples (158, 174, 184). All samples that underwent full

chemical pretreatment and continued on to AMS dating were provided a unique OxA- number. OxA- numbers followed by a 'X', denote samples that are research measurements using non-standard or experimental methods, or determinations that come with a warning as to the chemical parameters observed during pretreatment and measurement.

2.1.2.6. Calibration

The calibration of radiocarbon determinations was completed using the OxCal 4.3 software (185) and, depending on the location of the archaeological site (Northern or Southern Hemisphere) and material type, the IntCal13, Marine 13, or SHCal13 calibration curve (170, 171). As mentioned in section 2.1.1., calibration of radiocarbon measurements is necessary since these do not directly correlate with calendar years. This conversion is required for the comparison of archaeological events to each other and ice core records that detail past climate (186, 187). For the Holocene, atmospheric curves mainly rely on radiocarbon measurements from known-age tree rings that represent the atmospheric radiocarbon concentration in a particular year (188–191). Beyond the Holocene, U-Th dated speleothems (192–194) and corals (195–197), as well as plant macrofossils (198–203) and foraminifera from varved (204–207) and non-varved (200, 208, 209) sediments are employed. For atmospheric curves, measurements obtained from marine samples are corrected due to reservoir effects. In addition to these data (marine, terrestrial, and speleothem), marine curves are generated with the help of models that estimate the relationship between oceanic and atmospheric ^{14}C fluctuations, and are informed by the uptake and distribution of carbon in the ocean (210–212). Further details on curve construction and methodologies can be found in each publication and reference (213).

2.2. Bayesian age modelling

The following is a paraphrased excerpt from the methods section of Chapter IV, which deals entirely with Bayesian age modelling. Specifics on model construction and code can be found in the same chapter.

In brief, Bayesian age modelling is a statistical tool, here performed and discussed in the context of the OxCal software (185, 214), that allows the incorporation of relative prior information, e.g., stratigraphy, with absolute dates. The underlying mathematical basis derives from Bayes' Theorem (215):

$$p(t|y) \propto p(y|t)p(t) \quad (1)$$

where 't' is a set of parameters, 'y' the measurements made, 'p(t)' the prior or the information about the parameters independent of the measurements, 'p(y|t)' the likelihood for the measurements given a set of parameters, and 'p(t|y)' the posterior probability or likelihood for a given parameter set given the prior and the measurements. Simply put, this refers to the analysis of chronometric data (standardized likelihoods) in the context of existing, pertinent knowledge (prior beliefs), and the results obtained (posterior belief). Prior beliefs can involve absolute, e.g., historical accounts, or relative information, e.g., stratigraphy (216). Posterior beliefs are expressed as probability density functions (PDFs) through the use of Markhov Chain Monte Carlo (MCMC) methods which, by repeated sampling, calculate the highest probability distribution of dates as weighted towards the prior beliefs. At 95.4% confidence, a PDF is quoted as an age range that includes the 95.4% most likely results based on the prior. In OxCal, these are plotted over calibrated radiocarbon dates or non-radiocarbon measurements as a darker outline.

Bayesian age modeling assumes that time can be divided into units and treats archaeological events as groups defined by start and end boundaries. In this sense, a group can be incorporated as a `Phase` within a `Sequence` constrained by two `Boundary` commands. A `Phase` contains a group with unrelated, unordered items, whilst those in a `Sequence` follow an order. The items themselves can be phases or sequences, and these can be nested. The type of group can be defined by the type of boundary used—`Boundary`, `Zero_Boundary`, `Tau_Boundary` or `Sigma_Boundary`—and the distribution each denotes; uniform, ramped, exponential or normal (Figure 4 in (214)). For example, a `Boundary` placed at the start and end of a group defines a uniform phase. This assumes that all events included are equally likely to occur anywhere within the two boundaries. In case of multiple phases, these can be defined as contiguous, sequential or overlapping according to model construction (Figure 6 in reference 214). For contiguous phases, groups are assumed to be related, transitioning from one to the next. If included, outlier analysis [`Outlier_Model()` and `Outlier()`] can be used to address the assumption that all dates are correct. This defines the distribution and scale of outliers, and assigns each date a prior probability of being an outlier. The general t-type model,

[`Outlier_Model("General",T(5),U(0,4),"t");`],

for example, draws outliers from a Student's t-distribution with 5 degrees of freedom to account for extreme outliers, and sets the scale of offset to range widely, between 10^0 to 10^4 years (217). The analysis then identifies outliers by assessing the fit of chronometric data within the prior framework, and down-weights them automatically according to their degree of offset. This approach is more objective than manual exclusion of dates and, if a date is identified as an outlier at a posterior of 100%, it has a similar output (Figure 9 in reference 217). In archaeology, outlier analysis can be used to assess agreement within a sequence, often yielding important information regarding site-specific processes, e.g., geological unconformity or bioturbation.

In OxCal, there are a number of MCMC and non-MCMC functions that are relevant to archaeological investigations. These can be used to produce age estimates for archaeological features (`Date` within a `Phase`), the commencement of an occupational phase (start `Boundary`), or test goodness of fit between multiple dates relating to the same moment in time (`R_Combine` and `Combine`). Modeling the start of an archaeological occupation is particularly useful in the study of human dispersals, as human presence precedes an archaeological event. In addition, `KDE_Model` and `KDE_Plot` can be used to estimate the underlying distribution of datasets using kernel density estimation [(KDE; (218, 219)] (220). `KDE_Model`, in particular, is an MCMC approach that uses a normal kernel, assumes a normal distribution [estimating bandwidth according to Silverman's rule (221)], applies a shaping parameter to the bandwidth to overcome over-smoothing of multi-modal distributions, and treats events within a grouping as dependent. This has shown to be effective at retaining the original signal of a distribution and reducing noise (220).

III. Article 1: Reassessing the chronology of the archaeological site of Anzick

Published as below.

Becerra-Valdivia, L., Waters, M.R., Stafford, T.W., Anzick, S.L., Comeskey, D., Devièse, T. and Higham, T., 2018. Reassessing the chronology of the archaeological site of Anzick. *Proceedings of the National Academy of Sciences*, 115(27):7000-7003.

3.1. Main text

Reassessing the chronology of the archaeological site of Anzick

Abstract

Found in 1968, the archaeological site of Anzick (24PA506), Montana, contains the only known Clovis burial. Here, the partial remains of a male infant, Anzick-1, were found in association with a Clovis assemblage of over 100 lithic and osseous artifacts—all red-stained with ochre. The incomplete, unstained cranium of an unassociated, geologically younger individual, Anzick-2, was also recovered. Previous chronometric work has shown an age difference between Anzick-1 and the Clovis assemblage (represented by dates from two antler rod samples). This discrepancy has led to much speculation, with some discounting Anzick-1 as Clovis. To resolve this issue, we present the results of a comprehensive radiocarbon dating program that utilized different pre-treatment methods on osseous material from the site. Through this comparative approach, we obtained a robust chronometric dataset which suggests that Anzick-1 is temporally coeval with the dated antler rods. This implies that the individual is indeed temporally associated with the Clovis assemblage.

Significance Statement

The site of Anzick contains the only known Clovis burial. As such, it presents a significant opportunity to explore bio-cultural processes attributed to a key prehistoric complex within First Americans research. Considering the site's uniqueness and the existing ^{14}C age discrepancy between the human remains (Anzick-1) and the associated Clovis assemblage, obtaining robust chronometric data for this site is crucial. Through the use of different pre-treatment methods, this investigation has yielded a comprehensive chronometric dataset that shows, most relevantly, that Anzick-1 is temporally coeval with the Clovis artifacts found at the site.

Introduction

The timing and process of the initial peopling of the Americas has been, and continues to be, highly debated (1). Archaeological evidence suggests that humans first reached the American continent during the late Pleistocene through, or bordering, ancient Beringia (2, 3). In North America, evidence of early, widespread human settlement is found with the Clovis archaeological complex, recognized by eponymous and distinctive fluted bifacial points (4) and dated to 11,050-10,800 radiocarbon years before present [henceforth 'BP'; 5; see Waters et al. (6) on the exclusion of earlier dates from the sites of El Fin del Mundo and Aubrey]. Although Clovis artifacts are widespread in the North American record (7), human remains associated with the Clovis complex are rare. The only known Clovis burial was found in the archaeological site, Anzick.

Anzick (24PA506) was accidentally discovered in 1968 near Wilsall, Montana, by construction workers. The partial remains of a male infant, Anzick-1, were found in association with an assemblage of over 100 Clovis lithic and osseous artifacts—all red-stained with ochre (8–11). The incomplete, unstained cranium of an unassociated, geologically younger individual (12, 13), Anzick-2, was also recovered. Palaeogenomic data obtained for Anzick-1 suggest that this individual is i) genetically closer to modern Native Americans than any other group, ii) shares genetic information with the Upper Palaeolithic Siberian Mal'ta population, and iii) shows a closer affinity to central and south American indigenous groups than northern counterparts—likely indicating a divergence in Native American populations that predates Anzick-1 (11). Considering the geographic location and antiquity of the burial, these findings hold important spatio-temporal implications that further add to the complexity of the peopling process and render Anzick one of the most important archaeological sites within First Americans research. However, the chronology of the site has a ^{14}C age discrepancy that puts its status as the only Clovis burial into question.

For the last two and a half decades, the site of Anzick has been the subject of multiple chronometric investigations. These have produced radiocarbon dates obtained from different

chemical fractions, e.g., bulk collagen and 'compound specific' single amino acids, from Anzick-1, Anzick-2, and Clovis artifacts (two antler rods) found within the same archaeological context as Anzick-1 (5, 11–14). Although dates for Anzick-2 are consistent (SI Appendix, Table 1), Anzick-1 results show significant variation among different chemical fractions, with ages ranging from 8,690±310 BP (10,575-9,005 cal BP at 95.4% confidence) on decalcified collagen (AA-313A), to 11,550±60 BP (13,490-13,265 cal BP at 95.4% confidence) on 0.45 μm-filtered gelatin (CAMS-35912; Fig. 1). With the exception of AA-2979 (glutamic acid; 10,820±100 BP or 12,960-12,565 cal BP at 95.4% confidence) and AA-2981 (glycine; 10,940±90 BP or 13,020-12,700 cal BP at 95.4% confidence), most of the measurements for Anzick-1 fall outside the 95.4% confidence range of the antler rods, dated to 13,000-12,795 cal BP with good agreement (Fig. 1; SI Appendix, Table 2). The temporal discrepancy between the younger Anzick-1 ages and the artifacts has caused much speculation, with some archaeologists questioning the confidence ascribed to their association and discounting Anzick-1 as a Clovis individual (15). The compound-specific dates that agree with the antler rods should not be dismissed, however. Produced from a more pure fraction than bulk collagen, these likely point to the presence of a modern-carbon contaminant that might have eluded collagen pre-treatment and, in this case, co-eluted with other amino acids, e.g., aspartic acid and alanine.

In radiocarbon dating, contamination can be a major source of error (16). Methodological improvements, however, have seen a significant effect in dating accuracy and reliability (17–27). Given this and the variability shown by the Anzick-1 dataset, we sought to better define the chronology at the site by obtaining new radiocarbon measurements for Anzick-1, Anzick-2, and two Clovis bone artifacts using four different pre-treatment procedures. This approach would allow for cross-examination and a more comprehensive assessment of the chronometric data. While three of the protocols center on the decontamination of bulk collagen and are routinely employed in radiocarbon laboratories, the fourth was optimized at the Oxford Radiocarbon Accelerator Unit

(ORAU), and entails the extraction of a single amino acid, hydroxyproline (HYP), from bone collagen, using preparative High Performance Liquid Chromatography (prep-HPLC; 28). This protocol ensures sample purity through the complete removal of exogenous carbon, producing more accurate, robust results than alternative methods, particularly in the case of dating heavily contaminated bones (20, 28–33).

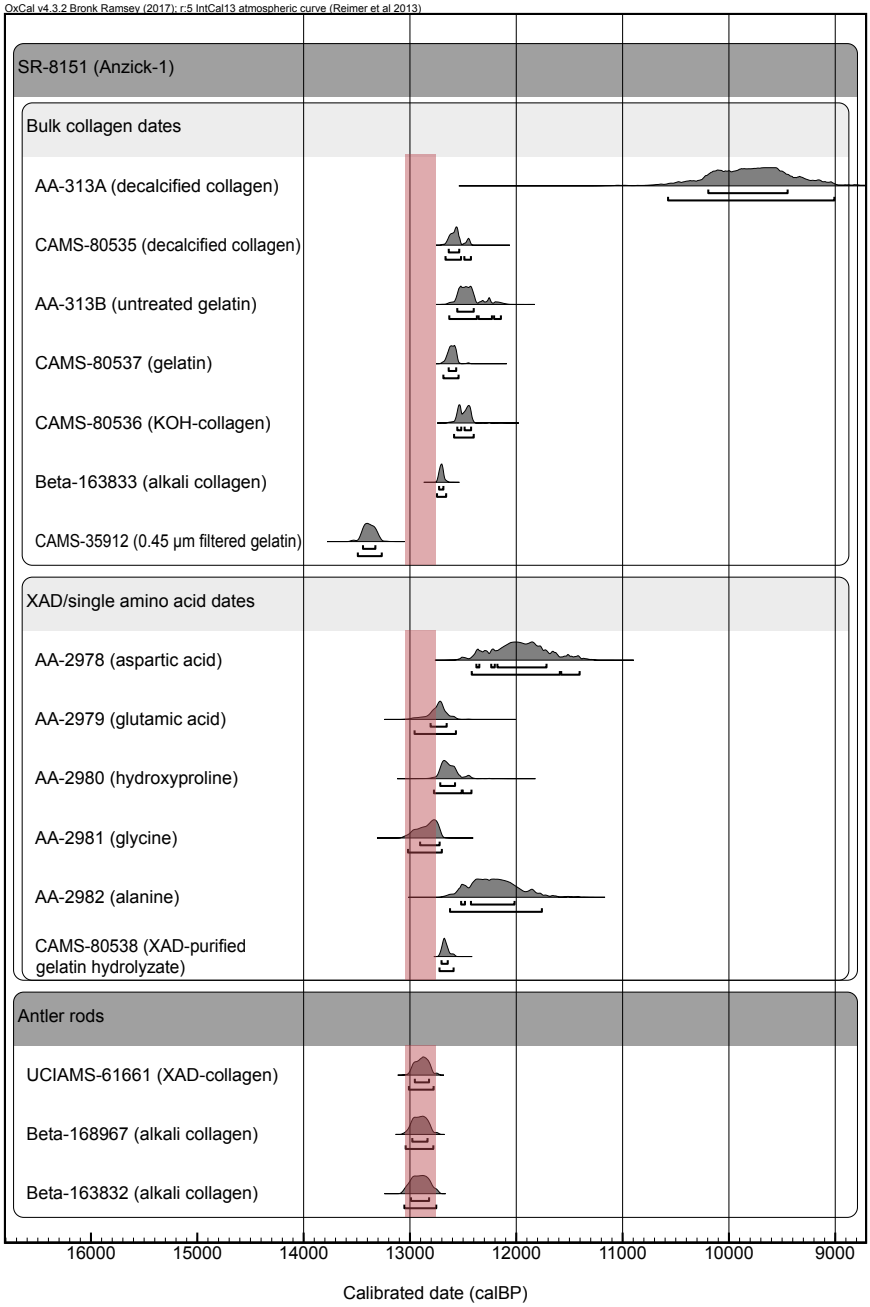


Figure 1. Previously-published radiocarbon dates (calibrated) for sample SR-8151 (Anzick-1) and two antler rods (SR-7599 and Rod #118/11) found within the same burial context. Data were compiled from multiple publications (5, 11–14; more detail on SI Appendix, Table 1). The red band

illustrates how a majority of the radiocarbon results for Anzick-1, with the exception of AA-2981 and AA-2979, fall outside the 95.4% confidence range of the dates obtained for the Clovis antler rods. This might suggest that Anzick-1 and the material assemblage represented by the antler rod samples are not temporally coeval and, in turn, unassociated.

Materials

Four osseous samples from the Anzick site were selected for AMS radiocarbon dating. These include Anzick-1 (SR-8151), Anzick-2 (SR-8147), and two Clovis artifacts (antler rods; SR-7599 and SR-7602). Three of these (SR-8151, SR-8147, and SR-7599) were previously dated using different pre-treatment methods (Fig. 1; SI Appendix, Table 1).

Results

Anzick-1, Anzick-2, and two antler rods were AMS radiocarbon dated following AG (Ezee-filtered collagen), AF (ultra-filtered collagen), and NRC (non-routine chemistry) protocols as described in Methods (Table 1, Fig. 2). Results show that while measurements within the SR-7599, SR-7602, and SR-8147 datasets are generally consistent with each other, the NRC-02 (HYP) date for SR-8151 (Anzick-1), at 10,915±50 BP or 12,905-12,695 cal BP at 95.4% confidence (OxA-X-2739-54), is considerably older than those produced using the other three methods and falls within the date range of the two antler rods at 95.4% confidence (SI Appendix, Table 2). Moreover, for all collagen samples, collagen yield, C:N, and %C values obtained are within the ORAU's accepted ranges—greater than 1% (weight), 2.9-3.5, and 30-50% (weight), respectively (34). These data indicate good collagen preservation and low levels of contamination. C:N values measured for all four NRC-02 (HYP) dates are slightly higher than the theoretical C:N value of hydroxyproline (5.0). Tests performed in our laboratory after the preparation of the Anzick material revealed that these higher values are likely due to the difference between the weight of the hydroxyproline

samples—estimated based on the peak area measured during the HPLC separation (28)—and the weight of the internal standards (alanine) used during the elemental analysis, having no significant effect on AMS measurement and the dates obtained (SI Appendix, Table 3).

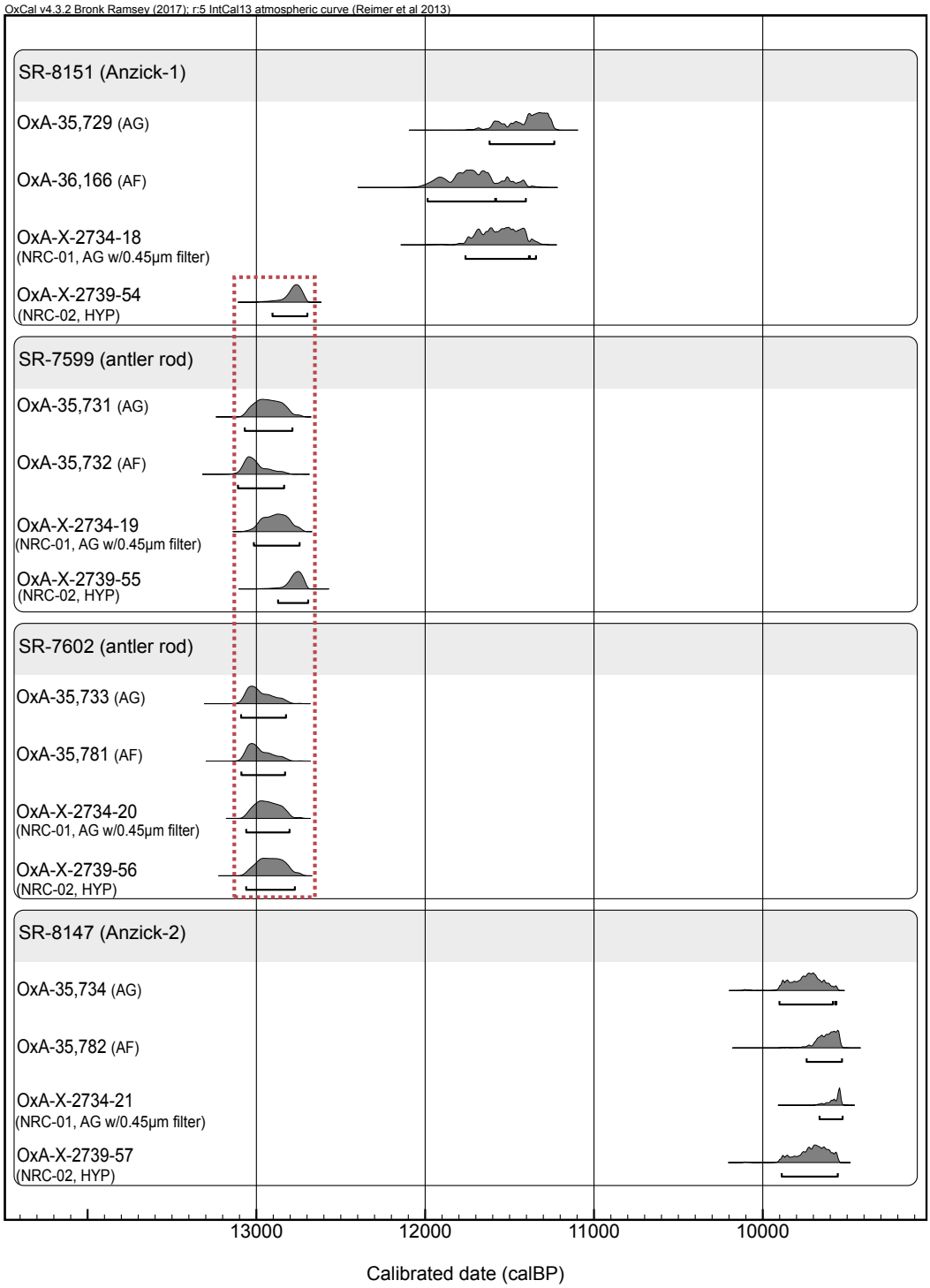


Figure 2. Oxford-obtained AMS results (calibrated) for the site of Anzick, arranged according to sample (SR-8151, -7599, -7602, and -8147) and pre-treatment protocol used (AG, AF, NRC-01, and NRC-02). This figure illustrates how the dates obtained for the Clovis assemblage (antler rods) and

the hydroxyproline-derived measurement for Anzick-1 (OxA-2739-54), fall within the 95.4% confidence range of each other (red, dashed square).

Discussion

The chronometric data obtained for samples SR-7599, SR-7602, and SR-8147, within each dataset, are in good agreement with each other and previously-published results (SI Appendix, Table 2). This suggests that i) the pre-treatment protocols used in this and other dating efforts were equally efficient in removing contaminants from the material, thus producing comparable results with no discernible trend or pattern, or ii) that the samples were not significantly contaminated with exogenous carbon and therefore produced reliable results regardless of the method used to pre-treat them. The Anzick-1 dataset, however, does not show the same consistency (SI Appendix, Table 2). The HYP date (OxA-X-2739-54), 10,915±50 BP or 12,905-12,695 cal BP at 95.4% confidence, is considerably older than the AG, AF, and NRC-01 dates (Table 1; Fig. 2), and agrees with previously-published glutamic acid (AA-2979; 10,820±100 BP or 12,960-12,565 cal BP at 95.4% confidence) and glycine (AA-2981; 10,940±90 BP or 13,020-12,700 cal BP at 95.4% confidence) determinations (SI Appendix, Table 2). This suggests that the sample was likely contaminated with modern carbon that less rigorous collagen-treating protocols did not eliminate or detect—C:N and %C values were acceptable—just as previously-published bulk collagen dates hinted (with the exception of CAMS-35912 at 11,550±60 BP or 13,490-13,265 cal BP at 95.4% confidence, which was likely contaminated with ^{14}C-depleted carbon during pretreatment and considered highly anomalous). Because no more material remains (see Statement Regarding Legal and Ethical Issues), identification of the contaminant through further analysis is impossible. As it stands, the HYP date suggests that Anzick-1 is temporally coeval with the antler rods measured. This implies that the individual is indeed associated with the Clovis artifact assemblage and dates within the Clovis period (5).

Conclusion

The site of Anzick contains the only known potential Clovis burial. The ^{14}C age discrepancy between the male infant, Anzick-1, and the Clovis assemblage found within the same archaeological context, has brought the association between the two into question. To solve this, we obtained multiple radiocarbon measurements for Anzick-1; Anzick-2, an unassociated, geologically younger individual; and two antler rods from the Clovis assemblage. Each sample was dated four times, following the use of different pre-treatment methods: collagen filtration (AG), collagen ultrafiltration (AF), collagen filtration with a 0.45 μm syringe filter (NRC-01), and hydroxyproline (HYP) extraction using prep-HPLC (NRC-02). This comprehensive approach showed that there is strong agreement between the Anzick-1 HYP date (10,915±50 BP or 12,905-12,695 cal BP at 95.4% confidence; OxA-X-2739-54) and all those obtained for the antler rods (12,990-12,840 cal BP at 95.4% confidence). The results therefore suggest that Anzick-1 is temporally coeval with the antler rods, associated with the Clovis assemblage, and dates within the Clovis period (5).

Methods

All samples were processed at the ORAU, using four different preparative protocols. The first, coded ‘AG’, is a routine procedure that entailed the decalcification, alkali wash, reacidification, gelatinization, and filtration of the bone sample using previously-cleaned 9 ml Ezee-filters™ (Elkay, UK), per (34). The second, coded ‘AF’, is a routine protocol that entailed the ultrafiltration (using Vivaspin™ 15–30 kD MWCO) of the gelatin following Ezee filtration (34). The third, coded ‘NRC’ (non-routine chemistry) -01, was the first of the non-routine procedures and involved the use of non-sterile, single-use, disposable Millex® syringe filters with a membrane porosity of 0.45 μm, instead of the routinely-used Ezee-filters™ (pore size of 45-90 μm; 37). The Millipore 0.45 μm syringe filters were flushed twice with MilliQ™ deionized water and once with 0.5M hydrochloric

acid prior to use. These particular filters were the same T. Stafford (CAMS and AA) used on his preparation of the material; keeping a higher degree of consistency between dating efforts. The fourth protocol, coded 'NRC-02, involved the separation of underivatized amino acids from ultrafiltered, hydrolyzed collagen using prep-HPLC, and the collection of hydroxyproline for dating. A full description of this protocol can be found in Deviese et al. (28). Collected collagen and hydroxyproline samples were dried, combusted, graphitized, and AMS-dated as per Brock et al. (34).

Statement Regarding Legal and Ethical Issues

Ethical and legal issues surround research of Native American human remains in the United States of America. The Anzick site was discovered on private land and the human remains recovered have not been under the control of a federally funded museum or federal agency and, thus, the Native American Graves Protection and Repatriation Act (NAGPRA) does not apply. Under Montana state law, unmarked human burials are not considered abandoned. Advice provided to the project by members of the Montana State Burial Board, however, confirmed that because no claimant has made a request for the remains, the human remains from the Anzick site remain under the control of the landowners, the Anzick family. However, to ensure that Native American concerns were addressed, in 2013, Native American groups with Reservations in the surrounding area of the Anzick site were informed about our work. Our research included the sampling of the Anzick-1 and Anzick-2 human remains for aDNA studies and radiocarbon dating. Samples collected for aDNA analysis went to the Center for GeoGenetics, Natural History Museum of Denmark, University of Copenhagen, Denmark. Samples for radiocarbon analysis were sent to the Oxford Radiocarbon Accelerator Unit (ORAU), University of Oxford, United Kingdom. The aDNA study was published in 2014 (11). The purpose of the radiocarbon dating was to resolve discrepancies between previously-reported ages for the human remains and the Clovis artifacts using a technique known as

specific-amino-acid dating. These samples were delayed in processing due to technical and personnel issues at Oxford and were processed in 2017, with the results reported here. All samples supplied to the ORAU have been consumed. With the support of the Anzick family and the research team, all human remains of Anzick-1 and Anzick-2 were reburied during a Native American ceremony in June, 2014.

Acknowledgements

L.B-V. would like to thank the Clarendon Fund and Merton College, University of Oxford, for supporting her research financially. T.W.S. would like to thank Mr. Earl Hill for funding his examination of the Anzick Site geology. T.D, L.B-V, D.C., and T.H. received support for this research from the European Research Council under the European Union's Seventh Framework Programme (FP7/2007-2013); ERC grant 324139 “PalaeoChron”, awarded to Professor T. Higham. We thank all members of the Oxford Radiocarbon Accelerator Unit, University of Oxford, particularly Eileen Jacob and Christopher Bronk Ramsey.

References

1. Meltzer DJ (2015) *The Great Paleolithic War: How Science Forged an Understanding of America’s Ice Age Past* (University of Chicago Press).

2. Goebel T, Waters MR, O’Rourke DH (2008) The late Pleistocene dispersal of modern humans in the Americas. *Science* 319(5869):1497–1502.

3. Meltzer DJ (2009) *First Peoples in a New World: Colonizing Ice Age America* (University of California Press).

4. Howard CD (1990) The Clovis Point: Characteristics and Type Description. *Plains Anthropol*

35(129):255–262.

5. Waters MR, Stafford TW Jr (2007) Redefining the age of Clovis: implications for the peopling of the Americas. *Science* 315(5815):1122–1126.

6. Waters MR, Stafford TW, Kooyman B, Hills LV (2015) Late Pleistocene horse and camel hunting at the southern margin of the ice-free corridor: Reassessing the age of Wally's Beach, Canada. *Proc Natl Acad Sci USA* 112(14):4263–4267.

7. Smallwood AM, Jennings TA (2014) *Clovis: On the Edge of a New Understanding* (Texas A&M University Press).

8. Lahren L, Bonnichsen R (1974) Bone Foreshafts From a Clovis Burial in Southwestern Montana. *Science* 186(4159):147–150.

9. Wilke PJ, Flenniken JJ, Ozbun TL (1991) Clovis Technology at the Anzick Site, Montana. *J Calif Gt Basin Anthropol* 13(2):242–272.

10. Owsley DW, Hunt DR, Macintyre IG, Logan MA (2001) Clovis and Early Archaic Crania from the Anzick Site (24PA506), Park County, Montana. *Plains Anthropol* 46(176):115–124.

11. Rasmussen M, et al. (2014) The genome of a Late Pleistocene human from a Clovis burial site in western Montana. *Nature* 506(7487):225–229.

12. Stafford TW, Jull AJT, Brendel K, Duhamel RC, Donahue D (1987) Study of Bone Radiocarbon Dating Accuracy at the University of Arizona NSF Accelerator Facility for Radioisotope Analysis. *Radiocarbon* 29(1):24–44.

13. Stafford TW, Hare PE, Currie L, Jull AJT, Donahue DJ (1991) Accelerator radiocarbon dating at the molecular level. *J Archaeol Sci* 18(1):35–72.

14. Morrow JE, Fiedel S (2006) New radiocarbon dates for the Clovis component of the Anzick Site, Park County, Montana. *Paleoindian Archaeology: A Hemispheric Perspective*, eds Morrow JE, Gnecco C (University Press of Florida), pp 123–138.

15. Stanford DJ, Bradley BA (2013) *Across Atlantic Ice: The Origin of America's Clovis Culture* (Univ of California Press).

16. Bronk Ramsey C (2008) Radiocarbon dating: revolutions in understanding. *Archaeometry* 50(2):249–275.

17. Bird MI, et al. (1999) Radiocarbon Dating of "Old" Charcoal Using a Wet Oxidation, Stepped-Combustion Procedure. *Radiocarbon* 41(2):127–140.

18. Bird MI, et al. (2003) Radiocarbon dating from 40 to 60kaBP at Border Cave, South Africa. *Quat Sci Rev* 22(8):943–947.

19. Brock F, Higham TFG (2009) AMS Radiocarbon Dating of Paleolithic-Aged Charcoal from Europe and the Mediterranean Rim Using ABOx-SC. *Radiocarbon* 51(2):839–846.

20. Devièse T, et al. (2017) Direct dating of Neanderthal remains from the site of Vindija Cave and implications for the Middle to Upper Paleolithic transition. *Proc Natl Acad Sci USA* 114(40): 10606–10611.

21. Douka K, Higham T, Sinitsyn A (2010) The influence of pretreatment chemistry on the radiocarbon dating of Campanian Ignimbrite-aged charcoal from Kostenki 14 (Russia). *Quat Res* 73(3):583–587.

22. Higham T, Ramsey CB, Karavanić I, Smith FH, Trinkaus E (2006) Revised direct radiocarbon dating of the Vindija G1 Upper Paleolithic Neandertals. *Proc Natl Acad Sci USA* 103(3):553–557.

23. Higham TFG, et al. (2009) Radiocarbon dating of charcoal from tropical sequences: results from the Niah Great Cave, Sarawak, and their broader implications. *J Quat Sci* 24(2):189–197.

24. Higham T, et al. (2009) Problems with radiocarbon dating the Middle to Upper Palaeolithic transition in Italy. *Quat Sci Rev* 28(13):1257–1267.

25. Marom A, McCullagh JSO, Higham TFG, Sinitsyn AA, Hedges REM (2012) Single amino acid radiocarbon dating of Upper Paleolithic modern humans. *Proc Natl Acad Sci USA* 109(18): 6878–6881.

26. Turney CSM, et al. (2001) Early human occupation at Devil's Lair, southwestern Australia 50,000 years ago. *Quat Res* 55(1):3–13.

27. Wood RE, et al. (2012) Testing the ABOx-SC method: Dating known-age charcoals associated with the Campanian Ignimbrite. *Quat Geochronol* 9:16–26.

28. Deviese T, Comeskey D, McCullagh J, Ramsey CB, Higham T (2017) New protocol for compound specific radiocarbon analysis of archaeological bones. *Rapid Commun Mass Spectrom* 32:373–379.

29. Bourrillon R, White R, Tartar E, Chiotti L (2017) A new Aurignacian engraving from Abri Blanchard, France: Implications for understanding Aurignacian graphic expression in Western and Central Europe. *Quaternary*. doi:10.1016/j.quaint.2016.09.063. Available online 24 Jan 2017.

30. Marom A, McCullagh JS, Higham TF, Sinitsyn AA, Hedges RE (2012) Single amino acid radiocarbon dating of Upper Paleolithic modern humans. *Proc Natl Acad Sci USA* 109(18): 6878–6881.

31. Nalawade-Chavan S, et al. (2014) New single amino acid hydroxyproline radiocarbon dates for

two problematic American Mastodon fossils from Alaska. *Quat Geochronol* 20:23–28.

32. Reynolds N, Dinnis R, Bessudnov AA, Devièse T, Higham T (2017) The Kostënki 18 child burial and the cultural and funerary landscape of Mid Upper Palaeolithic European Russia. *Antiquity* 91(360):1435–1450.

33. Sikora M, Seguin-Orlando A, Sousa VC (2017) Ancient genomes show social and reproductive behavior of early Upper Paleolithic foragers. *Science* eaao1807.

34. Brock F, Higham T, Ditchfield P, Ramsey CB (2010) Current Pretreatment Methods for AMS Radiocarbon Dating at the Oxford Radiocarbon Accelerator Unit (Orau). *Radiocarbon* 52(01): 103–112.

35. Bronk Ramsey C (2009) Bayesian Analysis of Radiocarbon Dates. *Radiocarbon* 51(1):337–360.

36. Reimer PJ, et al. (2013) IntCal13 and Marine13 Radiocarbon Age Calibration Curves 0–50,000 Years cal BP. *Radiocarbon* 55(4):1869–1887.

37. Brock F, Higham T, Ramsey CB (2013) Comments on the Use of Ezee-Filters™ and Ultrafilters at Orau. *Radiocarbon* 55(1):211–212.

3.2. Supplementary text

PNAS Supporting information for:

Reassessing the chronology of the archaeological site of Anzick

Lorena Becerra-Valdivia, Michael R. Waters, Thomas W. Stafford Jr., Sarah L. Anzick, Daniel Comeskey, Thibaut Devièse, Thomas Higham

This PDF includes:

- Table 1. Previously-published radiocarbon dates for osseous material from the site of Anzick
- Table 2. χ^2 test results on radiocarbon dates obtained for the site of Anzick
- Table 3. Data for four Oxford-obtained paired dates with differing C:N values

Table 1. Previously-published radiocarbon dates for osseous material from the site of Anzick, compiled from multiple publications (1–5). Calibration was done using the OxCal 4.3 software (6) and the IntCal13 calibration curve (7).

Sample number	Sample name	AMS laboratory number	Chemical fraction dated	Date (BP)	cal BP (95.4% confidence range)
SR-8151 (87NBS-280)	Anzick-1	AA-313A	decalcified collagen	8,690±310	10,575-9,005
SR-8151 (87NBS-280)	Anzick-1	AA-313B	untreated gelatin	10,500±400	12,630-12,140
SR-8151 (87NBS-280)	Anzick-1	AA-2978	aspartic acid	10,240±120	12,420-1,1400
SR-8151 (87NBS-280)	Anzick-1	AA-2979	glutamic acid	10,820±100	12,960-12,565
SR-8151 (87NBS-280)	Anzick-1	AA-2980	hydroxyproline	10,710±100	12,775-12,420
SR-8151 (87NBS-280)	Anzick-1	AA-2981	glycine	10,940±90	13,020-12,700
SR-8151 (87NBS-280)	Anzick-1	AA-2982	alanine	10,370±130	12,625-11,755
SR-8151 (87NBS-280)	Anzick-1	CAMS-80535	decalcified collagen	10,580±35	12,670-12,425

SR-8151 (87NBS-280)	Anzick-1	CAMS-80536	KOH-collagen	10,525±35	12,585-12,400
SR-8151 (87NBS-280)	Anzick-1	CAMS-80537	gelatin	10,610±30	12,690-12,540
SR-8151 (87NBS-280)	Anzick-1	CAMS-80538	XAD-purified gelatin hydrolyzate	10,705±35	12,725-12,585
SR-8151 (87NBS-280)	Anzick-1	CAMS-35912	0.45 µm-filtered gelatin	11,550±60	13,490-13,265
SR-8151 (87NBS-280)	Anzick-1	Beta-163833	alkali collagen	10,780±40	12,750-12,655
SR-8147 (87NBS-281)	Anzick-2	AA-313C	decalcified collagen	8,620±340	10,570-8,770
SR-8147 (87NBS-281)	Anzick-2	AA-313D	untreated gelatin	8,940±370	11,180-9,145
SR-8147 (87NBS-281)	Anzick-2	AA-2973	aspartic acid	8,510±120	9,890-9,140
SR-8147 (87NBS-281)	Anzick-2	AA-2974	glutamic acid	8,740±90	10,150-9,540
SR-8147 (87NBS-281)	Anzick-2	AA-2975	hydroxyproline	8,520±80	9,685-9,320
SR-8147 (87NBS-281)	Anzick-2	AA-2976	glycine	8,680±90	10,120-9,490
SR-8147 (87NBS-281)	Anzick-2	AA-2977	alanine	8,590±90	9,890-9,430
SR-7599 (rod #122)	Antler rod	UCIAMS-61661	XAD-collagen	11,025±30	13,010-12,775
SR-7599 (rod #122)	Antler rod	Beta-168967	alkali collagen	11,040±40	13,040-12,780
Rod #118/11	Antler rod	Beta-163832	alkali collagen	11,040±60	13,055-12,750

Table 2. χ^2 test results on radiocarbon dates obtained for the site of Anzick through this and previous (1–5; SI Appendix, Table 1) investigations. The statistical analysis was done with OxCal 4.3 (6) following Ward and Wilson (8), using R_combine and Combine commands (9). R_combine performs a χ^2 test on radiocarbon dates before calibration and was used when comparing multiple dates from a single sample, e.g., Anzick-1. Combine performs a χ^2 test on calibrated dates and was used when different samples were involved, e.g., Anzick-1 and the antler rods. The degrees of freedom are given by df and the χ^2 value calculated by T. Noted inside the brackets is the confidence level (at 5%) followed by the critical value of the χ^2 distribution. This value denotes the level above which T should not rise for the dates to be considered in good agreement or comparable.

Sample number	**Sample name(s)**	**Radiocarbon results included in test (by laboratory number)**	**Result**
SR-8151	Anzick-1	OxA-35,729; OxA-36,166; OxA-X-2734-18; OxA-X-2739-54	df=3 T=253.013 (5% 7.8)
SR-8151	Anzick-1	OxA-X-2739-54; AA-2979; AA-2981	df=2 T=0.939 (5% 5.991)
SR-7599	antler rod	OxA-35,731; OxA-35,732; OxA-X-2734-19; OxA-X-2739-55	df=3 T=11.525 (5% 7.8)
SR-7602	antler rod	OxA-35,733; OxA-35,781; OxA-X-2734-20; OxA-X-2739-56	df=3 T=1.4 (5% 7.8)
SR-7599 & SR-7602	antler rods	OxA-35,731; OxA-35,732; OxA-X-2734-19; OxA-X-2739-55; OxA-35,733; OxA-35,781; OxA-X-2734-20; OxA-X-2739-56	df=7 T=12.832 (5% 14.1)
SR-7599 & Rod #118/11	antler rods	UCIAMS-61661; Beta-168967; Beta-163832	df=2 T=0.1 (5% 6.0)
SR-7599, SR-7602, & Rod #118/11	antler rods	OxA-35,731; OxA-35,732; OxA-X-2734-19; OxA-X-2739-55; OxA-35,733; OxA-35,781; OxA-X-2734-20; OxA-X-2739-56; UCIAMS-61661; Beta-168967; Beta-163832	df=10 T=13.618 (5% 18.307)
SR-8147	Anzick-2	OxA-35,734; OxA-35,782; OxA-X-2734-21; OxA-X-2739-57	df=3 T=7.982 (5% 7.8)
SR-8147	Anzick-2	OxA-35,734; OxA-35,782; OxA-X-2734-21; OxA-X-2739-57; AA-313C; AA-313D; AA-2973; AA-2974; AA-2975; AA-2976; AA-2977	df=10 T=13.988 (5% 18.307)
SR-8151 & SR-7599	Anzick-1 (HYP date, only) and antler rod	OxA-X-2739-54; OxA-35,731; OxA-35,732; OxA-X-2734-19; OxA-X-2739-55;	df=4 T=11.104 (5% 9.5)
SR-8151 & SR-7602	Anzick-1 (HYP date, only) and antler rod	OxA-X-2739-54; OxA-35,733; OxA-35,781; OxA-X-2734-20; OxA-X-2739-56	df=4 T=8.896 (5% 9.5)

SR-8151, SR-7599, & SR-7602	Anzick-1 (HYP date, only) and two antler rods	OxA-X-2739-54; OxA-35,731; OxA-35,732; OxA-X-2734-19; OxA-X-2739-55; OxA-35,733; OxA-35,781; OxA-X-2734-20; OxA-X-2739-56	df=8 T=27.422 (5% 15.5)
SR-8151, SR-7599, & SR-7602	Anzick-1 (HYP date, only) and two antler rods (HYP dates, only)	OxA-X-2739-54; OxA-X-2739-55; OxA-X-2739-56	df=2 T=3.358 (5% 5.991)

Table 3. Data for four Oxford-obtained paired dates (two measurements obtained on the same sample) with differing C:N values, prepared using the same pretreatment protocol (P-code) as this study (10). The dates have not been corrected for HPLC background carbon, per Devièse et al. (10). Calibration was done using the OxCal 4.3 software (6) and the IntCal13 calibration curve (7). For the χ^2 test results, the degrees of freedom are given by df and the χ^2 value calculated by T. Noted inside the brackets is the confidence level (at 5%) followed by the critical value of the χ^2 distribution. This value denotes the level above which T should not rise for the dates to be considered in good agreement or comparable. Results show that although C:N values differ for the same sample, radiocarbon dates obtained are not widely disparate from one another.

Sample number	**Sub-sample**	**P-code**	**C:N**	**Date (BP)**	**±**	**cal BP (95.4% confidence range)**	**χ^2 test results**
1	a	NRC-02 (HYP)	5.2	11,360	50	13,300-13,090	df=1 T=5.645 (5%3.8)
	b	NRC-02 (HYP)	4.9	11,520	45	13,455-13,275	
2	a	NRC-02 (HYP)	5.3	11,190	50	13,160-12,930	df=1 T=0.6 (5%3.8)
	b	NRC-02 (HYP)	4.9	11,245	50	13,220-13,025	
3	a	NRC-02 (HYP)	5.3	10,920	50	12,915-12,700	df=1 T=3.1 (5%3.8)
	b	NRC-02 (HYP)	5.0	11,045	50	13,055-12,770	
4	a	NRC-02 (HYP)	5.7	10,915	50	12,905-12,695	df=1 T=10.576 (5%3.8)
	b	NRC-02 (HYP)	5.0	11,145	50	13,110-12,850	

References

1. Stafford TW, Jull AJT, Brendel K, Duhamel RC, Donahue D (1987) Study of Bone Radiocarbon Dating Accuracy at the University of Arizona NSF Accelerator Facility for Radioisotope Analysis. *Radiocarbon* 29(1):24–44.
2. Stafford TW, Hare PE, Currie L, Jull AJT, Donahue DJ (1991) Accelerator radiocarbon dating at the molecular level. *J Archaeol Sci* 18(1):35–72.
3. Morrow JE, Fiedel S (2006) New radiocarbon dates for the Clovis component of the Anzick Site, Park County, Montana. *Paleoindian Archaeology: A Hemispheric Perspective*, eds Morrow JE, Gnecco C (University Press of Florida), pp 123–138.
4. Waters MR, Stafford TW Jr (2007) Redefining the age of Clovis: implications for the peopling of the Americas. *Science* 315(5815):1122–1126.
5. Rasmussen M, et al. (2014) The genome of a Late Pleistocene human from a Clovis burial site in western Montana. *Nature* 506(7487):225–229.
6. Ramsey CB (2009) Bayesian Analysis of Radiocarbon Dates. *Radiocarbon* 51(1):337–360.
7. Reimer PJ, et al. (2013) IntCal13 and Marine13 Radiocarbon Age Calibration Curves 0–50,000 Years cal BP. *Radiocarbon* 55(4):1869–1887.
8. Ward GK, Wilson SR (1978) Procedures for comparing and combining radiocarbon age determinations: a critique. *Archaeometry* 20(1):19–31.
9. Ramsey CB (2018) OxCal Analysis. *OxCal 43 Manual*. Available at: http://c14.arch.ox.ac.uk/oxcalhelp/hlp_analysis.html [Accessed April 30, 2018].
10. Deviese T, Comeskey D, McCullagh J, Ramsey CB, Higham T (2017) New protocol for compound specific radiocarbon analysis of archaeological bones. *Rapid Commun Mass Spectrom* 32:373–379.

IV. Article 2: The timing and impact of the earliest human arrivals in North America

Accepted for review on 21/10/19, as below.

Becerra-Valdivia, L. & Higham, T., The timing and impact of the earliest human arrivals in North America. *Nature*.

4.1. Main text

The timing and impact of the earliest human arrivals in North America

Summary

The peopling of the Americas, during the Pleistocene-Holocene transition, marks a major event in the expansion of humans across the planet. Questions associated with this dispersal remain largely unanswered, however, since the previously accepted model, "Clovis-first", was effectively refuted. Considering the variable of *time* to be fundamental in the study of human dispersal, we analyze chronometric data from 41 North American and Beringian archaeological sites using a Bayesian age modelling approach. This allows us to create a chronological framework with which to elucidate spatio-temporal patterns and frame current genetic and climatic evidence. The data obtained indicate that although widespread occupation began during a period of abrupt warming, Greenland Interstadial 1 (~14.7-12.9 ka b2k)[1], humans were already present during or immediately after the Last Glacial Maximum (LGM; ~26.5-19 ka)[2,3]. This, in turn, suggests that the earliest arrivals to mid-latitude North America were humans from eastern Asia, who most likely crossed near the end of the LGM. In addition, we identify the synchronous commencement of Beringian, Clovis and Western Stemmed cultural traditions, and an overlap of each with the last appearance dates for 18 extinct faunal genera. This suggests that the widespread expansion of humans through North America was a key factor in the extinction of large terrestrial mammals occurring at the time.

Main Text

Until recently, the prevailing paradigm for initial human dispersal held that the first Americans were big-game hunters who first entered the continent ~13 thousand years ago from Asia via Beringia, moving southwards through an ice-free corridor between the Laurentide and

Cordilleran Ice Sheets (LIS and CIS). Once below the 48th parallel (N), it was suggested that they developed a material tradition named "Clovis"—dated to between 13,250-12,800 years before 1950 (cal BP)[4]—which spread across North America. This narrative, known as the 'Clovis-first' model, was widely accepted for most of the 20th century as it effectively answered every question associated with the peopling of the Americas—when, why, by whom, and from where[5]. The Clovis-first model has been refuted, however. New archaeo-chronometric data provide evidence for; i) sites that predate Clovis [often termed "pre-Clovis" or "other-than-Clovis"[6,7] (but see ref[8] for different terminology)][7,9–22], and; ii) distinct technological industries that occur coevally[23–28]. Currently, an earlier route along the Pacific Coast is considered most tenable[29–32] (but see ref[33]).

To understand the pattern of initial human dispersals, we have analyzed chronometric data from North America and Beringia using statistical methods on the OxCal 4.3 platform[34,35]. The results enable us to propose a new, chronology-centred model for the peopling of North America. High-precision chronometric models were built using Bayesian statistics and archaeo-chronometric information from 41 archaeological sites (see Supplementary Information; Table S1). This approach, known as Bayesian age modeling, enables the incorporation of scientific dates with stratigraphic and other relative age information (see Methods). The 39 archaeological sites comprise multiple or single cultural components that fall, according to the literature, within one of three technological traditions (Clovis, Western Stemmed, and Beringian; see Supplementary Information) or, as here defined, two exclusively temporal categories (pre-Clovis and 'Clovis-coeval'; Fig. 1). Probability density functions (PDFs) corresponding with temporal start boundaries or age estimates for each site and tradition were generated (see Methods and Supplementary Information, section 2; Table S2), and are reported below at a 95.4% confidence interval. Kernel density estimate (KDE) methods, which estimate the underlying distribution of a

dataset, were used to visualise the spatial and temporal distribution of the chronometric data (see Methods). To place our results in the context of past climatic changes, particularly the period comprising the Greenland Interstadial 1 (GI-1) and Greenland Stadial 1 (GS-1)—beginning at ~14.7 ka b2k (thousand years before AD 2000) and ending at ~11.7 ka b2k[1]—the Greenland ice core chronology (GICC05)[36] was used (see Figs. 2-3). Although GICC05 and the current radiocarbon dating calibration curve (IntCal13[37]) are not synchronous, between 14,000 and 11,000 years before present (AD 1950), the estimated offset is less than ~50 years[38]. Given the temporal resolution of this study (millennial), the effect of this offset is negligible.

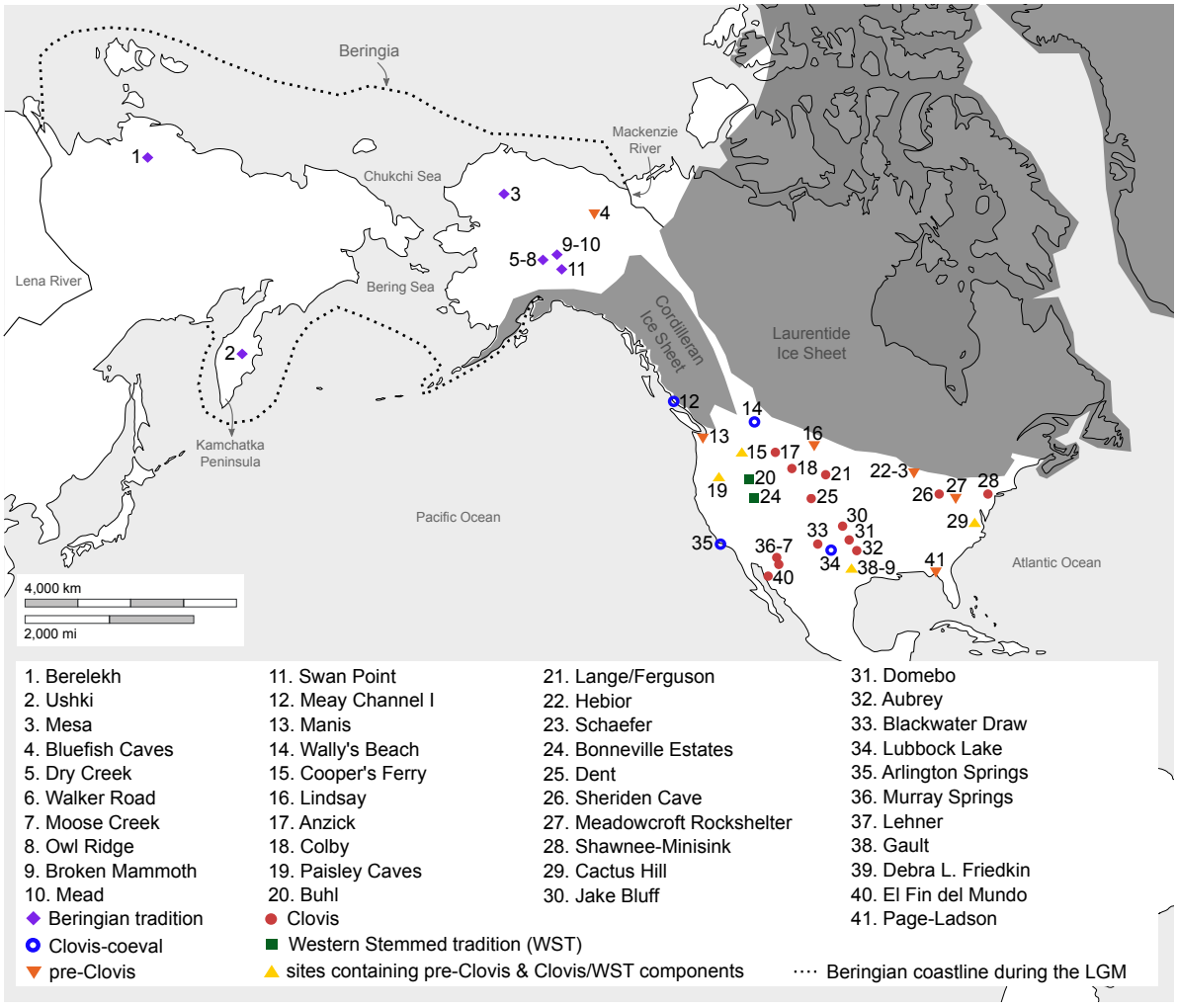


Fig. 1 | Map showing the location of the 41 archaeological sites included in this study. The extent of the ice-free corridor at 12,500 cal BP is according to ref[39], and the Beringian coastline during the LGM approximated from ref[40].

Start boundaries for pre-Clovis sites suggest that cultural occupations at Gault (Texas; 26,435-17,385 cal BP), Meadowcroft Rockshelter (Pennsylvania; 24,335-18,620 cal BP) and Cactus Hill (Virginia; 20,585-18,970 cal BP) began during, or immediately after, the Last Glacial Maximum (LGM; 26,500 to 20-19,000 years ago[2,3]) (Fig. 2a). In eastern Beringia, Bluefish Caves is represented by a single date obtained on a human-modified bone sample (24,035-23,310 cal BP; [41]), dating squarely to the LGM. Start boundaries for Cooper's Ferry (Idaho; 16,560-15,285 cal BP) and Debra L. Friedkin (Texas; 16,315-14,660 cal BP) suggest occupations at these sites began later, after the LGM and near GI-1. Following these, age estimates for Page-Ladson (Florida; 16,985-14,375 cal BP; see Supplementary Materials section 2.4.10 regarding the distribution's multimodality), Hebior (Wisconsin; 15,615-13975 cal BP), Schaefer (Wisconsin; 15,020-13,710 cal BP); Paisley Caves (Oregon; 14,755-13,780 cal BP), Lindsay (Montana; 14,625-13,945 cal BP) and Manis (Washington; 13,795-13,745 cal BP) fall within or near the GI-1. Chronometric data (n=162) from these twelve pre-Clovis components yielded a distribution with one main peak culminating at ~15-14,000 cal BP, which represents the bulk of chronometric data (Fig. 2b). For later traditions—Beringian, Western Stemmed and Clovis—start boundaries obtained suggest these began at 14,910-13,395 cal BP, 14,860-13,065 BP cal BP and 14,210-13,495 cal BP, respectively (Fig. 3; Extended Data Figs. 1-3). Of these, the estimate for Clovis is most robust due to sample size (n=16) and the constraint provided in the model by preceding dates in three of the archaeological sites included (Gault, Cactus Hill and Debra L. Friedkin).

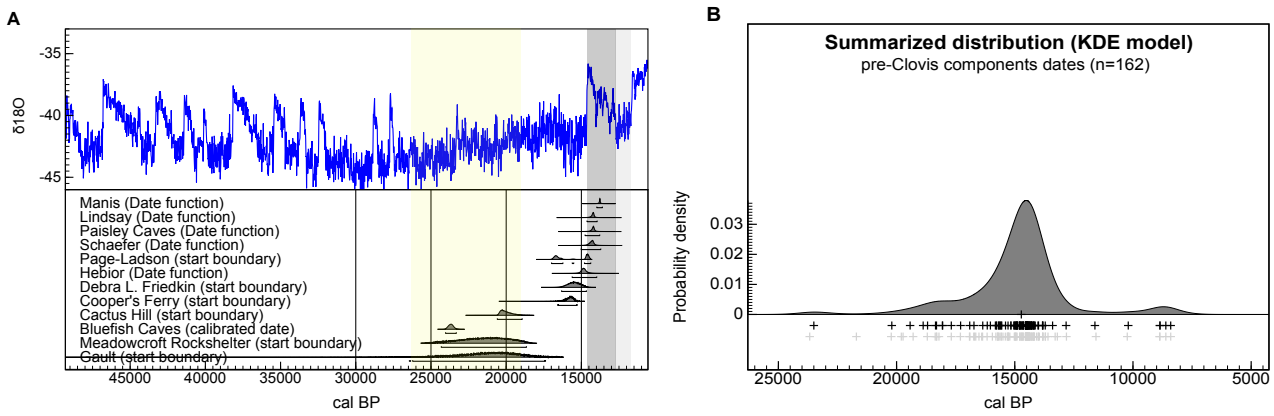


Fig. 2 | (A) Start boundaries or age estimates for twelve pre-Clovis sites/components and (B) a summarized distribution of chronometric data (i.e., dates; n=162) within these. In (**A**), the LGM span is according to ref[42] and is noted with a yellow band, whilst GI-1 (dark gray band) and GS-1 (light gray band) follow ref[1]. $\delta^{18}O$ data according to the Greenland ice core timescale (GICC05)[36]. Brackets beneath each age estimate show 95.4% confidence intervals. In (**B**), the light gray crosses show the medians of the likelihood distributions of the calibrated dates, whilst the black crosses show the medians of the marginal posterior distributions for each event from the KDE model analysis. Within this distribution, data are concentrated around a single peak at ~15-14,000 cal BP. Results suggest that humans were initially present in North America during or immediately after the LGM.

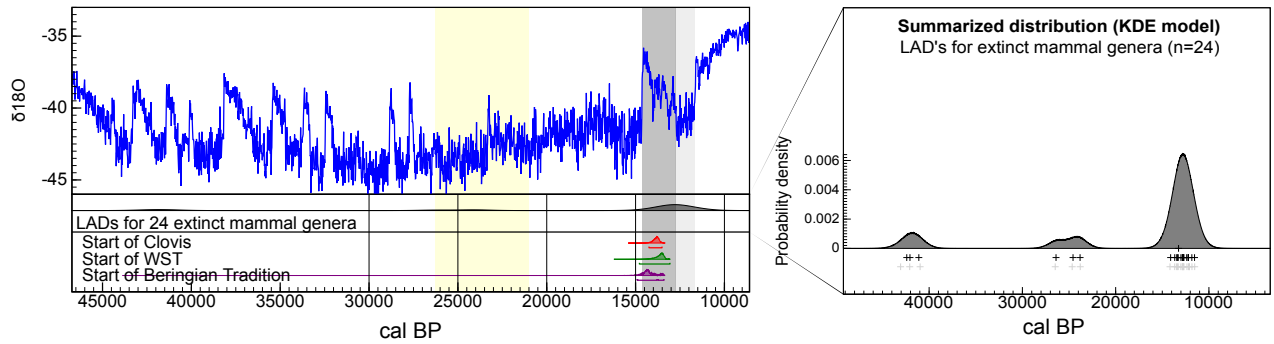


Fig. 3 | Start boundaries for Clovis, Western Stemmed and Beringian traditions, and a summarized distribution of last appearance dates (LADs) for 24 extinct mammal genera in North America. The LGM span is according to ref[42] and is noted with a yellow band, whilst GI-1 (dark gray band) and GS-1 (light gray band) follows ref[1]. $\delta^{18}O$ data according to the

Greenland ice core timescale (GICC05)[36]. Brackets beneath each age estimate show 95.4% confidence intervals. In the summarized distribution pane, the light gray crosses show the medians of the likelihood distributions of the calibrated dates, whilst the black crosses show the medians of the marginal posterior distributions for each event from the KDE model analysis. LAD data entered as compiled in ref[43]. Results suggest that the onset of the three traditions largely coincide with GI-1, a globally warmer period of drastic, short-lived climate changes[1]. Moreover, the highest density peak for the KDE model overlaps with the start of Clovis and Western traditions and coincides with the GI-1/GS-1 interface. This suggests that human expansion was strongly involved in North American Pleistocene extinctions.

The analysis shows that the earliest archaeological sequences in North America—Bluefish Caves, Gault, Meadowcroft and Cactus Hill—begin during, or immediately after, the LGM and, south of the 48th parallel (N), concentrate in the east (Fig. 1; Fig 4a-b). Whilst global climate was generally cooler and drier during the LGM, areas south of the North American ice sheets were relatively open and temperate[44–46], with evidence for high hydrological and ecological variability[47–52]. The distribution of early mid-latitude sites caught the attention of Solutrean Hypothesis advocates, who argue that North America was originally colonised by southwestern Europeans arriving via a transatlantic ice-corridor during the LGM[53–55]. The connection to Europe lies in purported typological and manufacturing similarities between Solutrean (appearing ~25-24,000 cal BP[56,57]) and Clovis technology, as well as evidence for pre-Columbian West Eurasian admixture. This hypothesis, however, is often rejected on technological and genetic grounds[42,58–60]. If transatlantic migration is discarded and an Asian origin assumed, the antiquity and distribution of these sites suggest that the initial crossing of the 48th parallel (N) occurred during Marine Isotope Stage (MIS) 3[61], when ice and sea level estimates[62–64] for this period indicate that land passage through Beringia was unlikely or interrupted, and an ice-free

corridor between LIS and CIS was probably present[64] (with evidence of terrestrial landscapes occurring 48-40 ka[65]), or the LGM terminus, when the Bering land bridge was viable but the ice-free corridor inacessible. This would have necessitated movement along the Pacific Coast, perhaps before the CIS reached maximum extent (~20-17 ka [66]). Both options suggest the earliest arrivals to North America had some degree of littoral adaptation, yet the latter is more compatible with current genetic findings, which suggest that ancestral Native Americans experienced genetic isolation in eastern Beringia during the LGM[67]—supported by LGM-dated human presence at Bluefish Caves[41] (but see refs[33,68])—and diverged from Ancient Beringians, descendants of the same founding population, at 22-18.1 ka[69,70]. This assumes the pre-Clovis occupants of Gault, Meadowcroft and Cactus Hill were of Native American ancestry. Once in mid-latitude North America, the paucity (n=11), distribution (Fig. 1) and characteristics of pre-Clovis evidence suggest that humans had unique adaptational behaviours and were spread widely, seemingly leaving little trace. Lithic industries at Gault, Meadowcroft and Cactus Hill, for example, are largely unrelated[6] (but see ref[71]).

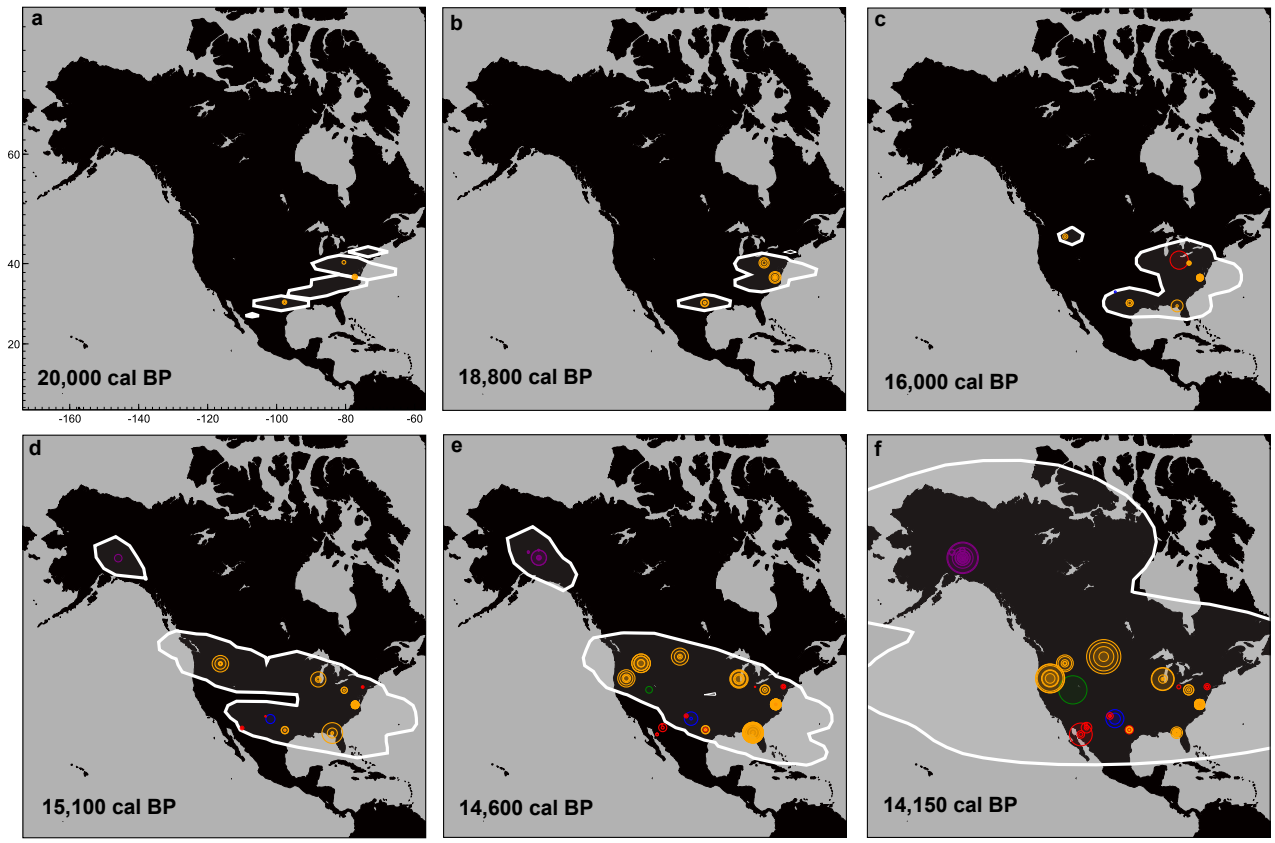


Fig. 4 | Spatio-temporal slices (a-f) of chronometric data (colored circles; i.e., dates; n=364) belonging to the cultural components analyzed, with a KDE analysis (white outlines). Chronometric data was summarized using a 'KDE_Model' analysis (see Methods). For each date, differences in circle size reflect increasing/decreasing probabilities at a 95.4% confidence interval and follow the color scheme in Fig. 1. The KDE analysis shows a marked increase in the frequency and distribution of the data immediately, before and during GI-1.

Bayesian age modelling shows that the start dates of the Beringian, Western Stemmed and Clovis traditions are statistically indistinguishable and occur synchronously, coinciding with GI-1 (Fig. 2)—a warmer period of sudden, short-lived climate changes[1]—and a peak in modelled chronometric data (Fig. 4d-f). Moreover, these likely follow a split of the ancestral Native American lineage into two branches[69,72–75], "Southern Native American" (SNA) and "Northern Native American" (NNA)[70], around 17.5-14.6 ka[70]. This probably occurs outside of Eastern Beringia and south of the North American ice sheets[69,70,72].

Technologically, the relationship between pre-Clovis and Clovis is uncertain[6], whilst the Western Stemmed tradition has been linked with multiple pre-Clovis[20,21,31] and circum-Pacific sites[8,30] due to perceived similarities in stemmed point technologies. Recently, however, the Debra L. Friedkin site was proposed to evidence the progression from stemmed to fluted (Clovis) technology, with a triangular lanceolate point noted as a possible link between the two[21]. Genetically, the connection between pre-Clovis populations and the makers of Clovis and Western Stemmed traditions requires further research. This is because, with the exception of the pre-Clovis component at Paisley Caves, where mitochondrial DNA data corresponds to Native American founding haplogroups[17], and Anzick, a burial site representing Clovis and the SNA lineage[73], genetic information from other Clovis-coeval or pre-Clovis archaeological sites has yet to be obtained. It is most likely, however, that these and the initial arrivals are related. Otherwise, a minimum of two Pleistocene-aged migrations should be expected. Given our results, a later dispersal would most likely predate GI-1 and estimates for the earliest bioavailability of the ice-free corridor, at ~13,000 cal BP[76,77], perhaps occurring after the western retreat of the CIS ~18-17 ka[66,78,79] and the Alaska Peninsula Glacier Complex ~17 ka, as well as the likely establishment of productive ecosystems in the North Pacific coast ~17 ka[66].

Human arrival in North America has been previously cited as causing the extinction of 37 faunal genera, i.e., the overkill hypothesis popularized by P. Martin[80–82]. Depending on the analysis, more recent studies are either in support[83] or suggest other factors, such as climate, ecological change and an extraterrestrial impact, as main or joint contributors[84–91]. Our results show that human presence in the continent precedes the majority of last appearance dates (LADs) for extinct genera in North America[43]. When these are summarized in a probability density distribution, the highest peak (containing 18 of the 24 dates included) occurs during the GI-1/

GS-1 boundary and overlaps with the start boundaries obtained for Clovis and Western Stemmed traditions (Fig. 3). This raises the distinct possibility that widespread human expansion was a key factor in the extinction of large terrestrial mammals, likely exacerbated by climate change. Further work, however, is required to better understand the relationship between human arrival, faunal extinctions, and climate change. In extinction research, this includes the definition of demographic histories for each extinct genus and species, increased chronometric data, and the application of a Bayesian approach in chronology building (see ref[92]). Results from the latter would allow formal integration with those in this study and their joint, quantitative analysis.

Using statistical modeling and current archaeo-chronometric records, we have focused on the timing of the initial human dispersals into Beringia and North America. Results suggest that humans were probably present in different settings during or immediately following the LGM, before the commencement of widespread occupation during GI-1. If population continuity is assumed, this pattern is consistent with phases of human exploration and colonization, and the degree of genetic structure already present in North America by GI-1. The bio-cultural relationship between humans represented by pre-Clovis sites and later North American and Beringian traditions, however, is largely unknown. Further research, including the extraction of ancient human DNA from sediments[93], has the potential to increase our knowledge and elucidate these questions. Finally, although this study focused on Beringia and North America, continued investigations in Central and South America—for which Late Pleistocene data is comparatively limited[94–101]—should allow for the chronological assessment of local archaeological sites[7,10,11,23,27,28,102–111] and the development of continent-wide spatio-temporal models. In this sense, future research in the First Americans field will undoubtedly test the chronological model here proposed, improving its precision and accuracy if new data is periodically assessed and integrated.

Methods

Previously published archaeo-chronometric data for 41 archaeological sites (see Supplementary Text, section 2; Table S1) were used to construct site- and tradition-level models using OxCal 4.3, a Bayesian modeling software[35], and the IntCal13 calibration curve[37]. In OxCal, models are built using Chronological Query Language (CQL), which is identified here in Courier New font.

Bayesian age modeling and OxCal

Bayesian age modeling is a statistical tool that enables the analysis of chronometric data (standardized likelihoods) in the context of existing, pertinent knowledge (prior), and the results obtained (posterior). Priors can involve absolute, e.g., historical accounts, or relative information, e.g., stratigraphy[112]. Results are expressed as probability density functions (PDFs) through the use of a random sampling technique, Markov Chain Monte Carlo (MCMC), that utilizes the Metropolis-Hastings algorithm and the Gibbs sampler[113,114]. The program is set to do 30,000 iterations, with convergence checked every 3,000 (a "pass") and new starting points at every 6,000. If convergence is less than 95%, the pass interval is increased by a factor of two until convergence is satisfactory. As preset, PDFs are quoted as age ranges including the 68.2, 95.4 or 99.7% most likely results based on the prior (the highest posterior density range). In plots, these are identifiable over individual calibrated radiocarbon likelihoods or non-radiocarbon measurements as a darker distribution. Bayesian age modeling assumes that time can be divided into units and treats archaeological events as groups defined by start and end boundaries. In this sense, a group can be incorporated into OxCal as a `Phase` within a `Sequence` constrained by two `Boundary` commands. A `Phase` contains a group with unrelated, unordered items, whilst those in a `Sequence` follow an order. The type of group can be defined by the type of boundary used (`Boundary`, `Zero_Boundary`, `Tau_Boundary` or `Sigma_Boundary`) and the distribution

each denotes—uniform, ramped, exponential or normal (Figure 4 in ref[35]). A `Boundary` at the start and end of a group, for example, defines a uniform phase and assumes that all events included are equally likely to occur anywhere within the two boundaries. If included, outlier analysis [`Outlier_Model()` and `Outlier()`] can be used to address the assumption that all dates are correct. This defines the distribution and scale of outliers, and assigns each date a prior probability of being an outlier. The general t-type model, for example, draws outliers from a Student's t-distribution with 5 degrees of freedom to account for extreme outliers, and sets the scale of offset to range widely, between 10^0 to 10^4 years[115]. The analysis then identifies outliers by assessing the fit of chronometric data within the prior framework, and down-weights them automatically according to their degree of offset. This approach is more objective than manual exclusion of dates and has a similar output (Fig. 9 in ref[115]). In archaeology, outlier analysis can be used to assess agreement between chronometric data and stratigraphic evidence, often yielding important information regarding site-specific processes, e.g., geological unconformity or bioturbation.

Model construction

Archaeological sites with dated stratified sequences were incorporated into single or multiple uniform phases, and start boundaries were used as temporal markers of human presence (see Supplementary Information, section 2). Unstratified sites containing roughly synchronous archaeological events—directly dated human burials with associated (dated) artifacts or faunal remains subjected to human predation—were included in a single, uniform `Phase`, and a `Date` function was used to provide an age estimate. For these, if applicable and available, only the latest bone collagen dates obtained through XAD[121,122] or HYP[123] protocols were used—recent studies show these to provide more reliable measurements, particularly for contaminated bone[4,16,124,125]. If these sites were best or solely represented by a single measurement, a calibrated date was employed. All modelled dates were assigned a 0.05 probability of being an outlier and the general t-type model

was used (using the same parameters noted above). We relied on outlier analysis to objectively identify and down-weight outliers within the models. Following these methods, site-specific age estimates (start boundaries, `Date` functions, or calibrated dates) were obtained for all archaeological sites (Supplementary Information, Table S2). Where appropriate, these were incorporated into uniform phases to build tradition-level models and PDFs for the start of Beringian, Western Stemmed and Clovis traditions were obtained (Extended Data Figs. 1-3). This allowed for the comparison of different traditions spatio-temporally, as informed by the statistical assessment of individual archaeological sequences. To visualize the temporal and/or spatial distribution of chronometric data, KDE methods were applied using the `KDE_Model` command (using default parameters noted above; in Figs. 2-4) and the 'Toggle KDE' option within map view (in Fig. 4). All age estimates are noted to 95.4% confidence interval (a standard width), unless otherwise specified, and rounded to five years (following a convention explained in ref[126]).

Data availability The data that support the findings of this study are available from the main text or Supplementary Information.

Acknowledgements Without implying their agreement with the content of this article, we thank Eileen Jacob (Oxford), Gorav Wali (Oxford), Jaime Swift (Oxford), Christopher Bronk Ramsey (Oxford), Julia Lee-Thorp (Oxford), Kelly Graf (Texas A&M) and Katerina Douka (MPI-SHH, Jena) for feedback on early versions of the manuscript. Funding was provided by the Clarendon Fund Scholarship, University of Oxford.

Author contributions L.B-V compiled and analyzed all data, built Bayesian age models and, with contribution from T.H., wrote the manuscript.

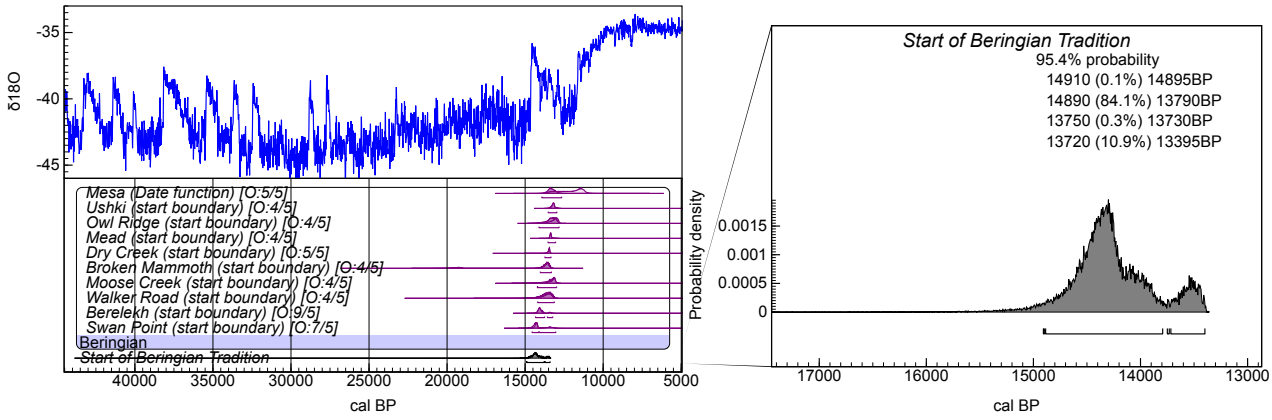
Competing interests The authors declare no competing interests.

Additional information

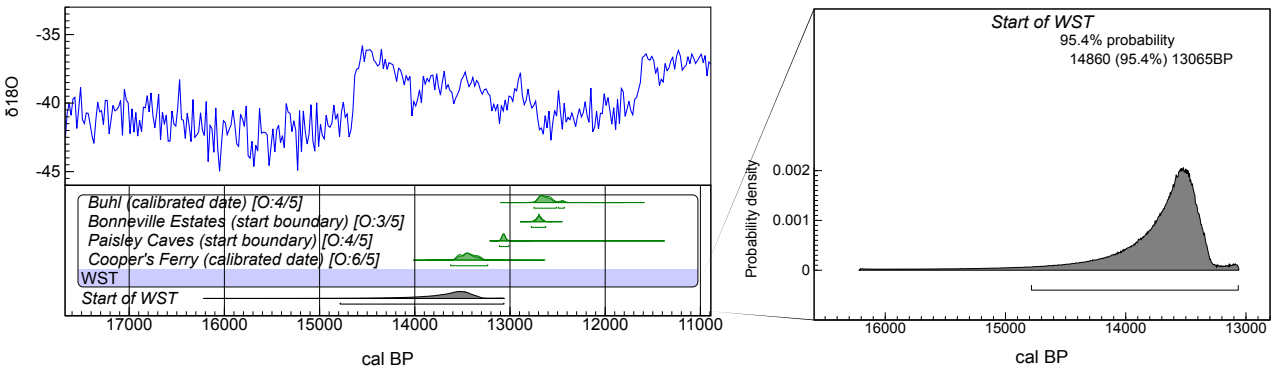
Supplementary Information is available for this paper.

Correspondence and requests for materials should be addressed to L.B-V. (lorena.becerravaldivia@arch.ox.ac.uk)

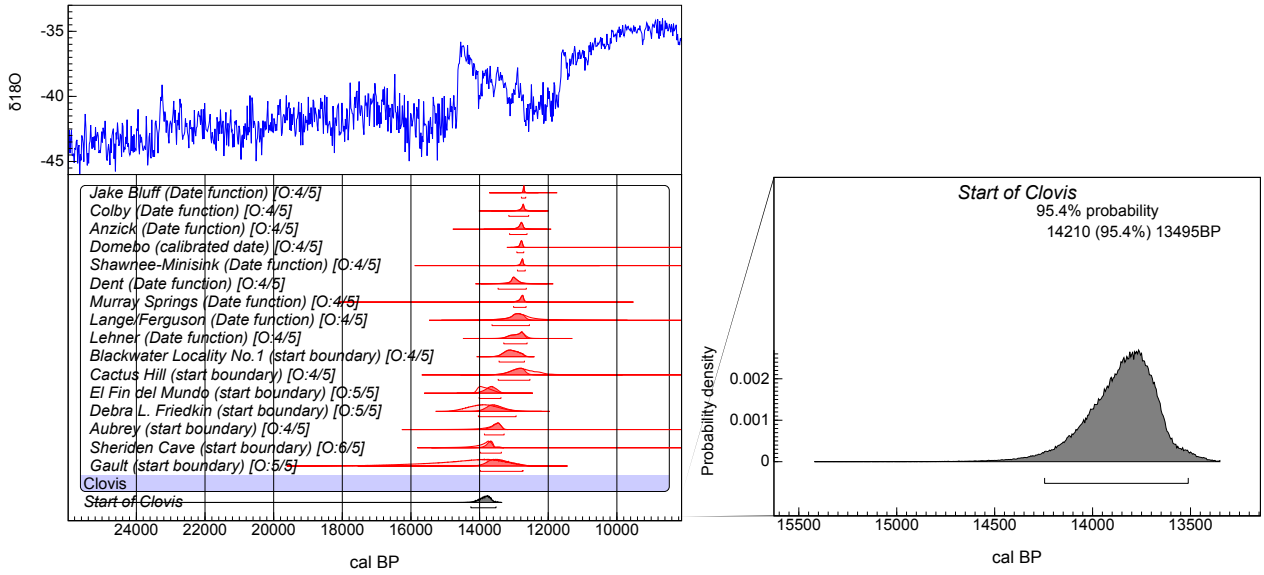
Reprints and permissions information is available at http://www.nature.com/reprints.



Extended Data Fig. 1 | Bayesian age model and start boundary for the Beringian tradition (14,910-13,395 cal BP). Outlier analysis output is noted as 'O:posterior probability/prior probability'. $\delta^{18}O$ data according to the Greenland ice core timescale (GICC05)[39].



Extended Data Fig. 2 | Bayesian age model and start boundary for the Western Stemmed tradition (14,860-13,065 cal BP). Outlier analysis output is noted as 'O:posterior probability/prior probability'. $\delta^{18}O$ data according to the Greenland ice core timescale (GICC05)[39].



Extended Data Fig. 3 | Bayesian age model and start boundary for the Clovis tradition (14,210-13,495 cal BP). Outlier analysis output is noted as 'O:posterior probability/prior probability'. $\delta^{18}O$ data according to the Greenland ice core timescale (GICC05)[39].

References

1. Rasmussen, S. O. *et al.* A stratigraphic framework for abrupt climatic changes during the Last Glacial period based on three synchronized Greenland ice-core records: refining and extending the INTIMATE event stratigraphy. *Quat. Sci. Rev.* **106**, 14–28 (2014).
2. Mix, A. C., Bard, E. & Schneider, R. Environmental processes of the ice age: land, oceans, glaciers (EPILOG). *Quat. Sci. Rev.* **20**, 627–657 (2001).
3. Clark, P. U. *et al.* The Last Glacial Maximum. *Science* **325**, 710–714 (2009).
4. Waters, M. R. & Stafford, T. W., Jr. Redefining the age of Clovis: implications for the peopling of the Americas. *Science* **315**, 1122–1126 (2007).
5. Meltzer, D. J. *The Great Paleolithic War: How Science Forged an Understanding of America's Ice Age Past*. (University of Chicago Press, 2015).
6. Haynes, G. The Millennium before Clovis. *PaleoAmerica* **1**, 134–162 (2015).

7. Dillehay, T. D. *Monte Verde, a Late Pleistocene Settlement in Chile: The archaeological context and interpretation*. (Smithsonian Institution Press, 1997).

8. Williams, T. J. & Madsen, D. B. The Upper Paleolithic of the Americas. *PaleoAmerica* 1–19 (2019).

9. Meltzer, D. J. *et al.* On the Pleistocene Antiquity of Monte Verde, Southern Chile. *Am. Antiq.* **62**, 659–663 (1997).

10. Dillehay, T. D. *et al.* Simple technologies and diverse food strategies of the Late Pleistocene and Early Holocene at Huaca Prieta, Coastal Peru. *Sci Adv* **3**, e1602778 (2017).

11. Dillehay, T. D. *et al.* A late pleistocene human presence at Huaca Prieta, Peru, and early Pacific Coastal adaptations. *Quat. Res.* **77**, 418–423 (2012).

12. Davis, L. G. *et al.* Late Upper Paleolithic occupation at Cooper's Ferry, Idaho, USA, ~16,000 years ago. *Science* **365**, 891–897 (2019).

13. Waters, M. R. *et al.* Pre-Clovis Mastodon Hunting 13,800 Years Ago at the Manis Site, Washington. *Science* **334**, 351–353 (2011).

14. Hill, C. L. & Davis, L. B. Stratigraphy, AMS radiocarbon age, and stable isotope biogeochemistry of the Lindsay Mammoth, eastern Montana. *Current Research in the Pleistocene* **15**, 109–112 (1998).

15. Davis, L. B. & Wilson, M. C. The late Pleistocene Lindsay mammoth (24DW501), eastern Montana: Possible man-mammoth association. *Current Research in the Pleistocene* **2**, 97–98 (1985).

16. Devièse, T. *et al.* Increasing accuracy for the radiocarbon dating of sites occupied by the first Americans. *Quaternary Science Research* **198**, 171–180 (2018).

17. Gilbert, M. T. P. *et al.* DNA from pre-Clovis human coprolites in Oregon, North America. *Science* **320**, 786–789 (2008).

18. Halligan, J. J. *et al.* Pre-Clovis occupation 14,550 years ago at the Page-Ladson site, Florida, and the peopling of the Americas. *Sci Adv* **2**, e1600375 (2016).

19. Feathers, J. K., Rhodes, E. J., Huot, S. & Mcavoy, J. M. Luminescence dating of sand deposits related to late Pleistocene human occupation at the Cactus Hill Site, Virginia, USA. *Quat. Geochronol.* **1**, 167–187 (2006/8).

20. Williams, T. J. *et al.* Evidence of an early projectile point technology in North America at the Gault Site, Texas, USA. *Sci Adv* **4**, eaar5954 (2018).

21. Waters, M. R. *et al.* Pre-Clovis projectile points at the Debra L. Friedkin site, Texas—Implications for the Late Pleistocene peopling of the Americas. *Science Advances* **4**, eaat4505 (2018).

22. Adovasio, J. M., Donahue, J. & Stuckenrath, R. The Meadowcroft Rockshelter Radiocarbon Chronology 1975-1990. *Am. Antiq.* **55**, 348–354 (1990).

23. Sandweiss, D. H. *et al.* Quebrada jaguay: early south american maritime adaptations. *Science* **281**, 1830–1832 (1998).

24. Goebel, T. & Keene, J. L. Are Great Basin stemmed points as old as Clovis in the Intermountain West? A review of the geochronological evidence. *Archaeology in the Great Basin and Southwest: Papers in Honor of Don D. Fowler* 35–60 (2014).

25. Méndez, C., Jackson, D., Seguel, R. & Delaunay, A. N. Early high-quality lithic procurement in the semiarid north of Chile. *Current Research in the Pleistocene* **27**, 19–21 (2010).

26. Méndez, C. & Jackson, D. Terminal Pleistocene lithic technology and use of space in Central Chile. *Chungara, Revista de Antropología Chilena* (2015).

27. Jones, K. B., Hodgins, G. W. L. & Sandweiss, D. H. Radiocarbon Chronometry of Site QJ-280, Quebrada Jaguay, a Terminal Pleistocene to Early Holocene Fishing Site in Southern Peru. *The Journal of Island and Coastal Archaeology* 1–19 (2017).

28. Roosevelt, A. C. *et al.* Paleoindian Cave Dwellers in the Amazon: The Peopling of the Americas. *Science* **272**, 373–384 (1996).

29. Erlandson, J. M. *et al.* The Kelp Highway Hypothesis: Marine Ecology, the Coastal Migration Theory, and the Peopling of the Americas. *The Journal of Island and Coastal Archaeology* **2**, 161–174 (2007).

30. Erlandson, J. M. & Braje, T. J. From Asia to the Americas by boat? Paleogeography, paleoecology, and stemmed points of the northwest Pacific. *Quat. Int.* **239**, 28–37 (2011).

31. Davis, L. G. *et al.* Late Upper Paleolithic Occupation at Cooper's Ferry, Idaho, USA Shows Americas Settled Before ~16,000 Years Ago. *Science* (2019).

32. Braje, T. J., Dillehay, T. D., Erlandson, J. M., Klein, R. G. & Rick, T. C. Finding the first Americans. *Science* **358**, 592–594 (2017).

33. Potter, B. A. *et al.* Current evidence allows multiple models for the peopling of the Americas. *Sci Adv* **4**, eaat5473 (2018).

34. Bronk Ramsey, C. Development of the radiocarbon program OxCal. *Radiocarbon* **43**, 355–363 (2001).

35. Bronk Ramsey, C. Bayesian Analysis of Radiocarbon Dates. *Radiocarbon* **51**, 337–360 (2009).

36. Rasmussen, S. O. *et al.* A new Greenland ice core chronology for the last glacial termination. *J. Geophys. Res.* **111**, 527 (2006).

37. Reimer, P. J. *et al.* IntCal13 and Marine13 Radiocarbon Age Calibration Curves 0–50,000 Years cal BP. *Radiocarbon* **55**, 1869–1887 (2013).

38. Adolphi, F. *et al.* Connecting the Greenland ice-core and U/ Th timescales via cosmogenic radionuclides: testing the synchroneity of Dansgaard--Oeschger events. *Clim. Past* **14**, (2018).

39. Dyke, A. S. An outline of North American deglaciation with emphasis on central and northern Canada. *Developments in Quaternary Sciences* **2**, 373–424 (2004).

40. Bond, J. D. Paleodrainage map of Beringia. (2019).

41. Bourgeon, L., Burke, A. & Higham, T. Earliest Human Presence in North America Dated to the Last Glacial Maximum: New Radiocarbon Dates from Bluefish Caves, Canada. *PLoS One* **12**, e0169486 (2017).

42. Clark, G. A. Deconstructing the North Atlantic Connection. *The Settlement of the American Continents* 103–112 (2004).

43. Grayson, D. K. & Meltzer, D. J. Revisiting Paleoindian exploitation of extinct North American mammals. *J. Archaeol. Sci.* **56**, 177–193 (2015).

44. Ray, N. & Adams, J. A GIS-based vegetation map of the world at the last glacial maximum (25,000-15,000 BP). *Internet archaeology* (2001).

45. Jackson, S. T. *et al.* Vegetation and environment in Eastern North America during the Last Glacial Maximum. *Quat. Sci. Rev.* **19**, 489–508 (2000).

46. Williams, J. W. Variations in tree cover in North America since the last glacial maximum. *Glob. Planet. Change* **35**, 1–23 (2003).

47. Lyle, M. *et al.* Out of the tropics: the Pacific, Great Basin lakes, and late Pleistocene water cycle in the western United States. *Science* **337**, 1629–1633 (2012).

48. Goebel, T., Hockett, B., Adams, K. D., Rhode, D. & Graf, K. Climate, environment, and humans in North America's Great Basin during the Younger Dryas, 12,900–11,600 calendar years ago. *Quat. Int.* **242**, 479–501 (2011).

49. Menking, K. M., Anderson, R. Y., Shafike, N. G., Syed, K. H. & Allen, B. D. Wetter or colder during the Last Glacial Maximum? Revisiting the pluvial lake question in southwestern North America. *Quat. Res.* **62**, 280–288 (2004).

50. Kirby, M. E. *et al.* A late Wisconsin (32--10k cal a BP) history of pluvials, droughts and vegetation in the Pacific south-west United States (Lake Elsinore, CA). *J. Quat. Sci.* **33**, 238–254 (2018).

51. Ibarra, D. E. *et al.* Warm and cold wet states in the western United States during the Pliocene–Pleistocene. *Geology* **46**, 355–358 (2018).

52. Feakins, S. J., Wu, M. S., Ponton, C. & Tierney, J. E. Biomarkers reveal abrupt switches in hydroclimate during the last glacial in southern California. *Earth Planet. Sci. Lett.* **515**, 164–172 (2019).

53. Stanford, D. J. & Bradley, B. A. *Across Atlantic Ice: The Origin of America's Clovis Culture*. (Univ of California Press, 2013).

54. Bradley, B. & Stanford, D. The North Atlantic ice-edge corridor: A possible Palaeolithic route to the New World. *World Archaeol.* **36**, 459–478 (2004).

55. Oppenheimer, S., Bradley, B. & Stanford, D. Solutrean hypothesis: genetics, the mammoth in the room. *World Archaeol.* **46**, 752–774 (2014).

56. Straus, L. G. The human occupation of southwestern Europe during the Last Glacial Maximum: Solutrean cultural adaptations in France and Iberia. *J. Anthropol. Res.* **71**, 465–492 (2015).

57. Aubry, T. & Almeida, M. Analyse critique des bases chronostratigraphiques de la structuration du Solutréen. *Le Solutréen* **40**, 37e52 (2013).

58. Straus, L. G., Meltzer, D. J. & Goebel, T. Ice Age Atlantis? Exploring the Solutrean-Clovis 'connection'. *World Archaeol.* **37**, 507–532 (2005).

59. Eren, M. I., Patten, R. J., O'Brien, M. J. & Meltzer, D. J. Refuting the technological cornerstone of the Ice-Age Atlantic crossing hypothesis. *J. Archaeol. Sci.* **40**, 2934–2941 (2013).

60. Raff, J. A. & Bolnick, D. A. Does Mitochondrial Haplogroup X Indicate Ancient Trans-Atlantic Migration to the Americas? A Critical Re-Evaluation. *PaleoAmerica* **1**, 297–304 (2015).

61. Lisiecki, L. E. & Raymo, M. E. A Pliocene-Pleistocene stack of 57 globally distributed benthic δ18O records. *Paleoceanography* **20**, (2005).

62. Spratt, R. M. & Lisiecki, L. E. A Late Pleistocene sea level stack. *Clim. Past* **12**, 1079–1092 (2016).

63. Pico, T., Mitrovica, J. X., Ferrier, K. L. & Braun, J. Global ice volume during MIS 3 inferred from a sea-level analysis of sedimentary core records in the Yellow River Delta. *Quat. Sci. Rev.* **152**, 72–79 (2016).

64. Batchelor, C. L. *et al.* The configuration of Northern Hemisphere ice sheets through the Quaternary. *Nat. Commun.* **10**, 3713 (2019).

65. Dalton, A. S., Finkelstein, S. A., Barnett, P. J. & Forman, S. L. Constraining the Late Pleistocene history of the Laurentide Ice Sheet by dating the Missinaibi Formation, Hudson Bay Lowlands, Canada. *Quat. Sci. Rev.* **146**, 288–299 (2016).

66. Lesnek, A. J., Briner, J. P., Lindqvist, C., Baichtal, J. F. & Heaton, T. H. Deglaciation of the Pacific coastal corridor directly preceded the human colonization of the Americas. *Sci Adv* **4**, eaar5040 (2018).

67. Tamm, E. *et al.* Beringian standstill and spread of Native American founders. *PLoS One* **2**, e829 (2007).

68. Graf, K. E. & Buvit, I. Human Dispersal from Siberia to Beringia: Assessing a Beringian Standstill in Light of the Archaeological Evidence. *Curr. Anthropol.* **58**, S583–S603 (2017).

69. Moreno-Mayar, J. V. *et al.* Early human dispersals within the Americas. *Science* **362**, eaav2621 (2018).

70. Moreno-Mayar, J. V. *et al.* Terminal Pleistocene Alaskan genome reveals first founding population of Native Americans. *Nature* **553**, 203–207 (2018).

71. Goodyear, A. C. Evidence of Pre-Clovis Sites in the Eastern United States. in *Paleoamerican Origins: Beyond Clovis* (eds. Bonnichesen, R., Lepper, B. T., Standford, D. & Waters, M. R.) 103–112 (2005).

72. Raghavan, M. *et al.* Genomic evidence for the Pleistocene and recent population history of Native Americans. *Science* **349**, aab3884 (2015).

73. Rasmussen, M. *et al.* The genome of a Late Pleistocene human from a Clovis burial site in western Montana. *Nature* **506**, 225–229 (2014).

74. Reich, D. *et al.* Reconstructing Native American population history. *Nature* **488**, 370–374 (2012).

75. Scheib, C. L. *et al.* Ancient human parallel lineages within North America contributed to a coastal expansion. *Science* **360**, 1024–1027 (2018).

76. Pedersen, M. W. *et al.* Postglacial viability and colonization in North America's ice-free corridor. *Nature* **537**, 45–49 (2016).

77. Heintzman, P. D. *et al.* Bison phylogeography constrains dispersal and viability of the Ice Free Corridor in western Canada. *Proc. Natl. Acad. Sci. U. S. A.* **113**, 8057–8063 (2016).

78. Darvill, C. M., Menounos, B., Goehring, B. M., Lian, O. B. & Caffee, M. W. Retreat of the western Cordilleran Ice Sheet margin during the last deglaciation. *Geophys. Res. Lett.* **45**, 9710–9720 (2018).

79. Taylor, M. A., Hendy, I. L. & Pak, D. K. Deglacial ocean warming and marine margin retreat of the Cordilleran Ice Sheet in the North Pacific Ocean. *Earth Planet. Sci. Lett.* **403**, 89–98 (2014).

80. *Pleistocene extinctions: The search for a cause*. (Yale University Press, 1967).

81. Martin, P. S. The discovery of America. *Science* **179**, 969–974 (1973).

82. Edwards, W. E. The late-Pleistocene extinction and diminution in size of many mammalian species. *Pleistocene extinctions: the search for a cause. Edited by PS Martin and HE Wright, Jr. Yale University Press, New Haven, Conn* 141–154 (1967).

83. Surovell, T. A., Pelton, S. R., Anderson-Sprecher, R. & Myers, A. D. Test of Martin's overkill hypothesis using radiocarbon dates on extinct megafauna. *Proc. Natl. Acad. Sci. U. S. A.* **113**, 886–891 (2016).

84. Robinson, G. S., Pigott Burney, L. & Burney, D. A. Landscape Paleoecology and megafaunal extinction in southwestern New York state. *Ecol. Monogr.* **75**, 295–315 (2005).

85. Guthrie, R. D. New carbon dates link climatic change with human colonization and Pleistocene extinctions. *Nature* **441**, 207–209 (2006).

86. Lorenzen, E. D. *et al.* Species-specific responses of Late Quaternary megafauna to climate and humans. *Nature* **479**, 359–364 (2011).

87. Prescott, G. W., Williams, D. R., Balmford, A., Green, R. E. & Manica, A. Quantitative global analysis of the role of climate and people in explaining late Quaternary megafaunal extinctions. *Proc. Natl. Acad. Sci. U. S. A.* **109**, 4527–4531 (2012).

88. Cooper, A. *et al.* Abrupt warming events drove Late Pleistocene Holarctic megafaunal turnover. *Science* **349**, 602–606 (2015).

89. Araujo, B. B. A., Oliveira-Santos, L. G. R., Lima-Ribeiro, M. S., Diniz-Filho, J. A. F. & Fernandez, F. A. S. Bigger kill than chill: The uneven roles of humans and climate on late Quaternary megafaunal extinctions. *Quat. Int.* **431**, 216–222 (2017).

90. Firestone, R. B. *et al.* Evidence for an extraterrestrial impact 12,900 years ago that contributed to the megafaunal extinctions and the Younger Dryas cooling. *Proceedings of the National Academy of Sciences* vol. 104 16016–16021 (2007).

91. Broughton, J. M. & Weitzel, E. M. Population reconstructions for humans and megafauna suggest mixed causes for North American Pleistocene extinctions. *Nat. Commun.* **9**, 5441 (2018).

92. Buck, C. E. & Bard, E. A calendar chronology for Pleistocene mammoth and horse extinction in North America based on Bayesian radiocarbon calibration. *Quat. Sci. Rev.* **26**, 2031–2035 (2007).

93. Slon, V. *et al.* Neandertal and Denisovan DNA from Pleistocene sediments. *Science* **356**, 605–608 (2017).

94. Bueno, L., Prates, L., Politis, G. G. & Steele, J. A Late Pleistocene/early Holocene archaeological 14C database for South America and the Isthmus of Panama: Palaeoenvironmental contexts and demographic interpretations. *Quat. Int.* 1–2 (2013).

95. Cooke, R., Ranere, A., Pearson, G. & Dickau, R. Radiocarbon chronology of early human settlement on the Isthmus of Panama (13,000–7000 BP) with comments on cultural affinities, environments, subsistence, and technological change. *Quat. Int.* **301**, 3–22 (2013).

96. Rademaker, K., Bromley, G. R. M. & Sandweiss, D. H. Peru archaeological radiocarbon database, 13,000–7000 14C B.P. *Quat. Int.* **301**, 34–45 (2013).

97. Capriles, J. M. & Albarracin-Jordan, J. The earliest human occupations in Bolivia: A review of the archaeological evidence. *Quat. Int.* **301**, 46–59 (2013).

98. Méndez Melgar, C. Terminal Pleistocene/early Holocene 14C dates form archaeological sites in Chile: Critical chronological issues for the initial peopling of the region. *Quat. Int.* **301**, 60–73 (2013).

99. Bueno, L., Dias, A. S. & Steele, J. The Late Pleistocene/Early Holocene archaeological record in Brazil: A geo-referenced database. *Quat. Int.* **301**, 74–93 (2013).

100. López Mazz, J. M. Early human occupation of Uruguay: Radiocarbon database and archaeological implications. *Quat. Int.* **301**, 94–103 (2013).

101. Prates, L., Politis, G. & Steele, J. Radiocarbon chronology of the early human occupation of Argentina. *Quat. Int.* **301**, 104–122 (2013).

102. Casamiquela, R., Montané, J. & Santana, R. Convivencia del hombre con el mastodonte en Chile central. *Noticiario Mensual del Museo Nacional de Historia Natural* **11**, 1–6 (1967).

103. Montané, J. Paleo-Indian remains from laguna de tagua tagua, central chile. *Science* **161**, 1137–1138 (1968).

104. Nuñez, L. *et al.* Cuenca de Taguatagua en Chile: el ambiente del Pleistoceno superior y ocupaciones humanas. *Revista Chilena de Historia Natural* **67**, 503–519 (1994).

105. Jackson, D., Méndez, C., Núñez, L. & Jackson, D. Procesamiento de fauna extinta durante la transición Pleistoceno-Holoceno en el centro-norte de Chile. *Boletín de Arqueología PUCP* 315–336 (2011).

106. Montane, J. Primera fecha radiocarbónica de Tagua-Tagua. *Not. Mens. Mus. Nac. Hist. Nat.* **139**, (1968).

107. Reitz, E. J., McInnis, H. E., Sandweiss, D. H. & Others. Terminal Pleistocene and Early Holocene fishing strategies at Quebrada Jaguay and the Ring Site, southern Peru. *Journal of Archaeological Science: Reports* **8**, 447–453 (2016).

108. Jackson, D., Méndez, C., Seguel, R., Maldonado, A. & Vargas, G. Initial Occupation of the Pacific Coast of Chile during Late Pleistocene Times. *Curr. Anthropol.* **48**, 725–731 (2007).

109. Roosevelt, A. C. Relatório preliminar sobre o levantamento e escavações na Caverna da Pedra Pintada, Monte Alegre, Pará, Brasil. *Segunda etapa de campo do projeto arqueológico Santarém* (1991).

110. Michab, M. *et al.* Luminescence dates for the Paleoindian site of Pedra Pintada, Brazil. *Quat. Sci. Rev.* **17**, 1041–1046 (1998).

111. Dillehay, T. D. *et al.* Monte Verde: seaweed, food, medicine, and the peopling of South America. *Science* **320**, 784–786 (2008).

112. Harris, E. C. *Principles of Archaeological Stratigraphy*. (Elsevier, 2014).

113. Gelfand, A. E. & Smith, A. F. M. Sampling-Based Approaches to Calculating Marginal Densities. *J. Am. Stat. Assoc.* **85**, 398–409 (1990).

114. Gilks, W. R., Richardson, S. & Spiegelhalter, D. *Markov chain Monte Carlo in practice*. (Chapman and Hall/CRC, 1995).

115. Bronk Ramsey, C. Dealing with Outliers and Offsets in Radiocarbon Dating. *Radiocarbon* **51**, 1023–1045 (2009).

116. Rosenblatt, M. Remarks on Some Nonparametric Estimates of a Density Function. *Ann. Math. Stat.* **27**, 832–837 (1956).

117. Parzen, E. On Estimation of a Probability Density Function and Mode. *Ann. Math. Stat.* **33**, 1065–1076 (1962).

118. Bronk Ramsey, C. Methods for Summarizing Radiocarbon Datasets. *Radiocarbon* **59**, 1809–1833 (2017).

119. Silverman, B. W. *Density Estimation for Statistics and Data Analysis*. (Chapman and Hall, 1986).

120. Bronk Ramsey, C. OxCal 4.3 Manual. *OxCal 4.3 Manual* https://c14.arch.ox.ac.uk/oxcalhelp/hlp_contents.html.

121. Stafford, T. W., Jr, Duhamel, R. C., Haynes, C. V., Jr & Brendel, K. Isolation of proline and hydroxyproline from fossil bone. *Life Sci.* **31**, 931–938 (1982).

122. Stafford, T. W., Brendel, K. & Duhamel, R. C. Radiocarbon, 13C and 15N analysis of fossil bone: Removal of humates with XAD-2 resin. *Geochim. Cosmochim. Acta* **52**, 2257–2267 (1988).

123. Deviese, T., Comeskey, D., McCullagh, J., Bronk Ramsey, C. & Higham, T. New protocol for compound specific radiocarbon analysis of archaeological bones. *Rapid Commun. Mass Spectrom.* **32**, 373–379 (2017).

124. Becerra-Valdivia, L. *et al.* Reassessing the chronology of the archaeological site of Anzick. *Proc. Natl. Acad. Sci. U. S. A.* **115**, 7000–7003 (2018).

125. Waters, M. R., Stafford, T. W., Jr, Kooyman, B. & Hills, L. V. Late Pleistocene horse and camel hunting at the southern margin of the ice-free corridor: reassessing the age of Wally's Beach, Canada. *Proc. Natl. Acad. Sci. U. S. A.* **112**, 4263–4267 (2015).

126. Derek Hamilton, W. & Krus, A. M. The myths and realities of Bayesian chronological modeling revealed. *Am. Antiq.* **83**, 187–203 (2018).

4.2. Supplementary text

1. Archaeological traditions discussed

1.1. Clovis

Clovis is the earliest, widespread cultural tradition of North America[1–4], dated in 2007 to 13,250-12,800 cal BP[5]. It is most commonly recognized by the presence of the Clovis projectile point, a fluted biface[6]. Clovis forms the basis of the 'Clovis-first' model, which stipulates that a group of big-game hunters initially entered North America from Asia ~13,5000 years ago via Beringia, moving southward through an ice-free corridor between the Laurentide and Cordilleran ice sheets. The technological origin of Clovis is yet unknown and it is generally believed to have developed in situ[7].

1.2. Western Stemmed tradition

Found in the Paleoindian record of the Intermountain West of North America, the Western Stemmed tradition (WST) is a non-fluted lithic technology dominated by large, generally narrow bifacial points with sloping shoulders and contracting, stem-like bases[8–12]. Through the dating of sites like Bonneville Estates, Cooper's Ferry, and Paisley Caves, this tradition is considered to be roughly coeval with or earlier than Clovis[8,9,13].

1.3. Beringian tradition

Reflecting the high degree of variability present in Beringia during the Pleistocene-Holocene transition, the Beringian tradition encompasses three main lithic industries[14–17]. Found in eastern Beringia, these include the Nenana, a non-microblade, biface-and-blade industry with Chindadn points (small and teardrop-shaped); the Denali, a distinctive microblade technology that generally postdates the Nenana; and the Northern Paleoindian, with bifacial, unfluted lanceolate

points. Technology found at western Beringian sites, Ushki (component 7) and Berelekh, share similarities with Nenana[14].

2. Archaeological sites included

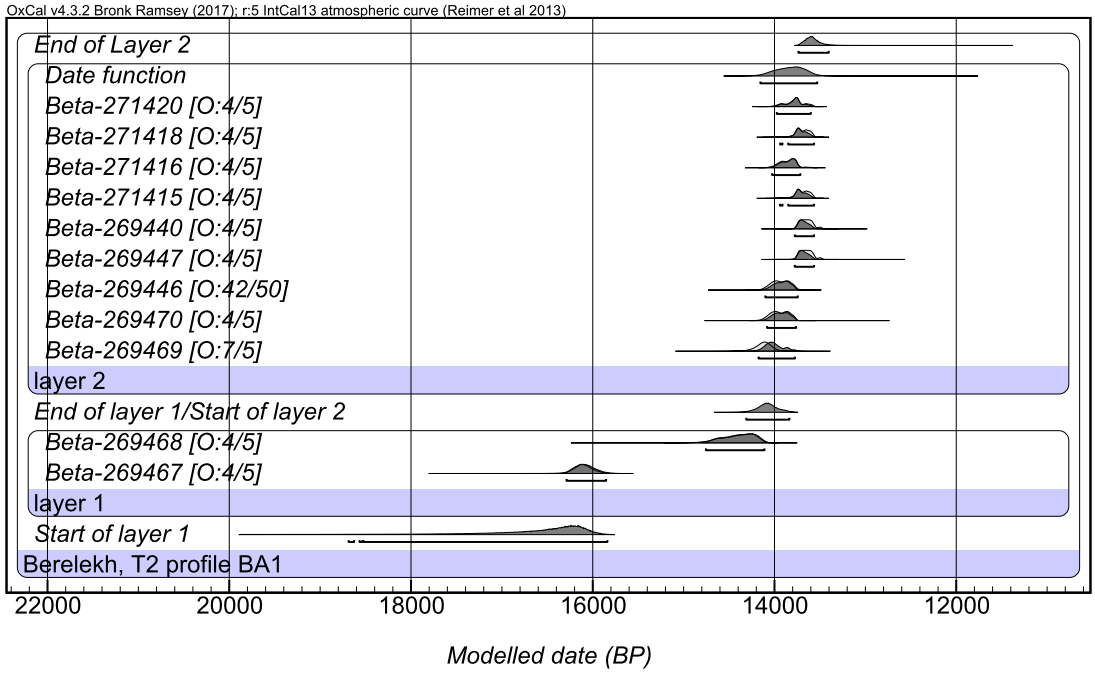
The 41 archaeological sites included in the analysis are listed alphabetically, according to category, and briefly described. Coordinates [noted in parentheses as 'latitude', 'longitude'; following the World Geodetic System (WGS84)], Bayesian age modeling notes and CQL code are provided for each. The latter can be copied into OxCal to replicate each model. For multiple-phase sequences, brief notes are made regarding the degree of cultural association for the chronometric data included. Multimodal or highly imprecise start boundaries are highlighted and discussed. Generally, these features are caused by taphonomic issues, sampling/radiocarbon dating biases and/or unreliable chronometric data. The latter is a possibility given that, for objectivity, dates deemed problematic in the literature were not manually excluded. Instead, as noted in the Methods section, we relied on outlier analysis to objectively identify and down-weight outliers within the models.

2.1. Beringian tradition

2.1.1. Berelekh, eastern Siberia (Russia)

The Berelekh geoarchaeological complex (at 70.500000, 144.033333) contains a mammoth bone bed ("graveyard") and a stratified archaeological site[18–20]. Although there is no evidence of human contribution to the former, cut-marked faunal bones and lithic artifacts are found within the latter. In 2009, test excavations were performed in a number of terraces within the complex. In terrace 2 (T2; profile BA1), cultural material was found within layer 2 and dates obtained provide stratigraphic control. Using chronometric data from this section, the model created dates the start of the cultural component at Berelekh to 14,315-13,835 cal BP (Fig. S1). T2 BA1 was

chosen as Beta-269470 and -269447 are the only two samples noted as belonging to a “culture-bearing layer”[19]. Directly dated human-modified osseous tools are noted as surface finds[19].



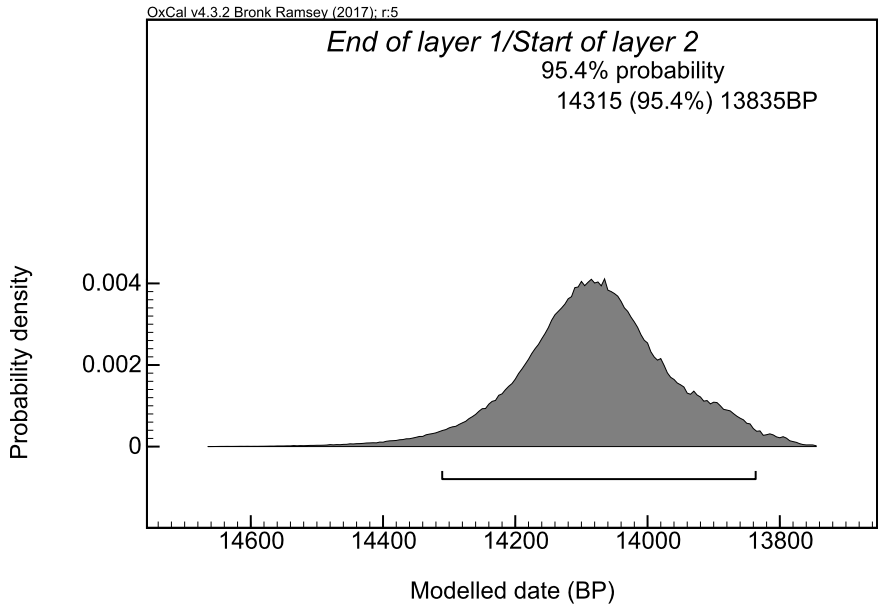


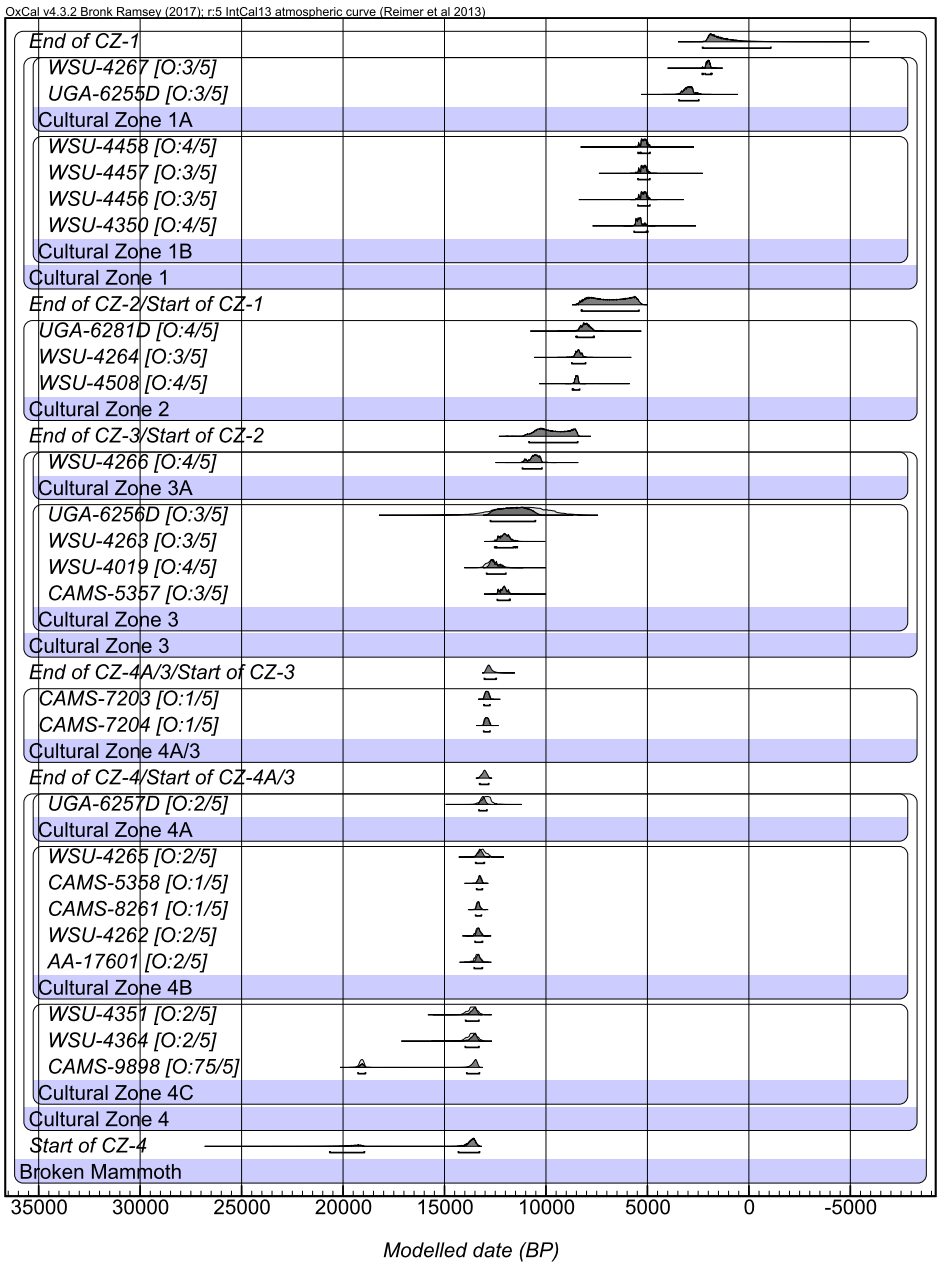
Fig. S1. Bayesian age model for Berelekh (T2; profile BA1; above), and start `Boundary` (below).

```
Plot()
 {
 Outlier_Model("General",T(5),U(0,4),"t");
 Sequence("Berelehk, T2 profile BA1")
  {
  Boundary("Start of layer 1");
  Phase("layer 1")
   {
   R_Date("Beta-269467", 13390, 60)
    {
    Outlier("General", 0.05);
    };
   R_Date("Beta-269468", 12350, 60)
    {
    Outlier("General", 0.05);
    };
   };
  Boundary("End of layer 1/Start of layer 2");
  Phase("layer 2")
   {
   R_Date("Beta-269469", 12220, 60)
    {
    Outlier("General", 0.05);
    };
   R_Date("Beta-269470", 12100, 60)
    {
```

```
 Outlier("General", 0.05);
 };
 R_Date("Beta-269446", 12090, 60)
 {
 Outlier("General", 0.5);
 };
 R_Date("Beta-269447", 11830, 60)
 {
 Outlier("General", 0.05);
 };
 R_Date("Beta-269440", 11830, 60)
 {
 Outlier("General", 0.05);
 };
 R_Date("Beta-271415", 11890, 60)
 {
 Outlier("General", 0.05);
 };
 R_Date("Beta-271416", 11990, 60)
 {
 Outlier("General", 0.05);
 };
 R_Date("Beta-271418", 11890, 60)
 {
 Outlier("General", 0.05);
 };
 R_Date("Beta-271420", 11940, 60)
 {
 Outlier("General", 0.05);
 };
 Date("Date function");
 };
 Boundary("End of Layer 2");
 };
};
```

2.1.2. Broken Mammoth, Alaska (U.S.A.)

Broken Mammoth (XBD-131; at 64.266667, -146.116667) is a stratified archaeological site containing four Cultural Zones, with Cultural Zone IV (C and B) representing the earliest human occupation[16,17,21–24]. Dates obtained provide stratigraphic control or date cultural features directly, e.g., hearth charcoal. Using these data, the model created places the start of Cultural Zone IV at 20,655-13,275 cal BP (Fig. S2). This boundary is multimodal due to date CAMS-9898 (15,830±70; from CZ-4C), which was rejected by Holmes as scavenged or old ivory[24]. The measurement is identified as an outlier at 75%, which means it is not fully down-weighted in the model; hence its influence.



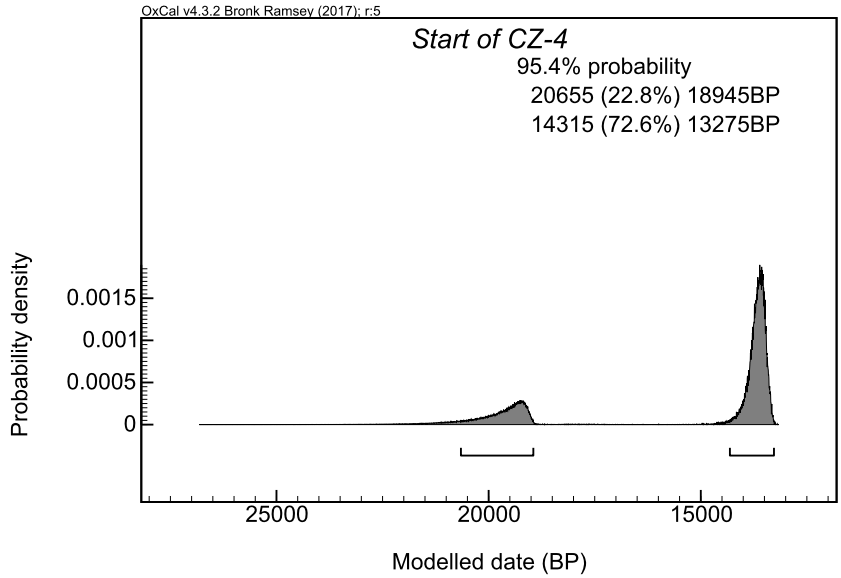


Fig. S2. Bayesian age model for Broken Mammoth (above), and start `Boundary` (below).

```
Plot()

{
 Outlier_Model("General",T(5),U(0,4),"t");
 Sequence("Broken Mammoth")
 {
  Boundary("Start of CZ-4");
  Sequence("Cultural Zone 4")
  {
  Phase("Cultural Zone 4C")
  {
  R_Date("CAMS-9898", 15830, 70)
  {
   Outlier("General", 0.05);
  };
  R_Date("WSU-4364", 11770, 220)
  {
   Outlier("General", 0.05);
  };
  R_Date("WSU-4351", 11770, 210)
  {
   Outlier("General", 0.05);
  };
 };
  Phase("Cultural Zone 4B")
  {
  R_Date("AA-17601", 11540, 140)
  {
   Outlier("General", 0.05);
  };
  R_Date("WSU-4262", 11510, 120)
  {
   Outlier("General", 0.05);
  };
  R_Date("CAMS-8261", 11500, 80)
  {
   Outlier("General", 0.05);
  };
  R_Date("CAMS-5358", 11420, 70)
  {
   Outlier("General", 0.05);
  };
  R_Date("WSU-4265", 11280, 190)
  {
   Outlier("General", 0.05);
  };
 };
  Phase("Cultural Zone 4A")
  {
  R_Date("UGA-6257D", 11040, 260)
  {
   Outlier("General", 0.05);
  };
 };
};
 Boundary("End of CZ-4/Start of CZ-4A/3 ");
 Phase("Cultural Zone 4A/3")
 {
 R_Date("CAMS-7204", 11060, 90)
 {
  Outlier("General", 0.05);
 };
 R_Date("CAMS-7203", 11040, 80)
 {
  Outlier("General", 0.05);
 };
};
 Boundary("End of CZ-4A/3/Start of CZ-3");
 Sequence("Cultural Zone 3")
 {
  Phase("Cultural Zone 3")
  {
  R_Date("CAMS-5357", 10290, 70)
  {
   Outlier("General", 0.05);
  };
  R_Date("WSU-4019", 10790, 230)
  {
   Outlier("General", 0.05);
  };
  R_Date("WSU-4263", 10270, 110)
  {
   Outlier("General", 0.05);
  };
  R_Date("UGA-6256D", 9690, 960)
  {
   Outlier("General", 0.05);
  };
 };
  Phase("Cultural Zone 3A")
  {
  R_Date("WSU-4266", 9310, 165)
  {
   Outlier("General", 0.05);
  };
 };
};
 Boundary("End of CZ-3/Start of CZ-2");
 Phase("Cultural Zone 2")
 {
 R_Date("WSU-4508", 7700, 80)
 {
  Outlier("General", 0.05);
 };
 R_Date("WSU-4264", 7600, 140)
 {
  Outlier("General", 0.05);
 };
 R_Date("UGA-6281D", 7200, 205)
 {
  Outlier("General", 0.05);
 };
};
 Boundary("End of CZ-2/Start of CZ-1");
 Sequence("Cultural Zone 1")
 {
  Phase("Cultural Zone 1B")
  {
  R_Date("WSU-4350", 4690, 110)
  {
   Outlier("General", 0.05);
  };
  R_Date("WSU-4456", 4540, 90)
  {
   Outlier("General", 0.05);
  };
  R_Date("WSU-4457", 4545, 90)
  {
   Outlier("General", 0.05);
  };
  R_Date("WSU-4458", 4525, 90)
  {
   Outlier("General", 0.05);
  };
 };
  Phase("Cultural Zone 1A")
  {
  R_Date("UGA-6255D", 2815, 180)
  {
   Outlier("General", 0.05);
  };
  R_Date("WSU-4267", 2040, 65)
  {
   Outlier("General", 0.05);
  };
 };
```

```
};
Boundary("End of CZ-1");
};
};
```

2.1.3. Dry Creek, Alaska (U.S.A.)

Dry Creek (HEA-005; at 63.883333, -149.033333) is a stratified site containing four cultural components, with I and II representing the earliest occupations[25–33]. Based on lithic technology and antiquity, Component I has been assigned to the Nenana complex, whilst Component II to the Denali. Using the latest chronometric data obtained from cultural features, e.g., hearth charcoal[33], the model created places the start of Component I at 13,700-13,350 cal BP (Fig. S3).

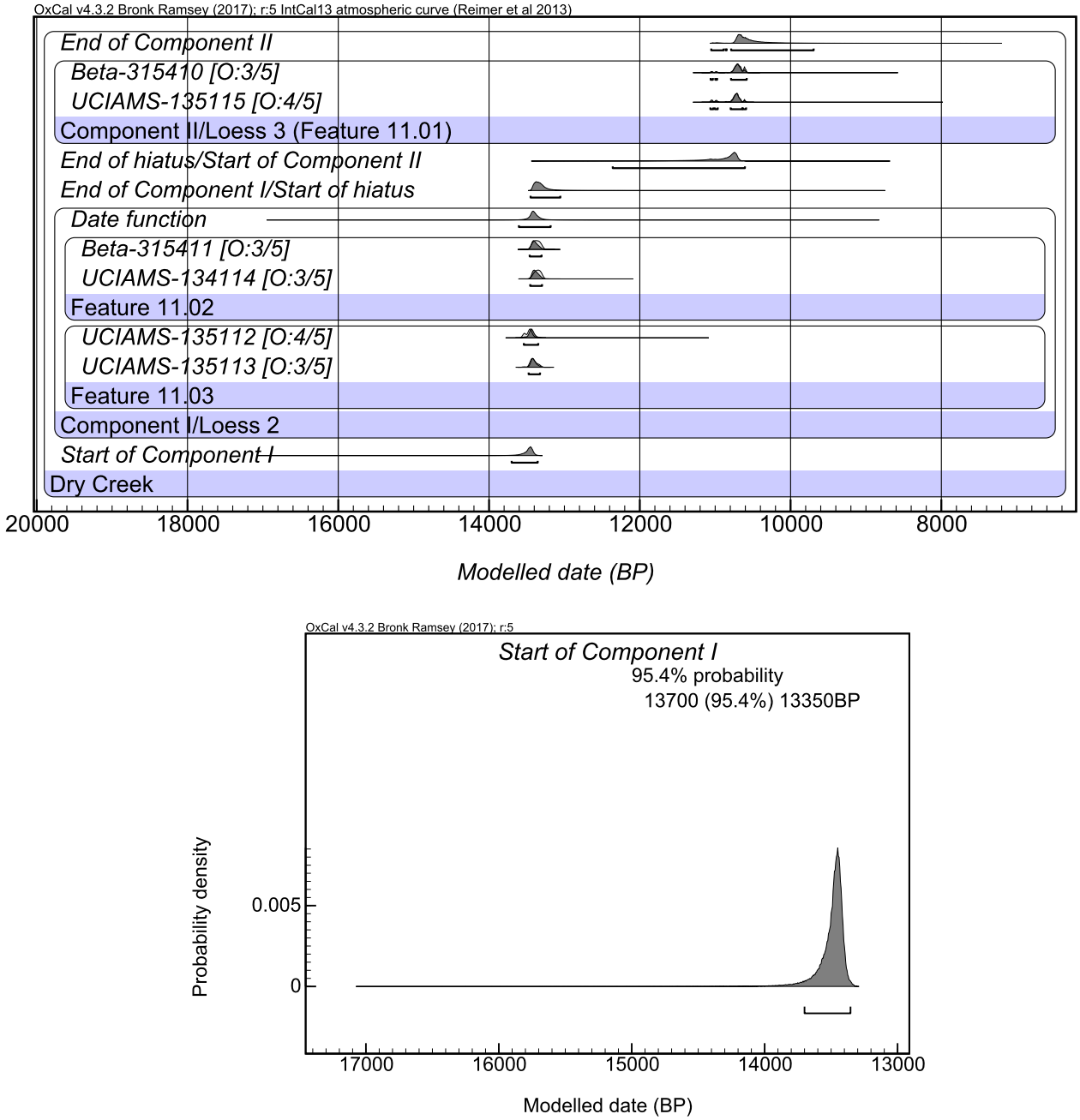


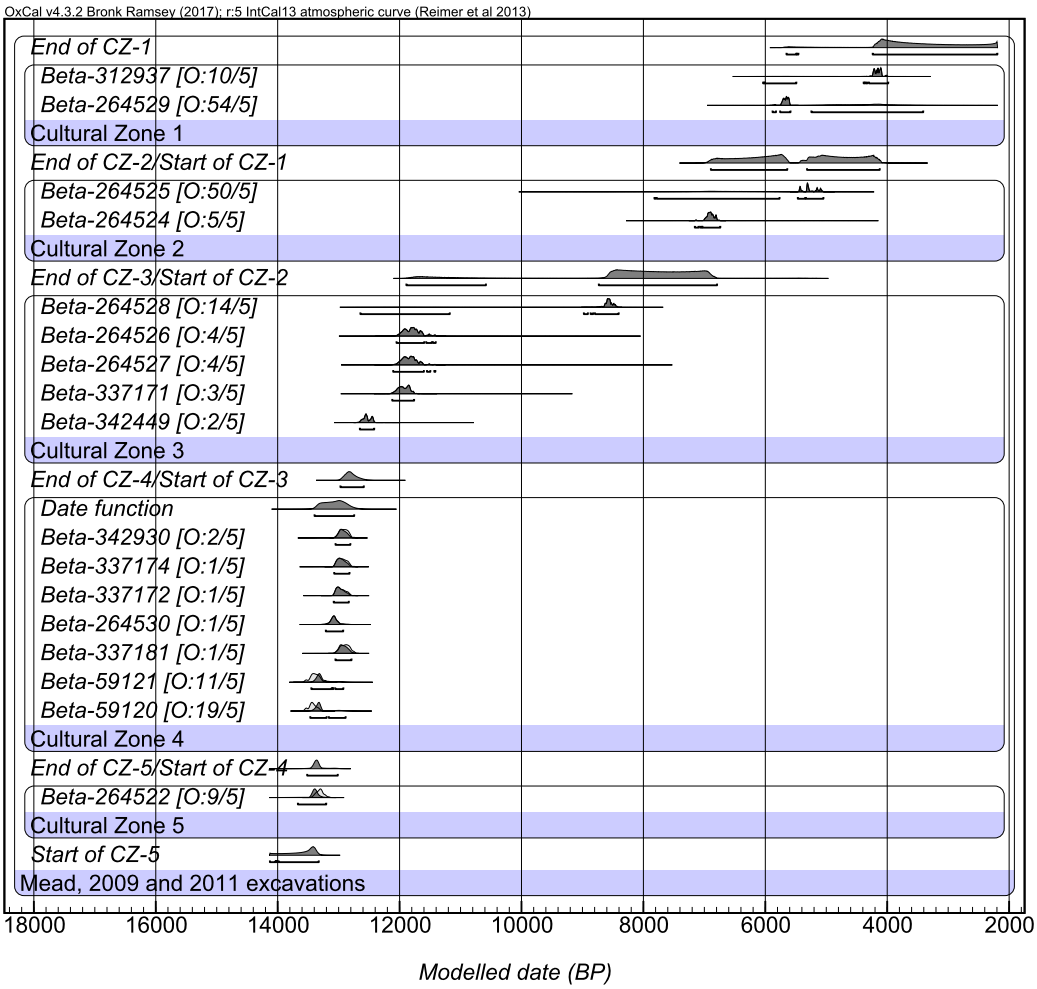
Fig. S3. Bayesian age model for Dry Creek (above), and start `Boundary` (below).

```
Plot()
{
 Outlier_Model("General",T(5),U(0,4),"t");
Sequence("Dry Creek")
 {
 Boundary("Start of Component I");
 Phase("Component I/Loess 2")
 {
 Phase("Feature 11.03")
 {
 R_Date("UCIAMS-135113", 11580, 40)
 {
 Outlier("General", 0.05);
 };
 R_Date("UCIAMS-135112", 11635, 40)
 {
 Outlier("General", 0.05);
 };
 };
 Phase("Feature 11.02")
 {
 R_Date("UCIAMS-134114", 11510, 40)
 {
 Outlier("General", 0.05);
 };
 R_Date("Beta-315411", 11530, 50)
 {
 Outlier("General", 0.05);
 };
 };
 Date("Date function");
 };
 Boundary("End of Component I/Start of hiatus");
 Boundary("End of hiatus/Start of Component II");
 Phase("Component II/Loess 3 (Feature 11.01)")
 {
 R_Date("UCIAMS-135115", 9480, 35)
 {
 Outlier("General", 0.05);
```

```
  };
  R_Date("Beta-315410", 9460, 40)
  {
   Outlier("General", 0.05);
  };
 };
 Boundary("End of Component II");
};
};
```

2.1.4. Mead, Alaska (U.S.A.)

Mead (XBD-071; at approximately 64.271001, -146.075173) is a stratified site containing five Cultural Zones, with Cultural Zone IV representing the earliest human occupation[16,17,21,34,35]. Using the latest chronometric data obtained for the 2009/2011 excavations[17,34,35], which provide stratigraphic control or date cultural features directly, e.g., hearth charcoal, the model created places the start of CZ-4 at 13,520-13,010 cal BP (Fig. S4).



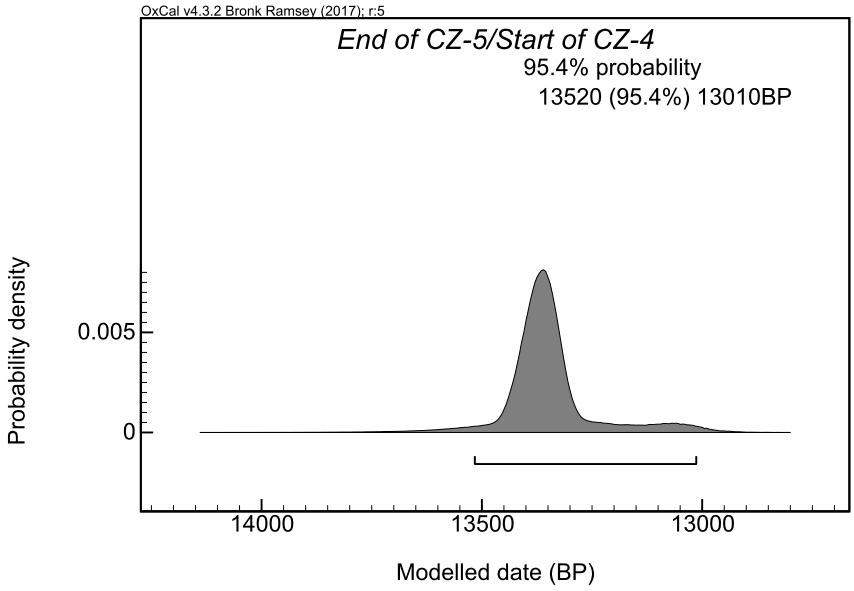


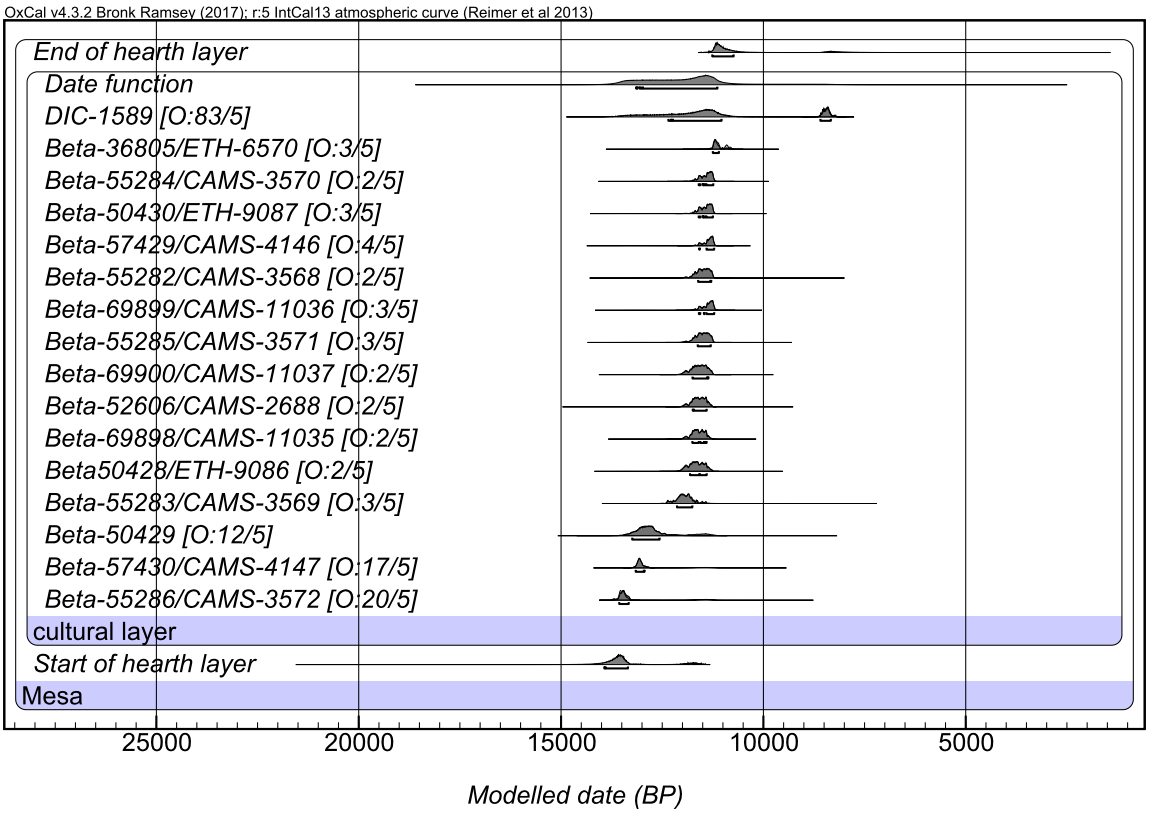
Fig. S4. Bayesian age model for Mead (above), and start `Boundary` (below).

```
Plot()
 {
 Outlier_Model("General",T(5),U(0,4),"t");
Sequence("Mead, 2009 and 2011 excavations")
 {
 Boundary("Start of CZ-5");
 Phase("Cultural Zone 5")
 {
 R_Date("Beta-264522", 11460, 50)
  {
  Outlier("General", 0.05);
  };
 };
 Boundary("End of CZ-5/Start of CZ-4");
 Phase("Cultural Zone 4")
 {
 R_Date("Beta-59120", 11600, 60)
```

```
 {
 Outlier("General", 0.05);
 };
 R_Date("Beta-59121", 11560, 80)
 {
 Outlier("General", 0.05);
 };
 R_Date("Beta-337181", 11030, 50)
 {
 Outlier("General", 0.05);
 };
 R_Date("Beta-264530", 11210, 60)
 {
 Outlier("General", 0.05);
 };
 R_Date("Beta-337172", 11100, 50)
 {
 Outlier("General", 0.05);
 };
 R_Date("Beta-337174", 11080, 50)
 {
 Outlier("General", 0.05);
 };
 R_Date("Beta-342930", 11050, 40)
 {
 Outlier("General", 0.05);
 };
 Date("Date function");
};
Boundary("End of CZ-4/Start of CZ-3");
Phase("Cultural Zone 3")
{
R_Date("Beta-342449", 10560, 40)
 {
 Outlier("General", 0.05);
 };
 R_Date("Beta-337171", 10220, 40)
 {
 Outlier("General", 0.05);
 };
 R_Date("Beta-264527", 10160, 50)
 {
 Outlier("General", 0.05);
 };
 R_Date("Beta-264526", 10140, 50)
 {
 Outlier("General", 0.05);
 };
 R_Date("Beta-264528", 7790, 50)
 {
 Outlier("General", 0.05);
 };
};
Boundary("End of CZ-3/Start of CZ-2");
Phase("Cultural Zone 2")
{
R_Date("Beta-264524", 6050, 40)
 {
 Outlier("General", 0.05);
 };
 R_Date("Beta-264525", 4580, 40)
 {
 Outlier("General", 0.05);
 };
};
Boundary("End of CZ-2/Start of CZ-1");
Phase("Cultural Zone 1")
{
 R_Date("Beta-264529", 4940, 40)
 {
 Outlier("General", 0.05);
 };
 R_Date("Beta-312937", 3780, 30)
 {
 Outlier("General", 0.05);
 };
};
 Boundary("End of CZ-1");
};
};
```

2.1.5. Mesa, Alaska (U.S.A.)

Mesa (KIR-102; at approximately 68.439857, -155.813683) is a multi-cluster site containing over fifteen hearths with associated Northern Paleoindian and microblade lithic industries[36–40]. All but one measurement obtained date cultural features directly, e.g., hearth charcoal. The exception was measured from “soil charcoal” and provides stratigraphic control. Using these data, a single `Phase` model was built, dating the cultural component to 13,910-9,355 cal BP (`Date` function; Fig. S5). The imprecision of this distribution is likely affected by date DIC-1589 (7,620±95 BP), which was rejected as an outlier by Kunz & Reanier[36,37], and is here identified as an outlier at 83% probability.



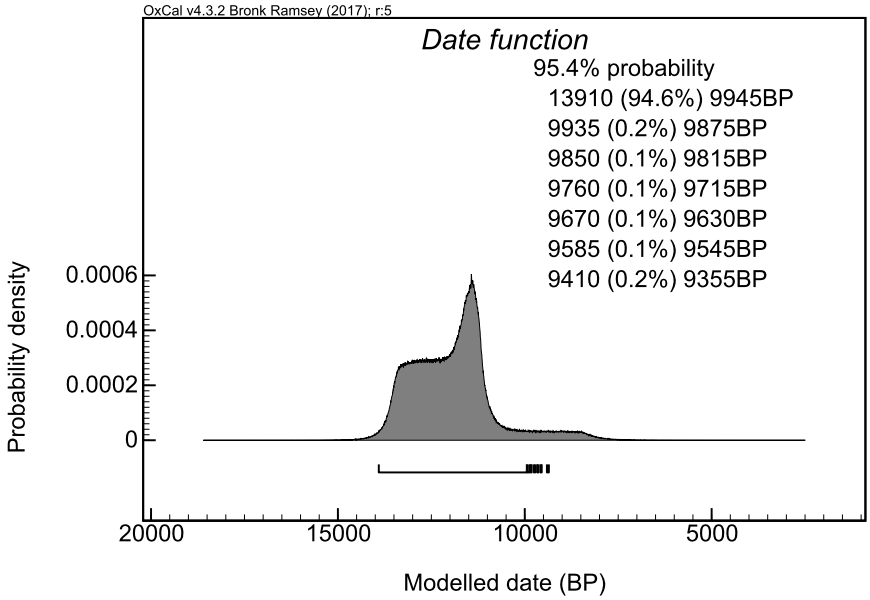


Fig. S5. Bayesian age model for Mesa (above), and `Date` function (below).

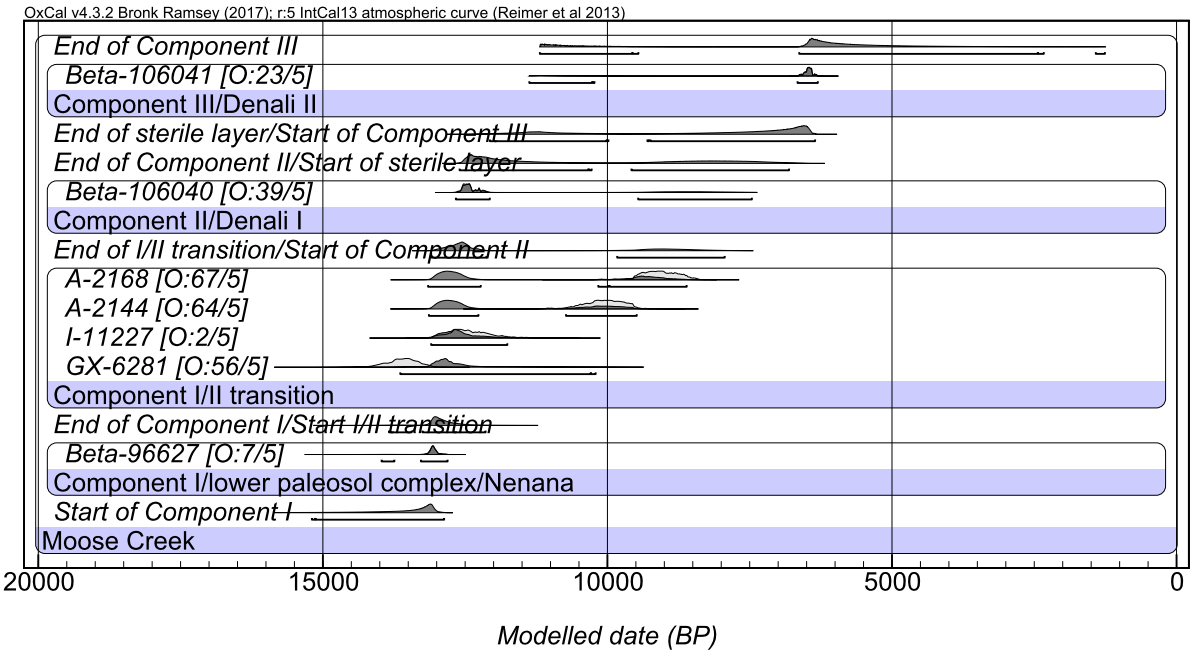
```
Plot()
{
 Outlier_Model("General",T(5),U(0,4),"t");
 Sequence("Mesa")
 {
  Boundary("Start of hearth layer");
  Phase("cultural layer")
  {
   R_Date("Beta-55286/CAMS-3572", 11660, 80)
   {
    Outlier("General", 0.05);
   };
   R_Date("Beta-57430/CAMS-4147", 11190, 70)
   {
    Outlier("General", 0.05);
   };
   R_Date("Beta-50429", 10980, 280)
   {
    Outlier("General", 0.05);
   };
   R_Date("Beta-55283/CAMS-3569", 10240, 80)
   {
    Outlier("General", 0.05);
   };
   R_Date("Beta50428/ETH-9086", 10090, 85)
   {
    Outlier("General", 0.05);
   };
   R_Date("Beta-69898/CAMS-11035", 10070, 60)
```

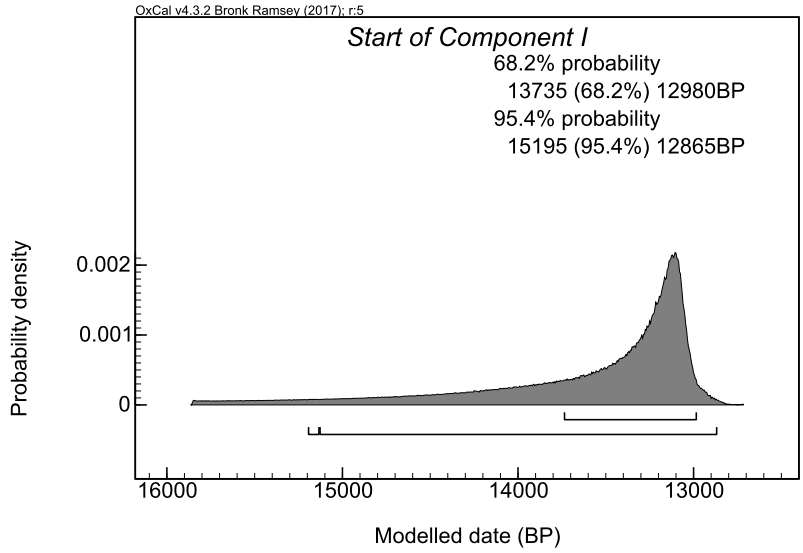
```
 {
 Outlier("General", 0.05);
 };
 R_Date("Beta-52606/CAMS-2688", 10060, 70)
 {
 Outlier("General", 0.05);
 };
 R_Date("Beta-69900/CAMS-11037", 10050, 90)
 {
 Outlier("General", 0.05);
 };
 R_Date("Beta-55285/CAMS-3571", 10000, 80)
 {
 Outlier("General", 0.05);
 };
 R_Date("Beta-69899/CAMS-11036", 9900, 80)
 {
 Outlier("General", 0.05);
 };
 R_Date("Beta-55282/CAMS-3568", 9990, 80)
 {
 Outlier("General", 0.05);
 };
 R_Date("Beta-57429/CAMS-4146", 9900, 70)
 {
 Outlier("General", 0.05);
 };
 R_Date("Beta-50430/ETH-9087", 9945, 75)
 {
 Outlier("General", 0.05);
 };
 R_Date("Beta-55284/CAMS-3570", 9930, 80)
 {
 Outlier("General", 0.05);
 };
 R_Date("Beta-36805/ETH-6570", 9730, 80)
 {
 Outlier("General", 0.05);
 };
 R_Date("DIC-1589", 7620, 95)
 {
 Outlier("General", 0.05);
 };
 Date("Date function");
 };
 Boundary("End of hearth layer");
 };
};
```

2.1.6. Moose Creek, Alaska (USA)

Moose Creek (FAI-206; at 64.066667, -149.100000) is a stratified site containing four cultural components[28,30,41–43]. Based on lithic technology and antiquity, Component I has been assigned to the Nenana complex, Component II to Denali I, and Component III to Denali II[41]. Only three dates obtained are considered to date cultural features directly (measured from hearth charcoal), whilst the rest are soil organics (in this case, located between Components I and II) and provide stratigraphic control. Using these data, the model created places the start of Component I at 15,195-12,865 cal BP (95.4% confidence) or 13,735-12,980 cal BP (68.2% confidence; Fig. S6).

Fig. S6. Bayesian age model for Moose C





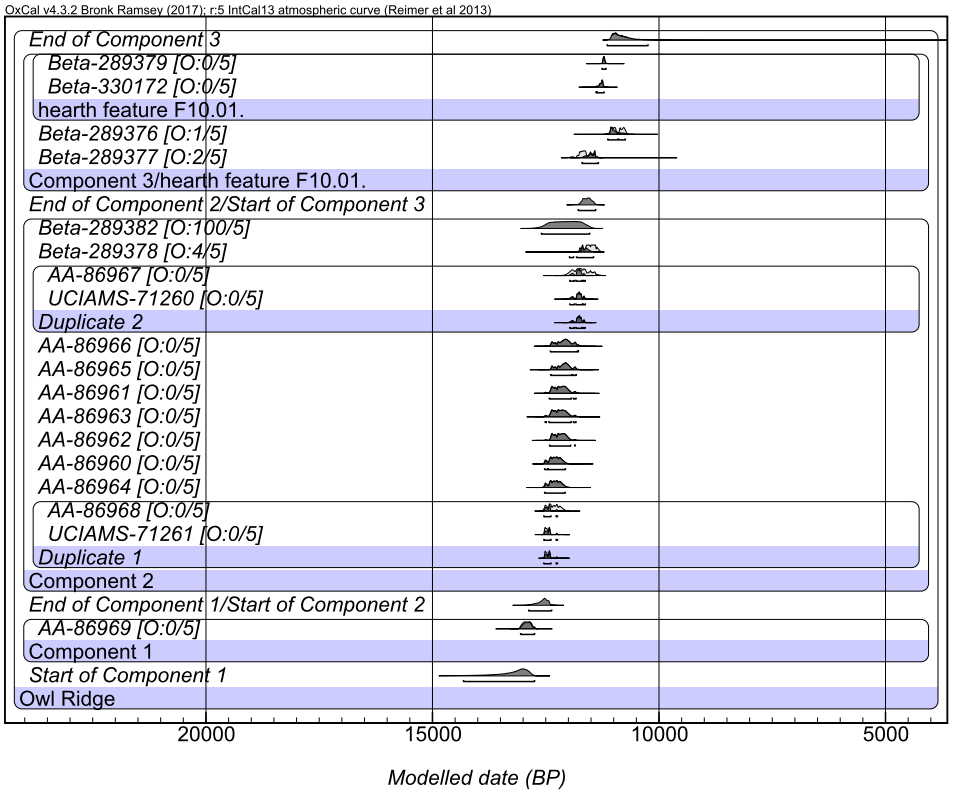
reek (above), and start `Boundary` (below).

```
Plot()
 {
 Outlier_Model("General",T(5),U(0,4),"t");
 Sequence("Moose Creek")
 {
 Boundary("Start of Component I");
 Phase("Component I/lower paleosol complex/Nenana")
 {
 R_Date("Beta-96627", 11190, 60)
 {
 Outlier("General", 0.05);
 };
 };
 Boundary("End of Component I/Start I/II transition");
 Phase("Component I/II transition")
 {
 R_Date("GX-6281", 11730, 250)
 {
 Outlier("General", 0.05);
 };
 R_Date("I-11227", 10640, 280)
 {
 Outlier("General", 0.05);
 };
 R_Date("A-2144", 8940, 270)
 {
 Outlier("General", 0.05);
 };
 R_Date("A-2168", 8160, 260)
 {
 Outlier("General", 0.05);
 };
 };
 Boundary("End of I/II transition/Start of Component II");
 Phase("Component II/Denali I")
 {
 R_Date("Beta-106040", 10500, 60)
 {
```

```
  Outlier("General", 0.05);
 };
};
Boundary("End of Component II/Start of sterile layer");
Boundary("End of sterile layer/Start of Component III");
Phase("Component III/Denali II")
{
 R_Date("Beta-106041", 5680, 50)
 {
  Outlier("General", 0.05);
 };
};
Boundary("End of Component III");
};
};
```

2.1.7. Owl Ridge, Alaska (U.S.A.)

Owl Ridge (FAI-91; at 64.0125, -149.556944) is a stratified archaeological site containing three cultural components[30,44–46]. Based on lithic technology and antiquity, Component 1 has been assigned to the Nenana complex, whilst Component 2-3 to the Denali[46]. Using the latest chronometric data obtained for the 2007/2009/2010 excavations[46] (those clearly denoted from Components 1-3), the model created places the start of Component I at 14,315-12,745 cal BP (Fig. S7). Only two dates obtained are considered to directly date a cultural feature (hearth F10.01; Beta-289379 and -330172), whilst the rest are wood charcoals that provide stratigraphic control[46].



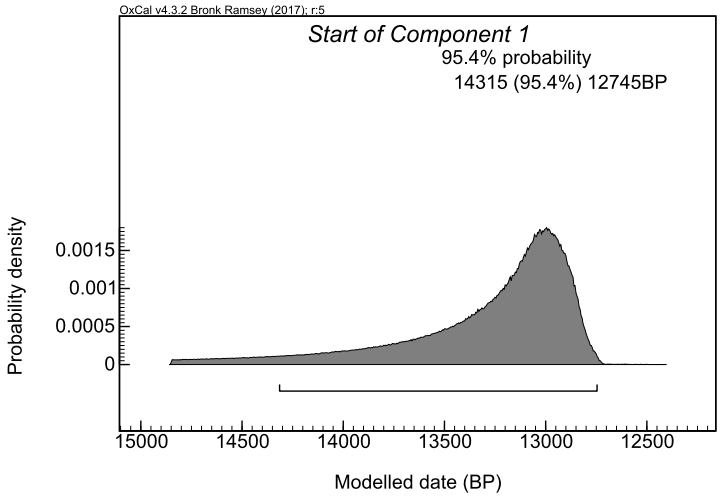


Fig. S7. Bayesian age model for Owl Ridge (above), and start `Boundary` (below).

```
Plot()
{
 Outlier_Model("General",T(5),U(0,4),"t");
 Sequence("Owl Ridge")
 {
  Boundary("Start of Component 1");
  Phase("Component 1")
  {
   R_Date("AA-86969", 11060, 60)
   {
    Outlier("General", 0.05);
   };
  };
  Boundary("End of Component 1/Start of Component 2");
  Phase("Component 2")
  {
   Combine("Duplicate 1")
   {
    R_Date("UCIAMS-71261", 10485, 25)
    {
     Outlier("General", 0.05);
    };
    R_Date("AA-86968", 10440, 60)
    {
     Outlier("General", 0.05);
    };
   };
   R_Date("AA-86964", 10420, 60)
   {
    Outlier("General", 0.05);
   };
   R_Date("AA-86960", 10415, 60)
   {
    Outlier("General", 0.05);
   };
   R_Date("AA-86962", 10335, 60)
   {
    Outlier("General", 0.05);
   };
```

```
R_Date("AA-86963", 10340, 75)
 {
 Outlier("General", 0.05);
};
R_Date("AA-86961", 10330, 70)
 {
 Outlier("General", 0.05);
};
R_Date("AA-86965", 10295, 60)
 {
 Outlier("General", 0.05);
};
R_Date("AA-86966", 10290, 75)
 {
 Outlier("General", 0.05);
};
Combine("Duplicate 2")
 {
 R_Date("UCIAMS-71260", 10125, 20)
  {
  Outlier("General", 0.05);
  };
 R_Date("AA-86967", 10120, 75)
  {
  Outlier("General", 0.05);
  };
 };
R_Date("Beta-289378", 10020, 40)
 {
 Outlier("General", 0.05);
};
R_Date("Beta-289382", 80, 40)
 {
 Outlier("General", 0.05);
};
};
Boundary("End of Component 2/Start of Component 3");
Phase("Component 3/hearth feature F10.01.")
 {
 R_Date("Beta-289377", 10080, 40)
  {
  Outlier("General", 0.05);
  };
 R_Date("Beta-289376", 9550, 40)
  {
  Outlier("General", 0.05);
  };
 Phase("hearth feature F10.01.")
  {
  R_Date("Beta-330172", 9880, 40)
   {
   Outlier("General", 0.05);
   };
  R_Date("Beta-289379", 9790, 40)
   {
   Outlier("General", 0.05);
   };
  };
 };
 Boundary("End of Component 3");
};
};
```

2.1.8. Swan Point, Alaska (U.S.A.)

Swan Point (XBD-156; at 63.300000, -146.033333) is a stratified archaeological site containing four Cultural Zones [16,30,47–50]. Cultural Zone 4b, the earliest occupational layer, contains microblade technology that has been linked[51] to the Siberian Diuktai culture[52]. Dates obtained provide stratigraphic control or date cultural features directly, e.g., hearth charcoal. Using these data, the model created places its start at 14,680-14,155 cal BP (Fig. S8).

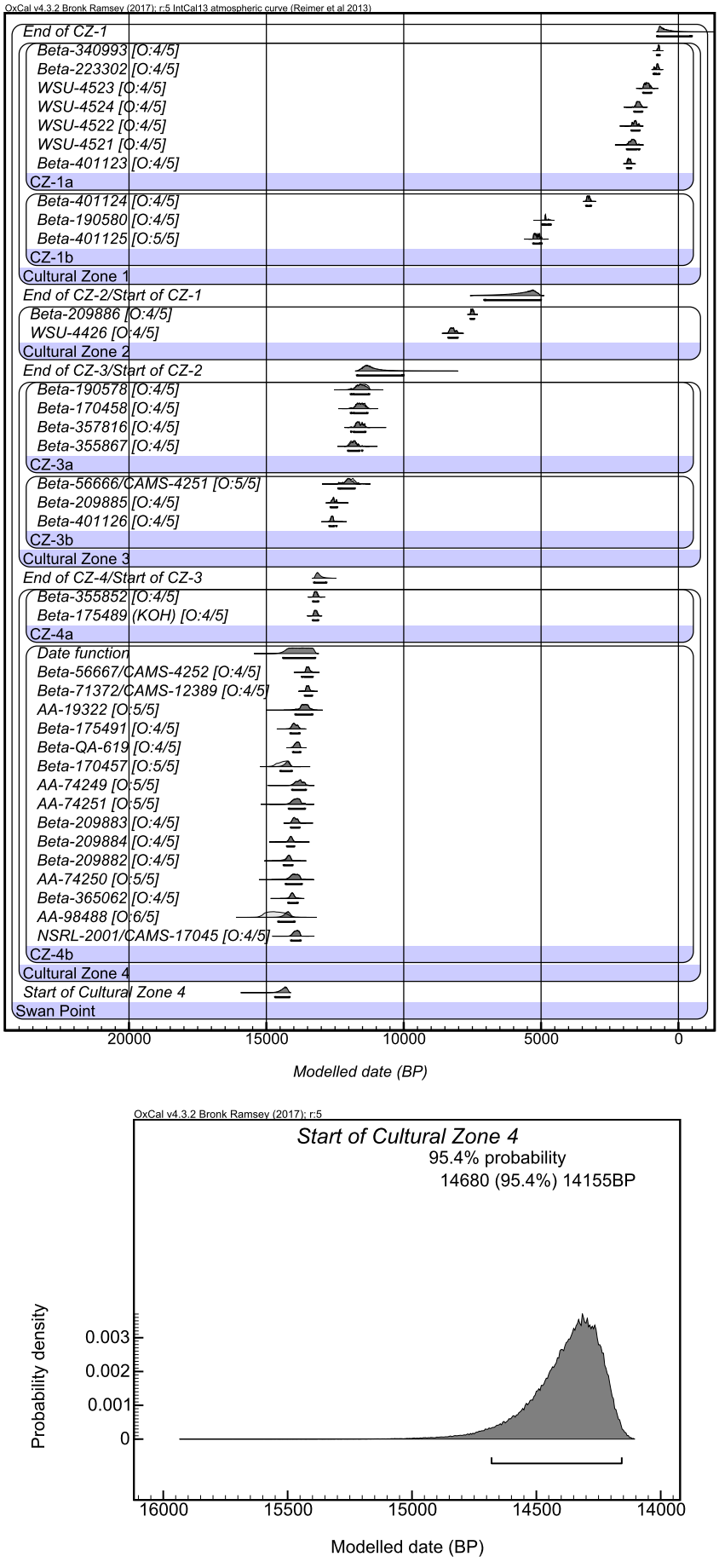


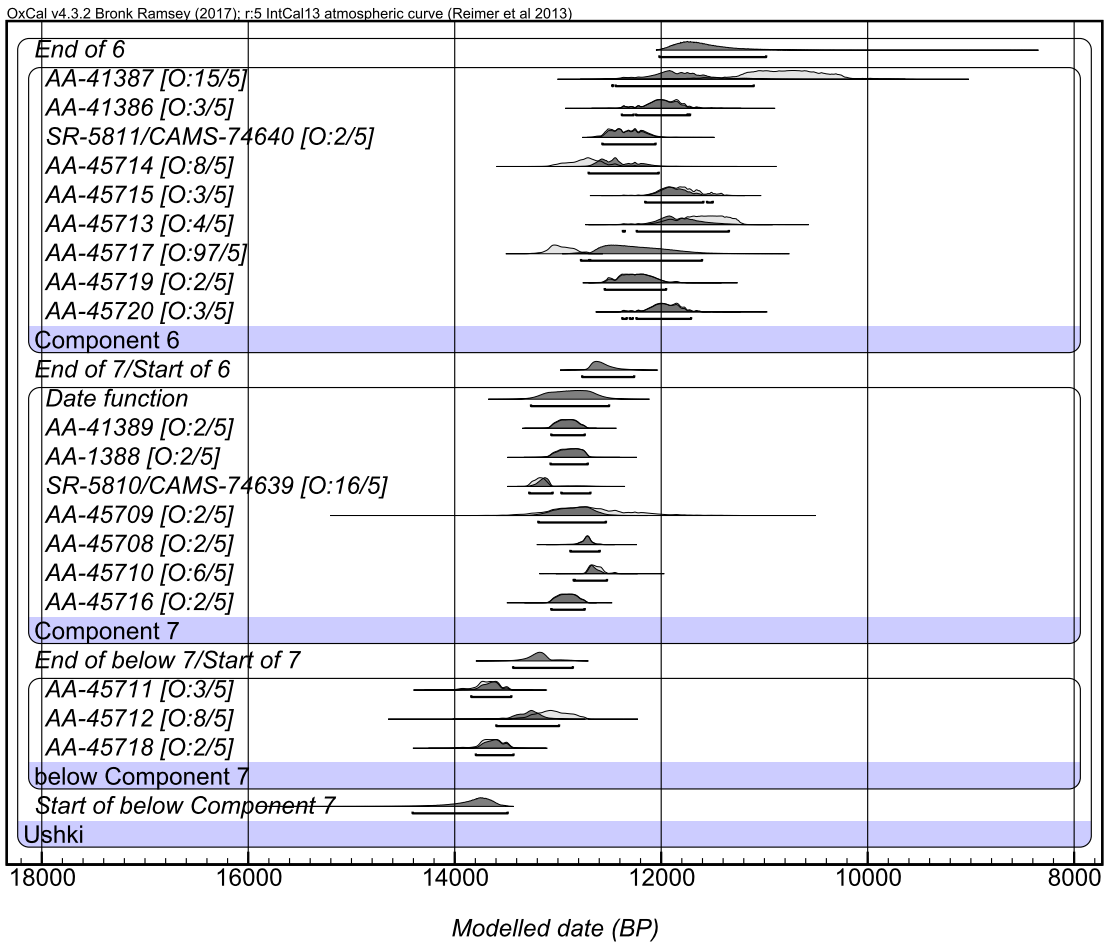
Fig. S8. Bayesian age model for Swan Point (above), and start `Boundary` (below).

```
Plot()
{
 Outlier_Model("General",T(5),U(0,4),"t");
 Sequence("Swan Point")
 {
  Boundary("Start of Cultural Zone 4");
  Sequence("Cultural Zone 4")
  {
   Phase("CZ-4b")
   {
    R_Date("NSRL-2001/CAMS-17045", 12060, 70)
    {
     Outlier("General", 0.05);
    };
    R_Date("AA-98488", 12500, 150)
    {
     Outlier("General", 0.05);
    };
    R_Date("Beta-365062", 12170, 50)
    {
     Outlier("General", 0.05);
    };
    R_Date("AA-74250", 12110, 120)
    {
     Outlier("General", 0.05);
    };
    R_Date("Beta-209882", 12290, 40)
    {
     Outlier("General", 0.05);
    };
    R_Date("Beta-209884", 12220, 40)
    {
     Outlier("General", 0.05);
    };
    R_Date("Beta-209883", 12100, 40)
    {
     Outlier("General", 0.05);
    };
    R_Date("AA-74251", 12050, 120)
    {
     Outlier("General", 0.05);
    };
    R_Date("AA-74249", 11950, 100)
    {
     Outlier("General", 0.05);
    };
    R_Date("Beta-170457", 12360, 60)
    {
     Outlier("General", 0.05);
    };
    R_Date("Beta-QA-619", 12040, 40)
    {
     Outlier("General", 0.05);
    };
    R_Date("Beta-175491", 12110, 50)
    {
     Outlier("General", 0.05);
    };
    R_Date("AA-19322", 11770, 140)
    {
     Outlier("General", 0.05);
    };
    R_Date("Beta-71372/CAMS-12389", 11660, 60)
    {
     Outlier("General", 0.05);
    };
    R_Date("Beta-56667/CAMS-4252", 11660, 70)
    {
     Outlier("General", 0.05);
    };
    Date("Date function");
   };
   Phase("CZ-4a")
   {
    R_Date("Beta-175489 (KOH)", 11360, 50)
    {
     Outlier("General", 0.05);
    };
    R_Date("Beta-355852", 11350, 50)
    {
     Outlier("General", 0.05);
    };
   };
  };
  Boundary("End of CZ-4/Start of CZ-3 ");
  Sequence("Cultural Zone 3")
  {
   Phase("CZ-3b")
   {
    R_Date("Beta-401126", 10620, 40)
    {
     Outlier("General", 0.05);
    };
    R_Date("Beta-209885", 10570, 40)
    {
     Outlier("General", 0.05);
    };
    R_Date("Beta-56666/CAMS-4251", 10230, 80)
    {
     Outlier("General", 0.05);
    };
   };
   Phase("CZ-3a")
   {
    R_Date("Beta-355867", 10160, 50)
    {
     Outlier("General", 0.05);
    };
    R_Date("Beta-357816", 10070, 40)
    {
     Outlier("General", 0.05);
    };
    R_Date("Beta-170458", 10050, 60)
    {
     Outlier("General", 0.05);
    };
    R_Date("Beta-190578", 10010, 90)
    {
     Outlier("General", 0.05);
    };
   };
  };
  Boundary("End of CZ-3/Start of CZ-2");
  Phase("Cultural Zone 2")
  {
   R_Date("WSU-4426", 7400, 80)
   {
    Outlier("General", 0.05);
   };
   R_Date("Beta-209886", 6610, 40)
   {
    Outlier("General", 0.05);
   };
  };
  Boundary("End of CZ-2/Start of CZ-1");
  Sequence("Cultural Zone 1")
  {
   Phase("CZ-1b")
   {
    R_Date("Beta-401125", 4480, 30)
    {
     Outlier("General", 0.05);
    };
    R_Date("Beta-190580", 4260, 40)
```

```
 {
 Outlier("General", 0.05);
 };
 R_Date("Beta-401124", 3060, 30)
 {
 Outlier("General", 0.05);
 };
};
Phase("CZ-1a")
{
R_Date("Beta-401123", 1860, 30)
 {
 Outlier("General", 0.05);
 };
 R_Date("WSU-4521", 1750, 80)
 {
 Outlier("General", 0.05);
 };
 R_Date("WSU-4522", 1670, 60)
 {
 Outlier("General", 0.05);
 };
 R_Date("WSU-4524", 1570, 70)
 {
 Outlier("General", 0.05);
 };
 R_Date("WSU-4523", 1220, 70)
 {
 Outlier("General", 0.05);
 };
 R_Date("Beta-223302", 860, 40)
 {
 Outlier("General", 0.05);
 };
 R_Date("Beta-340993", 810, 30)
 {
 Outlier("General", 0.05);
 };
};
};
Boundary("End of CZ-1");
};
};
```

2.1.9. Ushki, Kamchatka (Russia)

Ushki-1 and -5 (at approximately 56.206208, 159.994846) are archaeological sites containing two, stratified Paleoindian components—7 and 6[53]. Component 7 relates to the Nenana complex, whilst Component 6 has affinities with the Siberian Diuktai[52] culture and Denali. Dates obtained provide stratigraphic control or date cultural features directly, e.g., hearth charcoal. Using these data, the model created places the start of Component 7 at 13,435-12,855 cal BP (Fig. S9).



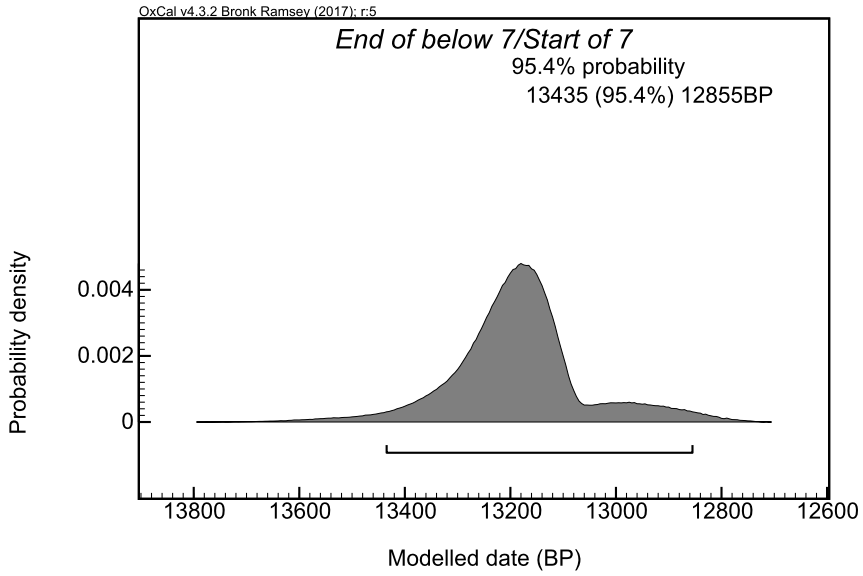


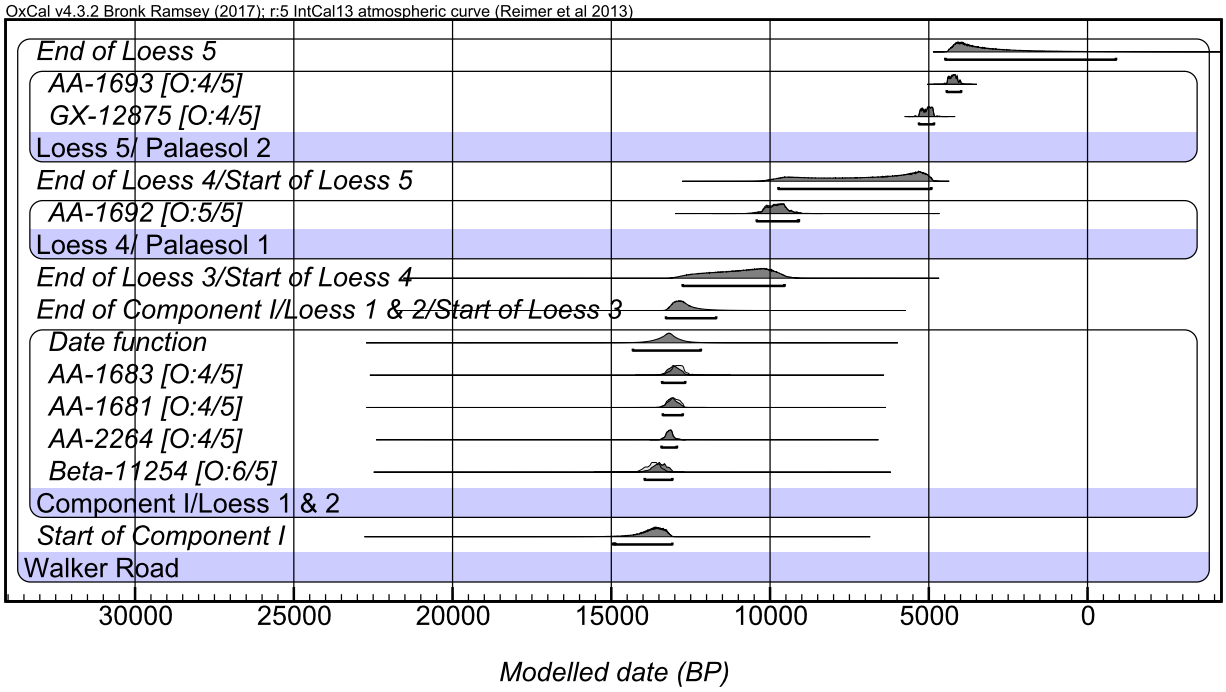
Fig. S9. Bayesian age model for Ushki (above), and start `Boundary` (below).

```
Plot()
 {
 Outlier_Model("General",T(5),U(0,4),"t");
Sequence("Ushki")
 {
 Boundary("Start of below Component 7");
 Phase("below Component 7")
 {
 R_Date("AA-45718", 11820, 100)
 {
 Outlier("General", 0.05);
 };
 R_Date("AA-45712", 11200, 160)
 {
 Outlier("General", 0.05);
 };
 R_Date("AA-45711", 11870, 90)
 {
 Outlier("General", 0.05);
 };
 };
```

```
Boundary("End of below 7/Start of 7");
Phase("Component 7")
{
 R_Date("AA-45716", 11050, 75)
 {
  Outlier("General", 0.05);
 };
 R_Date("AA-45710", 10675, 75)
 {
  Outlier("General", 0.05);
 };
 R_Date("AA-45708", 10810, 75)
 {
  Outlier("General", 0.05);
 };
 R_Date("AA-45709", 10850, 320)
 {
  Outlier("General", 0.05);
 };
 R_Date("SR-5810/CAMS-74639", 11330, 50)
 {
  Outlier("General", 0.05);
 };
 R_Date("AA-1388", 11005, 115)
 {
  Outlier("General", 0.05);
 };
 R_Date("AA-41389", 11050, 75)
 {
  Outlier("General", 0.05);
 };
 Date("Date function");
};
Boundary("End of 7/Start of 6");
Phase("Component 6")
{
 R_Date("AA-45720", 10230, 70)
 {
  Outlier("General", 0.05);
 };
 R_Date("AA-45719", 10385, 90)
 {
  Outlier("General", 0.05);
 };
 R_Date("AA-45717", 11130, 100)
 {
  Outlier("General", 0.05);
 };
 R_Date("AA-45713", 10040, 130)
 {
  Outlier("General", 0.05);
 };
 R_Date("AA-45715", 10160, 75)
 {
  Outlier("General", 0.05);
 };
 R_Date("AA-45714", 10800, 175)
 {
  Outlier("General", 0.05);
 };
 R_Date("SR-5811/CAMS-74640", 10460, 80)
 {
  Outlier("General", 0.05);
 };
 R_Date("AA-41386", 10240, 75)
 {
  Outlier("General", 0.05);
 };
 R_Date("AA-41387", 9485, 275)
 {
  Outlier("General", 0.05);
 };
};
Boundary("End of 6");
};
};
```

2.1.10. Walker Road, Alaska (U.S.A.)

Walker Road (HEA-130; at 63.966667, -149.083333) is a stratified site containing two cultural components, I and II. Based on lithic technology and antiquity, Component I has been assigned to the Nenana complex, whilst II is late Holocene[26,28,30,54]. Dates obtained provide stratigraphic control or date cultural features directly, e.g., hearth charcoal. Using these data, the model created places the start of Component I at 14,950-13,075 cal BP (Fig. S10).



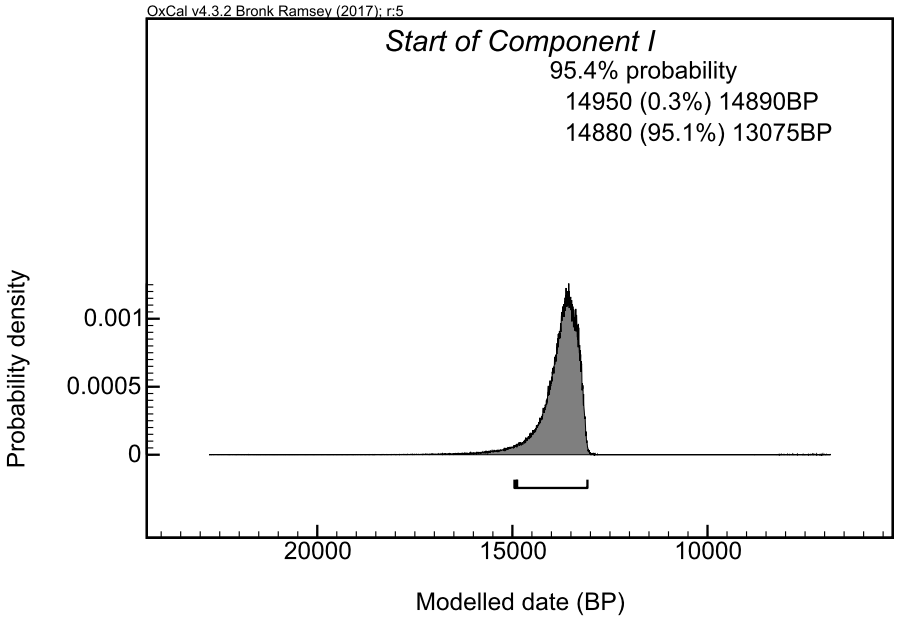


Fig. S10. Bayesian age model for Walker Road (above), and start `Boundary` (below).

```
Plot()
 {
 Outlier_Model("General",T(5),U(0,4),"t");
 Sequence("Walker Road")
  {
  Boundary("Start of Component I");
  Phase("Component I/Loess 1 & 2")
   {
   R_Date("Beta-11254", 11820, 200)
    {
    Outlier("General", 0.05);
    };
   R_Date("AA-2264", 11300, 120)
    {
    Outlier("General", 0.05);
    };
   R_Date("AA-1681", 11170, 180)
    {
    Outlier("General", 0.05);
    };
   R_Date("AA-1683", 11010, 230)
    {
    Outlier("General", 0.05);
    };
   Date("Date function");
   };
  Boundary("End of Component I/Loess 1 & 2/Start of Loess 3");
  Boundary("End of Loess 3/Start of Loess 4");
  Phase("Loess 4/ Palaesol 1")
  {
  R_Date("AA-1692", 8720, 250)
   {
   Outlier("General", 0.05);
   };
  };
  Boundary("End of Loess 4/Start of Loess 5");
```

```
 Phase("Loess 5/ Palaesol 2")
 {
 R_Date("GX-12875", 4415, 95)
  {
  Outlier("General", 0.05);
  };
 R_Date("AA-1693", 3816, 79)
  {
  Outlier("General", 0.05);
  };
 };
 Boundary("End of Loess 5");
};
};
```

2.2. Clovis tradition

2.2.1. Anzick, Montana (U.S.A.)

Anzick site (24PA506; at approximately 45.977128, -110.660209) contains the partial remains of a human individual (Anzick-1) with associated, and temporally coeval, Clovis osseous and lithic tool technology [5,55–62]. Although multiple dates have been obtained for the burial, HYP ages for Anzick-1 and the two Clovis antler rods are considered most reliable[62]. The incorporation of these into a single `Phase` model dates the Clovis component to 13,175-12,485 cal BP (`Date` function; Fig. S11).

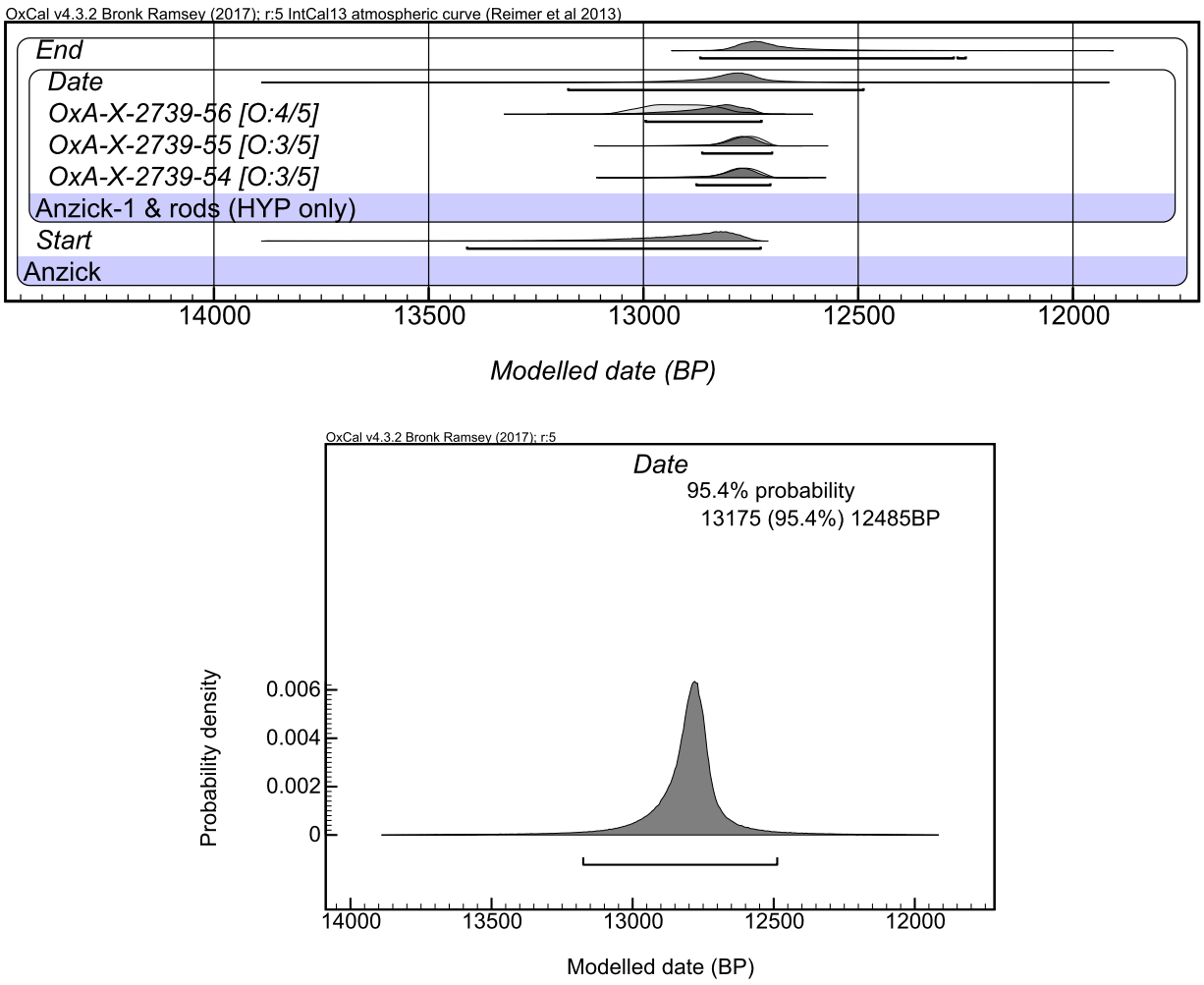


Fig. S11. Bayesian age model for Anzick (above), and `Date` function (below).

```
Sequence("Anzick")
{
 Outlier_Model("General",T(5),U(0,4),"t");
 Boundary("Start");
 Phase("Anzick-1 & rods (HYP only)")
 {
 R_Date("OxA-X-2739-54", 10915, 50)
  {
  Outlier("General", 0.05);
  };
 R_Date("OxA-X-2739-55", 10900, 50)
  {
  Outlier("General", 0.05);
  };
 R_Date("OxA-X-2739-56", 11050, 55)
  {
  Outlier("General", 0.05);
  };
 Date("Date");
 };
 Boundary("End");
};
```

2.2.2. Aubrey, Texas (U.S.A.)

Aubrey (41DN479; at approximately 33.353936, -97.087474) is a multi-cluster (e.g., Camp B and pond), stratified (units A-K) site containing Clovis lithic technology, hearths, and a well[63,64]. The Clovis component is found between units D and E. At Camp B, the Clovis occupation is dated by two charcoal dates from a hearth (AA-5271 and AA-5274) and further extrapolated from a dated pond deposit. Although both Camp B and the pond were modeled (see CQL code

below), only the PDF belonging to the start of the Clovis camp (surface of unit A2) was incorporated into large-scale models, as the extrapolation introduces unnecessary uncertainty. The model created places the start of the Clovis component at 14,750-13,245 cal BP (Fig. S12).

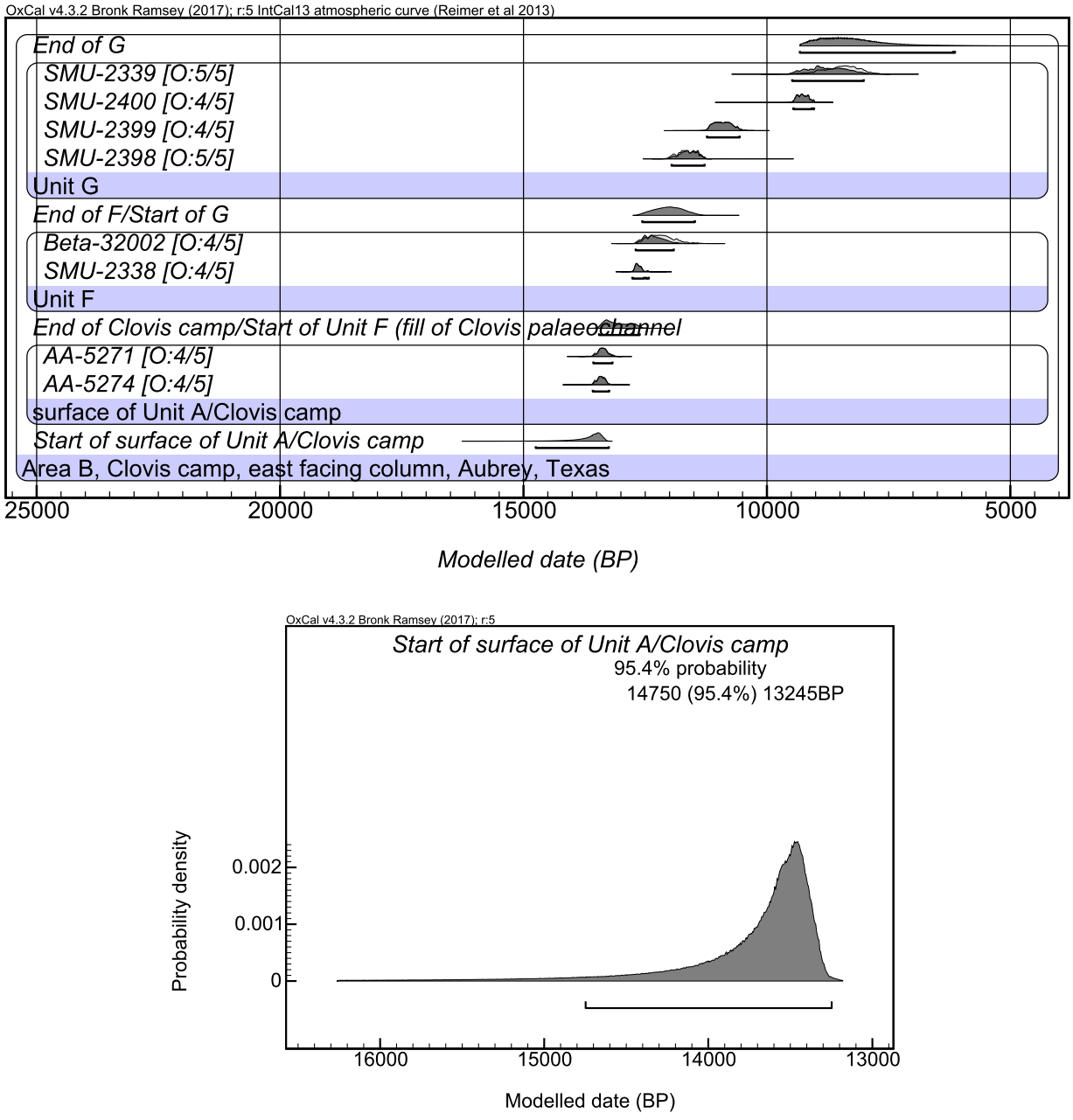


Fig. S12. Bayesian age model for Aubrey (Clovis camp; above), and start `Boundary` (below).

```
Plot()
 {
 Outlier_Model("General",T(5),U(0,4),"t");
 Sequence("Area B, Clovis camp, east facing column, Aubrey, Texas")
  {
  Boundary("Start of surface of Unit A/Clovis camp");
  Phase("surface of Unit A/Clovis camp")
   {
   R_Date("AA-5274", 11590, 93)
    {
    Outlier("General", 0.05);
    };
   R_Date("AA-5271", 11542, 111)
    {
    Outlier("General", 0.05);
    };
   };
 };
```

```
 Boundary("End of Clovis camp/Start of Unit F (fill of Clovis palaeochannel");
 Phase("Unit F")
 {
  R_Date("SMU-2338", 10718, 90)
  {
   Outlier("General", 0.05);
  };
  R_Date("Beta-32002", 10360, 150)
  {
   Outlier("General", 0.05);
  };
 };
 Boundary("End of F/Start of G");
 Phase("Unit G")
 {
  R_Date("SMU-2398", 10084, 80)
  {
   Outlier("General", 0.05);
  };
  R_Date("SMU-2399", 9572, 130)
  {
   Outlier("General", 0.05);
  };
  R_Date("SMU-2400", 8275, 70)
  {
   Outlier("General", 0.05);
  };
  R_Date("SMU-2339", 7582, 320)
  {
   Outlier("General", 0.05);
  };
 };
 Boundary("End of G");
 };
};

Plot()
{
 Outlier_Model("General",T(5),U(0,4),"t");
 Sequence("Area A pond, west facing column, Aubrey, Texas")
 {
  Boundary("Start of B");
  Sequence("Unit B")
  {
   Phase("B1")
   {
    R_Date("SMU-2236", 14202, 220)
    {
     Outlier("General", 0.05);
    };
    R_Date("SMU-2304", 13569, 400)
    {
     Outlier("General", 0.05);
    };
   };
   Phase("B2")
   {
    R_Date("SMU-2303", 13575, 100)
    {
     Outlier("General", 0.05);
    };
    R_Date("SMU-2302", 13665, 170)
    {
     Outlier("General", 0.05);
    };
    R_Date("SMU-2202", 13344, 410)
    {
     Outlier("General", 0.05);
    };
    R_Date("SMU-2305", 13263, 105)
    {
     Outlier("General", 0.05);
    };
   };
  };
  Boundary("End of B/Start of C");
  Phase("Unit C")
  {
   R_Date("SMU-2478", 12334, 170)
   {
    Outlier("General", 0.05);
   };
  };
  Boundary("End of C/Start of D");
  Boundary("End of D/Start of E");
  Phase("Unit E")
  {
   R_Date("SMU-2194", 10937, 80)
   {
    Outlier("General", 0.05);
   };
   R_Date("SMU-2406", 10390, 80)
   {
    Outlier("General", 0.05);
   };
  };
  Boundary("End of E");
 };
};
```

2.2.3. Blackwater Locality No. 1, New Mexico (U.S.A.)

Blackwater Locality No. 1 (29RV2; at 34.276686, -103.322134), the type-site for Clovis, is a stratified (units A-G) site containing Clovis, Folsom, Midland, and Agate Basin material, as well as evidence for mammoth butchering[65–69]. The Clovis component is found within Unit C. Although no bone dates exist (the first author attempted to extract collagen from one human-modified bone sample without success), the geochronology at the site is well established[65,66].

Using these data, the model created places the start of the Clovis component at 13,440-12,675 cal BP (Fig. S13).

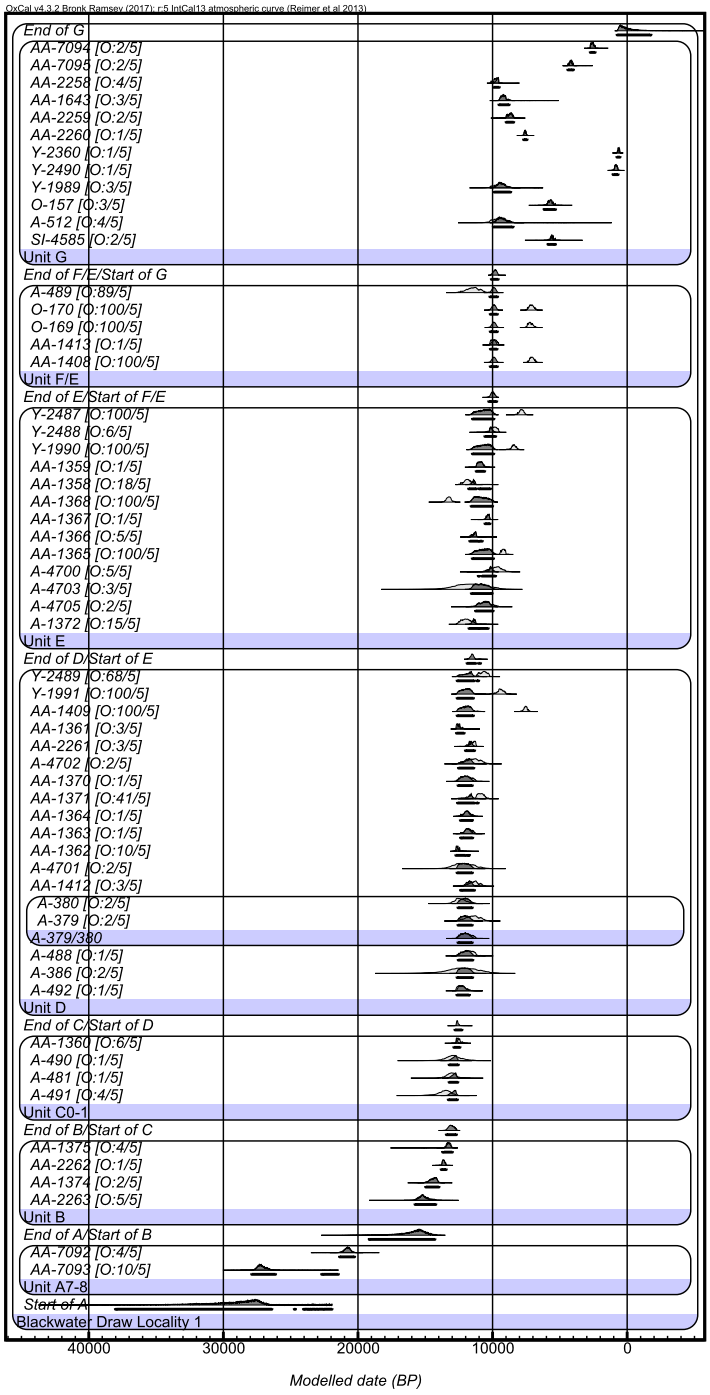


Fig. S13. Bayesian age model for Blackwater Locality No. 1 (above), and start `Boundary` (below).

```
Plot()
 {
 Outlier_Model("General",T(5),U(0,4),"t");
 Sequence("Blackwater Draw Locality 1")
 {
 Boundary("Start of A");
 Phase("Unit A7-8")
 {
 R_Date("AA-7093", 22930, 290)
 {
 Outlier("General", 0.05);
 };
 R_Date("AA-7092", 17220, 170)
 {
 Outlier("General", 0.05);
 };
 };
 Boundary("End of A/Start of B");
 Phase("Unit B")
 {
 R_Date("AA-2263", 12790, 160)
 {
 Outlier("General", 0.05);
 };
 R_Date("AA-1374", 12330, 110)
 {
 Outlier("General", 0.05);
 };
 R_Date("AA-2262", 11810, 90)
 {
 Outlier("General", 0.05);
 };
 R_Date("AA-1375", 11380, 150)
 {
 Outlier("General", 0.05);
 };
 };
 Boundary("End of B/Start of C");
 Phase("Unit C0-1")
 {
 R_Date("A-491", 11630, 400)
 {
 Outlier("General", 0.05);
 };
 R_Date("A-481", 11170, 360)
 {
 Outlier("General", 0.05);
 };
 R_Date("A-490", 11040, 500)
 {
 Outlier("General", 0.05);
 };
 R_Date("AA-1360", 10580, 100)
 {
 Outlier("General", 0.05);
 };
 };
 Boundary("End of C/Start of D");
 Phase("Unit D")
 {
 R_Date("A-492", 10490, 200)
 {
 Outlier("General", 0.05);
 };
 R_Date("A-386", 10490, 900)
 {
 Outlier("General", 0.05);
 };
 R_Date("A-488", 10170, 260)
 {
 Outlier("General", 0.05);
 };
 R_Combine("A-379/380")
 {
  R_Date("A-379", 9900, 320)
  {
  Outlier("General", 0.05);
  };
  R_Date("A-380", 10600, 320)
  {
  Outlier("General", 0.05);
  };
 };
 R_Date("AA-1412", 9860, 210)
 {
 Outlier("General", 0.05);
 };
 R_Date("A-4701", 10470, 580)
 {
 Outlier("General", 0.05);
 };
 R_Date("AA-1362", 10740, 100)
 {
 Outlier("General", 0.05);
 };
 R_Date("AA-1363", 10160, 120)
 {
 Outlier("General", 0.05);
 };
 R_Date("AA-1364", 10210, 110)
 {
 Outlier("General", 0.05);
 };
 R_Date("AA-1371", 9560, 180)
 {
 Outlier("General", 0.05);
 };
 R_Date("AA-1370", 10260, 230)
 {
 Outlier("General", 0.05);
 };
 R_Date("A-4702", 9870, 320)
 {
 Outlier("General", 0.05);
 };
 R_Date("AA-2261", 9950, 100)
 {
 Outlier("General", 0.05);
 };
 R_Date("AA-1361", 10640, 110)
 {
 Outlier("General", 0.05);
 };
 R_Date("AA-1409", 6660, 160)
 {
 Outlier("General", 0.05);
 };
 R_Date("Y-1991", 8430, 200)
 {
 Outlier("General", 0.05);
 };
 R_Date("Y-2489", 9400, 200)
 {
 Outlier("General", 0.05);
 };
 };
 Boundary("End of D/Start of E");
 Phase("Unit E")
 {
 R_Date("A-1372", 10250, 200)
 {
 Outlier("General", 0.05);
 };
 R_Date("A-4705", 9296, 320)
 {
 Outlier("General", 0.05);
```

```
};
R_Date("A-4703", 10000, 910)
{
 Outlier("General", 0.05);
};
R_Date("A-4700", 8630, 310)
{
 Outlier("General", 0.05);
};
R_Date("AA-1365", 8230, 100)
{
 Outlier("General", 0.05);
};
R_Date("AA-1366", 9890, 100)
{
 Outlier("General", 0.05);
};
R_Date("AA-1367", 9150, 90)
{
 Outlier("General", 0.05);
};
R_Date("AA-1368", 11400, 190)
{
 Outlier("General", 0.05);
};
R_Date("AA-1358", 10190, 130)
{
 Outlier("General", 0.05);
};
R_Date("AA-1359", 9590, 120)
{
 Outlier("General", 0.05);
};
R_Date("Y-1990", 7610, 160)
{
 Outlier("General", 0.05);
};
R_Date("Y-2488", 8830, 160)
{
 Outlier("General", 0.05);
};
R_Date("Y-2487", 7020, 180)
{
 Outlier("General", 0.05);
};
};
Boundary("End of E/Start of F/E");
Phase("Unit F/E")
{
R_Date("AA-1408", 6190, 130)
{
 Outlier("General", 0.05);
};
R_Date("AA-1413", 8830, 120)
{
 Outlier("General", 0.05);
};
R_Date("O-169", 6300, 150)
{
 Outlier("General", 0.05);
};
R_Date("O-170", 6230, 150)
{
 Outlier("General", 0.05);
};
R_Date("A-489", 9890, 290)
{
 Outlier("General", 0.05);
};
};
Boundary("End of F/E/Start of G");
Phase("Unit G")
{
R_Date("SI-4585", 4855, 90)
{
 Outlier("General", 0.05);
};
R_Date("A-512", 8470, 350)
{
 Outlier("General", 0.05);
};
R_Date("O-157", 4950, 150)
{
 Outlier("General", 0.05);
};
R_Date("Y-1989", 8450, 280)
{
 Outlier("General", 0.05);
};
R_Date("Y-2490", 910, 100)
{
 Outlier("General", 0.05);
};
R_Date("Y-2360", 680, 80)
{
 Outlier("General", 0.05);
};
R_Date("AA-2260", 6720, 80)
{
 Outlier("General", 0.05);
};
R_Date("AA-2259", 7850, 110)
{
 Outlier("General", 0.05);
};
R_Date("AA-1643", 8230, 140)
{
 Outlier("General", 0.05);
};
R_Date("AA-2258", 8730, 90)
{
 Outlier("General", 0.05);
};
R_Date("AA-7095", 3800, 60)
{
 Outlier("General", 0.05);
};
R_Date("AA-7094", 2500, 60)
{
 Outlier("General", 0.05);
};
};
Boundary("End of G");
};
};
```

2.2.4. Cactus Hill, Virginia (U.S.A.)

Cactus Hill (44SX202; at approximately 36.986668, -77.322360) is a multi-cluster, stratified (levels 1-7) archaeological site containing pre-Clovis and Clovis, Archaic, Woodland, and

historic material[70–75]. Optically-stimulated luminescence (OSL) and radiocarbon dating methods have been used to date the deposits[71], providing stratigraphic control. Using these data, the model created places the start of the pre-Clovis component at 20,585-18,970 cal BP, and the start of Clovis at 13,605-11,390 cal BP (Fig. S14).

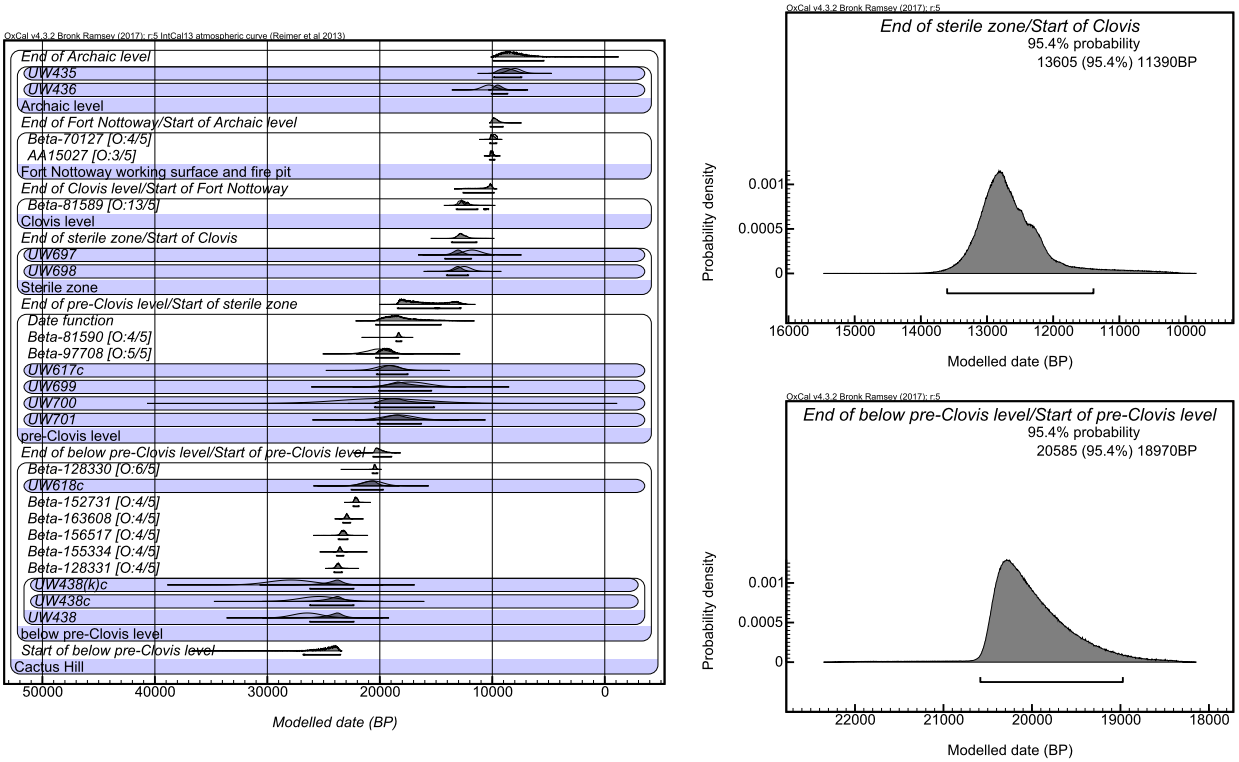


Fig. S14. Bayesian age model for Cactus Hill (above), and start boundaries for both pre-Clovis and Clovis components (adjacent).

```
Plot()
{
 Outlier_Model("General",T(5),U(0,4),"t");
Sequence("Cactus Hill")
 {
 Boundary("Start of below pre-Clovis level");
 Phase("below pre-Clovis level")
 {
 Combine("UW438")
 {
 Age("UW438c", N(25400, 1700))
  {
  Outlier("General", 0.05);
 };
 Age("UW438(k)c", N(27900, 2000))
  {
  Outlier("General", 0.05);
 };
};
 R_Date("Beta-128331", 19700, 130)
 {
 Outlier("General", 0.05);
};
 R_Date("Beta-155334", 19540, 70)
 {
 Outlier("General", 0.05);
};
 R_Date("Beta-156517", 19310, 150)
 {
 Outlier("General", 0.05);
};
 R_Date("Beta-163608", 19050, 80)
 {
 Outlier("General", 0.05);
};
 R_Date("Beta-152731", 18250, 80)
 {
 Outlier("General", 0.05);
};
 Age("UW618c", N(20600, 900))
 {
 Outlier("General", 0.05);
};
```

```
 R_Date("Beta-128330", 16940, 50)
 {
  Outlier("General", 0.05);
 };
};
Boundary("End of below pre-Clovis level/Start of pre-Clovis level");
Phase("pre-Clovis level")
{
 Age("UW701", N(18300, 1400))
 {
  Outlier("General", 0.05);
 };
 Age("UW700", N(19800, 3800))
 {
  Outlier("General", 0.05);
 };
 Age("UW699", N(17300, 1600))
 {
  Outlier("General", 0.05);
 };
 Age("UW617c", N(19300, 1000))
 {
  Outlier("General", 0.05);
 };
 R_Date("Beta-97708", 16670, 730)
 {
  Outlier("General", 0.05);
 };
 R_Date("Beta-81590", 15070, 70)
 {
  Outlier("General", 0.05);
 };
 Date("Date function");
};
Boundary("End of pre-Clovis level/Start of sterile zone");
Phase("Sterile zone")
{
 Age("UW698", N(12500, 600))
 {
  Outlier("General", 0.05);
 };
 Age("UW697", N(11800, 800))
 {
  Outlier("General", 0.05);
 };
};
Boundary("End of sterile zone/Start of Clovis");
Phase("Clovis level")
{
 R_Date("Beta-81589", 10920, 250)
 {
  Outlier("General", 0.05);
 };
};
Boundary("End of Clovis level/Start of Fort Nottoway");
Phase("Fort Nottoway working surface and fire pit")
{
 R_Date("AA15027", 8920, 65)
 {
  Outlier("General", 0.05);
 };
 R_Date("Beta-70127", 8800, 120)
 {
  Outlier("General", 0.05);
 };
};
Boundary("End of Fort Nottoway/Start of Archaic level");
Phase("Archaic level")
{
 Age("UW436", N(10300, 600))
 {
  Outlier("General", 0.05);
 };
 Age("UW435", N(8000, 600))
 {
  Outlier("General", 0.05);
 };
};
Boundary("End of Archaic level");
};
};
```

2.2.5. Colby, Wyoming (U.S.A.)

Colby (48WA322; at approximately 44.020499, -107.854297) is a Clovis, mammoth-butchering site with associated lithic tool technology[5,76,77]. The incorporation of two XAD bone dates (UCIAMS-11342 and UCIAMS-11343) into a single `Phase`, dates the archaeological event to 13,165-12,350 cal BP (`Date` function; Fig. S15).

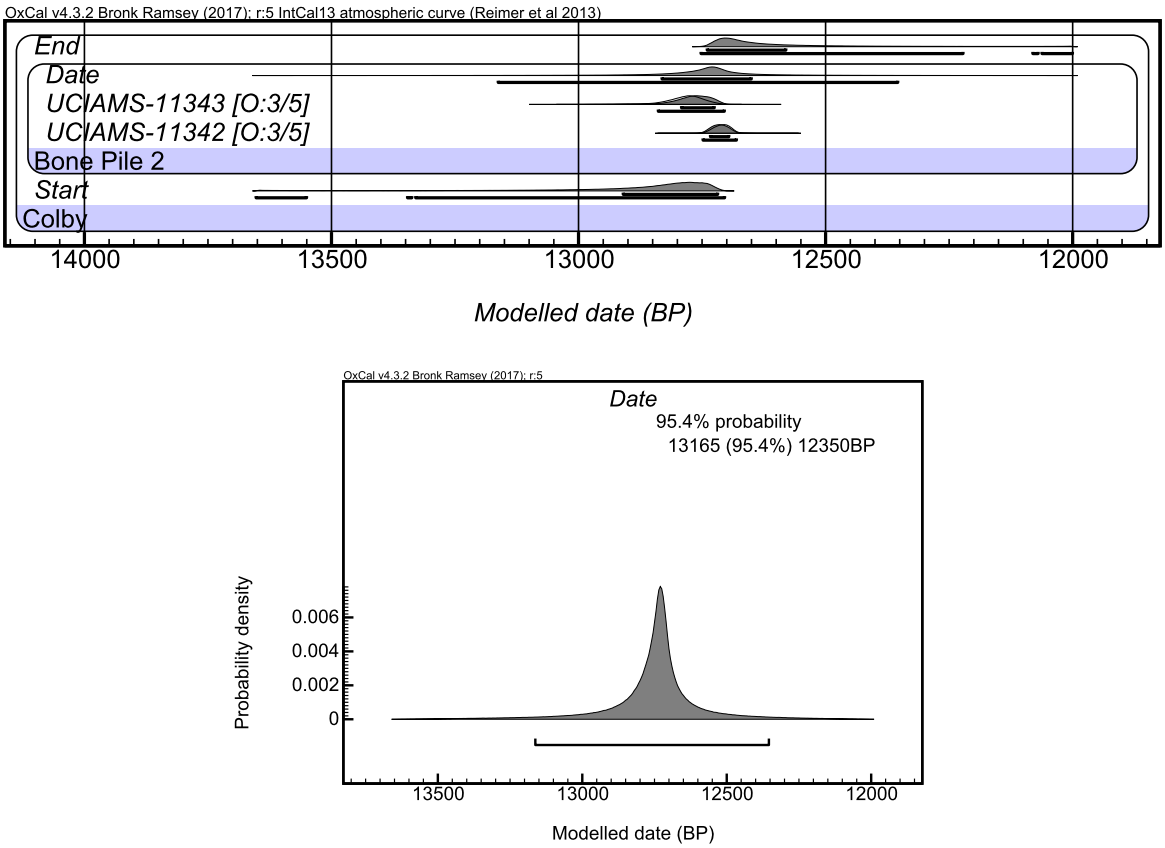


Fig. S15. Bayesian age model for Colby (above), and `Date` function (below).

```
Sequence("Colby")
{
 Outlier_Model("General",T(5),U(0,4),"t");
 Boundary("Start");
 Phase("Bone Pile 2")
 {
  R_Date("UCIAMS-11342", 10790, 30)
  {
   Outlier("General", 0.05);
  };
  R_Date("UCIAMS-11343", 10950, 30)
  {
   Outlier("General", 0.05);
  };
  Date("Date");
 };
 Boundary("End");
};
```

2.2.6. Debra L. Friedkin, Texas (U.S.A.)

The Debra L. Friedkin site (41BL1239; at approximately 30.892283, -97.709742) is a stratified, multicomponent site (blocks A and B) containing pre-Clovis ("Buttermilk complex"; but see ref[78]), Clovis, Folsom, late Paleoindian, and Archaic material[79–82]. OSL has been used to date the deposits. Using the latest chronometric evidence[82], the model created places the start of the Buttermilk complex at 16,330-14,690 cal BP, and the start of Clovis at 14,755-13,120 cal BP (Fig. S16). This includes dates within "Boundary Date" categories in preceding phases. If

incorporated in succeeding phases, the same date to 17,495-15,275 and 14,960-13,295 cal BP, correspondingly. CQL code for both models are provided below.

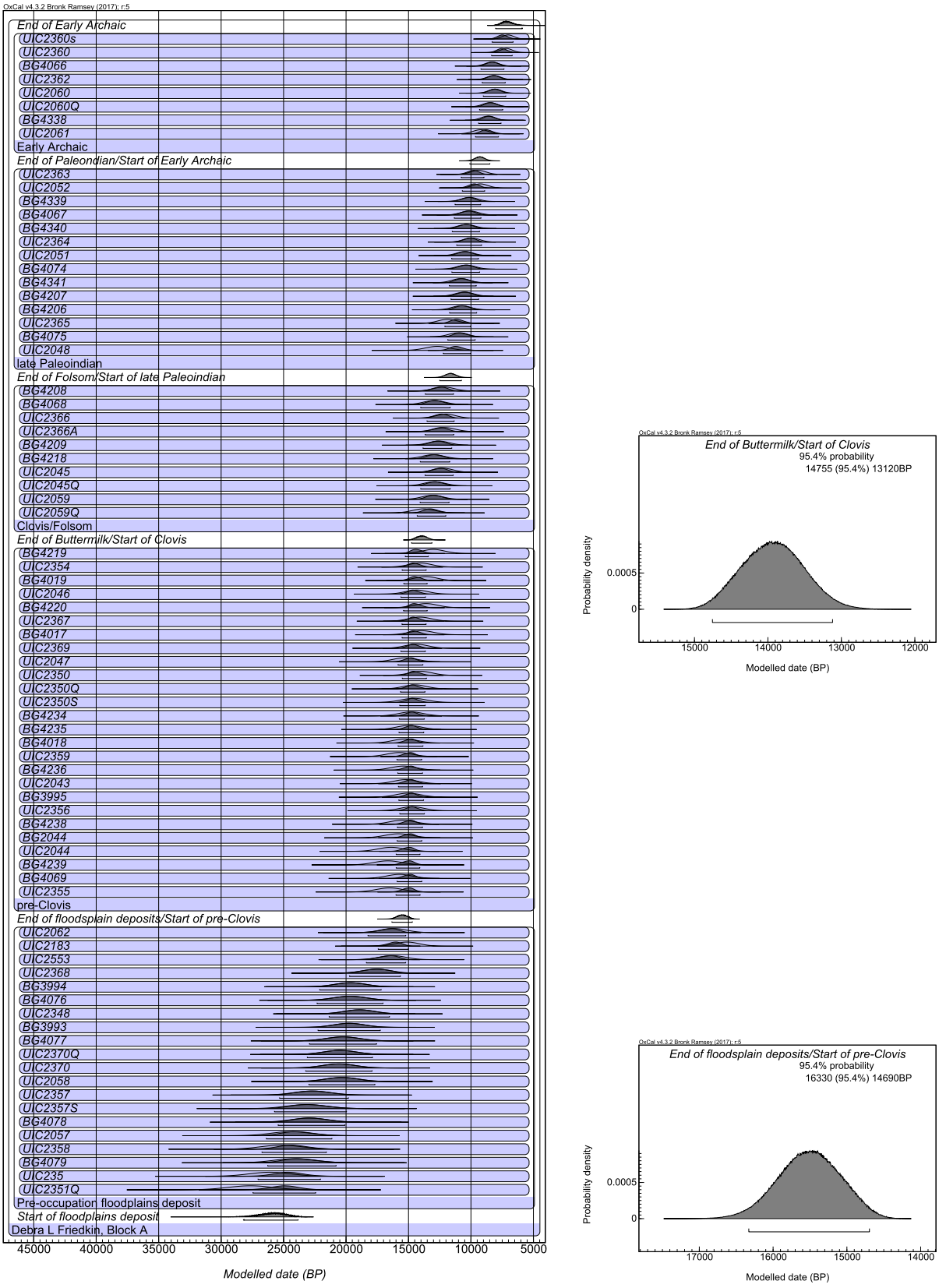


Fig. S16. Bayesian age model for Debra L. Friedkin (above), and start boundaries for both pre-Clovis and Clovis components (adjacent).

```
Plot()
 {
 Outlier_Model("General",T(5),U(0,4),"t");
 Sequence("Debra L Friedkin, Block A, dates in Boundary Date in preceding phases")
  {
  Boundary("Start of floodplains deposit");
  Phase("Pre-occupation floodplains deposit")
   {
   Age("UIC2351Q", N(27650, 1800))
    {
    Outlier("General", 0.05);
    };
   Age("UIC235", N(26090, 1670))
    {
    Outlier("General", 0.05);
    };
   Age("BG4079", N(24145, 1635))
    {
    Outlier("General", 0.05);
    };
   Age("UIC2358", N(25185, 1640))
    {
    Outlier("General", 0.05);
    };
   Age("UIC2057", N(24420, 1580))
    {
    Outlier("General", 0.05);
    };
   Age("BG4078", N(22950, 1445))
    {
    Outlier("General", 0.05);
    };
   Age("UIC2357S", N(23150, 1600))
    {
    Outlier("General", 0.05);
    };
   Age("UIC2357", N(22710, 1450))
    {
    Outlier("General", 0.05);
    };
   Age("UIC2058", N(20330, 1320))
    {
    Outlier("General", 0.05);
    };
   Age("UIC2370", N(20565, 1325))
    {
    Outlier("General", 0.05);
    };
   Age("UIC2370Q", N(20490, 1305))
    {
    Outlier("General", 0.05);
    };
   Age("BG4077", N(20250, 1340))
    {
    Outlier("General", 0.05);
    };
   Age("BG3993", N(19750, 1245))
    {
    Outlier("General", 0.05);
    };
   Age("UIC2348", N(18930, 1210))
    {
    Outlier("General", 0.05);
    };
   Age("BG4076", N(19680, 1320))
    {
    Outlier("General", 0.05);
    };
   Age("BG3994", N(19650, 1230))
    {
    Outlier("General", 0.05);
    };
   Age("UIC2368", N(17530, 1140))
    {
    Outlier("General", 0.05);
    };
   Age("UIC2553", N(16270, 1040))
    {
    Outlier("General", 0.05);
    };
   Age("UIC2183", N(15110, 960))
    {
    Outlier("General", 0.05);
    };
   Age("UIC2062", N(16170, 1030))
    {
    Outlier("General", 0.05);
    };
   };
  Boundary("End of floodsplain deposits/Start of pre-Clovis");
  Phase("pre-Clovis")
   {
   Age("UIC2355", N(16515, 1075))
    {
    Outlier("General", 0.05);
    };
   Age("BG4069", N(15725, 1030))
    {
    Outlier("General", 0.05);
    };
   Age("BG4239", N(16650, 1110))
    {
    Outlier("General", 0.05);
    };
   Age("UIC2044", N(16400, 1040))
    {
    Outlier("General", 0.05);
    };
   Age("BG2044", N(15800, 1080))
    {
    Outlier("General", 0.05);
    };
   Age("BG4238", N(15500, 1020))
    {
    Outlier("General", 0.05);
    };
   Age("UIC2356", N(14710, 940))
    {
    Outlier("General", 0.05);
    };
   Age("BG3995", N(15020, 1010))
    {
    Outlier("General", 0.05);
    };
   Age("UIC2043", N(15210, 960))
    {
    Outlier("General", 0.05);
    };
   Age("BG4236", N(15400, 1015))
    {
    Outlier("General", 0.05);
    };
   Age("UIC2359", N(15730, 1010))
    {
    Outlier("General", 0.05);
    };
   Age("BG4018", N(15265, 1000))
    {
    Outlier("General", 0.05);
    };
   Age("BG4235", N(14965, 985))
    {
    Outlier("General", 0.05);
    };
   Age("BG4234", N(14790, 985))
    {
```

```
 Outlier("General", 0.05);
 };
 Age("UIC2350S", N(14580, 1030))
 {
 Outlier("General", 0.05);
 };
 Age("UIC2350Q", N(14480, 920))
 {
 Outlier("General", 0.05);
 };
 Age("UIC2350", N(14000, 890))
 {
 Outlier("General", 0.05);
 };
 Age("UIC2047", N(15270, 960))
 {
 Outlier("General", 0.05);
 };
 Age("UIC2369", N(14370, 930))
 {
 Outlier("General", 0.05);
 };
 Age("BG4017", N(13960, 965))
 {
 Outlier("General", 0.05);
 };
 Age("UIC2367", N(14080, 920))
 {
 Outlier("General", 0.05);
 };
 Age("BG4220", N(13595, 930))
 {
 Outlier("General", 0.05);
 };
 Age("UIC2046", N(14350, 910))
 {
 Outlier("General", 0.05);
 };
 Age("BG4019", N(13620, 880))
 {
 Outlier("General", 0.05);
 };
 Age("UIC2354", N(14070, 910))
 {
 Outlier("General", 0.05);
 };
 Age("BG4219", N(13010, 905))
 {
 Outlier("General", 0.05);
 };
};
Boundary("End of Buttermilk/Start of Clovis");
Phase("Clovis/Folsom")
{
 Age("UIC2059Q", N(13780, 885))
 {
 Outlier("General", 0.05);
 };
 Age("UIC2059", N(13090, 830))
 {
 Outlier("General", 0.05);
 };
 Age("UIC2045Q", N(12925, 845))
 {
 Outlier("General", 0.05);
 };
 Age("UIC2045", N(12240, 800))
 {
 Outlier("General", 0.05);
 };
 Age("BG4218", N(13020, 870))
 {
 Outlier("General", 0.05);
 };
 Age("BG4209", N(12560, 830))
 {
 Outlier("General", 0.05);
 };
 Age("UIC2366A", N(12100, 860))
 {
 Outlier("General", 0.05);
 };
 Age("UIC2366", N(12000, 770))
 {
 Outlier("General", 0.05);
 };
 Age("BG4068", N(12940, 855))
 {
 Outlier("General", 0.05);
 };
 Age("BG4208", N(12170, 820))
 {
 Outlier("General", 0.05);
 };
};
Boundary("End of Folsom/Start of late Paleoindian");
Phase("late Paleoindian")
{
 Age("UIC2048", N(12690, 955))
 {
 Outlier("General", 0.05);
 };
 Age("BG4075", N(11060, 735))
 {
 Outlier("General", 0.05);
 };
 Age("UIC2365", N(11870, 760))
 {
 Outlier("General", 0.05);
 };
 Age("BG4206", N(10785, 715))
 {
 Outlier("General", 0.05);
 };
 Age("BG4207", N(10530, 750))
 {
 Outlier("General", 0.05);
 };
 Age("BG4341", N(10830, 695))
 {
 Outlier("General", 0.05);
 };
 Age("BG4074", N(10375, 740))
 {
 Outlier("General", 0.05);
 };
 Age("UIC2051", N(10480, 675))
 {
 Outlier("General", 0.05);
 };
 Age("UIC2364", N(9930, 640))
 {
 Outlier("General", 0.05);
 };
 Age("BG4340", N(10360, 705))
 {
 Outlier("General", 0.05);
 };
 Age("BG4067", N(10100, 695))
 {
 Outlier("General", 0.05);
 };
 Age("BG4339", N(10095, 655))
 {
 Outlier("General", 0.05);
 };
```

```
 Age("UIC2052", N(9250, 600))
 {
 Outlier("General", 0.05);
 };
 Age("UIC2363", N(9405, 610))
 {
 Outlier("General", 0.05);
 };
};
Boundary("End of Paleondian/Start of Early Archaic");
Phase("Early Archaic")
{
Age("UIC2061", N(9215, 620))
 {
 Outlier("General", 0.05);
 };
 Age("BG4338", N(8655, 550))
 {
 Outlier("General", 0.05);
 };
 Age("UIC2060Q", N(8490, 560))
 {
 Outlier("General", 0.05);
 };
 Age("UIC2060", N(8070, 520))
 {
 Outlier("General", 0.05);
 };
 Age("UIC2362", N(8160, 540))
 {
 Outlier("General", 0.05);
 };
 Age("BG4066", N(8315, 540))
 {
 Outlier("General", 0.05);
 };
 Age("UIC2360", N(7160, 470))
 {
 Outlier("General", 0.05);
 };
 Age("UIC2360s", N(7030, 470))
 {
 Outlier("General", 0.05);
 };
};
Boundary("End of Early Archaic");
};
};

Plot()
{
 Outlier_Model("General",T(5),U(0,4),"t");
 Sequence("Debra L Friedkin, Block A, dates in Boundary Date in succeeding phases")
 {
 Boundary("Start of floodplains deposit");
 Phase("Pre-occupation floodplains deposit")
 {
 Age("UIC2351Q", N(27650, 1800))
 {
 Outlier("General", 0.05);
 };
 Age("UIC235", N(26090, 1670))
 {
 Outlier("General", 0.05);
 };
 Age("BG4079", N(24145, 1635))
 {
 Outlier("General", 0.05);
 };
 Age("UIC2358", N(25185, 1640))
 {
 Outlier("General", 0.05);
 };
 Age("UIC2057", N(24420, 1580))
 {
 Outlier("General", 0.05);
 };
 Age("BG4078", N(22950, 1445))
 {
 Outlier("General", 0.05);
 };
 Age("UIC2357S", N(23150, 1600))
 {
 Outlier("General", 0.05);
 };
 Age("UIC2357", N(22710, 1450))
 {
 Outlier("General", 0.05);
 };
 Age("UIC2058", N(20330, 1320))
 {
 Outlier("General", 0.05);
 };
 Age("UIC2370", N(20565, 1325))
 {
 Outlier("General", 0.05);
 };
 Age("UIC2370Q", N(20490, 1305))
 {
 Outlier("General", 0.05);
 };
 Age("BG4077", N(20250, 1340))
 {
 Outlier("General", 0.05);
 };
 Age("BG3993", N(19750, 1245))
 {
 Outlier("General", 0.05);
 };
 Age("UIC2348", N(18930, 1210))
 {
 Outlier("General", 0.05);
 };
 Age("BG4076", N(19680, 1320))
 {
 Outlier("General", 0.05);
 };
 Age("BG3994", N(19650, 1230))
 {
 Outlier("General", 0.05);
 };
};
 Boundary("End of floodsplain deposits/Start of pre-Clovis");
 Phase("pre-Clovis")
 {
 Age("UIC2368", N(17530, 1140))
 {
 Outlier("General", 0.05);
 };
 Age("UIC2553", N(16270, 1040))
 {
 Outlier("General", 0.05);
 };
 Age("UIC2183", N(15110, 960))
 {
 Outlier("General", 0.05);
 };
 Age("UIC2062", N(16170, 1030))
 {
 Outlier("General", 0.05);
 };
 Age("UIC2355", N(16515, 1075))
 {
 Outlier("General", 0.05);
 };
 Age("BG4069", N(15725, 1030))
```

```
 {
 Outlier("General", 0.05);
 };
 Age("BG4239", N(16650, 1110))
 {
 Outlier("General", 0.05);
 };
 Age("UIC2044", N(16400, 1040))
 {
 Outlier("General", 0.05);
 };
 Age("BG2044", N(15800, 1080))
 {
 Outlier("General", 0.05);
 };
 Age("BG4238", N(15500, 1020))
 {
 Outlier("General", 0.05);
 };
 Age("UIC2356", N(14710, 940))
 {
 Outlier("General", 0.05);
 };
 Age("BG3995", N(15020, 1010))
 {
 Outlier("General", 0.05);
 };
 Age("UIC2043", N(15210, 960))
 {
 Outlier("General", 0.05);
 };
 Age("BG4236", N(15400, 1015))
 {
 Outlier("General", 0.05);
 };
 Age("UIC2359", N(15730, 1010))
 {
 Outlier("General", 0.05);
 };
 Age("BG4018", N(15265, 1000))
 {
 Outlier("General", 0.05);
 };
 Age("BG4235", N(14965, 985))
 {
 Outlier("General", 0.05);
 };
 Age("BG4234", N(14790, 985))
 {
 Outlier("General", 0.05);
 };
 Age("UIC2350S", N(14580, 1030))
 {
 Outlier("General", 0.05);
 };
 Age("UIC2350Q", N(14480, 920))
 {
 Outlier("General", 0.05);
 };
 Age("UIC2350", N(14000, 890))
 {
 Outlier("General", 0.05);
 };
 Age("UIC2047", N(15270, 960))
 {
 Outlier("General", 0.05);
 };
 Age("UIC2369", N(14370, 930))
 {
 Outlier("General", 0.05);
 };
 Age("BG4017", N(13960, 965))
 {
 Outlier("General", 0.05);
 };
 Age("UIC2367", N(14080, 920))
 {
 Outlier("General", 0.05);
 };
 Age("BG4220", N(13595, 930))
 {
 Outlier("General", 0.05);
 };
};
Boundary("End of Buttermilk/Start of Clovis");
Phase("Clovis/Folsom")
{
 Age("UIC2046", N(14350, 910))
 {
 Outlier("General", 0.05);
 };
 Age("BG4019", N(13620, 880))
 {
 Outlier("General", 0.05);
 };
 Age("UIC2354", N(14070, 910))
 {
 Outlier("General", 0.05);
 };
 Age("BG4219", N(13010, 905))
 {
 Outlier("General", 0.05);
 };
 Age("UIC2059Q", N(13780, 885))
 {
 Outlier("General", 0.05);
 };
 Age("UIC2059", N(13090, 830))
 {
 Outlier("General", 0.05);
 };
 Age("UIC2045Q", N(12925, 845))
 {
 Outlier("General", 0.05);
 };
 Age("UIC2045", N(12240, 800))
 {
 Outlier("General", 0.05);
 };
 Age("BG4218", N(13020, 870))
 {
 Outlier("General", 0.05);
 };
 Age("BG4209", N(12560, 830))
 {
 Outlier("General", 0.05);
 };
 Age("UIC2366A", N(12100, 860))
 {
 Outlier("General", 0.05);
 };
 Age("UIC2366", N(12000, 770))
 {
 Outlier("General", 0.05);
 };
 Age("BG4068", N(12940, 855))
 {
 Outlier("General", 0.05);
 };
 Age("BG4208", N(12170, 820))
 {
 Outlier("General", 0.05);
 };
};
Boundary("End of Folsom/Start of late Paleoindian");
Phase("late Paleoindian")
```

```
 {
 Age("UIC2048", N(12690, 955))
 {
 Outlier("General", 0.05);
 };
 Age("BG4075", N(11060, 735))
 {
 Outlier("General", 0.05);
 };
 Age("UIC2365", N(11870, 760))
 {
 Outlier("General", 0.05);
 };
 Age("BG4206", N(10785, 715))
 {
 Outlier("General", 0.05);
 };
 Age("BG4207", N(10530, 750))
 {
 Outlier("General", 0.05);
 };
 Age("BG4341", N(10830, 695))
 {
 Outlier("General", 0.05);
 };
 Age("BG4074", N(10375, 740))
 {
 Outlier("General", 0.05);
 };
 Age("UIC2051", N(10480, 675))
 {
 Outlier("General", 0.05);
 };
 Age("UIC2364", N(9930, 640))
 {
 Outlier("General", 0.05);
 };
 Age("BG4340", N(10360, 705))
 {
 Outlier("General", 0.05);
 };
 Age("BG4067", N(10100, 695))
 {
 Outlier("General", 0.05);
 };
 Age("BG4339", N(10095, 655))
 {
 Outlier("General", 0.05);
 };
 Age("UIC2052", N(9250, 600))
 {
 Outlier("General", 0.05);
 };
 Age("UIC2363", N(9405, 610))
 {
 Outlier("General", 0.05);
 };
};
Boundary("End of Paleondian/Start of Early Archaic");
Phase("Early Archaic")
{
Age("UIC2061", N(9215, 620))
 {
 Outlier("General", 0.05);
 };
 Age("BG4338", N(8655, 550))
 {
 Outlier("General", 0.05);
 };
 Age("UIC2060Q", N(8490, 560))
 {
 Outlier("General", 0.05);
 };
 Age("UIC2060", N(8070, 520))
 {
 Outlier("General", 0.05);
 };
 Age("UIC2362", N(8160, 540))
 {
 Outlier("General", 0.05);
 };
 Age("BG4066", N(8315, 540))
 {
 Outlier("General", 0.05);
 };
 Age("UIC2360", N(7160, 470))
 {
 Outlier("General", 0.05);
 };
 Age("UIC2360s", N(7030, 470))
 {
 Outlier("General", 0.05);
 };
};
Boundary("End of Early Archaic");
};
};
```

2.2.7. Dent, Colorado (U.S.A.)

Dent (5WL269; at approximately 40.319080, -104.829562) is a Clovis, mammoth-butchering site with associated lithic tool technology[5,57,58,83–88]. Although multiple dates have been obtained for the site, two HYP dates (OxA-X-2736-11 and OxA-X-2736-12) produced from mammoth bone samples are considered most reliable[88]. The incorporation of these into a single `Phase` model dates the Clovis component to 13,545-12,415 cal BP (`Date` function; Fig. S17).

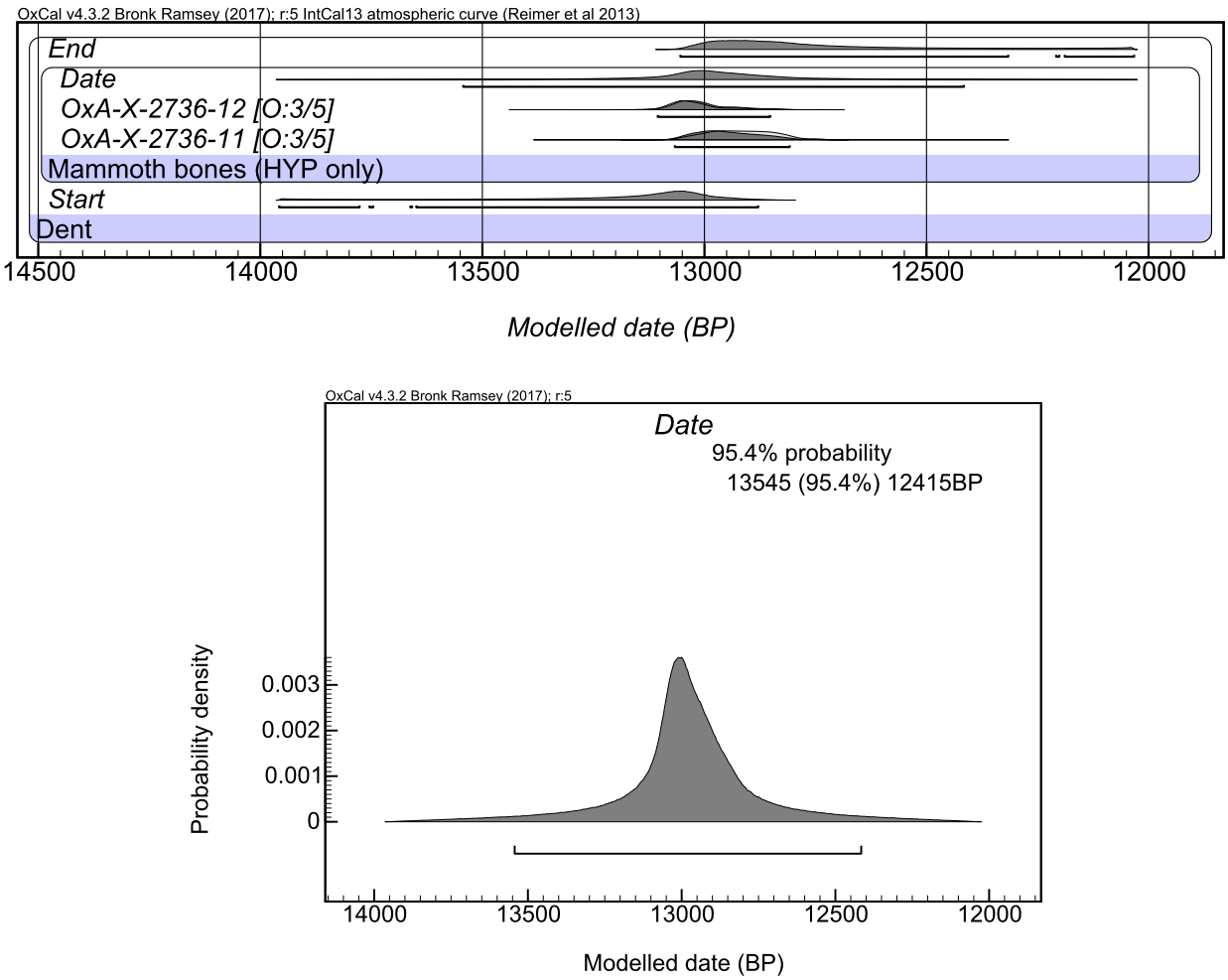


Fig. S17. Bayesian age model for Dent (above), and `Date` function (below).

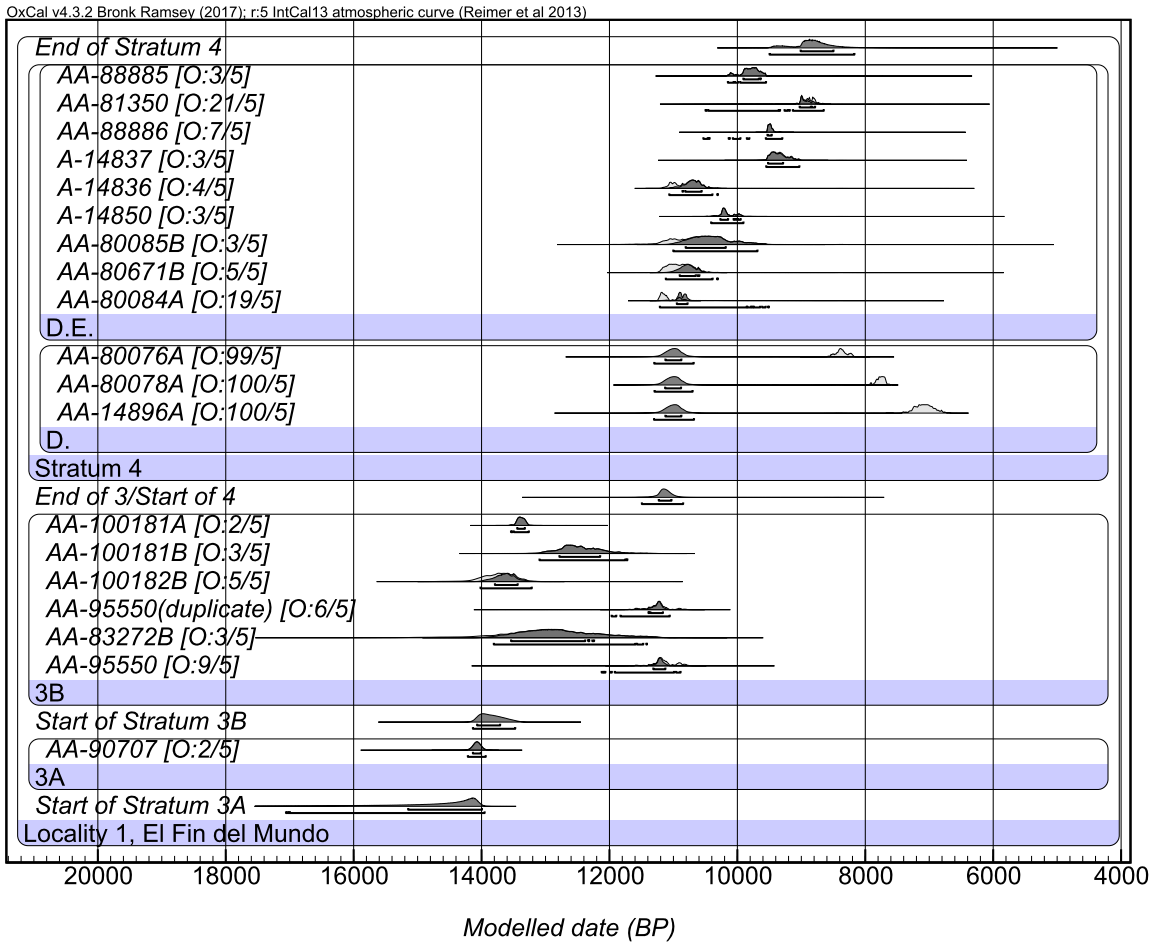
```
Sequence("Dent")
 {
 Outlier_Model("General",T(5),U(0,4),"t");
 Boundary("Start");
 Phase("Mammoth bones (HYP only)")
 {
 R_Date("OxA-X-2736-11", 11055, 50)
  {
  Outlier("General", 0.05);
  };
 R_Date("OxA-X-2736-12", 11155, 50)
  {
  Outlier("General", 0.05);
  };
 Date("Date");
 };
 Boundary("End");
};
```

2.2.8. Domebo, Oklahoma (U.S.A.)

Domebo (34CD50; at approximately 34.957529, -98.271482) is a Clovis, mammoth-butchering site with associated lithic tool technology[57,89,90]. Although multiple dates have been obtained for the site, an XAD date (UCIAMS-11341; 12,910-12,710 cal BP) produced from mammoth bone is considered the most reliable[5] and is here used.

2.2.9. El Fin del Mundo, Sonora (Mexico)

El Fin del Mundo (at approximately 29.733406, -111.760384) is a multi-cluster, stratified (units 2-4) site containing Clovis lithic technology and evidence for gomphothere butchering[91]. Within Locality 1, the Clovis component is found in stratum 3, member 3B. Although multiple dates have been obtained, "poor chronostratigraphic integrity best characterizes the sequence exposed"[91]. Regardless, Sanchez et al.[91] assign the age of the Clovis component to AA-100181B (11,550±60 BP), a date obtained from a charcoal fleck among the same level as lithic flakes (gomphothere bone was not directly dated due to poor collagen preservation). Using these data, the model created places the start of the Clovis component at 14,135-13,470 cal BP (Fig. S18). Further chronometric work is required to better define the chronology at this site, however.



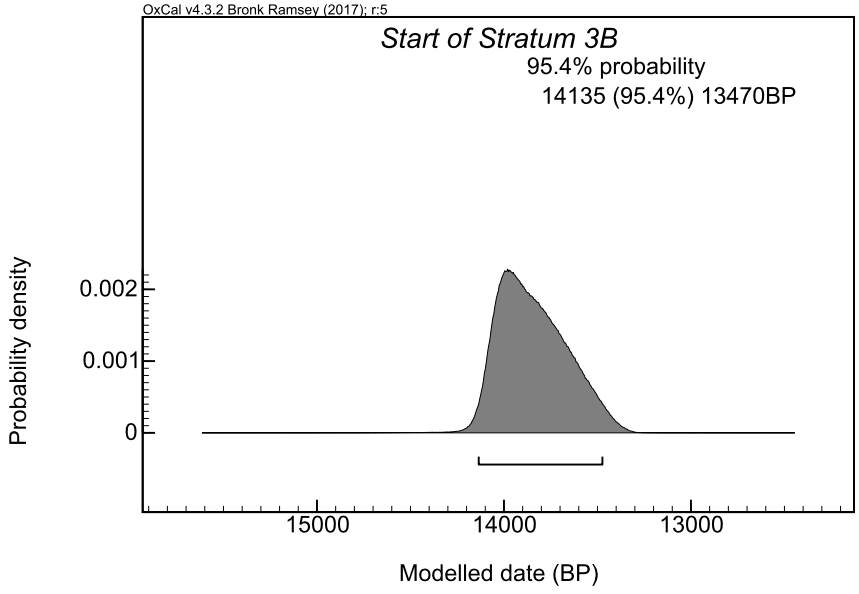


Fig. S18. Bayesian age model for El Fin del Mundo (above), and start `Boundary` (below).

```
Plot()
 {
 Outlier_Model("General",T(5),U(0,4),"t");
Sequence("Locality 1, El Fin del Mundo")
 {
 Boundary("Start of Stratum 3A");
 Phase("3A")
 {
 R_Date("AA-90707", 12180, 40)
  {
  Outlier("General", 0.05);
  };
 };
 Boundary("Start of Stratum 3B");
 Phase("3B")
 {
 R_Date("AA-95550", 9755, 92)
  {
  Outlier("General", 0.05);
```

```
  };
  R_Date("AA-83272B", 11040, 580)
  {
   Outlier("General", 0.05);
  };
  R_Date("AA-95550(duplicate)", 9804, 93)
  {
   Outlier("General", 0.05);
  };
  R_Date("AA-100182B", 11880, 200)
  {
   Outlier("General", 0.05);
  };
  R_Date("AA-100181B", 10650, 250)
  {
   Outlier("General", 0.05);
  };
  R_Date("AA-100181A", 11550, 60)
  {
   Outlier("General", 0.05);
  };
 };
 Boundary("End of 3/Start of 4");
 Sequence("Stratum 4")
 {
  Phase("D.")
  {
   R_Date("AA-14896A", 6185, 115)
   {
    Outlier("General", 0.05);
   };
   R_Date("AA-80078A", 6921, 58)
   {
    Outlier("General", 0.05);
   };
   R_Date("AA-80076A", 7570, 93)
   {
    Outlier("General", 0.05);
   };
  };
  Phase("D.E.")
  {
   R_Date("AA-80084A", 9715, 64)
   {
    Outlier("General", 0.05);
   };
   R_Date("AA-80671B", 9560, 120)
   {
    Outlier("General", 0.05);
   };
   R_Date("AA-80085B", 9290, 290)
   {
    Outlier("General", 0.05);
   };
   R_Date("A-14850", 9030, 75)
   {
    Outlier("General", 0.05);
   };
   R_Date("A-14836", 9465, 100)
   {
    Outlier("General", 0.05);
   };
   R_Date("A-14837", 8375, 110)
   {
    Outlier("General", 0.05);
   };
   R_Date("AA-88886", 8470, 50)
   {
    Outlier("General", 0.05);
   };
   R_Date("AA-81350", 8030, 50)
   {
    Outlier("General", 0.05);
   };
   R_Date("AA-88885", 8770, 60)
   {
    Outlier("General", 0.05);
   };
  };
 };
 Boundary("End of Stratum 4");
};
};
```

2.2.10. Gault, Texas (U.S.A.)

Gault (41BL323; at 30.892283, -97.709742) is a multi-cluster, stratified (units 1-10) site containing pre-Clovis ("Gault Assemblage"), Clovis, Late Paleoindian, and Archaic material[92–97]. The pre-Clovis level is represented by small-projectile-point technology and a blade-and-core tradition. OSL was used to date the deposits[96,97]. Using these data, the model created places the start of the pre-Clovis (Gault Assemblage) component at 26,435-17,385 cal BP, and the start of Clovis at 16,895-12,705 cal BP (Fig. S19). Particularly for the pre-Clovis boundary, the lack of precision is largely due to the OSL measurements (with large error margins) and a lack of constraint from preceding dates.

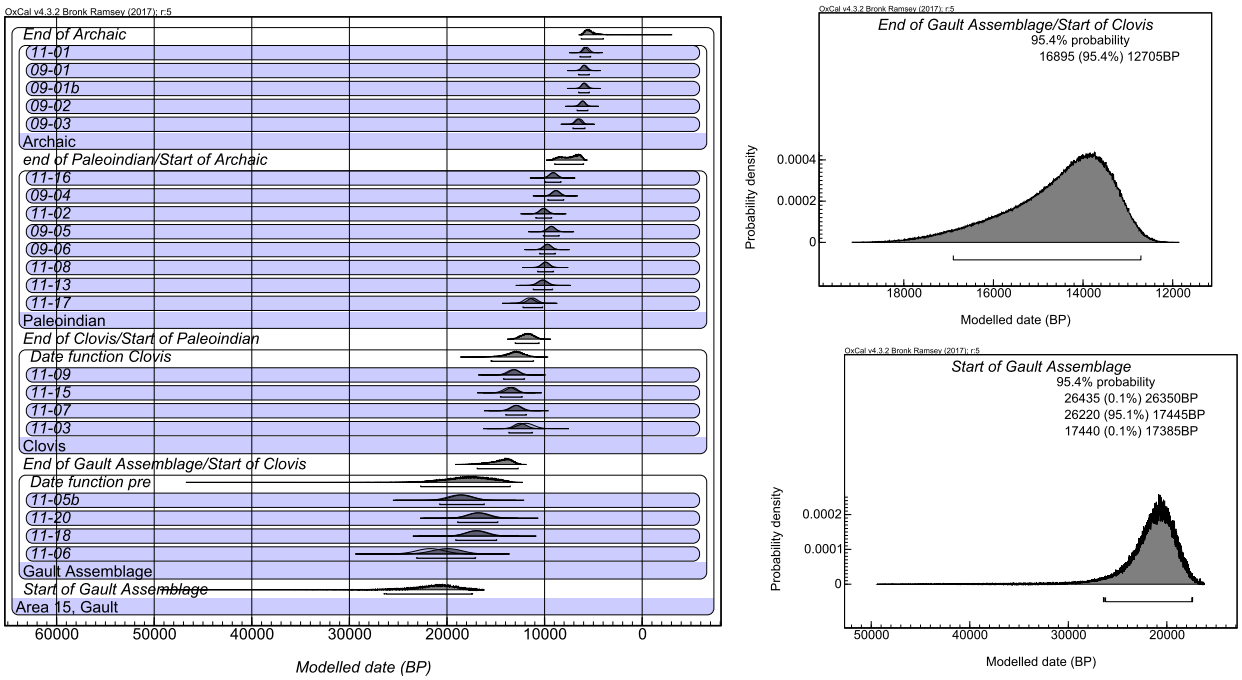


Fig. S19. Bayesian age model for Gault (above), and start boundaries for both pre-Clovis and Clovis components (adjacent).

```
Plot()
 {
 Outlier_Model("General",T(5),U(0,4),"t");
 Sequence("Area 15, Gault")
 {
 Boundary("Start of Gault Assemblage");
 Phase("Gault Assemblage")
 {
 Age("11-06", N(21700, 1400))
 {
 Outlier("General", 0.05);
 };
 Age("11-18", N(16900, 1100))
 {
 Outlier("General", 0.05);
 };
 Age("11-20", N(16700, 1100))
 {
 Outlier("General", 0.05);
 };
 Age("11-05b", N(18700, 1200))
 {
 Outlier("General", 0.05);
 };
 Date("Date function pre");
 };
 Boundary("End of Gault Assemblage/Start of Clovis");
 Phase("Clovis")
 {
 Age("11-03", N(11900, 800))
 {
 Outlier("General", 0.05);
 };
 Age("11-07", N(12900, 600))
 {
 Outlier("General", 0.05);
 };
 Age("11-15", N(13600, 600))
 {
 Outlier("General", 0.05);
 };
 Age("11-09", N(13200, 600))
 {
 Outlier("General", 0.05);
 };
 Date("Date function Clovis");
 };
 Boundary("End of Clovis/Start of Paleoindian");
 Phase("Paleoindian")
 {
 Age("11-17", N(11600, 500))
 {
 Outlier("General", 0.05);
 };
 Age("11-13", N(10200, 500))
 {
 Outlier("General", 0.05);
 };
 Age("11-08", N(9900, 400))
 {
 Outlier("General", 0.05);
 };
 Age("09-06", N(9700, 400))
 {
 Outlier("General", 0.05);
 };
 Age("09-05", N(9300, 400))
 {
 Outlier("General", 0.05);
 };
 Age("11-02", N(10100, 400))
 {
 Outlier("General", 0.05);
 };
 Age("09-04", N(8800, 400))
 {
 Outlier("General", 0.05);
 };
 Age("11-16", N(9100, 400))
```

```
  {
   Outlier("General", 0.05);
  };
 };
 Boundary("end of Paleoindian/Start of Archaic");
 Phase("Archaic")
 {
  Age("09-03", N(6600, 300))
  {
   Outlier("General", 0.05);
  };
  Age("09-02", N(6100, 300))
  {
   Outlier("General", 0.05);
  };
  Age("09-01b", N(5900, 300))
  {
   Outlier("General", 0.05);
  };
  Age("09-01", N(5900, 300))
  {
   Outlier("General", 0.05);
  };
  Age("11-01", N(5700, 300))
  {
   Outlier("General", 0.05);
  };
 };
 Boundary("End of Archaic");
};
};
```

2.2.11. Jake Bluff, Oklahoma (U.S.A.)

Jake Bluff (34HP60; at approximately 36.596874, -99.514348) is a Clovis, bison-butchering site with associated lithic tool technology[98–100]. The incorporation of five bone dates into a single `Phase`, dates the archaeological event to 12,775-12,645 cal BP (`Date` function; Fig. S20).

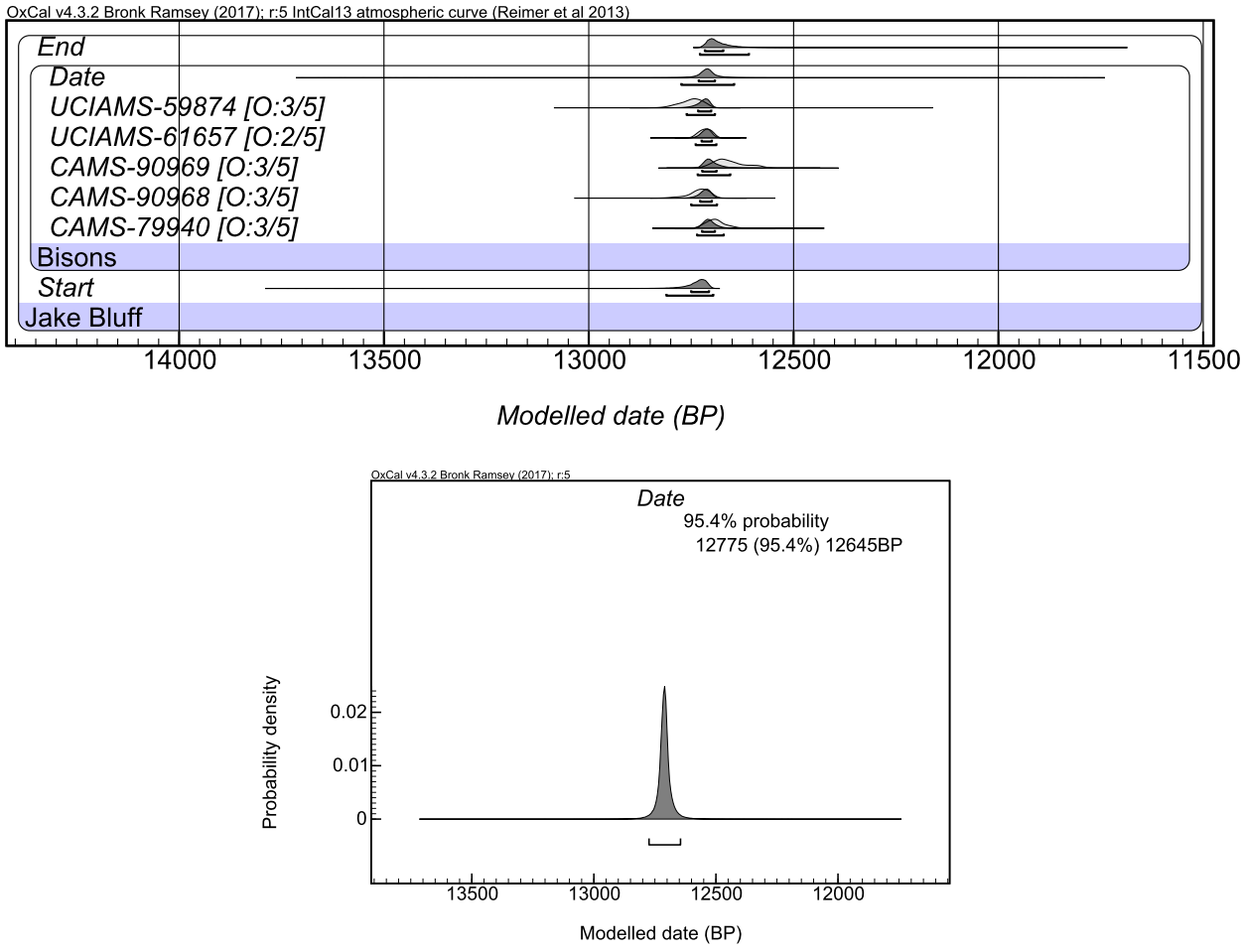


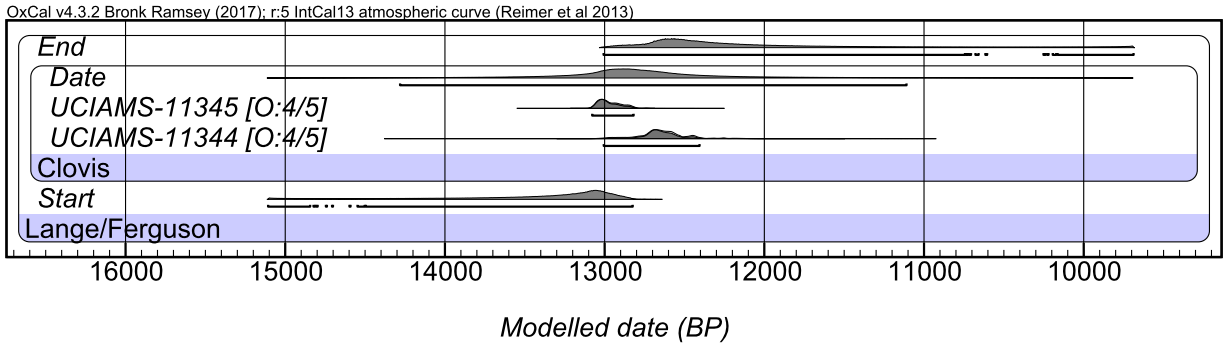
Fig. S20. Bayesian age model for Jake Bluff (above), and `Date` function (below).

```
Sequence("Jake Bluff")
 {
 Outlier_Model("General",T(5),U(0,4),"t");
 Boundary("Start");
```

```
Phase("Bisons")
 {
 R_Date("CAMS-79940", 10750, 40)
  {
  Outlier("General", 0.05);
  };
 R_Date("CAMS-90968", 10840, 45)
  {
  Outlier("General", 0.05);
  };
 R_Date("CAMS-90969", 10700, 45)
  {
  Outlier("General", 0.05);
  };
 R_Date("UCIAMS-61657", 10810, 25)
  {
  Outlier("General", 0.05);
  };
 R_Date("UCIAMS-59874", 10885, 35)
  {
  Outlier("General", 0.05);
  };
 Date("Date");
 };
Boundary("End");
};
```

2.2.12. Lange/Ferguson, South Dakota (U.S.A.)

Lange/Ferguson (39SH33; at approximately 43.334567, -102.104490) is a Clovis, mammoth-butchering site with associated lithic and osseous tool technology[5,101–105]. Although geochronological data has been obtained from the site's stratified deposits[106], two XAD dates (UCIAMS-11344 and UCIAMS-11345) were measured directly from mammoth bone samples[5]. The incorporation of these into a single `Phase` model dates the Clovis component to 14,285-11,105 cal BP (`Date` function; Fig. S21).



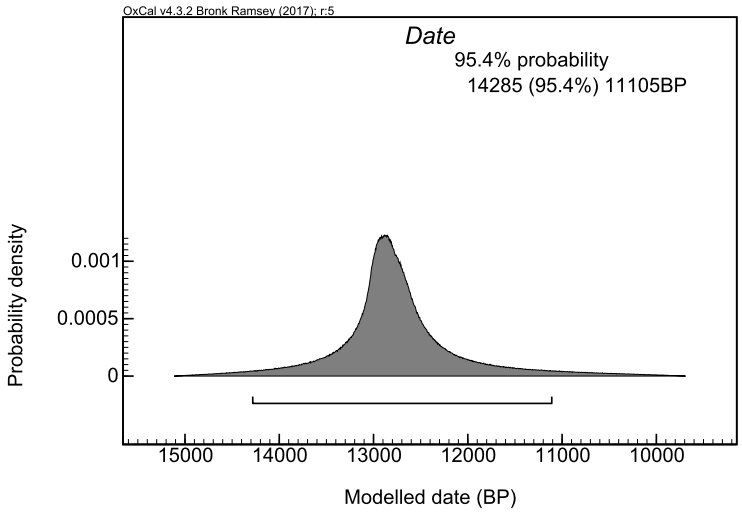
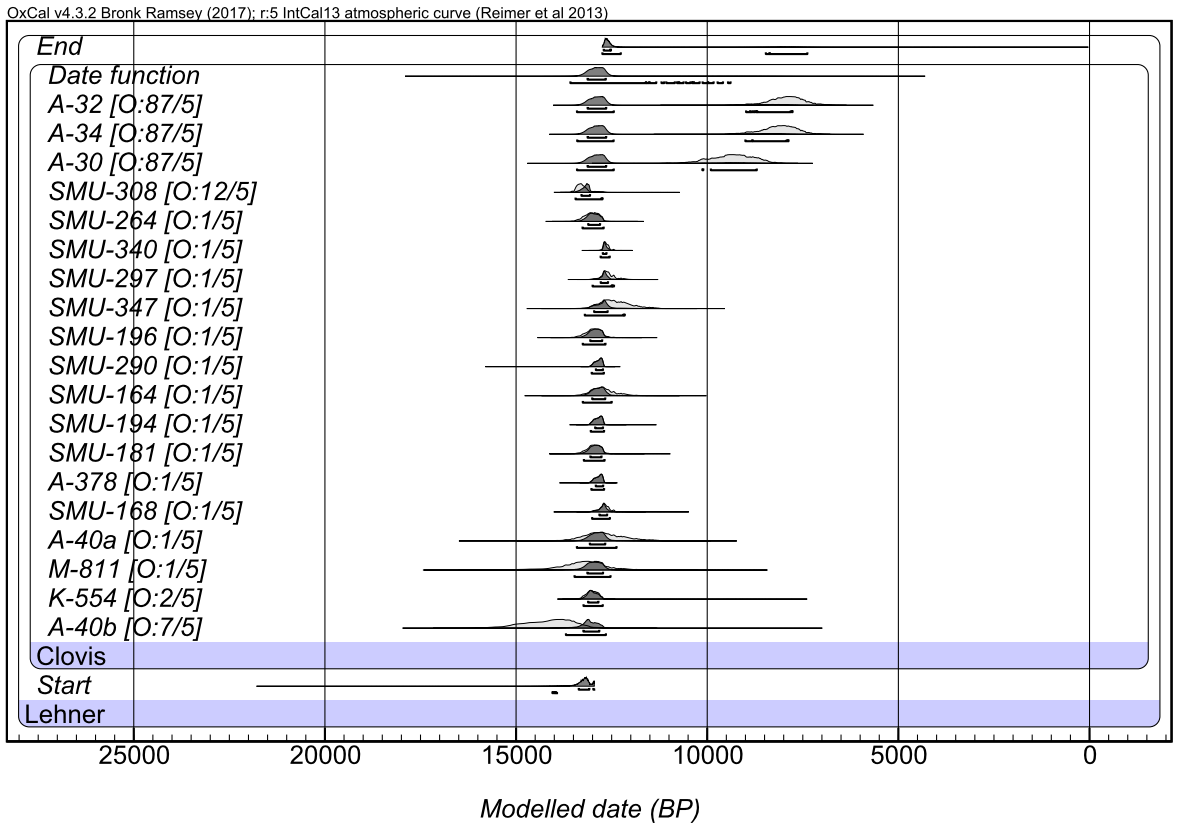


Fig. S21. Bayesian age model for Lange/Ferguson (above), and `Date` function (below).

```
\Plot()
 {
 Outlier_Model("General",T(5),U(0,4),"t");
 Sequence("Lange/Ferguson")
 {
 Boundary("Start");
 Phase("Clovis")
 {
 R_Date("UCIAMS-11344", 10710, 130)
 {
 Outlier("General", 0.05);
 };
 R_Date("UCIAMS-11345", 11110, 40)
 {
 Outlier("General", 0.05);
 };
 Date("Date");
 };
 Boundary("End");
 };
};
```

2.2.13. Lehner, Arizona (U.S.A.)

Lehner (Arizona EE:12:1; at 31.421691, -110.114805) is a Clovis, mammoth-butchering site with associated lithic tool technology and hearth features[103,107]. There are no direct bone dates, just charcoal-obtained measurements from hearth features. The incorporation of fourteen hearth-extracted, charcoal measurements into a single `Phase` model, dates the Clovis component at Lehner to 13,579-9,390 (`Date` function; Fig. S22). The span of this distribution is likely affected by five conventional radiocarbon dates—ranged from 7,205±450 (A-34) to 12,000±450 (A-40b)—which were rejected by archaeologists due to their large spread and perceived contamination[103,107].



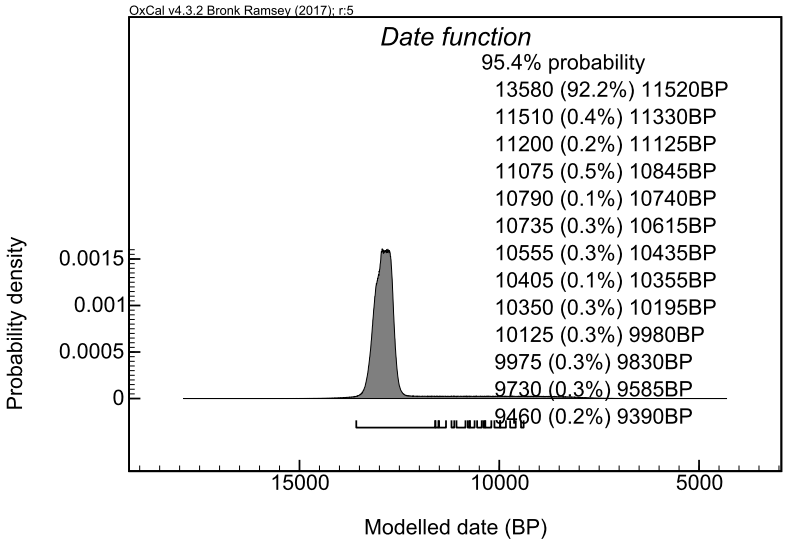


Fig. S22. Bayesian age model for Lehner (above), and `Date` function (below).

```
Plot()
{
 Outlier_Model("General",T(5),U(0,4),"t");
 Sequence("Lehner")
 {
  Boundary("Start");
  Phase("Clovis")
  {
   R_Date("A-40b", 12000, 450)
   {
    Outlier("General", 0.05);
   };
   R_Date("K-554", 11180, 140)
   {
    Outlier("General", 0.05);
   };
   R_Date("M-811", 11290, 500)
   {
    Outlier("General", 0.05);
   };
   R_Date("A-40a", 10900, 450)
   {
    Outlier("General", 0.05);
   };
   R_Date("SMU-168", 10770, 140)
   {
    Outlier("General", 0.05);
   };
   R_Date("A-378", 10940, 100)
```

```
  {
   Outlier("General", 0.05);
  };
  R_Date("SMU-181", 11080, 200)
  {
   Outlier("General", 0.05);
  };
  R_Date("SMU-194", 10950, 110)
  {
   Outlier("General", 0.05);
  };
  R_Date("SMU-164", 10860, 280)
  {
   Outlier("General", 0.05);
  };
  R_Date("SMU-290", 10950, 90)
  {
   Outlier("General", 0.05);
  };
  R_Date("SMU-196", 11080, 230)
  {
   Outlier("General", 0.05);
  };
  R_Date("SMU-347", 10620, 300)
  {
   Outlier("General", 0.05);
  };
  R_Date("SMU-297", 10700, 150)
  {
   Outlier("General", 0.05);
  };
  R_Date("SMU-340", 10710, 90)
  {
   Outlier("General", 0.05);
  };
  R_Date("SMU-264", 11170, 200)
  {
   Outlier("General", 0.05);
  };
  R_Date("SMU-308", 11470, 110)
  {
   Outlier("General", 0.05);
  };
  R_Date("A-30", 8330, 450)
  {
   Outlier("General", 0.05);
  };
  R_Date("A-34", 7205, 450)
  {
   Outlier("General", 0.05);
  };
  R_Date("A-32", 7022, 450)
  {
   Outlier("General", 0.05);
  };
  Date("Date function");
 };
 Boundary("End");
};
```

2.2.14. Murray Springs, Arizona, (U.S.A.)

Murray Springs (Arizona EE:8:25; at approximately 32.236196, -110.330801) is a Clovis, mammoth- and bison-butchering site with associated lithic and osseous tool technology[103,108,109]. Although there are no bone dates, eight charcoal samples from the Graveyard Member (F1) have been dated and are deemed to represent the Clovis occupation at the site[108]. The incorporation of these into a single `Phase` model dates the Clovis component to 13,015-12,615 (`Date` function; Fig. S23).

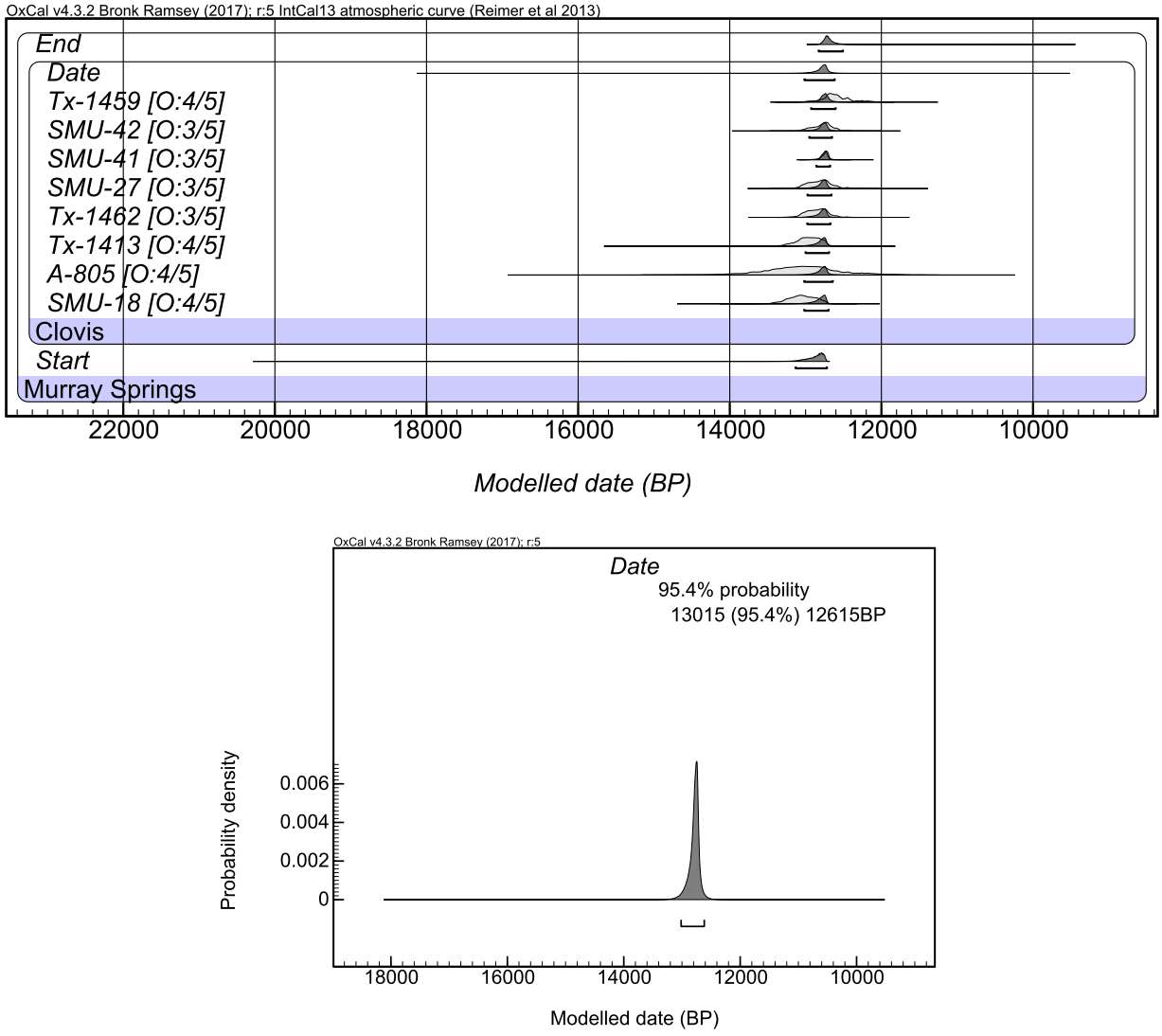


Fig. S23. Bayesian age model for Murray Springs (above), and `Date` function (below).

```
Plot()
{
 Outlier_Model("General",T(5),U(0,4),"t");
 Sequence("Murray Springs")
 {
  Boundary("Start");
  Phase("Graveyard Member F1")
  {
  R_Date("SMU-18", 11190, 180)
   {
   Outlier("General", 0.05);
   };
  R_Date("A-805", 11150, 450)
   {
   Outlier("General", 0.05);
   };
  R_Date("Tx-1413", 11080, 180)
   {
   Outlier("General", 0.05);
   };
  R_Date("Tx-1462", 10930, 170)
   {
   Outlier("General", 0.05);
   };
  R_Date("SMU-27", 10890, 180)
   {
   Outlier("General", 0.05);
   };
  R_Date("SMU-41", 10840, 70)
   {
   Outlier("General", 0.05);
   };
  R_Date("SMU-42", 10840, 140)
   {
   Outlier("General", 0.05);
   };
  R_Date("Tx-1459", 10710, 160)
   {
   Outlier("General", 0.05);
   };
  Date("Date function");
  };
  Boundary("End");
 };
};
```

2.2.15. Shawnee-Minisink, Pennsylvania, U.S.A.

Shawnee-Minisink (36MR43; at approximately 40.995474, -75.13735) is a stratified site (zones 1-4) containing Clovis, Archaic, and Woodland material[5,110–116]. Zone 4 (per ref[110]), the Clovis level, includes lithic tool technology and hearth features. Apart from this layer, only the Middle Woodland has been dated[110]. Thus, all dates obtained (from hearth charcoal samples) for the Clovis component have been entered into a single `Phase` model. This dates the Clovis component to 12,910-12,650 cal BP (`Date` function; Fig. S24).

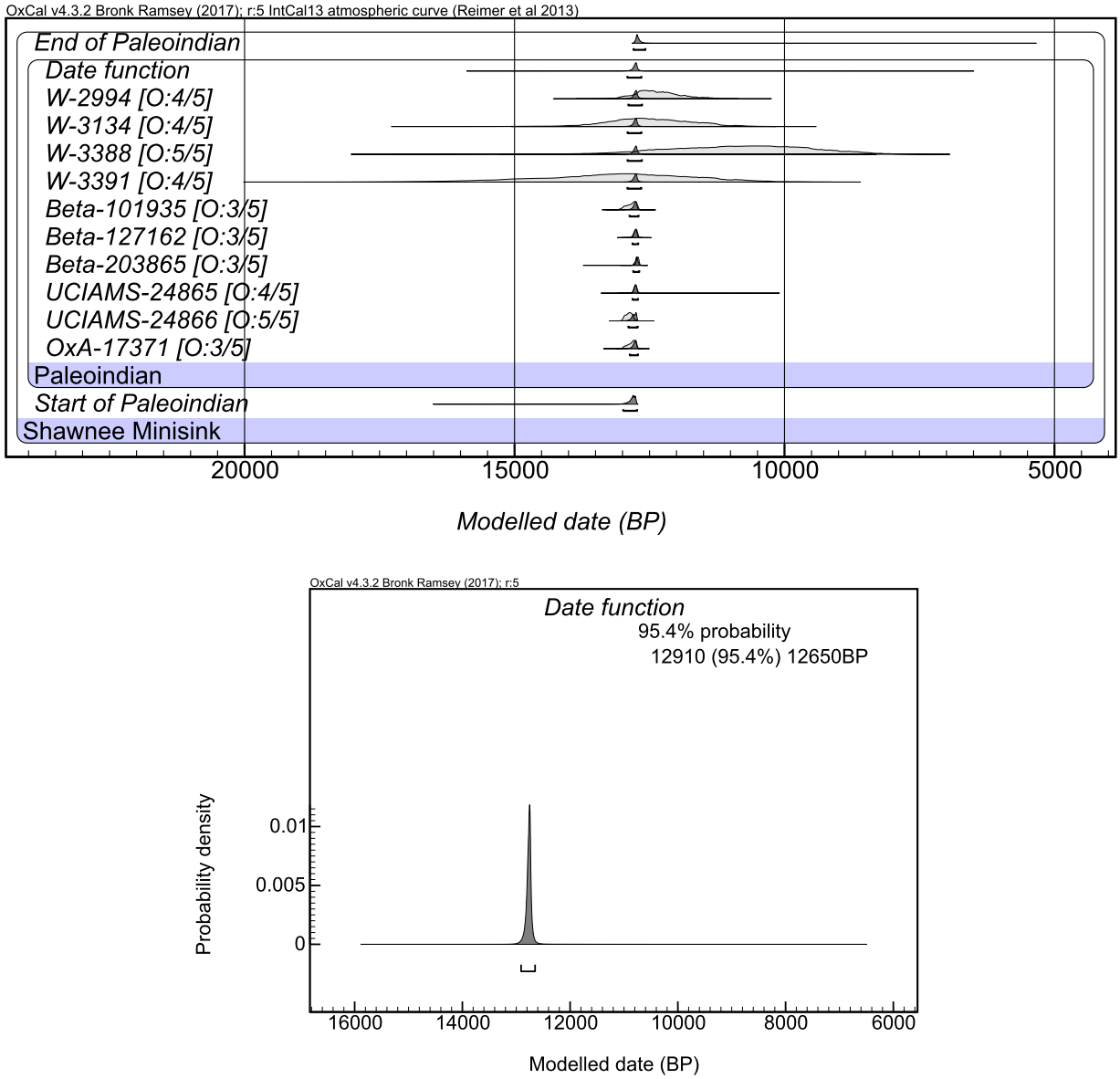


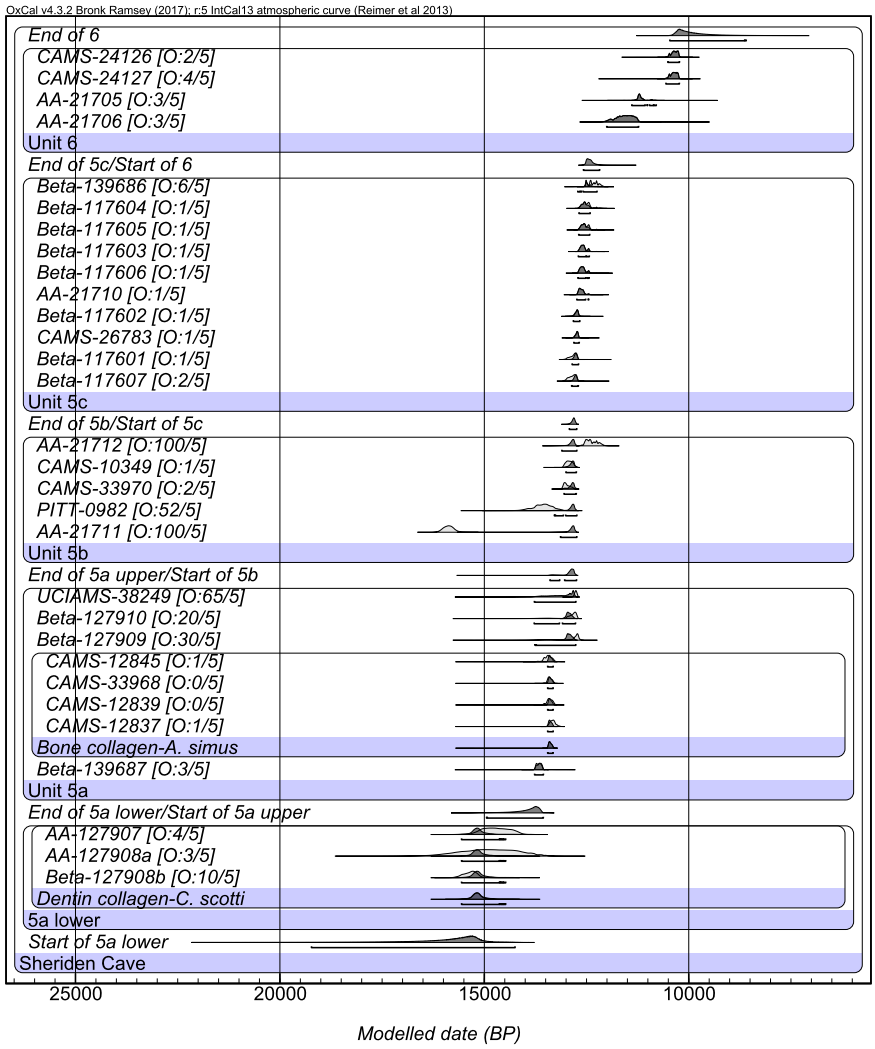
Fig. S24. Bayesian age model for Shawnee-Minisink (above), and `Date` function (below).

```
Plot()
 {
 Outlier_Model("General",T(5),U(0,4),"t");
 Sequence("Shawnee-Minisink")
  {
  Boundary("Start of Paleoindian");
```

```
Phase("Paleoindian")
 {
 R_Date("OxA-17371", 10970, 50)
  {
  Outlier("General", 0.05);
 };
 R_Date("UCIAMS-24866", 11020, 30)
 {
  Outlier("General", 0.05);
 };
 R_Date("UCIAMS-24865", 10915, 25)
 {
  Outlier("General", 0.05);
 };
 R_Date("Beta-203865", 10820, 50)
 {
  Outlier("General", 0.05);
 };
 R_Date("Beta-127162", 10900, 40)
 {
  Outlier("General", 0.05);
 };
 R_Date("Beta-101935", 10940, 90)
 {
  Outlier("General", 0.05);
 };
 R_Date("W-3391", 11050, 1000)
 {
  Outlier("General", 0.05);
 };
 R_Date("W-3388", 9310, 1000)
 {
  Outlier("General", 0.05);
 };
 R_Date("W-3134", 10750, 600)
 {
  Outlier("General", 0.05);
 };
 R_Date("W-2994", 10590, 300)
 {
  Outlier("General", 0.05);
 };
 Date("Date function");
 };
 Boundary("End of Paleoindian");
};
};
```

2.2.16. Sheriden Cave, Ohio (U.S.A.)

Sheriden Cave (33WY252; at approximately 40.945194, -83.346083) is a stratified (units 1-6b) site containing Clovis lithic and osseous tool technology[117–123]. The Clovis assemblage was found at the upper portion of stratum 5a, at the very interface with 5b. Dates obtained provide stratigraphic control or date cultural features/artefacts directly, e.g., bone point (UCIAMS-38249). Using these data, the model created places the start of the Clovis component at 14,950-13,555 cal BP (Fig. S25).



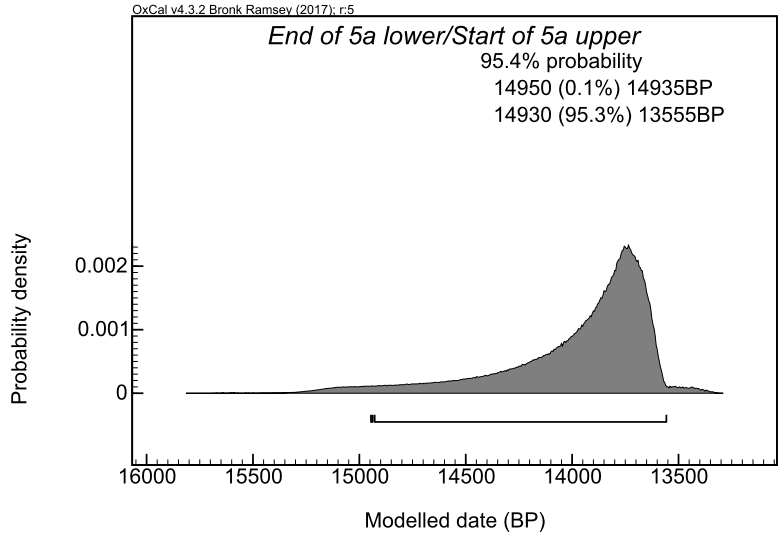


Fig. S25. Bayesian age model for Sheriden Cave (above), and start `Boundary` (below).

```
Plot()
 {
 Outlier_Model("General",T(5),U(0,4),"t");
 Sequence("Sheriden Cave")
  {
  Boundary("Start of 5a lower");
  Phase("Unit 5a lower")
   {
   Combine("Dentin collagen-C. scotti")
    {
    R_Date("Beta-127908b", 12840, 100)
     {
     Outlier("General", 0.05);
     };
    R_Date("AA-127908a", 12590, 450)
     {
     Outlier("General", 0.05);
```

```
 };
 R_Date("AA-127907", 12520, 170)
 {
 Outlier("General", 0.05);
 };
};
};
Boundary("End of 5a lower/Start of 5a upper");
Phase("Unit 5a upper")
{
R_Date("Beta-139687", 11860, 40)
{
Outlier("General", 0.05);
};
Combine("Bone collagen-A. simus")
{
R_Date("CAMS-12837", 11480, 60)
{
Outlier("General", 0.05);
};
R_Date("CAMS-12839", 11570, 70)
{
Outlier("General", 0.05);
};
R_Date("CAMS-33968", 11570, 50)
{
Outlier("General", 0.05);
};
R_Date("CAMS-12845", 11610, 90)
{
Outlier("General", 0.05);
};
};
R_Date("Beta-127909", 10840, 80)
{
Outlier("General", 0.05);
};
R_Date("Beta-127910", 10960, 60)
{
Outlier("General", 0.05);
};
R_Date("UCIAMS-38249", 10915, 30)
{
Outlier("General", 0.05);
};
};
Boundary("End of 5a upper/Start of 5b");
Phase("Unit 5b")
{
R_Date("AA-21711", 13210, 80)
{
Outlier("General", 0.05);
};
R_Date("PITT-0982", 11710, 220)
{
Outlier("General", 0.05);
};
R_Date("CAMS-33970", 11130, 60)
{
Outlier("General", 0.05);
};
R_Date("CAMS-10349", 11060, 60)
{
Outlier("General", 0.05);
};
R_Date("AA-21712", 10470, 70)
{
Outlier("General", 0.05);
};
};
Boundary("End of 5b/Start of 5c");
Phase("Unit 5c")
{
R_Date("Beta-117607", 10970, 70)
{
Outlier("General", 0.05);
};
R_Date("Beta-117601", 10940, 70)
{
Outlier("General", 0.05);
};
R_Date("CAMS-26783", 10850, 60)
{
Outlier("General", 0.05);
};
R_Date("Beta-117602", 10850, 70)
{
Outlier("General", 0.05);
};
R_Date("AA-21710", 10680, 80)
{
Outlier("General", 0.05);
};
R_Date("Beta-117606", 10620, 70)
{
Outlier("General", 0.05);
};
R_Date("Beta-117603", 10600, 60)
{
Outlier("General", 0.05);
};
R_Date("Beta-117605", 10570, 70)
{
Outlier("General", 0.05);
};
R_Date("Beta-117604", 10550, 70)
{
Outlier("General", 0.05);
};
R_Date("Beta-139686", 10440, 40)
{
Outlier("General", 0.05);
};
};
Boundary("End of 5c/Start of 6");
Phase("Unit 6")
{
R_Date("AA-21706", 10020, 115)
{
Outlier("General", 0.05);
};
R_Date("AA-21705", 9775, 70)
{
Outlier("General", 0.05);
};
R_Date("CAMS-24127", 9190, 60)
{
Outlier("General", 0.05);
};
R_Date("CAMS-24126", 9170, 60)
{
Outlier("General", 0.05);
};
};
Boundary("End of 6");
};
};
```

2.3. Clovis-coeval

2.3.1. Arlington Springs, California (U.S.A.)

Arlington Springs (CA-SRI-173; at approximately 34.005591, -120.177117) is a Clovis-coeval site containing two human femora[124,125]. Two XAD dates were obtained on one of the femurs (CAMS-16814 and CAMS-16810). The oldest, CAMS-16810 (10,960±80 BP), was considered to be a more accurate date for the skeleton due to differences in collagen preservation within the bone[5,124]. Calibrated, the human femur dates to 13,015-12,705 cal BP.

2.3.2. Meay Channel I, Calvert Island (Canada)

Meay Channel I (EjTa-4; at approximately 51.659051, -128.098817) is a site containing several human footprints impressed into a paleosol (Stratum X)[126]. All dates obtained provide stratigraphic control. Using these data, the model created place the start of strata X/XI to 13,825-13,200 cal BP (Fig. S26). Date UCIAMS-186383 (720±15 BP), from a much younger stratum (II), was excluded as it skewed the model unnecessarily.

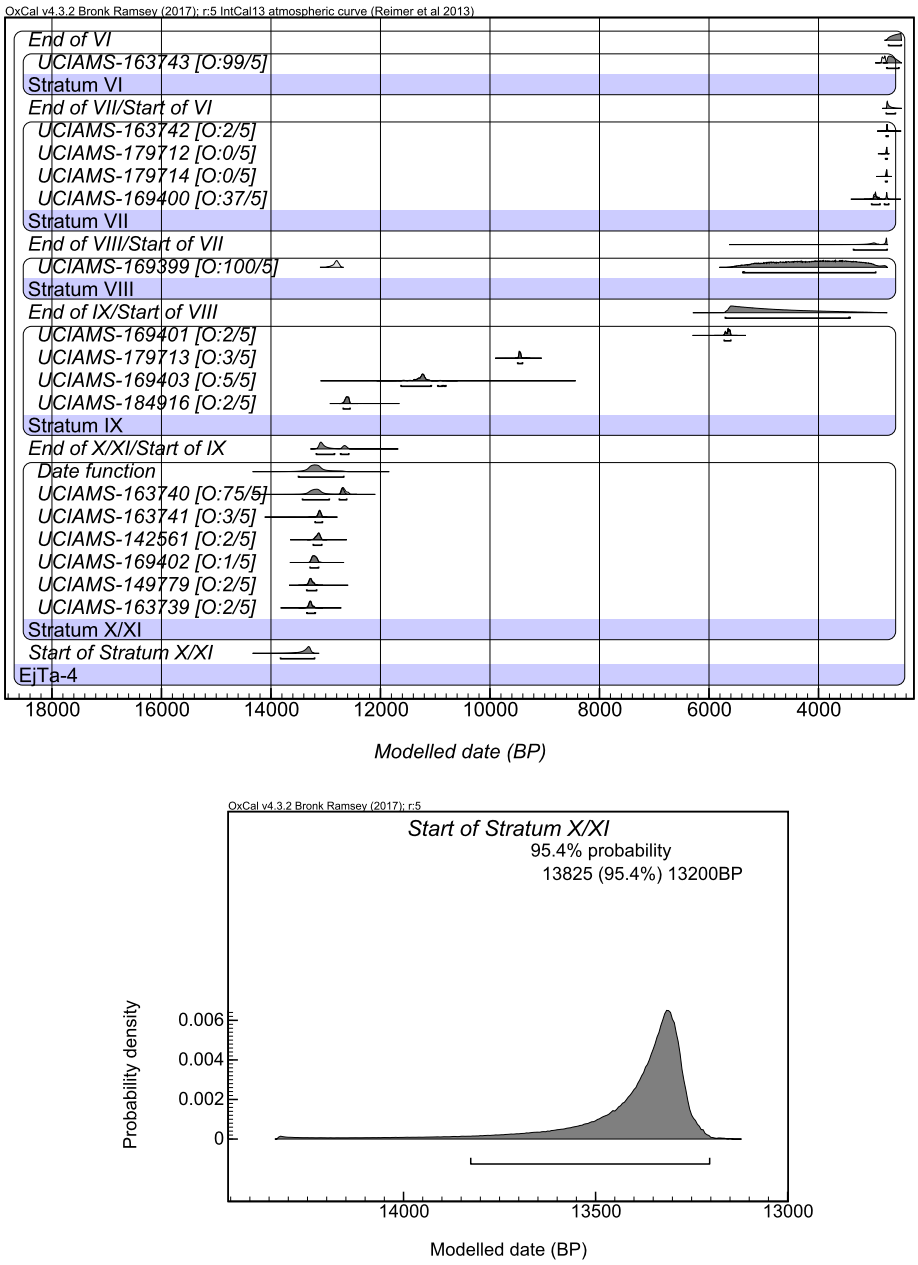


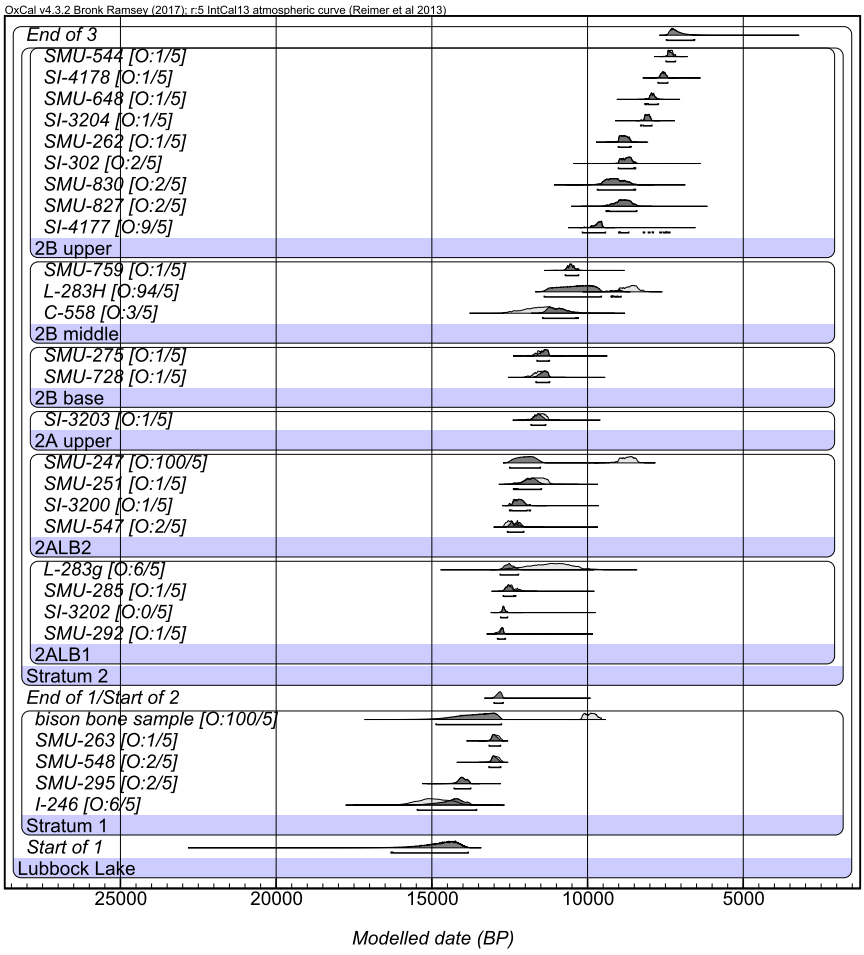
Fig. S26. Bayesian age model for Meay Channel I (above), and start `Boundary` (below).

```
Plot()
 {
 Outlier_Model("General",T(5),U(0,4),"t");
 Sequence("Meay Channel I")
  {
  Boundary("Start of Stratum X/XI");
  Phase("Stratum X/XI")
   {
   R_Date("UCIAMS-163739", 11440, 25)
    {
    Outlier("General", 0.05);
    };
   R_Date("UCIAMS-149779", 11435, 30)
    {
    Outlier("General", 0.05);
    };
   R_Date("UCIAMS-169402", 11365, 25)
    {
    Outlier("General", 0.05);
    };
   R_Date("UCIAMS-142561", 11295, 30)
    {
    Outlier("General", 0.05);
    };
   R_Date("UCIAMS-163741", 11260, 25)
    {
    Outlier("General", 0.05);
    };
   R_Date("UCIAMS-163740", 10720, 60)
    {
    Outlier("General", 0.05);
    };
   Date("Date function");
  };
  Boundary("End of X/XI/Start of IX");
  Phase("Stratum IX")
  {
  R_Date("UCIAMS-184916", 10625, 20)
   {
   Outlier("General", 0.05);
   };
  R_Date("UCIAMS-169403", 9820, 80)
   {
```

```
 Outlier("General", 0.05);
 };
 R_Date("UCIAMS-179713", 8410, 20)
 {
 Outlier("General", 0.05);
 };
 R_Date("UCIAMS-169401", 4935, 25)
 {
 Outlier("General", 0.05);
 };
};
Boundary("End of IX/Start of VIII");
Phase("Stratum VIII")
{
R_Date("UCIAMS-169399", 10980, 25)
 {
 Outlier("General", 0.05);
 };
};
Boundary("End of VIII/Start of VII");
Phase("Stratum VII")
{
R_Date("UCIAMS-169400", 2855, 15)
 {
 Outlier("General", 0.05);
 };
 R_Date("UCIAMS-179714", 2650, 15)
 {
 Outlier("General", 0.05);
 };
 R_Date("UCIAMS-179712", 2645, 15)
 {
 Outlier("General", 0.05);
 };
 R_Date("UCIAMS-163742", 2605, 20)
 {
 Outlier("General", 0.05);
 };
};
Boundary("End of VII/Start of VI");
Phase("Stratum VI")
{
 R_Date("UCIAMS-163743", 2715, 20)
 {
 Outlier("General", 0.05);
 };
};
Boundary("End of VI");
};
};
```

2.3.3. Lubbock Lake, Texas (U.S.A.)

Lubbock Lake (41LU1; at 33.622424, -101.889496) is a multi-cluster, stratified (strata 1-5) site containing Clovis-coeval, Folsom, Archaic, and Protohistoric material[127–131]. There is evidence for human predation of mammoth in the Clovis-coeval component (stratum 1)[132,133], and bison within the Folsom stratum (2). Using data from strata 1-3 (providing stratigraphic control and dating the bison directly), only, the model created places the start of the Clovis-coeval occupation at 16,310-13,830 cal BP (Fig. S27). If adding strata 4-5, the model finds no agreement due to poor agreement with the stratigraphic evidence.



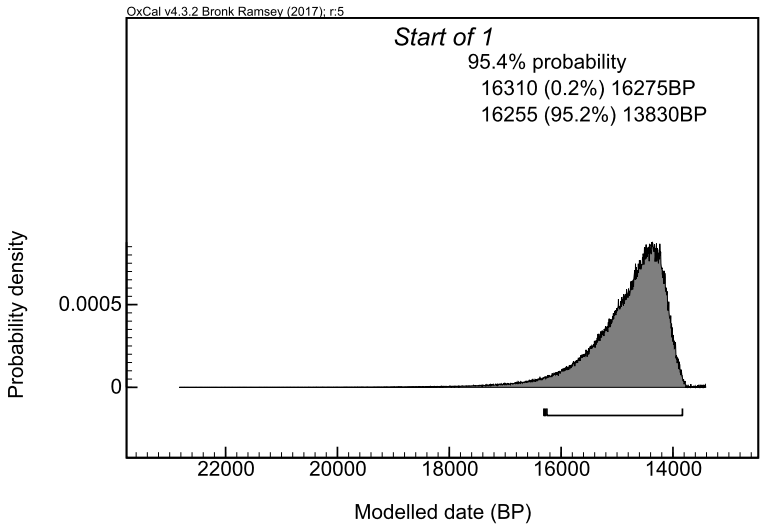


Fig. S27. Bayesian age model for Lubbock Lake (above), and start `Boundary` (below).

```
Plot()
 {
 Outlier_Model("General",T(5),U(0,4),"t");
 Sequence("Lubbock Lake")
  {
  Boundary("Start of 1");
  Phase("Stratum 1")
   {
   R_Date("I-246", 12650, 290)
    {
    Outlier("General", 0.05);
    };
   R_Date("SMU-295", 12150, 90)
    {
    Outlier("General", 0.05);
    };
   R_Date("SMU-548", 11100, 100)
    {
    Outlier("General", 0.05);
    };
   R_Date("SMU-263", 11100, 100)
    {
    Outlier("General", 0.05);
    };
   R_Combine("bison bone sample")
```

```
 {
 R_Date("SMU-317", 8860, 90);
 R_Date("SMU-367", 7040, 600);
 Outlier("General", 0.05);
 };
};
Boundary("End of 1/Start of 2");
Sequence("Stratum 2")
{
Phase("2ALB1")
{
R_Date("SMU-292", 10880, 90)
 {
 Outlier("General", 0.05);
 };
R_Date("SI-3202", 10780, 80)
 {
 Outlier("General", 0.05);
 };
R_Date("SMU-285", 10530, 90)
 {
 Outlier("General", 0.05);
 };
R_Date("L-283g", 9700, 450)
 {
 Outlier("General", 0.05);
 };
};
Phase("2ALB2")
{
R_Date("SMU-547", 10540, 100)
 {
 Outlier("General", 0.05);
 };
R_Date("SI-3200", 10360, 80)
 {
 Outlier("General", 0.05);
 };
R_Date("SMU-251", 10060, 170)
 {
 Outlier("General", 0.05);
 };
R_Date("SMU-247", 7840, 170)
 {
 Outlier("General", 0.05);
 };
};
Phase("2A upper")
 {
 R_Date("SI-3203", 10015, 75)
 {
 Outlier("General", 0.05);
 };
};
Phase("2B base")
{
R_Date("SMU-728", 9990, 100)
 {
 Outlier("General", 0.05);
 };
R_Date("SMU-275", 9960, 80)
 {
 Outlier("General", 0.05);
 };
};
Phase("2B middle")
{
R_Date("C-558", 9883, 350)
 {
 Outlier("General", 0.05);
 };
R_Date("L-283H", 7765, 200)
 {
 Outlier("General", 0.05);
 };
R_Date("SMU-759", 9330, 70)
 {
 Outlier("General", 0.05);
 };
};
Phase("2B upper")
{
R_Date("SI-4177", 8655, 90)
 {
 Outlier("General", 0.05);
 };
R_Date("SMU-827", 7980, 180)
 {
 Outlier("General", 0.05);
 };
R_Date("SMU-830", 8210, 240)
 {
 Outlier("General", 0.05);
 };
R_Date("SI-302", 7890, 100)
 {
 Outlier("General", 0.05);
 };
R_Date("SMU-262", 7970, 70)
 {
 Outlier("General", 0.05);
 };
R_Date("SI-3204", 7255, 75)
 {
 Outlier("General", 0.05);
 };
R_Date("SMU-648", 7100, 80)
 {
 Outlier("General", 0.05);
 };
R_Date("SI-4178", 6705, 95)
 {
 Outlier("General", 0.05);
 };
R_Date("SMU-544", 6400, 80)
 {
 Outlier("General", 0.05);
 };
 };
};
Boundary("End of 3");
};
};
```

2.3.4. Wally's Beach, Alberta (Canada)

Wally's Beach (DhPg-8; at approximately 49.381404, -114.077366) is a Clovis-coeval, horse- and camel-butchering site with associated lithic tool technology[88,134–137]. Considering that XAD/

HYP have been obtained for one camel, seven horses, and one muskox (nearby and unbutchered), a single `Phase` model was built. This dates the butchering events to 13,340-13,220 cal BP (`Date` function; Fig. S28).

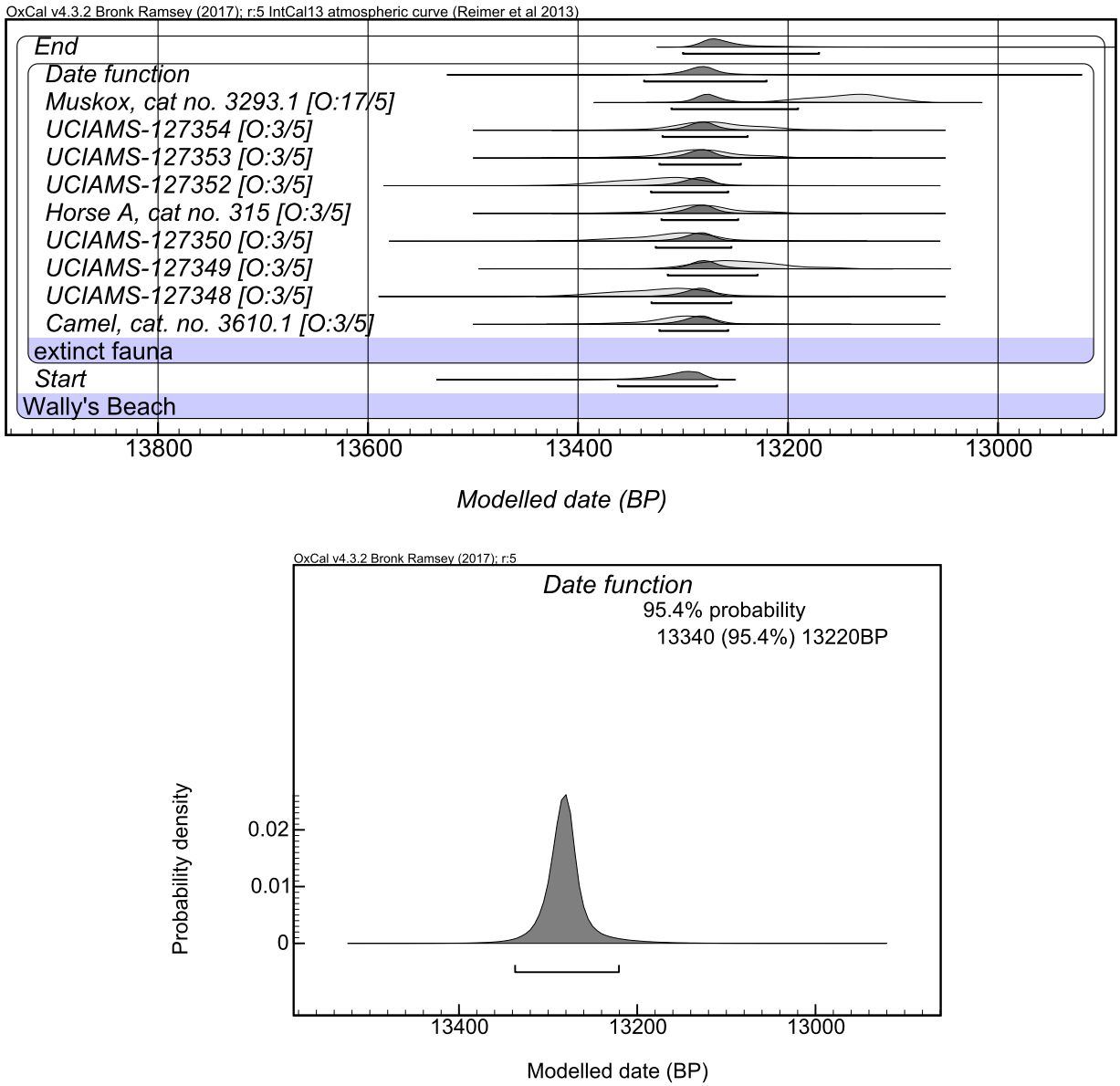


Fig. S28. Bayesian age model for Wally's Beach (above), and `Date` function (below).

```
Plot()
 {
 Outlier_Model("General", T(5), U(0,4), "t");
 Sequence("Wally's Beach")
 {
 Boundary("Start");
 Phase("extinct fauna")
 {
 R_Combine("Camel, cat. no. 3610.1")
 {
 R_Date("UCIAMS-116400", 11465, 40);
 R_Date("UCIAMS-127347", 11425, 30);
 R_Date("OxA-X-2736-8", 11530, 50);
 Outlier("General", 0.05);
 };
 //Horse 1, cat no.3594 XAD
 R_Date("UCIAMS-127348", 11470, 35)
 {
 Outlier("General", 0.05);
 };
 //Horse 2, cat no. 2988.1 XAD
 R_Date("UCIAMS-127349", 11410, 30)
 {
 Outlier("General", 0.05);
 };
 //Horse 3, cat no. 944 XAD
 R_Date("UCIAMS-127350", 11460, 30)
 {
 Outlier("General", 0.05);
```

```
  };
  R_Combine("Horse A, cat no. 315")
  {
   R_Date("UCIAMS-127351", 11440, 30);
   R_Date("OxA-X-2736-10", 11445, 55);
   Outlier("General", 0.05);
  };
  //Horse B, cat. no. 164 XAD
  R_Date("UCIAMS-127352", 11475, 30)
  {
   Outlier("General", 0.05);
  };
  //Horse C, cat. no 683 XAD
  R_Date("UCIAMS-127353", 11440, 30)
  {
   Outlier("General", 0.05);
  };
  //Horse D, cat. no 77.1 XAD
  R_Date("UCIAMS-127354", 11430, 30)
  {
   Outlier("General", 0.05);
  };
  R_Combine("Muskox, cat no. 3293.1")
  {
   R_Date("UCIAMS-127373", 11320, 30);
   R_Date("OxA-X-2736-9", 11255, 50);
   Outlier("General", 0.05);
  };
  Date("Date function");
 };
 Boundary("End");
};
```

2.4. Pre-Clovis

In First Americans research, pre-Clovis sites are often controversial and viewed with skepticism[138]. Scrutiny is generally placed on the reliability of the archaeological evidence, rather than the chronometric data (given the relatively young age of this period, in radiocarbon dating terms, dated materials are less prone to modern carbon contamination). This study, however, considers all sites included analysis to provide unequivocal evidence of human activity. If there is uncertainty regarding cultural association for any given site, however, alternate views are noted. In the case of Meadowcroft Rockshelter, uncertainty regarding the cultural aspect of stratum IIa is taken into account, and a conservative modelling approach is taken (see site for details).

2.4.1. Bluefish Caves, Yukon (Canada)

Bluefish Caves site (at 67.15, -140.75) is composed of three karstic cavities (Caves I, II, and III) with stratified deposits (Units A-D) and lithic technology (within Unit B)[139,140]. In 2017, six human-modified bones (but see refs[14,141]) from Caves I and II were dated and published[140]. Results ranged from 10,490±55 BP (OxA-33776) to 19,650±130 BP (OxA-33778). Sample J7.8.17 (OxA-33778) is the only bone with a known stratigraphic location, however. Considering this and its antiquity, OxA-33778 (24,035-23,310 cal BP) has been used to represent the earliest human presence at Bluefish Caves.

2.4.2. Cactus Hill, Virginia (U.S.A.)

See in Clovis section.

2.4.3. Cooper's Ferry, Idaho (U.S.A.)

Cooper's Ferry (10IH73; at approximately 45.90538, -116.39751) is a multi-cluster, stratified [lithostratigraphic units (LU) 1-9] site containing lithics and faunal remains[8,12,142–145]. The oldest evidence for human activity occurs at LU3, where a number of prehistoric pit features were identified. In situ WST technology was found at the upper portion of LU3. All dates obtained provide stratigraphic control. Bayesian age modeling performed in ref[145] places the start of LU3 at 16,560-15,280 cal BP (95.4% confidence), whilst WST technology is best anchored by one date from upper LU3, OxA-X-2792-45 (13,610-13,275 cal BP). All dates directly obtained from pit features from the model were excluded as in ref[145] and not included in the sensitivity testing (section 4) due to their context.

2.4.4. Debra L. Friedkin, Texas (U.S.A.)

See Clovis section.

2.4.5. Gault, Texas (U.S.A.)

See Clovis section.

2.4.6. Hebior and Schaefer, Wisconsin (U.S.A.)

The sites of Hebior (47KN265) and Schaefer (47KN252) (both at approximately 42.643, -88.010) contain mammoth remains showing human modification and associated lithic technology[146–152]. The archaeological status of the sites has been rejected by Grayson and Meltzer, due to perceived data insufficiencies and doubts regarding the association between the mammoths and the lithic artefacts[132,133]. Although multiple dates have been obtained[146,151,153,154],

XAD dates produced from mammoth bone samples are considered the most reliable. The incorporation of these into a single `Phase` model for each site dates the components to 15,615-13,975 cal BP (Hebior; `Date` function; Fig. S29) and 15,020-13,710 cal BP (Schaefer; `Date` function; Fig. S30).

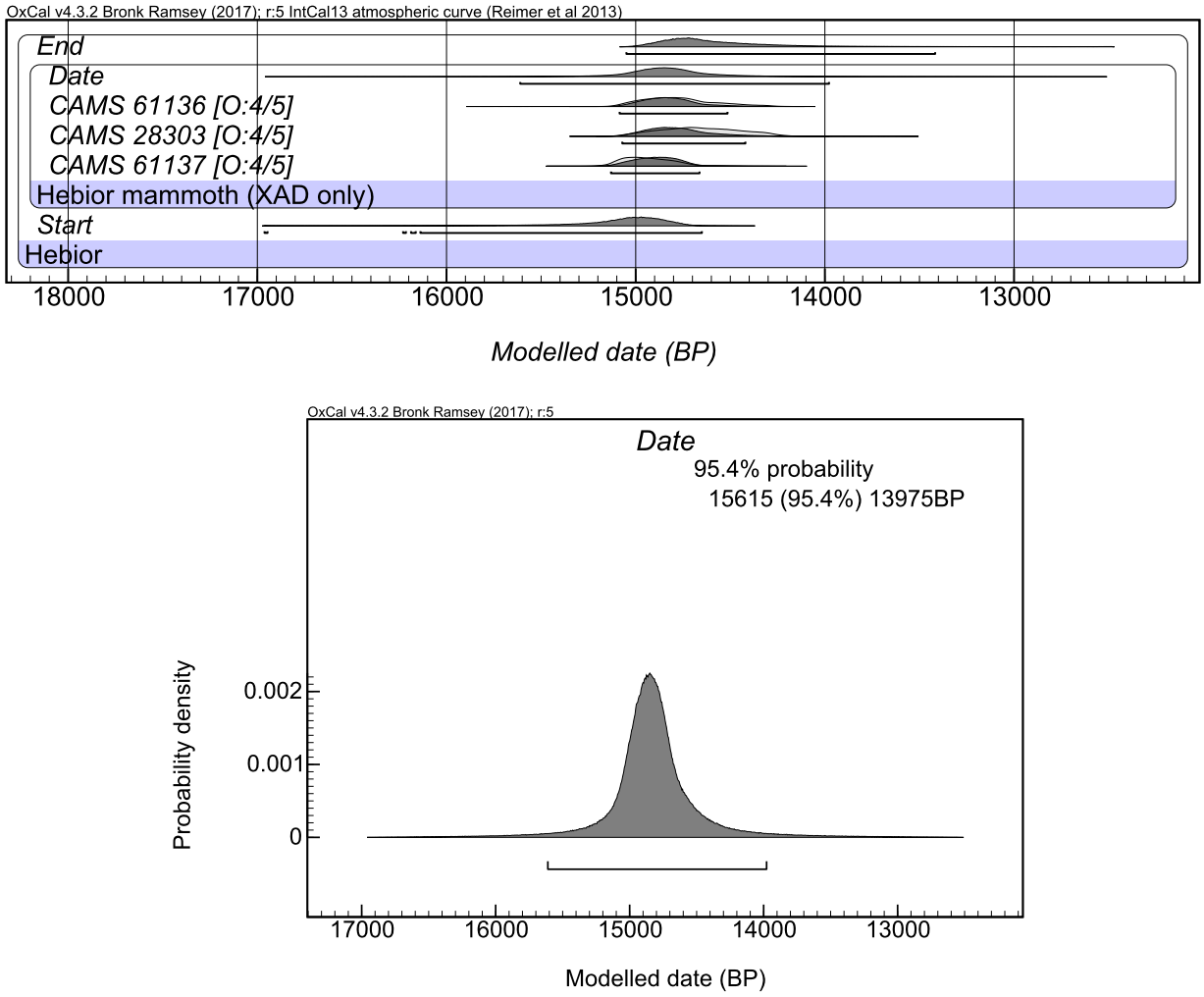


Fig. S29. Bayesian age model for Hebior (above), and `Date` function (below).

```
Sequence("Hebior")
{
 Outlier_Model("General",T(5),U(0,4),"t");
 Boundary("Start");
 Phase("Hebior mammoth (XAD only)")
 {
  R_Date("CAMS 61137", 12590, 50)
  {
   Outlier("General", 0.05);
  };
  R_Date("CAMS 28303", 12480, 60)
  {
   Outlier("General", 0.05);
  };
  R_Date("CAMS 61136", 12520, 50)
  {
   Outlier("General", 0.05);
  };
  Date("Date");
 };
 Boundary("End");
};
```

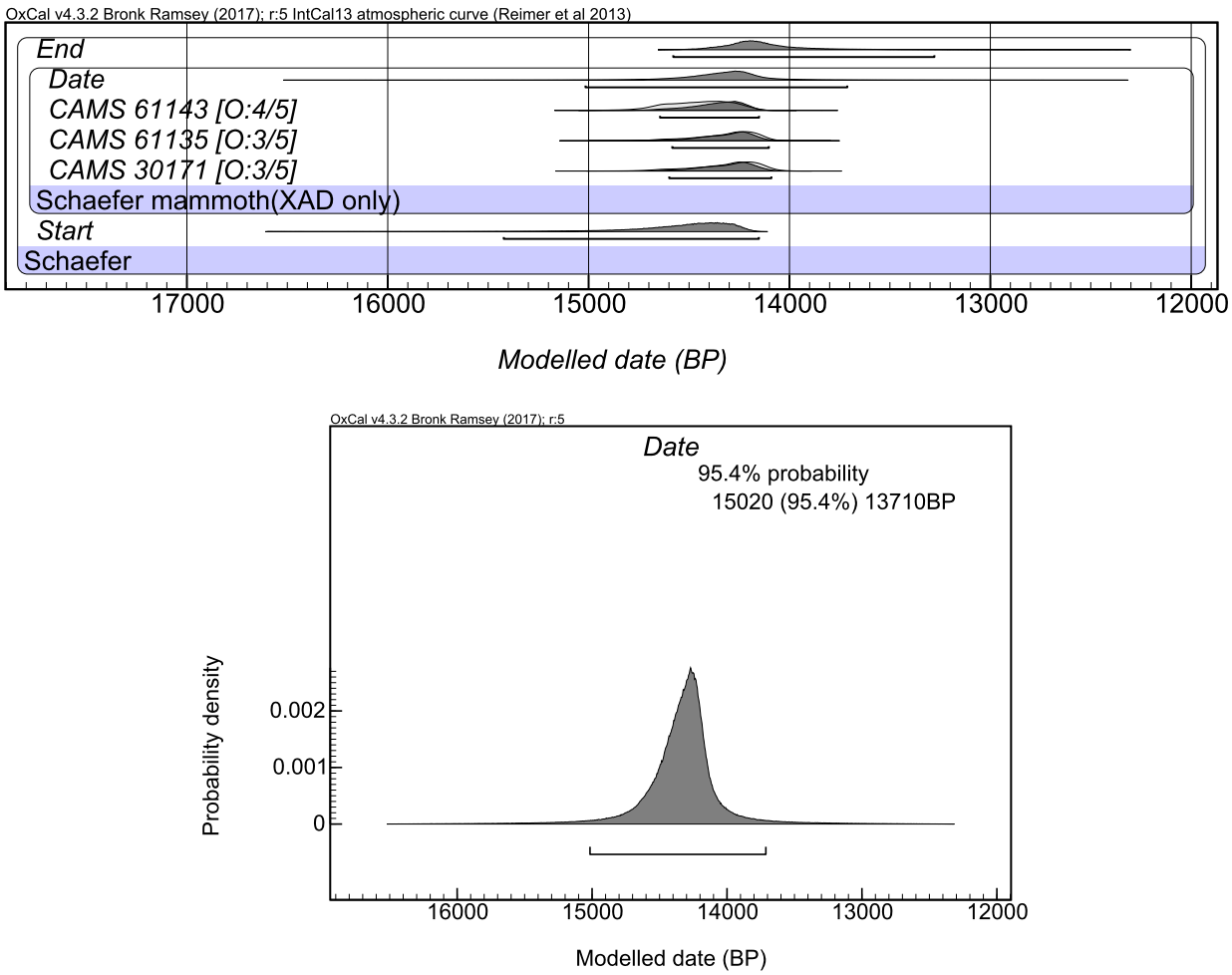


Fig. S30. Bayesian age model for Schaefer (above), and `Date` function (below).

```
Sequence("Schaefer")
 {
 Outlier_Model("General",T(5),U(0,4),"t");
 Boundary("Start");
 Phase("Schaefer mammoth(XAD only)")
  {
  R_Date("CAMS 30171", 12310, 60)
  {
  Outlier("General", 0.05);
  };
  R_Date("CAMS 61135", 12320, 50)
  {
  Outlier("General", 0.05);
  };
  R_Date("CAMS 61143", 12390, 40)
  {
  Outlier("General", 0.05);
  };
  Date("Date");
 };
 Boundary("End");
};
```

2.4.7. Lindsay, Montana (U.S.A.)

Lindsay site (24DW501; also known as Deer Creek; at approximately at 47.232458, -105.128239) contains the remains of a single mammoth[88,155,156]. Cut marks on the bones suggest evidence of disarticulation and meat stripping[157] (but see ref[132]). Although multiple dates have been obtained, four HYP and XAD dates produced from mammoth bone samples [88,158,159] are

considered the most reliable. The incorporation of these into a single `Phase` model dates the component to 14,625-13,945cal BP (`Date` function; Fig. S31).

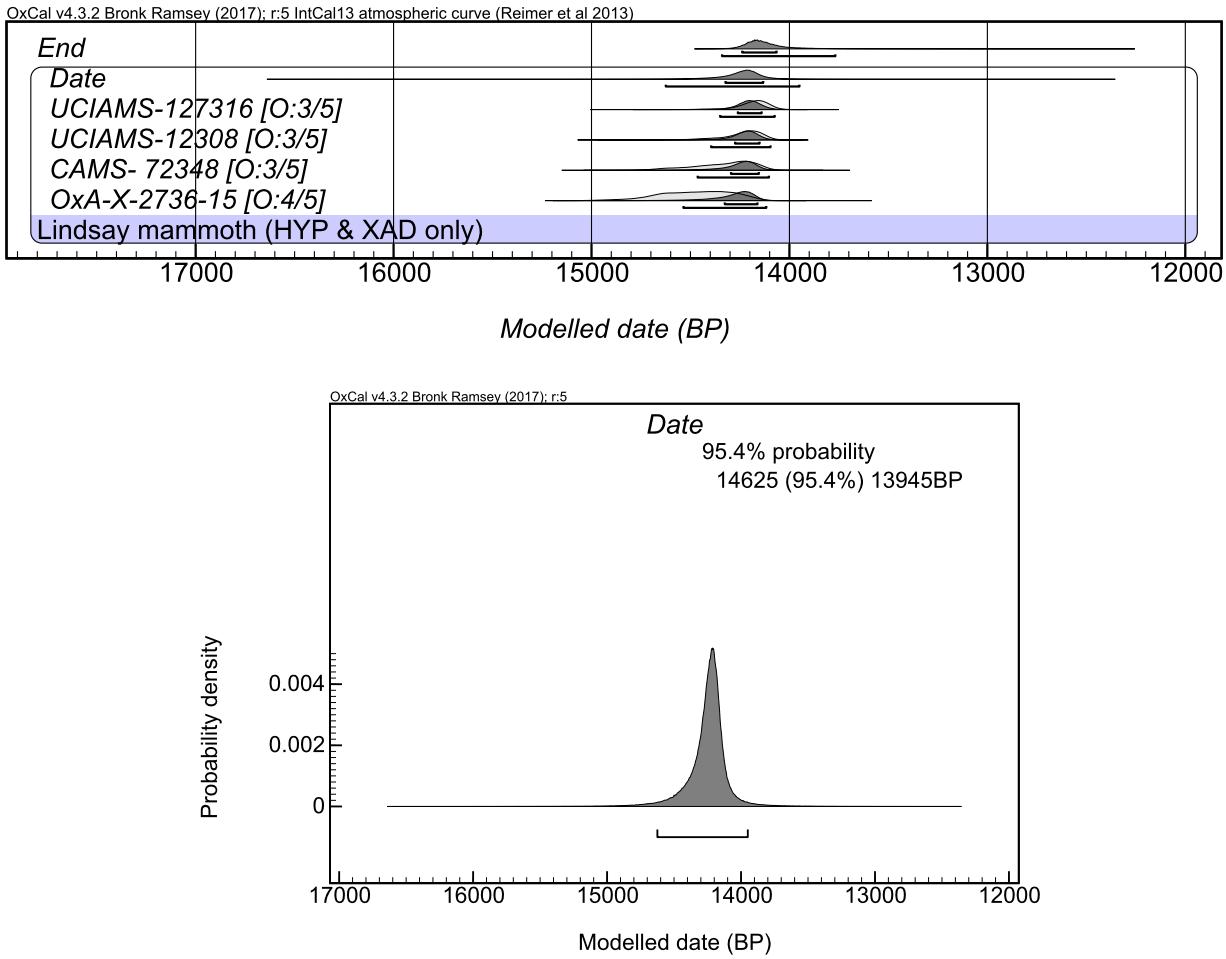


Fig. S31. Bayesian age model for Lindsay (above), and `Date` function (below).

```
Sequence("Lindsay")
 {
 Outlier_Model("General",T(5),U(0,4),"t");
 Boundary("Start");
 Phase("Lindsay mammoth (HYP & XAD only)")
 {
  R_Date("OxA-X-2736-15", 12395, 55)
  {
  Outlier("General", 0.05);
  };
  R_Date("CAMS- 72348", 12330, 50)
  {
  Outlier("General", 0.05);
  };
  R_Date("UCIAMS-12308", 12300, 35)
  {
  Outlier("General", 0.05);
  };
  R_Date("UCIAMS-127316", 12270, 35)
  {
  Outlier("General", 0.05);
  };
  Date("Date");
 };
 Boundary("End");
};
```

2.4.8. Manis, Washington (U.S.A.)

Manis site (45CA218; at approximately 48.032304, -123.101320) contains the remains of a single mastodon with an osseous (mastodon bone) projectile point embedded in its rib[160–162], but see refs[132,163]. Although multiple dates have been obtained for the site, four XAD dates produced

from mastodon bone samples are considered most reliable[160]. The incorporation of these into a single `Phase` model dates the component to 13,975-13,600 cal BP (`Date` function; Fig. S32).

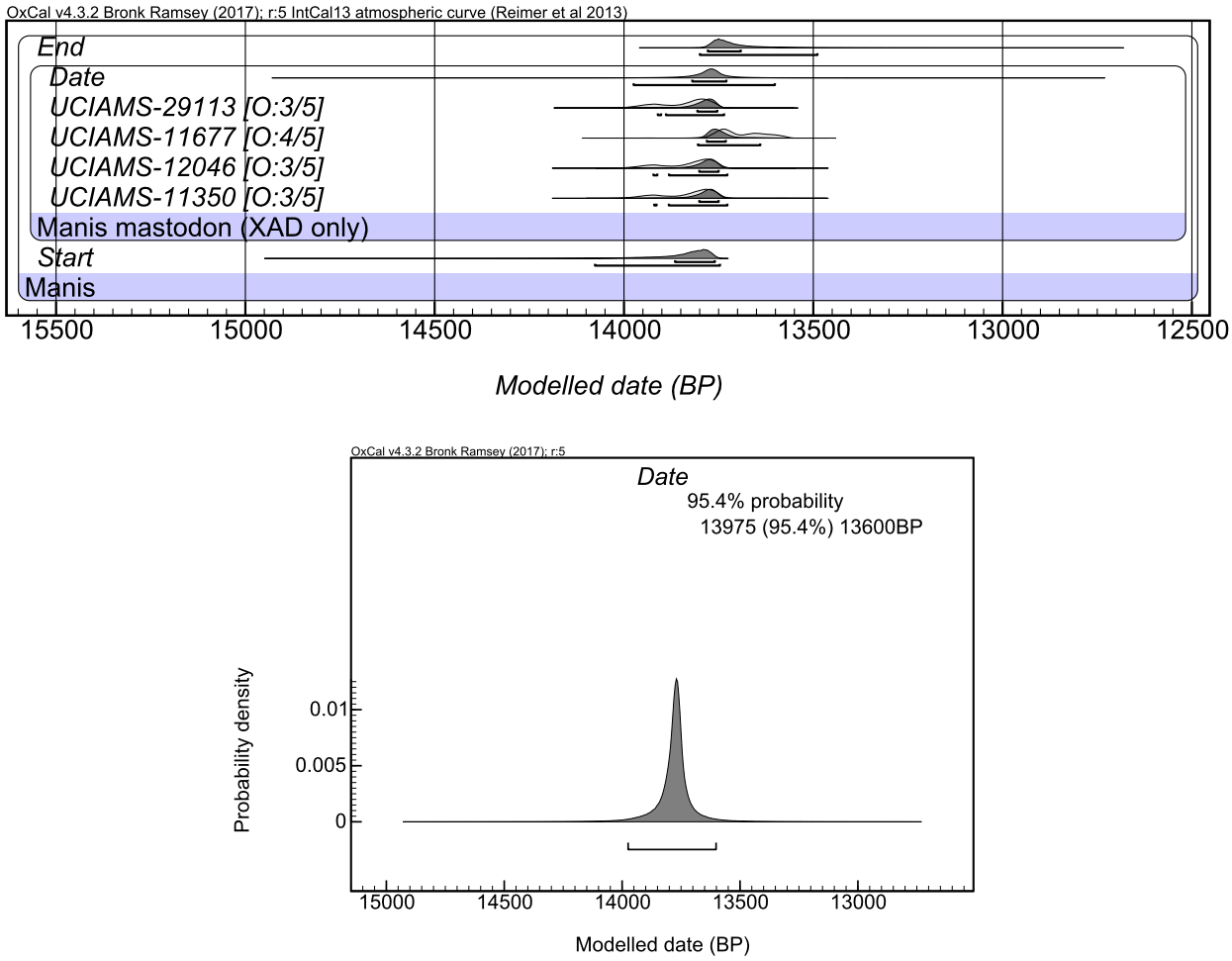


Fig. S32. Bayesian age model for Manis (above), and `Date` function (below).

```
Sequence("Manis")
 {
 Outlier_Model("General",T(5),U(0,4),"t");
 Boundary("Start");
 Phase("Manis mastodon (XAD only)")
 {
 R_Date("UCIAMS-11350",11975,35)
 {
 Outlier("General", 0.05);
 };
 R_Date("UCIAMS-12046",11975,35)
 {
 Outlier("General", 0.05);
 };
 R_Date("UCIAMS-11677",11890,35)
 {
 Outlier("General", 0.05);
 };
 R_Date("UCIAMS-29113",11990,30)
 {
 Outlier("General", 0.05);
 };
 Date("Date");
 };
 Boundary("End");
};
```

2.4.9. Meadowcroft Rockshelter, Pennsylvania (U.S.A.)

Meadowcroft Rockshelter (36WH297; at 40.286445, -80.488813) is a multi-component, stratified (strata I-XI) site containing pre-Clovis ("Miller complex"), Archaic, Woodland, and historic material[75,164–168]. Miller technology is found within Stratum IIa and all dates obtained provide stratigraphic control[165,168]. The antiquity of the basal strata [I and IIa (deepest levels)] has caused much controversy; some argue that old-carbon contamination has overestimated the radiocarbon results[169] and others note that insufficient data has been published[170]. For this reason, the start of Stratum IIa (F-46 Lower)—instead of Stratum IIa (deepest levels)—has been used to estimate the start of the pre-Clovis component at the site, placing it at 24,335-18,620 cal BP (Fig. S33). The imprecision of this boundary is likely due to a small temporal gap between the deepest levels of Stratum IIa and F-46 lower. Given the good agreement between chronometric data and stratigraphic evidence at this level, this, in turn, probably reflects a real taphonomic event or an artefact of sampling/dating bias.

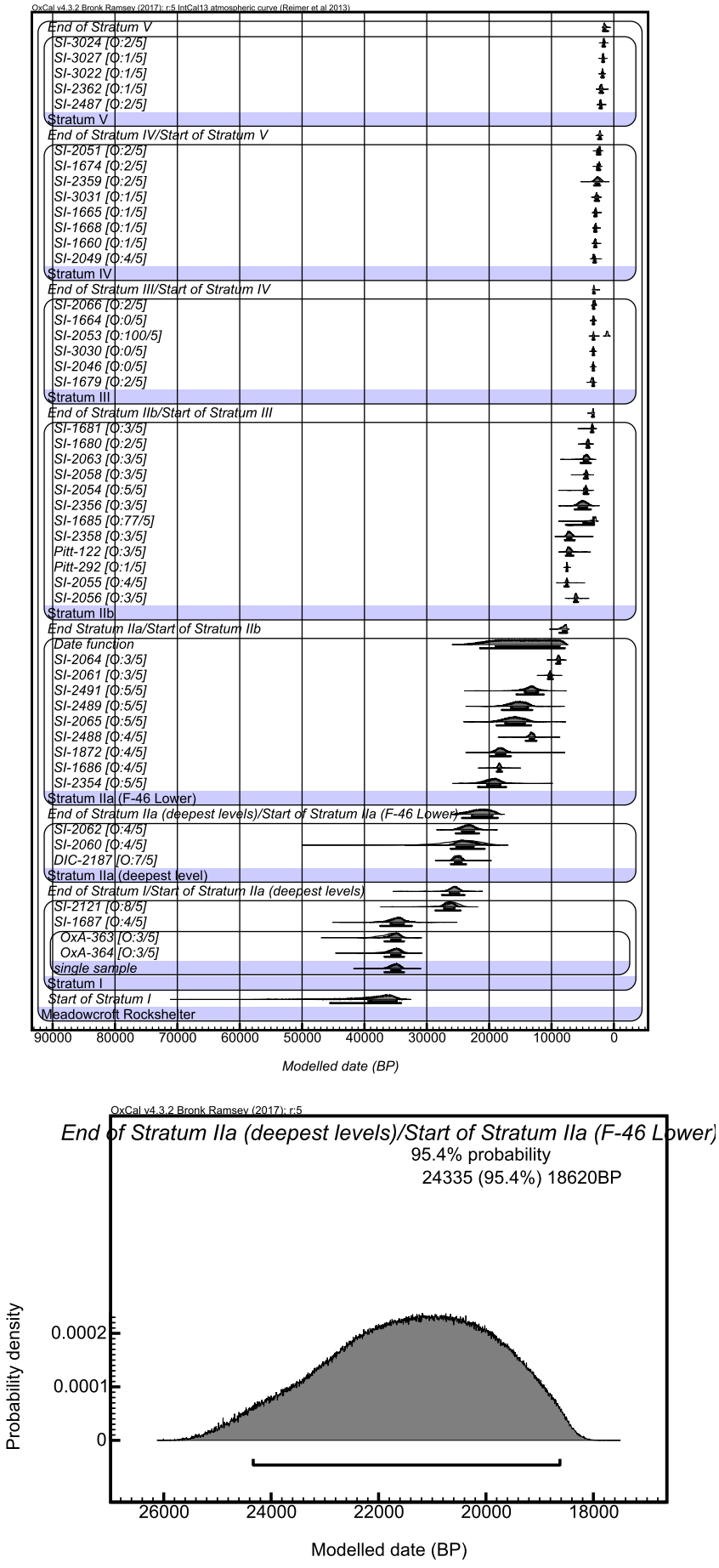


Fig. S33. Bayesian age model for Meadowcroft Rockshelter (above), and start `Boundary` (below).

```
Plot()
 {
 Outlier_Model("General",T(5),U(0,4),"t");
 Sequence("Meadowcroft Rockshelter")
 {
  Boundary("Start of Stratum I");
  Phase("Stratum I")
  {
  R_Combine("single sample")
   {
   R_Date("OxA-364", 30900, 1100)
    {
    Outlier("General", 0.05);
    };
   R_Date("OxA-363", 31400, 1200)
    {
    Outlier("General", 0.05);
    };
   };
  R_Date("SI-1687", 30710, 1140)
  {
   Outlier("General", 0.05);
  };
  R_Date("SI-2121", 21380, 800)
  {
   Outlier("General", 0.05);
  };
 };
 Boundary("End of Stratum I/Start of Stratum IIa (deepest levels)");
 Phase("Stratum IIa (deepest level)")
 {
 R_Date("DIC-2187", 21070, 475)
 {
  Outlier("General", 0.05);
 };
 //small diluted sample
 R_Date("SI-2060", 19600, 2400)
 {
  Outlier("General", 0.05);
 };
 //small diluted sample
 R_Date("SI-2062", 19100, 810)
 {
  Outlier("General", 0.05);
 };
};
Boundary("End of Stratum IIa (deepest levels)/Start of Stratum IIa (F-46 Lower)");
Phase("Stratum IIa (F-46 Lower)")
 {
 R_Date("SI-2354", 16175, 975)
 {
  Outlier("General", 0.05);
 };
 R_Date("SI-1686", 15120, 165)
 {
  Outlier("General", 0.05);
 };
 R_Date("SI-1872", 14975, 620)
 {
  Outlier("General", 0.05);
 };
 R_Date("SI-2488", 11320, 340)
 {
  Outlier("General", 0.05);
 };
 R_Date("SI-2065", 13240, 1010)
 {
  Outlier("General", 0.05);
 };
 R_Date("SI-2489", 12800, 870)
 {
  Outlier("General", 0.05);
 };
 R_Date("SI-2491", 11300, 700)
 {
  Outlier("General", 0.05);
 };
 R_Date("SI-2061", 9075, 115)
 {
  Outlier("General", 0.05);
 };
 R_Date("SI-2064", 8010, 110)
 {
  Outlier("General", 0.05);
 };
 Date("Date function");
};
Boundary("End Stratum IIa/Start of Stratum IIb");
Phase("Stratum IIb")
 {
 R_Date("SI-2056", 5300, 130)
 {
  Outlier("General", 0.05);
 };
 R_Date("SI-2055", 6670, 140)
 {
  Outlier("General", 0.05);
 };
 R_Date("Pitt-292", 6630, 70)
 {
  Outlier("General", 0.05);
 };
 R_Date("Pitt-122", 6315, 280)
 {
  Outlier("General", 0.05);
 };
 R_Date("SI-2358", 6290, 355)
 {
  Outlier("General", 0.05);
 };
 R_Date("SI-1685", 2870, 85)
 {
  Outlier("General", 0.05);
 };
 R_Date("SI-2356", 4380, 500)
 {
  Outlier("General", 0.05);
 };
 R_Date("SI-2054", 4005, 85)
 {
  Outlier("General", 0.05);
 };
 R_Date("SI-2058", 3970, 85)
 {
  Outlier("General", 0.05);
 };
 R_Date("SI-2063", 3950, 240)
 {
  Outlier("General", 0.05);
 };
 R_Date("SI-1680", 3770, 90)
 {
  Outlier("General", 0.05);
 };
 R_Date("SI-1681", 3210, 95)
 {
  Outlier("General", 0.05);
 };
};
Boundary("End of Stratum IIb/Start of Stratum III");
Phase("Stratum III")
 {
 R_Date("SI-1679", 3255, 115)
 {
  Outlier("General", 0.05);
 };
```

```
R_Date("SI-2046", 3115, 70)
 {
 Outlier("General", 0.05);
};
R_Date("SI-3030", 3100, 90)
 {
 Outlier("General", 0.05);
};
R_Date("SI-2053", 1140, 115)
 {
 Outlier("General", 0.05);
};
R_Date("SI-1664", 3065, 80)
 {
 Outlier("General", 0.05);
};
R_Date("SI-2066", 2930, 75)
 {
 Outlier("General", 0.05);
};
};
Boundary("End of Stratum III/Start of Stratum IV");
Phase("Stratum IV")
{
R_Date("SI-2049", 3050, 85)
 {
 Outlier("General", 0.05);
};
R_Date("SI-1660", 2860, 80)
 {
 Outlier("General", 0.05);
};
R_Date("SI-1668", 2820, 75)
 {
 Outlier("General", 0.05);
};
R_Date("SI-1665", 2815, 80)
 {
 Outlier("General", 0.05);
};
R_Date("SI-3031", 2655, 120)
 {
 Outlier("General", 0.05);
};
R_Date("SI-2359", 2485, 350)
 {
 Outlier("General", 0.05);
};
R_Date("SI-1674", 2325, 75)
 {
 Outlier("General", 0.05);
};
R_Date("SI-2051", 2290, 90)
 {
 Outlier("General", 0.05);
};
};
Boundary("End of Stratum IV/Start of Stratum V");
Phase("Stratum V")
{
R_Date("SI-2487", 2155, 65)
 {
 Outlier("General", 0.05);
};
R_Date("SI-2362", 2075, 125)
 {
 Outlier("General", 0.05);
};
R_Date("SI-3022", 1880, 65)
 {
 Outlier("General", 0.05);
};
R_Date("SI-3027", 1790, 60)
 {
 Outlier("General", 0.05);
};
R_Date("SI-3024", 1665, 65)
 {
 Outlier("General", 0.05);
};
};
Boundary("End of Stratum V");
};
};
```

2.4.10. Page-Ladson, Florida (U.S.A)

Page-Ladson (8JE591; at approximately 30.173805, -83.956282) is a stratified (units 2-4), underwater site containing a butchered mastodon with associated lithic tool technology. Radiocarbon data obtained from the 2013 excavations were used, where the pre-Clovis component is found within units 3c and 4[171,172]. Although the dates provide stratigraphic control, some of the measurements made on twigs are reported as mastodon digesta[171]. Using these data, the model created places the start of unit 3c at 16,985-14,375 cal BP (Fig. S34). The boundary is multimodal, however, due to poor agreement between dates and stratigraphic evidence in unit 3. This might be due to reliability of the chronometric data, taphonomic issues, or an artifact of

sampling/dating. Given the ages obtained for unit 3c in two cores at the site[171], the younger distribution is likely most accurate.

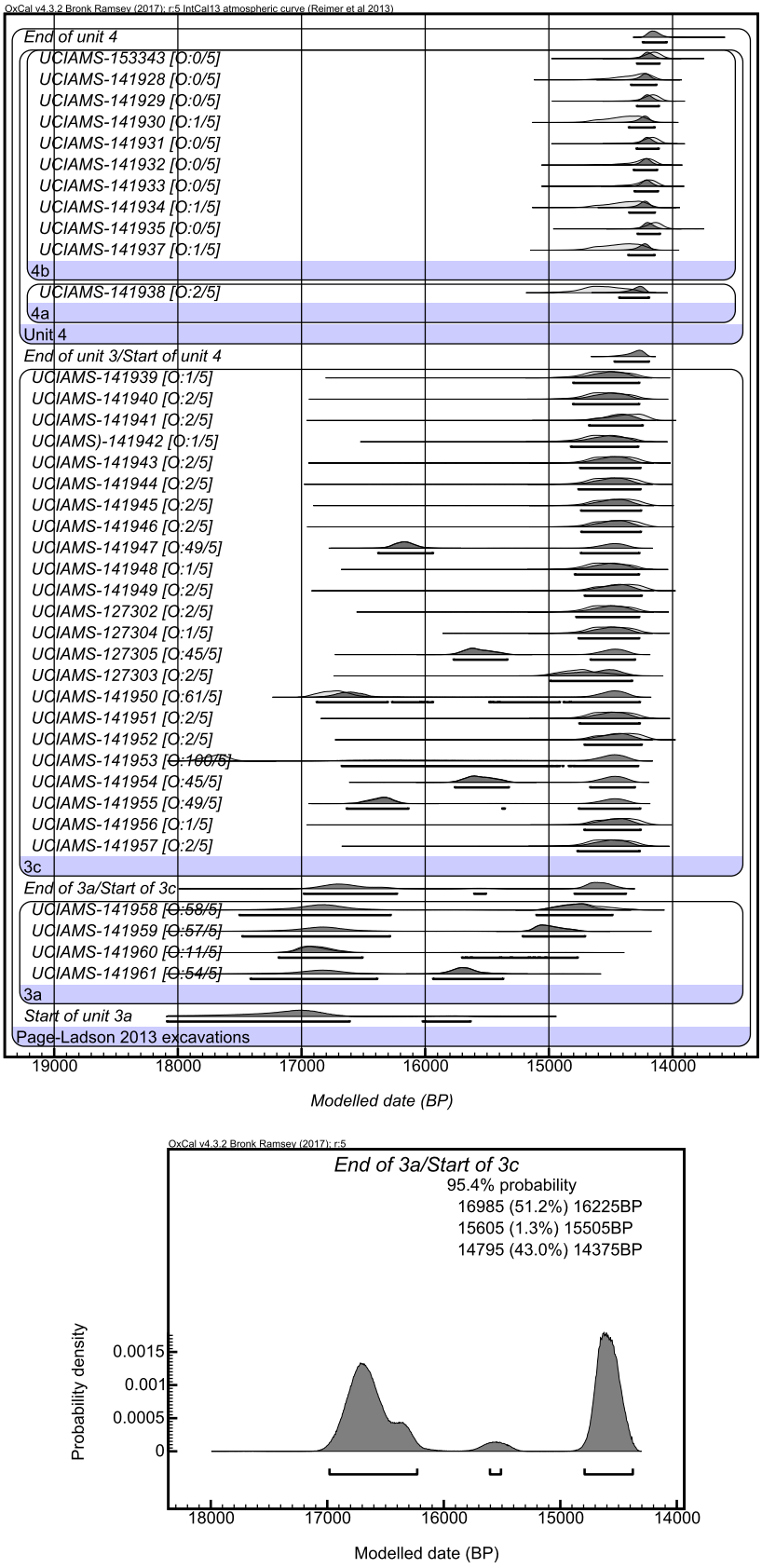


Fig. S34. Bayesian age model for Page-Ladson (above), and start `Boundary` (below).

```
Plot()
 {
 Outlier_Model("General", T(5), U(0,4), "t");
 Sequence("Page-Ladson 2013 excavations")
 {
  Boundary("Start of unit 3a");
  Phase("3a")
  {
  R_Date("UCIAMS-141961", 13080, 40)
   {
   Outlier("General", 0.05);
   };
  R_Date("UCIAMS-141960", 13945, 50)
   {
   Outlier("General", 0.05);
   };
  R_Date("UCIAMS-141959", 12615, 35)
   {
   Outlier("General", 0.05);
   };
  R_Date("UCIAMS-141958", 12495, 35)
   {
   Outlier("General", 0.05);
   };
  };
  Boundary("End of 3a/Start of 3c");
  Phase("3c")
  {
  R_Date("UCIAMS-141957", 12420, 30)
   {
   Outlier("General", 0.05);
   };
  R_Date("UCIAMS-141956", 12395, 30)
   {
   Outlier("General", 0.05);
   };
  R_Date("UCIAMS-141955", 13585, 35)
   {
   Outlier("General", 0.05);
   };
  R_Date("UCIAMS-141954", 13005, 35)
   {
   Outlier("General", 0.05);
   };
  R_Date("UCIAMS-141953", 14510, 40)
   {
   Outlier("General", 0.05);
   };
  R_Date("UCIAMS-141952", 12385, 35)
   {
   Outlier("General", 0.05);
   };
  R_Date("UCIAMS-141951", 12415, 30)
   {
   Outlier("General", 0.05);
   };
  R_Date("UCIAMS-141950", 13830, 35)
   {
   Outlier("General", 0.05);
   };
  R_Date("UCIAMS-127303", 12495, 30)
   {
   Outlier("General", 0.05);
   };
  R_Date("UCIAMS-127305", 13015, 30)
   {
   Outlier("General", 0.05);
   };
  R_Date("UCIAMS-127304", 12420, 30)
   {
   Outlier("General", 0.05);
   };
  R_Date("UCIAMS-127302", 12425, 30)
   {
   Outlier("General", 0.05);
   };
  R_Date("UCIAMS-141949", 12385, 35)
   {
   Outlier("General", 0.05);
   };
  R_Date("UCIAMS-141948", 12430, 30)
   {
   Outlier("General", 0.05);
   };
  R_Date("UCIAMS-141947", 13440, 40)
   {
   Outlier("General", 0.05);
   };
  R_Date("UCIAMS-141946", 12400, 35)
   {
   Outlier("General", 0.05);
   };
  R_Date("UCIAMS-141945", 12400, 35)
   {
   Outlier("General", 0.05);
   };
  R_Date("UCIAMS-141944", 12410, 35)
   {
   Outlier("General", 0.05);
   };
  R_Date("UCIAMS-141943", 12410, 30)
   {
   Outlier("General", 0.05);
   };
  R_Date("UCIAMS)-141942", 12440, 30)
   {
   Outlier("General", 0.05);
   };
  R_Date("UCIAMS-141941", 12365, 30)
   {
   Outlier("General", 0.05);
   };
  R_Date("UCIAMS-141940", 12430, 30)
   {
   Outlier("General", 0.05);
   };
  R_Date("UCIAMS-141939", 12430, 35)
   {
   Outlier("General", 0.05);
   };
  };
  Boundary("End of unit 3/Start of unit 4");
  Sequence("Unit 4")
  {
  Phase("4a")
   {
   R_Date("UCIAMS-141938", 12440, 30)
    {
    Outlier("General", 0.05);
    };
   };
  Phase("4b")
   {
   R_Date("UCIAMS-141937", 12380, 35)
    {
    Outlier("General", 0.05);
    };
   R_Date("UCIAMS-141935", 12250, 35)
    {
    Outlier("General", 0.05);
    };
   R_Date("UCIAMS-141934", 12365, 30)
    {
    Outlier("General", 0.05);
    };
   R_Date("UCIAMS-141933", 12295, 35)
```

```
 {
 Outlier("General", 0.05);
 };
 R_Date("UCIAMS-141932", 12310, 30)
 {
 Outlier("General", 0.05);
 };
 R_Date("UCIAMS-141931", 12275, 30)
 {
 Outlier("General", 0.05);
 };
 R_Date("UCIAMS-141930", 12370, 30)
 {
 Outlier("General", 0.05);
 };
 R_Date("UCIAMS-141929", 12270, 30)
 {
 Outlier("General", 0.05);
 };
 R_Date("UCIAMS-141928", 12335, 35)
 {
 Outlier("General", 0.05);
 };
 R_Date("UCIAMS-153343", 12260, 35)
 {
 Outlier("General", 0.05);
 };
 };
 };
 Boundary("End of unit 4");
 };
};
```

2.4.11. Paisley Caves, Oregon (U.S.A.)

Paisley Caves (or Paisley Five Mile Point Caves; 35LK3400; at approximately 42.776636, -120.667361) is a multi-cluster (caves 1, 2, 3, and 5), stratified (LU 1-7) with pre-Clovis and WST components[9,173–178]. In Cave 5, human coprolites found below WST artifacts have been found in the lowest level (LU 1), whilst the earliest WST projectile point base is found within the Indurated Silt Lense (ISL) in LU 2. The latter is bounded by dated samples 2010PC-223 (on top and within the ISL) and 2010PC-224 (beneath the ISL)[174]. Although the site is stratified, modeling Paisley Caves within a bounded sequence is not straightforward; 203 radiocarbon dates have been obtained from different caves, profiles, units, and multiple, distinct archeological events[174]. These provide stratigraphic control and date cultural features directly, e.g., human coprolites. If data from Cave 5, LU's 1-3, are incorporated in a model, the order of the sequence cannot be resolved. For this reason, the age for the pre-Clovis component has been obtained through a `Date` function (14,755-13,780 cal BP) for the three earliest human coprolites (Fig. S35). Given that these date human presence directly, this is likely an accurate estimate. Moreover, considering that the age of the earliest WST artifact is extrapolated from dating done at Profile III[174], we have modelled this sequence to obtain a PDF for the start of the Western Stemmed tradition component at the site (13,110-13,015 cal BP; Fig. S36).

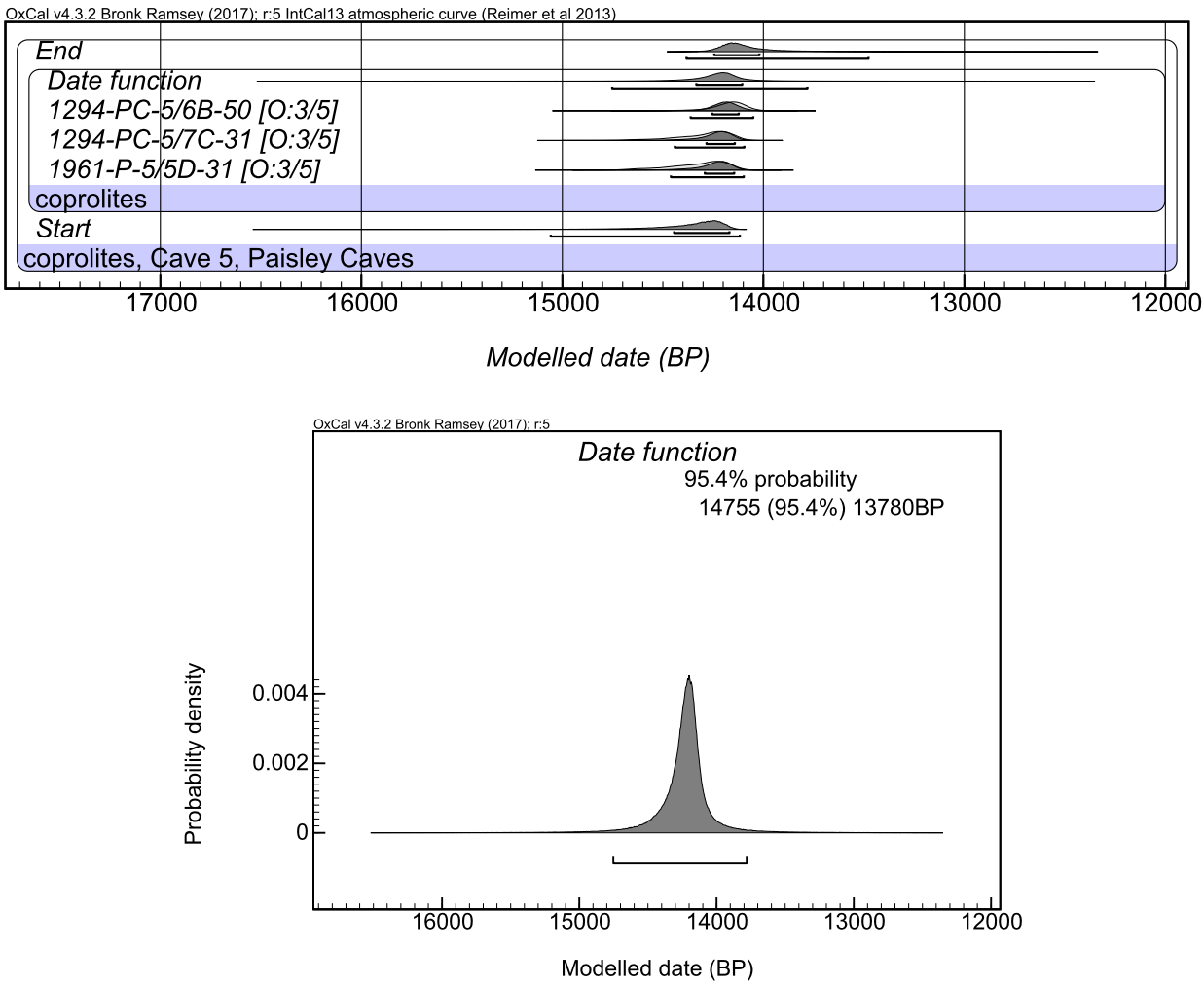
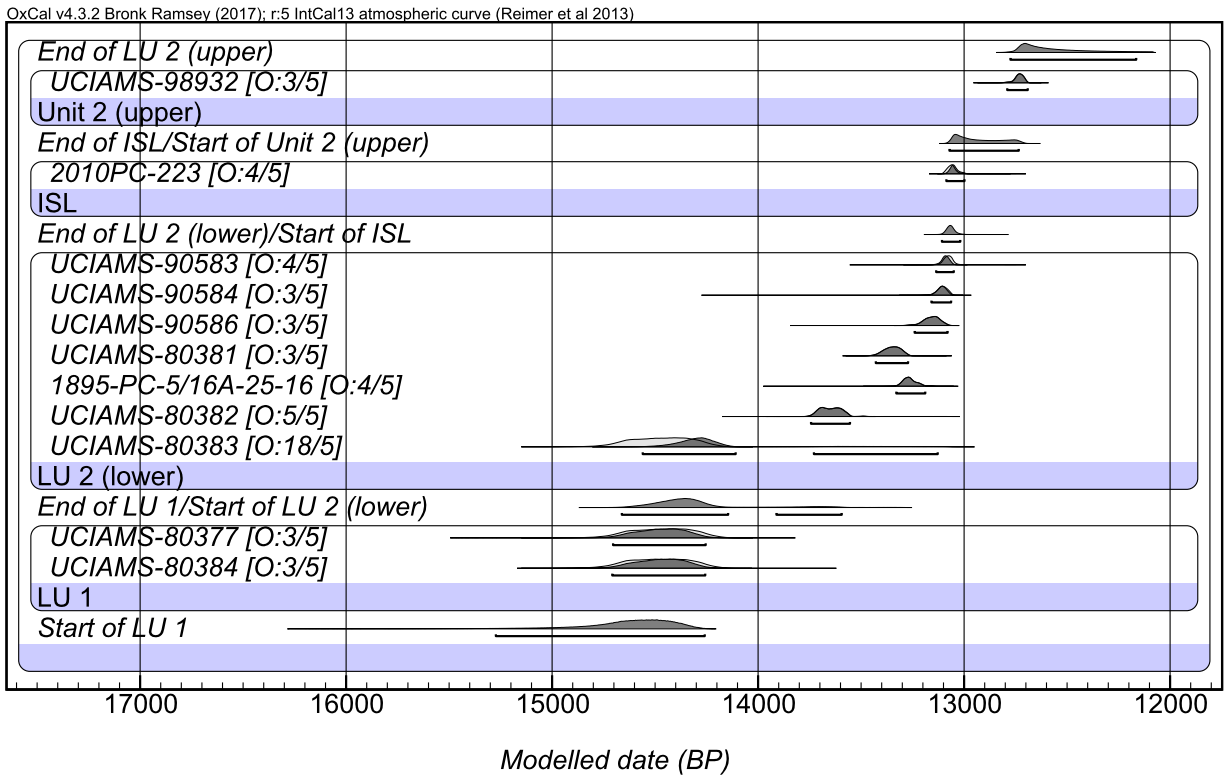


Fig. S35. Bayesian age model for Paisley Caves (coprolites; above), and `Date` function (below).



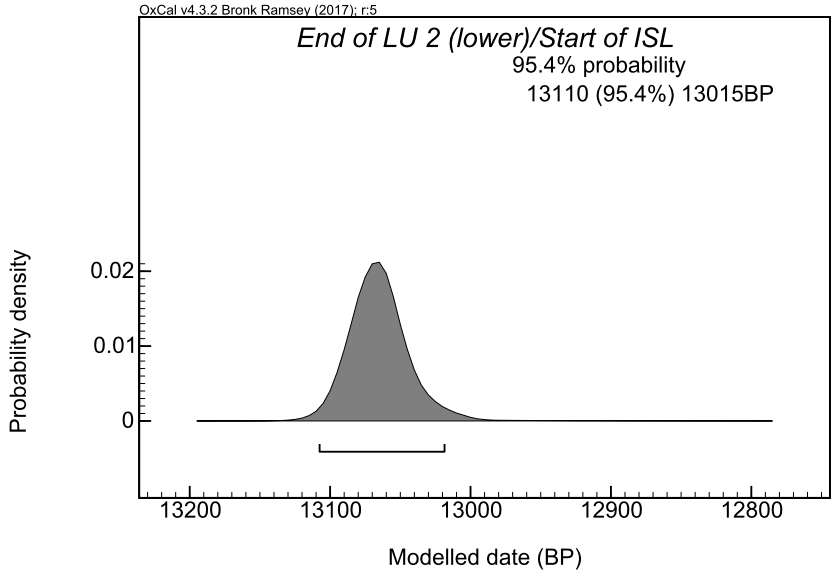


Fig. S36. Bayesian age model for Paisley Caves (Profile III; above), and start `Boundary` (below).

```
Plot()
 {
 Outlier_Model("General",T(5),U(0,4),"t");
 Sequence("human coprolites, Cave 5, Paisley Caves")
  {
  Boundary("Start");
  Phase()
  {
  R_Combine("1961-P-5/5D-31")
   {
   R_Date("Beta-213424", 12400, 60);
   R_Date("OxA-16498", 12275, 55);
   Outlier("General", 0.05);
   };
  R_Combine("1294-PC-5/7C-31")
   {
   R_Date("OxA-16497", 12345, 55);
   R_Date("Beta-213426", 12290, 60);
   Outlier("General", 0.05);
   };
  R_Combine("1294-PC-5/6B-50")
   {
   R_Date("Beta-216474", 12260, 60);
   R_Date("OxA-16495", 12140, 70);
   Outlier("General", 0.05);
   };
```

```
  R_Combine("1294-PC-5/6B-40")
  {
   R_Date("Beta-213423", 10050, 50);
   R_Date("OxA-16376", 10965, 50);
   Outlier("General", 0.05);
  };
  Date("Date function");
 };
 Boundary("End");
};
};

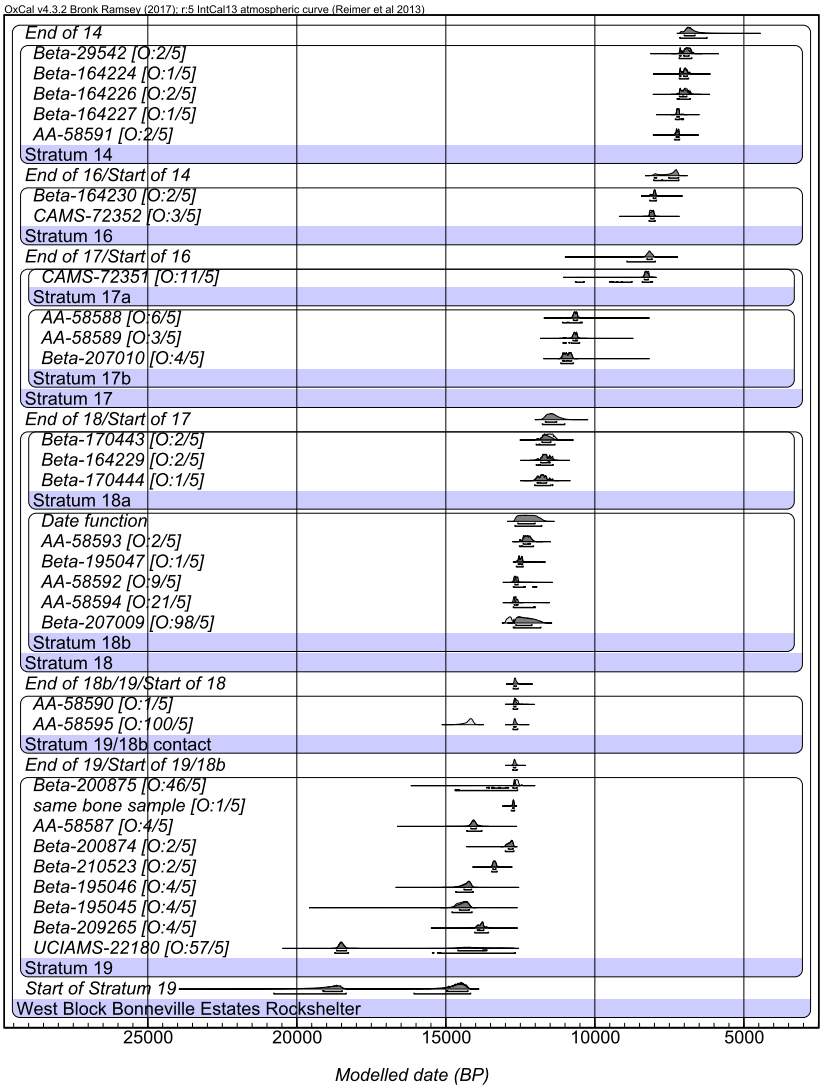
Plot()
{
 Outlier_Model("General",T(5),U(0,4),"t");
 Sequence("Profile II, Cave 5, Paisley Caves")
 {
  Boundary("Start of LU 1");
  Phase("LU 1")
  {
   R_Date("UCIAMS-80384", 12410, 25)
   {
    Outlier("General", 0.05);
   };
   R_Date("UCIAMS-80377", 12405, 25)
   {
    Outlier("General", 0.05);
   };
  };
  Boundary("End of LU 1/Start of LU 2 (lower)");
  Phase("LU 2 (lower)")
  {
   R_Date("UCIAMS-80383", 12405, 25)
   {
    Outlier("General", 0.05);
   };
   R_Date("UCIAMS-80382", 11815, 25)
   {
    Outlier("General", 0.05);
   };
   R_Combine("1895-PC-5/16A-25-16")
   {
    R_Date("UCIAMS-90582", 11505, 30);
    R_Date("UCIAMS-90581", 11340, 30);
    Outlier("General", 0.05);
   };
   R_Date("UCIAMS-80381", 11500, 30)
   {
    Outlier("General", 0.05);
   };
   R_Date("UCIAMS-90586", 11315, 25)
   {
    Outlier("General", 0.05);
   };
   R_Date("UCIAMS-90584", 11250, 25)
   {
    Outlier("General", 0.05);
   };
   R_Date("UCIAMS-90583", 11205, 25)
   {
    Outlier("General", 0.05);
   };
  };
  Boundary("End of LU 2 (lower)/Start of ISL");
  Phase("ISL")
  {
   R_Combine("2010PC-223")
   {
    R_Date("UCIAMS-80379", 11295, 25);
    R_Date("UCIAMS-80380", 11165, 25);
    R_Date("UCIAMS-80378", 11070, 25);
    Outlier("General", 0.05);
   };
  };
  Boundary("End of ISL/Start of Unit 2 (upper)");
  Phase("Unit 2 (upper)")
  {
   R_Date("UCIAMS-98932", 10855, 30)
   {
    Outlier("General", 0.05);
   };
  };
  Boundary("End of LU 2 (upper)");
 };
};
```

2.5. Western Stemmed tradition

2.5.1. Bonneville Estates Rockshelter, Nevada (U.S.A.)

Bonneville Estates Rockshelter (26EK3682; at approximately 40.294985, -114.076284) is a multi-cluster (e.g., East and West blocks), stratified (strata 1-19) site containing WST lithic technology and hearth features[8,179–184]. The earliest cultural components are represented in stratum 12, for East block, and 18b, for West block. Dates obtained provide stratigraphic control or date cultural features directly, e.g., hearth charcoal. Using these data, the models created place the start of the WST to 12,740-12,570 cal BP, at the East block, and 12,760-12,605 at cal BP, at the West block (see below for both sets of CQL code). The PDF for the start of stratum 19/18b

contact for the West block (Fig. S37) was used in the tradition-level model, due to a larger sample size.



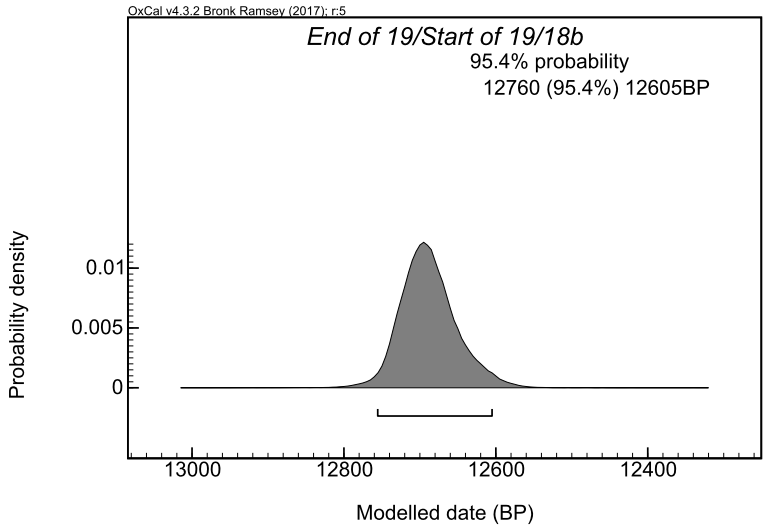


Fig. S37. Bayesian age model for Bonneville Estates Rockshelter (above), and start `Boundary` (below).

```
Plot()
{
 Outlier_Model("General",T(5),U(0,4),"t");
 Sequence("West Block, Bonneville Estates Rockshelter")
 {
  Boundary("Start of Stratum 19");
  Phase("Stratum 19")
  {
   R_Date("UCIAMS-22180", 15240, 50)
   {
    Outlier("General", 0.05);
   };
   R_Date("Beta-209265", 11960, 60)
   {
    Outlier("General", 0.05);
   };
   R_Date("Beta-195045", 12390, 40)
   {
    Outlier("General", 0.05);
   };
   R_Date("Beta-195046", 12330, 40)
   {
    Outlier("General", 0.05);
   };
   R_Date("Beta-210523", 11530, 40)
   {
    Outlier("General", 0.05);
   };
   R_Date("Beta-200874", 10970, 60)
   {
    Outlier("General", 0.05);
   };
   R_Date("AA-58587", 12180, 60)
   {
    Outlier("General", 0.05);
   };
   R_Combine("same bone sample")
   {
    R_Date("UCIAMS-22176", 10900, 50);
    R_Date("Beta-210524", 10830, 40);
    Outlier("General", 0.05);
   };
   R_Date("Beta-200875", 10640, 60)
   {
    Outlier("General", 0.05);
   };
  };
  Boundary("End of 19/Start of 19/18b");
  Phase("Stratum 19/18b contact")
  {
   R_Date("AA-58595", 12270, 60)
   {
    Outlier("General", 0.05);
   };
   R_Date("AA-58590", 10690, 70)
   {
    Outlier("General", 0.05);
   };
  };
  Boundary("End of 18b/19/Start of 18");
  Sequence("Stratum 18")
  {
   Phase("Stratum 18b")
   {
    R_Date("Beta-207009", 11010, 40)
    {
     Outlier("General", 0.05);
    };
    R_Date("AA-58594", 10800, 60)
    {
     Outlier("General", 0.05);
    };
    R_Date("AA-58592", 10760, 70)
    {
     Outlier("General", 0.05);
    };
    R_Date("Beta-195047", 10540, 40)
    {
     Outlier("General", 0.05);
    };
    R_Date("AA-58593", 10405, 50)
    {
     Outlier("General", 0.05);
    };
    Date("Date function");
   };
   Phase("Stratum 18a")
   {
    R_Date("Beta-170444", 10130, 60)
    {
     Outlier("General", 0.05);
    };
    R_Date("Beta-164229", 10080, 50)
    {
     Outlier("General", 0.05);
    };
    R_Date("Beta-170443", 10040, 70)
    {
     Outlier("General", 0.05);
    };
   };
  };
  Boundary("End of 18/Start of 17");
  Sequence("Stratum 17")
  {
   Phase("Stratum 17b")
   {
    R_Date("Beta-207010", 9580, 40)
    {
     Outlier("General", 0.05);
    };
    R_Date("AA-58589", 9440, 50)
    {
     Outlier("General", 0.05);
    };
    R_Date("AA-58588", 9430, 50)
    {
     Outlier("General", 0.05);
    };
   };
   Phase("Stratum 17a")
   {
    R_Date("CAMS-72351", 7420, 50)
    {
     Outlier("General", 0.05);
    };
   };
  };
  Boundary("End of 17/Start of 16");
  Phase("Stratum 16")
  {
   R_Date("CAMS-72352", 7280, 50)
   {
    Outlier("General", 0.05);
   };
   R_Date("Beta-164230", 7190, 50)
   {
    Outlier("General", 0.05);
   };
  };
  Boundary("End of 16/Start of 14");
  Phase("Stratum 14")
  {
   R_Date("AA-58591", 6315, 40)
   {
    Outlier("General", 0.05);
```

```
  };
  R_Date("Beta-164227", 6280, 40)
  {
   Outlier("General", 0.05);
  };
  R_Date("Beta-164226", 6100, 80)
  {
   Outlier("General", 0.05);
  };
  R_Date("Beta-164224", 6100, 50)
  {
   Outlier("General", 0.05);
  };
  R_Date("Beta-29542", 6040, 80)
  {
   Outlier("General", 0.05);
  };
 };
 Boundary("End of 14");
};
};

Plot()
{
 Outlier_Model("General",T(5),U(0,4),"t");
 Sequence("East Block, Bonneville Estates Rockshelter")
 {
  Boundary("Start of Stratum 12");
  Phase("Stratum 12")
  {
  R_Date("Beta-195013", 10390, 40)
   {
   Outlier("General", 0.05);
   };
  R_Date("Beta-203504", 10340, 60)
   {
   Outlier("General", 0.05);
   };
  R_Date("Beta-206278", 10250, 50)
   {
   Outlier("General", 0.05);
   };
  R_Date("AA-58600", 10380, 60)
   {
   Outlier("General", 0.05);
   };
  R_Date("Beta-182935", 10050, 50)
   {
   Outlier("General", 0.05);
   };
  R_Date("Beta-182934", 10030, 50)
   {
   Outlier("General", 0.05);
   };
  R_Date("Beta-182931", 10560, 50)
   {
   Outlier("General", 0.05);
   };
  R_Date("AA-58598", 9990, 50)
   {
   Outlier("General", 0.05);
   };
  };
  Boundary("End of 12/Start of 10");
  Phase("Stratum 10")
  {
  R_Date("Beta-195042", 9580, 40)
   {
   Outlier("General", 0.05);
   };
  R_Date("Beta-195044", 9570, 40)
   {
   Outlier("General", 0.05);
   };
  R_Date("Beta-161891", 9520, 60)
   {
   Outlier("General", 0.05);
   };
  R_Date("AA-58599", 9440, 80)
   {
   Outlier("General", 0.05);
   };
  R_Date("Beta-203507", 8830, 60)
   {
   Outlier("General", 0.05);
   };
  };
  Boundary("End of 10/Start of 9b");
  Phase("Stratum 9b")
  {
  R_Date("AA-58596", 7240, 50)
   {
   Outlier("General", 0.05);
   };
  R_Date("Beta-182933", 5350, 70)
   {
   Outlier("General", 0.05);
   };
  R_Date("Beta-182928", 5160, 80)
   {
   Outlier("General", 0.05);
   };
  };
  Boundary("End of Stratum 9");
 };
};
```

2.5.2. Buhl, Idaho (U.S.A.)

Buhl (10TF1019; at approximately 42.658225, -114.788668) is a burial site containing the partial remains of a female individual associated with osseous artifacts and an obsidian stemmed point[8,143,185]. A direct bone (collagen) date (10,675±95 BP; Beta-43055 & ETH-7729) places the site at 12,740-12,420 cal BP.

2.5.3. Cooper's Ferry, Idaho (U.S.A.)

See pre-Clovis section.

2.5.4. Paisley Caves, Oregon (U.S.A.)

See pre-Clovis section.

3. Data tabulation

Following the analysis in section 2, two tables were compiled. The first, Table S1, is a tabulation of chronometric data included in Bayesian age models, according to each archaeological site. Provenience, material type and sources are noted. The second, Table S2, is a summary of age estimates obtained for the tradition or temporal components of interest. Where applicable, these were incorporated into tradition-level models (Figs. S1-S3).

Table S1. Chronometric data (n=711) from the 41 archaeological sites included in the Bayesian age modeling (noted as in sources).

Site name	Provenience	Sample material	Laboratory code	Date (BP or ka)	Source	Notes
Anzick	-	human bone (Anzick-1; HYP)	OxA-X-2739-54	10915±50	*62*	
Anzick	-	antler rod (HYP)	OxA-X-2739-55	10900±50	*62*	
Anzick	-	antler rod (HYP)	OxA-X-2739-56	11050±55	*62*	
Arlington Springs	-	human femur	CAMS-16810	10,960±80	*5*	
Aubrey	surface of Unit A/ Clovis camp	charcoal	AA-5274	11590±93	*63*	
Aubrey	surface of Unit A/ Clovis camp	charcoal	AA-5271	11542±111	*63*	
Aubrey	Unit F	humate	SMU-2338	10718±90	*63*	
Aubrey	Unit F	sediment	Beta-32002	10360±150	*63*	
Aubrey	Unit G	humate	SMU-2398	10084±80	*63*	
Aubrey	Unit G	humate	SMU-2399	9572±130	*63*	
Aubrey	Unit G	humate	SMU-2400	8275±70	*63*	
Aubrey	Unit G	humate	SMU-2339	7582±320	*63*	
Berelehk	T2 profile BA1; layer1	silt with plant macro remains	Beta-269467	13390±60	*19*	

Site name	Provenience	Sample material	Laboratory code	Date (BP or ka)	Source	Notes
Berelehk	T2 profile BA1; layer1	silt with plant macro remains	Beta-269468	12350±60	*19*	
Berelehk	T2 profile BA1; layer 2	silt with plant macro remains	Beta-269469	12220±60	*19*	
Berelehk	T2 profile BA1; layer 2	charred material screened from culture-bearing layer	Beta-269470	12100±60	*19*	
Berelehk	T2 profile BA1; layer 2	wolf phalanx	Beta-269446	12090±60	*19*	
Berelehk	T2 profile BA1; layer 2	twigs, material screened from culture-bearing layer	Beta-269447	11830±60	*19*	
Berelehk	T2 profile BA1; layer 2	arctic fox	Beta-269440	11830±60	*19*	
Berelehk	T2 profile BA1; layer 2	Pleistocene hare	Beta-271415	11890±60	*19*	
Berelehk	T2 profile BA1; layer 2	Pleistocene hare	Beta-271416	11990±60	*19*	
Berelehk	T2 profile BA1; layer 2	Pleistocene hare	Beta-271418	11890±60	*19*	
Berelehk	T2 profile BA1; layer 2	bird bone/ ptarmigan (?), screened material	Beta-271420	11940±60	*19*	
Blackwater Locality No. 1	Unit A7-8	humates	AA-7093	22930±290	*66*	
Blackwater Locality No. 1	Unit A7-8	organic residue	AA-7092	17220±170	*66*	
Blackwater Locality No. 1	Unit B	sediment (humates)	AA-2262	11810±90	*66*	
Blackwater Locality No. 1	Unit B	sediment (humates)	AA-2263	12790±160	*66*	
Blackwater Locality No. 1	Unit B	sediment (humates)	AA-1374	12330±110	*66*	
Blackwater Locality No. 1	Unit B	sediment (humates)	AA-1375	11380±150	*66*	
Blackwater Locality No. 1	Unit C0-1	carbonized plant remains	A-491	11630±400	*66*	
Blackwater Locality No. 1	Unit C0-1	carbonized plant remains	A-481	11170±360	*66*	
Blackwater Locality No. 1	Unit C0-1	soluble plant remains	A-490	11040±500	*66*	
Blackwater Locality No. 1	Unit C0-1	carbonized wood flecks	AA-1360	10580±100	*66*	
Blackwater Locality No. 1	Unit D	soluble plant remains	A-492	10490±200	*66*	

Site name	Provenience	Sample material	Laboratory code	Date (BP or ka)	Source	Notes
Blackwater Locality No. 1	Unit D	sediment humic acids	A-386	10490±900	*66*	
Blackwater Locality No. 1	Unit D	soluble plant remains	A-488	10170±260	*66*	
Blackwater Locality No. 1	Unit D	sediment organic residue	A-379	9900±320	*66*	
Blackwater Locality No. 1	Unit D	sediment organic acids from A-379	A-380	10600±320	*66*	
Blackwater Locality No. 1	Unit D	sediment (humates)	AA-1412	9860±210	*66*	
Blackwater Locality No. 1	Unit D	sediment	A-4701	10470±580	*66*	
Blackwater Locality No. 1	Unit D	sediment	AA-1362	10740±100	*66*	
Blackwater Locality No. 1	Unit D	sediment	AA-1363	10160±120	*66*	
Blackwater Locality No. 1	Unit D	sediment	AA-1364	10210±110	*66*	
Blackwater Locality No. 1	Unit D	charcoal flecks	AA-1371	9560±180	*66*	
Blackwater Locality No. 1	Unit D	charcoal lump	AA-1370	10260±230	*66*	
Blackwater Locality No. 1	Unit D	sediment (humates)	A-4702	9870±320	*66*	
Blackwater Locality No. 1	Unit D	sediment (humates)	AA-2261	9950±100	*66*	
Blackwater Locality No. 1	Unit D	carbonized plants (humates)	AA-1361	10640±110	*66*	
Blackwater Locality No. 1	Unit D	bone	AA-1409	6660±160	*66*	
Blackwater Locality No. 1	Unit D	bison bone	Y-1991	8430±200	*66*	
Blackwater Locality No. 1	Unit D	sediment organic residue	Y-2489	9400±200	*66*	
Blackwater Locality No. 1	Unit E/D	humates	A-1372	10250±200	*66*	
Blackwater Locality No. 1	Unit E	sediment (humate)	A-4705	9296±320	*66*	
Blackwater Locality No. 1	Unit E	sediment (humates)	A-4703	10000±910	*66*	

Site name	Provenience	Sample material	Laboratory code	Date (BP or ka)	Source	Notes
Blackwater Locality No. 1	Unit E	sediment (humates)	A-4700	8630±310	*66*	
Blackwater Locality No. 1	Unit E	sediment (organic residue)	AA-1365	8230±100	*66*	
Blackwater Locality No. 1	Unit E	sediment (humates)	AA-1366	9890±100	*66*	
Blackwater Locality No. 1	Unit E	sediment (organic residue)	AA-1367	9150±90	*66*	
Blackwater Locality No. 1	Unit E	sediment (humates)	AA-1368	11400±190	*66*	
Blackwater Locality No. 1	Unit E	sediment (organic residue)	AA-1358	10190±130	*66*	
Blackwater Locality No. 1	Unit E	sediment (humates)	AA-1359	9590±120	*66*	
Blackwater Locality No. 1	Unit E	bison bone	Y-1990	7610±160	*66*	
Blackwater Locality No. 1	Unit E	sediment organic residue	Y-2488	8830±160	*66*	
Blackwater Locality No. 1	Unit E	sediment organic residue	Y-2487	7020±180	*66*	
Blackwater Locality No. 1	Unit F/E	bone	AA-1408	6190±130	*66*	
Blackwater Locality No. 1	Unit F/E	burned bone	AA-1413	8830±120	*66*	
Blackwater Locality No. 1	Unit F/E	bison bone	O-169	6300±150	*66*	
Blackwater Locality No. 1	Unit F/E	bison bone	O-170	6230±150	*66*	
Blackwater Locality No. 1	Unit F/E	soluble plant remains	A-489	9890±290	*66*	
Blackwater Locality No. 1	Unit G	soil organic residue	SI-4585	4855±90	*66*	
Blackwater Locality No. 1	Unit G	burned bison bone	A-512	8470±350	*66*	
Blackwater Locality No. 1	Unit G	burned bison bone	O-157	4950±150	*66*	
Blackwater Locality No. 1	Unit G	bison metacarpal	Y-1989	8450±280	*66*	
Blackwater Locality No. 1	Unit G	soil organic residue	Y-2490	910±100	*66*	

Site name	Provenience	Sample material	Laboratory code	Date (BP or ka)	Source	Notes
Blackwater Locality No. 1	Unit G	soil organic residue	Y-2360	680±80	*66*	
Blackwater Locality No. 1	Unit G	charcoal	AA-2260	6720±80	*66*	
Blackwater Locality No. 1	Unit G	charcoal (humates)	AA-2259	7850±110	*66*	
Blackwater Locality No. 1	Unit G	burned bone	AA-1643	8230±140	*66*	
Blackwater Locality No. 1	Unit G	burned bone (humates)	AA-2258	8730±90	*66*	
Blackwater Locality No. 1	Unit G	brown aeolian sand (organic residue)	AA-7094	2500±60	*66*	
Blackwater Locality No. 1	Unit G	brown aeolian sand (organic residue)	AA-7095	3800±60	*66*	
Bluefish Caves	Cave II, basal loess, 142 cam below datum	bone (# J7.8.17)	OxA-33778	19650±130	*140*	
Bonneville Estates Rockshelter	West Block, Stratum 19	bone	UCIAMS-22180	15240±50	*180*	
Bonneville Estates Rockshelter	West Block, Stratum 19	hearth charcoal	Beta-209265	11960±60	*180*	
Bonneville Estates Rockshelter	West Block, Stratum 19	hearth charcoal	Beta-195045	12390±40	*180*	
Bonneville Estates Rockshelter	West Block, Stratum 19	hearth charcoal	Beta-195046	12330±40	*180*	
Bonneville Estates Rockshelter	West Block, Stratum 19	bone	Beta-210523	11530±40	*180*	
Bonneville Estates Rockshelter	West Block, Stratum 19	bone	Beta-200874	10970±60	*180*	
Bonneville Estates Rockshelter	West Block, Stratum 19	hearth charcoal	AA-58587	12180±60	*180*	
Bonneville Estates Rockshelter	West Block, Stratum 19	bone	UCIAMS-22176	10900±50;	*180*	
Bonneville Estates Rockshelter	West Block, Stratum 19	bone	Beta-210524	10830±40;	*180*	
Bonneville Estates Rockshelter	West Block, Stratum 19	hearth charcoal	Beta-200875	10640±60	*180*	
Bonneville Estates Rockshelter	West Block, Stratum 19/18b contact	hearth charcoal	AA-58595	12270±60	*180*	
Bonneville Estates Rockshelter	West Block, Stratum 19/18b contact	hearth charcoal	AA-58590	10690±70	*180*	

Site name	Provenience	Sample material	Laboratory code	Date (BP or ka)	Source	Notes
Bonneville Estates Rockshelter	West Block, Stratum 18b	hearth charcoal	Beta-207009	11010±40	*180*	
Bonneville Estates Rockshelter	West Block, Stratum 18b	hearth charcoal	AA-58594	10800±60	*180*	
Bonneville Estates Rockshelter	West Block, Stratum 18b	hearth charcoal	AA-58592	10760±70	*180*	
Bonneville Estates Rockshelter	West Block, Stratum 18b	hearth charcoal	Beta-195047	10540±40	*180*	
Bonneville Estates Rockshelter	West Block, Stratum 18b	hearth charcoal	AA-58593	10405±50	*180*	
Bonneville Estates Rockshelter	West Block, Stratum 18a	hearth charcoal	Beta-170444	10130±60	*180*	
Bonneville Estates Rockshelter	West Block, Stratum 18a	hearth charcoal	Beta-164229	10080±50	*180*	
Bonneville Estates Rockshelter	West Block, Stratum 18a	hearth charcoal	Beta-170443	10040±70	*180*	
Bonneville Estates Rockshelter	West Block, Stratum 18a/17b contact	hearth charcoal	Beta-207010	9580±40	*180*	
Bonneville Estates Rockshelter	West Block, Stratum 17b	hearth charcoal	AA-58589	9440±50	*180*	
Bonneville Estates Rockshelter	West Block, Stratum 17b	hearth charcoal	AA-58588	9430±50	*180*	
Bonneville Estates Rockshelter	West Block, Stratum 17a	hearth charcoal	CAMS-72351	7420±50	*180*	
Bonneville Estates Rockshelter	West Block, Stratum 16	dispersed charcoal	CAMS-72352	7280±50	*180*	
Bonneville Estates Rockshelter	West Block, Stratum 16	textile fragment	Beta-164230	7190±50	*180*	
Bonneville Estates Rockshelter	West Block, Stratum 14	garbage pit charcoal	AA-58591	6315±40	*180*	
Bonneville Estates Rockshelter	West Block, Stratum 14	hearth charcoal	Beta-164227	6280±40	*180*	
Bonneville Estates Rockshelter	West Block, Stratum 14	hearth charcoal	Beta-164227	6280±40	*180*	
Bonneville Estates Rockshelter	West Block, Stratum 14	cordage fragment	Beta-164224	6100±50	*180*	
Bonneville Estates Rockshelter	West Block, Stratum 14	bulk charcoal	Beta-29542	6040±80	*180*	
Broken Mammoth	CZ-4C	ivory artifact	CAMS-9898	15830±70	*24*	

Site name	Provenience	Sample material	Laboratory code	Date (BP or ka)	Source	Notes
Broken Mammoth	CZ-4C	charcoal	WSU-4364	11770±220	*24*	
Broken Mammoth	CZ-4C	charcoal	WSU-4351	11770±210	*24*	
Broken Mammoth	CZ-4B	hearth charcoal	WSU-4262	11510±120	*24*	
Broken Mammoth	CZ-4B	swan bone	CAMS-8261	11500±80	*24*	
Broken Mammoth	CZ-4B	hearth charcoal	CAMS-5358	11420±70	*24*	
Broken Mammoth	CZ-4B	charcoal	WSU-4265	11280±190	*24*	
Broken Mammoth	CZ-3/4A?	charcoal	UGA-6257D	11040±260	*24*	
Broken Mammoth	CZ-3/4A?	wapiti bone	CAMS-7204	11060±90	*24*	
Broken Mammoth	CZ-3/4A?	mammal bone	CAMS-7203	11040±80	*24*	
Broken Mammoth	CZ-3	hearth charcoal	CAMS-5357	10290±70	*24*	
Broken Mammoth	CZ-3	charcoal	WSU-4019	10790±110	*24*	
Broken Mammoth	CZ-3	hearth charcoal	WSU-4263	10270±110	*24*	
Broken Mammoth	CZ-3	hearth charcoal	UGA-6256D	9690±90	*24*	
Broken Mammoth	CZ-3A	charcoal	WSU-4266	9310±165	*24*	
Broken Mammoth	CZ-2	charcoal	WSU-4508	7700±80	*24*	
Broken Mammoth	CZ-2	charcoal	WSU-4264	7600±140	*24*	
Broken Mammoth	CZ-2	charcoal	UGA-6281D	7200±205	*24*	
Broken Mammoth	CZ-1B	hearth charcoal	WSU-4350	4690±110	*24*	
Broken Mammoth	CZ-1B	charcoal	WSU-4456	4540±90	*24*	
Broken Mammoth	CZ-1B	charcoal	WSU-4457	4545±90	*24*	
Broken Mammoth	CZ-1B	charcoal	WSU-4448	4525±90	*24*	
Broken Mammoth	CZ-1A	charcoal	WSU-4267	2040±65	*24*	
Broken Mammoth	CZ-1A	charcoal	UGA-6255D	2815±180	*24*	
Buhl	burial locale (909 masl)	human bone	Beta-43055 & ETH-7729	10675±95	*185*	
Cactus Hill	below pre-Clovis level	sediment	UW438c	25400±1700	*71*	OSL
Cactus Hill	below pre-Clovis level	sediment	UW438(kc)	27900±2000	*71*	OSL
Cactus Hill	below pre-Clovis level	wood charcoal	Beta-128331	19700±130	*71*	
Cactus Hill	below pre-Clovis level	charred organic matter	Beta-155334	19540±70	*71*	
Cactus Hill	below pre-Clovis level	charred organic matter	Beta-156517	19310±150	*71*	

Site name	Provenience	Sample material	Laboratory code	Date (BP or ka)	Source	Notes
Cactus Hill	below pre-Clovis level	charred organic matter	Beta-163608	19050±80	*71*	
Cactus Hill	below pre-Clovis level	wood charcoal	Beta-152731	18250±80	*71*	
Cactus Hill	below pre-Clovis level	sediment	UW618c	20600±900	*71*	OSL
Cactus Hill	below pre-Clovis level	wood charcoal	Beta-128330	16940±50	*71*	
Cactus Hill	pre-Clovis level	sediment	UW701	18300±1400	*71*	OSL
Cactus Hill	pre-Clovis level	sediment	UW700	19800±3800	*71*	OSL
Cactus Hill	pre-Clovis level	sediment	UW699	17300±1600	*71*	OSL
Cactus Hill	pre-Clovis level	sediment	UW617c	19300±1000	*71*	OSL
Cactus Hill	pre-Clovis level	wood charcoal	Beta-97708	16670±730	*71*	
Cactus Hill	pre-Clovis level	wood charcoal	Beta-81590	15070±70	*71*	
Cactus Hill	sterile zone	sediment	UW698	12500±600	*71*	OSL
Cactus Hill	sterile zone	sediment	UW697	11800±800	*71*	OSL
Cactus Hill	Clovis level	wood charcoal	Beta-81589	10920±250	*71*	
Cactus Hill	Phase("Fort Nottoway working surface and fire pit"	wood charcoal	AA-15027	8920±65	*71*	
Cactus Hill	Phase("Fort Nottoway working surface and fire pit"	wood charcoal	Beta-70127	8800±120	*71*	
Cactus Hill	Archaic level	sediment	UW436	10300±600	*71*	OSL
Cactus Hill	Archaic level	sediment	UW435	8000±600	*71*	OSL
Colby	Bone Pile 2	mammoth bone (XAD)	UCIAMS-11342	10790±30	*5*	
Colby	Bone Pile 2	mammoth bone (XAD)	UCIAMS-11343	10950±30	*5*	
Cooper’s Ferry	Mid LU5	bone	OxA-37169	8141±38	*13*	
Cooper’s Ferry	Mid LU5	sediment	CFA019	12170±2320	*13*	OSL
Cooper’s Ferry	Upper LU4	bone	OxA-38048	9775±50	*13*	
Cooper’s Ferry	Upper LU4	bone	OxA-X-2792-41	9110±50	*13*	
Cooper’s Ferry	Mid LU4	bone	OxA-38103	10055±55	*13*	
Cooper’s Ferry	Mid LU4	sediment	CFA018	12730±2400	*13*	OSL
Cooper’s Ferry	Mid LU4	bone	OxA-X-2792-42	13165±70	*13*	
Cooper’s Ferry	Lower LU4	bone	OxA-37171	10005±40	*13*	
Cooper’s Ferry	Lower LU4	charcoal	D-AMS 029850	9714±57	*13*	
Cooper’s Ferry	Lower LU4	bone	OxA-X-2792-43	10050±60	*13*	
Cooper’s Ferry	Lower LU4	charcoal	D-AMS 029851	7944±39	*13*	
Cooper’s Ferry	Near surface of LU3	charcoal	TO-7349	11410±120	*13*	
Cooper’s Ferry	Upper LU3	bone	OxA-X-2792-45	11630±80	*13*	

Site name	Provenience	Sample material	Laboratory code	Date (BP or ka)	Source	Notes
Cooper's Ferry	Mid LU3	bone	OxA-38104	7605±40	*13*	
Cooper's Ferry	Mid LU3	sediment	CFA017	13710±2620	*13*	OSL
Cooper's Ferry	Mid LU3 (F129)	charcoal	D-AMS 029846	12348±71	*13*	
Cooper's Ferry	Mid LU3	charcoal	OxA-38050	7831±40	*13*	
Cooper's Ferry	Mid LU3 (F129)	charcoal	D-AMS 029749	12598±54	*13*	
Cooper's Ferry	Mid LU3 (F129)	charcoal	D-AMS 029847	12472±61	*13*	
Cooper's Ferry	Mid LU3	charcoal	D-AMS 029848	12363±49	*13*	
Cooper's Ferry	Lower LU3	bone	OxA-37284	12475±60	*13*	
Cooper's Ferry	Lower LU3	charcoal	OxA-38051	13070±80	*13*	
Cooper's Ferry	Lower LU3	bone	OxA-X-2792-48	12830±65	*13*	
Cooper's Ferry	Lower LU3	bone	OxA-38106	7985±40	*13*	
Cooper's Ferry	Within pit (F144)	bone	OxA-38197	11720±80	*13*	excluded from models (see site description for further information)
Cooper's Ferry	Within first pit (PFA2)	charcoal	Beta-114949	11370±40	*13*	excluded from models (see site description for further information)
Cooper's Ferry	Within second pit (F134)	bone	OxA-38049	10010±50	*13*	excluded from models (see site description for further information)
Cooper's Ferry	Within second pit (F134)	bone	OxA-38052	13335±75	*13*	excluded from models (see site description for further information)
Cooper's Ferry	Within third pit (F135)	bone	OxA-38105	9955±50	*13*	excluded from models (see site description for further information)
Debra L. Friedkin (Block A)	Pre-Occupation Floodplain deposits	sediment	UIC2351Q	27650±1800	*82*	OSL
Debra L. Friedkin (Block A)	Pre-Occupation Floodplain deposits	sediment	UIC235	26090±1670	*82*	OSL
Debra L. Friedkin (Block A)	Pre-Occupation Floodplain deposits	sediment	BG4079	24145±1635	*82*	OSL
Debra L. Friedkin (Block A)	Pre-Occupation Floodplain deposits	sediment	UIC2358	25185±1640	*82*	OSL
Debra L. Friedkin (Block A)	Pre-Occupation Floodplain deposits	sediment	UIC2057	24420±1580	*82*	OSL
Debra L. Friedkin (Block A)	Pre-Occupation Floodplain deposits	sediment	BG4078	22950±1445	*82*	OSL
Debra L. Friedkin (Block A)	Pre-Occupation Floodplain deposits	sediment	UIC2357S	23150±1600	*82*	OSL

Site name	Provenience	Sample material	Laboratory code	Date (BP or ka)	Source	Notes
Debra L. Friedkin (Block A)	Pre-Occupation Floodplain deposits	sediment	UIC2357	22710±1450	*82*	OSL
Debra L. Friedkin (Block A)	Pre-Occupation Floodplain deposits	sediment	UIC2058	20330±1320	*82*	OSL
Debra L. Friedkin (Block A)	Pre-Occupation Floodplain deposits	sediment	UIC2370	20565±1325	*82*	OSL
Debra L. Friedkin (Block A)	Pre-Occupation Floodplain deposits	sediment	UIC2370Q	20490±1305	*82*	OSL
Debra L. Friedkin (Block A)	Pre-Occupation Floodplain deposits	sediment	BG4077	20250±1340	*82*	OSL
Debra L. Friedkin (Block A)	Pre-Occupation Floodplain deposits	sediment	BG3993	19750±1245	*82*	OSL
Debra L. Friedkin (Block A)	Pre-Occupation Floodplain deposits	sediment	UIC2348	18930±1210	*82*	OSL
Debra L. Friedkin (Block A)	Pre-Occupation Floodplain deposits	sediment	BG4076	19680±1320	*82*	OSL
Debra L. Friedkin (Block A)	Pre-Occupation Floodplain deposits	sediment	BG3994	19650±1230	*82*	OSL
Debra L. Friedkin (Block A)	Boundary Date	sediment	UIC2368	17530±1140	*82*	OSL
Debra L. Friedkin (Block A)	Boundary Date	sediment	UIC2553	16270±1040	*82*	OSL
Debra L. Friedkin (Block A)	Boundary Date	sediment	UIC2183	15110±960	*82*	OSL
Debra L. Friedkin (Block A)	Boundary Date	sediment	UIC2062	16170±1030	*82*	OSL
Debra L. Friedkin (Block A)	Pre-Clovis	sediment	UIC2355	16515±1075	*82*	OSL
Debra L. Friedkin (Block A)	Pre-Clovis	sediment	BG4069	15725±1030	*82*	OSL
Debra L. Friedkin (Block A)	Pre-Clovis	sediment	BG4239	16650±1110	*82*	OSL
Debra L. Friedkin (Block A)	Pre-Clovis	sediment	UIC2044	16400±1040	*82*	OSL
Debra L. Friedkin (Block A)	Pre-Clovis	sediment	BG2044	15800±1080	*82*	OSL
Debra L. Friedkin (Block A)	Pre-Clovis	sediment	BG4238	15500±1020	*82*	OSL
Debra L. Friedkin (Block A)	Pre-Clovis	sediment	UIC2356	14710±940	*82*	OSL

Site name	Provenience	Sample material	Laboratory code	Date (BP or ka)	Source	Notes
Debra L. Friedkin (Block A)	Pre-Clovis	sediment	BG3995	15020±1010	*82*	OSL
Debra L. Friedkin (Block A)	Pre-Clovis	sediment	UIC2043	15210±960	*82*	OSL
Debra L. Friedkin (Block A)	Pre-Clovis	sediment	BG4236	15400±1015	*82*	OSL
Debra L. Friedkin (Block A)	Pre-Clovis	sediment	UIC2359	15730±1010	*82*	OSL
Debra L. Friedkin (Block A)	Pre-Clovis	sediment	BG4018	15265±1000	*82*	OSL
Debra L. Friedkin (Block A)	Pre-Clovis	sediment	BG4235	14965±985	*82*	OSL
Debra L. Friedkin (Block A)	Pre-Clovis	sediment	BG4234	14790±985	*82*	OSL
Debra L. Friedkin (Block A)	Pre-Clovis	sediment	UIC2350S	14580±1030	*82*	OSL
Debra L. Friedkin (Block A)	Pre-Clovis	sediment	UIC2350Q	14480±920	*82*	OSL
Debra L. Friedkin (Block A)	Pre-Clovis	sediment	UIC2350	14000±890	*82*	OSL
Debra L. Friedkin (Block A)	Pre-Clovis	sediment	UIC2047	15270±960	*82*	OSL
Debra L. Friedkin (Block A)	Pre-Clovis	sediment	UIC2369	14370±930	*82*	OSL
Debra L. Friedkin (Block A)	Pre-Clovis	sediment	BG4017	13960±965	*82*	OSL
Debra L. Friedkin (Block A)	Pre-Clovis	sediment	UIC2367	14080±920	*82*	OSL
Debra L. Friedkin (Block A)	Pre-Clovis	sediment	BG4220	13595±930	*82*	OSL
Debra L. Friedkin (Block A)	Boundary Date	sediment	UIC2046	14350±910	*82*	OSL
Debra L. Friedkin (Block A)	Boundary Date	sediment	BG4019	13620±880	*82*	OSL
Debra L. Friedkin (Block A)	Boundary Date	sediment	UIC2354	14070±910	*82*	OSL
Debra L. Friedkin (Block A)	Boundary Date	sediment	BG4219	13010±905	*82*	OSL
Debra L. Friedkin (Block A)	Clovis and Folsom	sediment	UIC2059Q	13780±885	*82*	OSL

Site name	Provenience	Sample material	Laboratory code	Date (BP or ka)	Source	Notes
Debra L. Friedkin (Block A)	Clovis and Folsom	sediment	UIC2059	13090±830	*82*	OSL
Debra L. Friedkin (Block A)	Clovis and Folsom	sediment	UIC2045Q	12925±845	*82*	OSL
Debra L. Friedkin (Block A)	Clovis and Folsom	sediment	UIC2045	12240±800	*82*	OSL
Debra L. Friedkin (Block A)	Clovis and Folsom	sediment	BG4218	13020±870	*82*	OSL
Debra L. Friedkin (Block A)	Clovis and Folsom	sediment	BG4209	12560±830	*82*	OSL
Debra L. Friedkin (Block A)	Clovis and Folsom	sediment	UIC2366A	12100±860	*82*	OSL
Debra L. Friedkin (Block A)	Clovis and Folsom	sediment	UIC2366	12000±770	*82*	OSL
Debra L. Friedkin (Block A)	Clovis and Folsom	sediment	BG4068	12940±855	*82*	OSL
Debra L. Friedkin (Block A)	Clovis and Folsom	sediment	BG4208	12170±820	*82*	OSL
Debra L. Friedkin (Block A)	Paleoindian	sediment	UIC2050	12970±830	*82*	OSL; not in Waters et al., 2018; excluded
Debra L. Friedkin (Block A)	Late Paleoindian	sediment	UIC2048	12690±955	*82*	OSL
Debra L. Friedkin (Block A)	Late Paleoindian	sediment	BG4075	11060±735	*82*	OSL
Debra L. Friedkin (Block A)	Late Paleoindian	sediment	UIC2365	11870±760	*82*	OSL
Debra L. Friedkin (Block A)	Late Paleoindian	sediment	BG4206	10785±715	*82*	OSL
Debra L. Friedkin (Block A)	Late Paleoindian	sediment	BG4207	10530±750	*82*	OSL
Debra L. Friedkin (Block A)	Late Paleoindian	sediment	BG4341	10830±695	*82*	OSL
Debra L. Friedkin (Block A)	Late Paleoindian	sediment	BG4074	10375±740	*82*	OSL
Debra L. Friedkin (Block A)	Late Paleoindian	sediment	UIC2051	10480±675	*82*	OSL
Debra L. Friedkin (Block A)	Late Paleoindian	sediment	UIC2364	9930±640	*82*	OSL
Debra L. Friedkin (Block A)	Late Paleoindian	sediment	BG4340	10360±705	*82*	OSL

Site name	Provenience	Sample material	Laboratory code	Date (BP or ka)	Source	Notes
Debra L. Friedkin (Block A)	Late Paleoindian	sediment	BG4067	10100±695	*82*	OSL
Debra L. Friedkin (Block A)	Late Paleoindian	sediment	BG4339	10095±655	*82*	OSL
Debra L. Friedkin (Block A)	Late Paleoindian	sediment	UIC2052	9250±600	*82*	OSL
Debra L. Friedkin (Block A)	Late Paleoindian	sediment	UIC2363	9405±610	*82*	OSL
Debra L. Friedkin (Block A)	Early Archaic	sediment	UIC2061	9215±620	*82*	OSL
Debra L. Friedkin (Block A)	Early Archaic	sediment	BG4338	8655±550	*82*	OSL
Debra L. Friedkin (Block A)	Early Archaic	sediment	UIC2060Q	8490±560	*82*	OSL
Debra L. Friedkin (Block A)	Early Archaic	sediment	UIC2060	8070±520	*82*	OSL
Debra L. Friedkin (Block A)	Early Archaic	sediment	UIC2362	8160±540	*82*	OSL
Debra L. Friedkin (Block A)	Early Archaic	sediment	BG4066	8315±540	*82*	OSL
Debra L. Friedkin (Block A)	Early Archaic	sediment	UIC2360	7160±470	*82*	OSL
Debra L. Friedkin (Block A)	Early Archaic	sediment	UIC2360s	7030±470	*82*	OSL
Dent	mammoth bone bed	mammoth bone (HYP)	OxA-X-2736-11	11055±50	*88*	
Dent	mammoth bone bed	mammoth bone (HYP)	OxA-X-2736-12	11155±50	*88*	
Domebo	Clovis mammoth bone bed	mammoth bone	UCIAMS-11341	10960±30	*5*	
Dry Creek	Loess 2; component I; feature 11.02	hearth charcoal (Salix sp.)	Beta-315411	11530±50	*33*	
Dry Creek	Loess 2; component I; feature 11.02	hearth charcoal (Salix sp.)	UCIAMS-135114	11510±40	*33*	
Dry Creek	Loess 2; component I; feature 11.03	hearth charcoal (Salix sp.)	UCIAMS-135112	11635±40	*33*	
Dry Creek	Loess 2; component I; feature 11.03	hearth charcoal (Salix sp.)	UCIAMS-135113	11580±40	*33*	
Dry Creek	Loess 3; component II; feature 11.01	hearth charcoal (Salix sp.)	Beta-315410	9460±60	*33*	
Dry Creek	Loess 3; component II; feature 11.01	hearth charcoal (Salix sp.)	UCIAMS-135115	9480±35	*33*	
El Fin del Mundo	Stratum 3 (A)	shell (Planorbid)	AA-90707	12180±40	*91*	
El Fin del Mundo	Stratum 3 (B)	tooth enamel	AA-95550	9755±92	*91*	

Site name	Provenience	Sample material	Laboratory code	Date (BP or ka)	Source	Notes
El Fin del Mundo	Stratum 3 (B)	organic matter	AA-83272B	11040±580	*91*	
El Fin del Mundo	Stratum 3 (B)	tooth enamel	AA-95550 (duplicate)	9804±93	*91*	
El Fin del Mundo	Stratum 3 (B)	charcoal	AA-100182B	11880±200	*91*	
El Fin del Mundo	Stratum 3 (B)	charcoal	AA-100181B	10650±250	*91*	
El Fin del Mundo	Stratum 3 (B)	charcoal	AA-100181A	11550±60	*91*	
El Fin del Mundo	Stratum 4 (D)	organic matter	AA-14896A	6185±115	*91*	
El Fin del Mundo	Stratum 4 (D)	organic matter	AA-80078A	6921±58	*91*	
El Fin del Mundo	Stratum 4 (D)	organic matter	AA-80076A	7570±93	*91*	
El Fin del Mundo	Stratum 4 (D.E)	charcoal	AA-80084A	9715±64	*91*	
El Fin del Mundo	Stratum 4 (D.E)	charcoal	AA-80671B	9560±120	*91*	
El Fin del Mundo	Stratum 4 (D.E)	charcoal	AA-80085B	9290±290	*91*	
El Fin del Mundo	Stratum 4 (D.E)	organic matter	A-14850	9030±75	*91*	
El Fin del Mundo	Stratum 4 (D.E)	organic matter	A-14836	9465±100	*91*	
El Fin del Mundo	Stratum 4 (D.E)	organic matter	A-14837	8375±110	*91*	
El Fin del Mundo	Stratum 4 (D.E)	shell (Succinid)	AA-88886	8470±50	*91*	
El Fin del Mundo	Stratum 4 (D.E)	shell (Succinid)	AA-81350	8030±50	*91*	
El Fin del Mundo	Stratum 4 (D.E)	shell (Succinid)	AA-88885	8770±60	*91*	
Gault	Gault Assemblage	sediment	11-06	21700±1400	*97*	OSL
Gault	Gault Assemblage	sediment	11-18	16900±1100	*97*	OSL
Gault	Gault Assemblage	sediment	11-20	16700±1100	*97*	OSL
Gault	Gault Assemblage	sediment	11-05b	18700±1200	*97*	OSL
Gault	Clovis	sediment	11-03	11900±800	*97*	OSL
Gault	Clovis	sediment	11-07	12900±600	*97*	OSL
Gault	Clovis	sediment	11-15	13600±600	*97*	OSL
Gault	Clovis	sediment	11-09	13200±600	*97*	OSL
Gault	Paleoindian	sediment	11-17	11600±500	*97*	OSL
Gault	Paleoindian	sediment	11-13	10200±500	*97*	OSL
Gault	Paleoindian	sediment	11-08	9900±400	*97*	OSL
Gault	Paleoindian	sediment	09-06	9700±400	*97*	OSL
Gault	Paleoindian	sediment	09-05	9300±400	*97*	OSL
Gault	Paleoindian	sediment	11-02	10100±400	*97*	OSL
Gault	Paleoindian	sediment	09-04	8800±400	*97*	OSL
Gault	Paleoindian	sediment	11-16	9100±400	*97*	OSL
Gault	Archaic	sediment	09-03	6600±300	*97*	OSL
Gault	Archaic	sediment	09-02	6100±300	*97*	OSL
Gault	Archaic	sediment	09-01b	5900±300	*97*	OSL

Site name	Provenience	Sample material	Laboratory code	Date (BP or ka)	Source	Notes
Gault	Archaic	sediment	09-01	5900±300	*97*	OSL
Gault	Archaic	sediment	11-01	5700±300	*97*	OSL
Hebior	Paleoindian	mammoth bone (XAD)	CAMS-61137	12590±50	*151*	
Hebior	Paleoindian	mammoth bone (XAD)	CAMS-28303	12480±60	153	
Hebior	Paleoindian	mammoth bone (XAD)	CAMS-61136	12520±50	*151*	Although they might not be the same, this same date is noted as CAMS 24943 in ref[153].
Jake Bluff	Clovis bison bone bed	bison bone (XAD)	CAMS-79940	10750±40	*98*	
Jake Bluff	Clovis bison bone bed	bison bone (XAD)	CAMS-90968	10840±45	*98*	
Jake Bluff	Clovis bison bone bed	bison bone (XAD)	CAMS-90969	10700±45	*98*	
Jake Bluff	Clovis bison bone bed	bison bone (XAD)	UCIAMS-61657	10810±25	*99*	
Jake Bluff	Clovis bison bone bed	bison bone (XAD)	UCIAMS-59874	10885±35	*99*	
Lange/ Ferguson	Clovis mammoth bone bed	mammoth bone (XAD)	UCIAMS-11344	10710±130	*5*	
Lange/ Ferguson	Clovis mammoth bone bed	mammoth bone (XAD)	UCIAMS-11345	11110±40	*5*	
Lehner	hearth 2	hearth charcoal	K-554	11180±140	*107*	
Lehner	hearth 2	hearth charcoal	M-811	11290±500	*107*	
Lehner	F1	hearth charcoal	SMU-168	10770±140	*103*	
Lehner	F1	hearth charcoal	A-378	10940±100	*103*	
Lehner	F1	hearth charcoal	SMU-181	11080±200	*103*	
Lehner	F2/D,Z	hearth charcoal	SMU-194	10950±110	*103*	
Lehner	F2/D,Z	hearth charcoal	SMU-164	10860±280	*103*	
Lehner	F2/D,Z	hearth charcoal	SMU-290	10950±90	*103*	
Lehner	F2/D,Z	hearth charcoal	SMU-196	11080±230	*103*	
Lehner	F2/F0	hearth charcoal	SMU-347	10620±300	*103*	
Lehner	F2/F0	hearth charcoal	SMU-297	10700±150	*103*	
Lehner	F2/F0	hearth charcoal	SMU-340	10710±90	*103*	
Lehner	F2/F0	hearth charcoal	SMU-264	11170±200	*103*	
Lehner	F2/F0	hearth charcoal	SMU-308	11470±110	*103*	
Lehner	hearth 1	hearth charcoal	A-34	7205±450	*107*	
Lehner	hearth 2	hearth charcoal	A-32	7022±450	*107*	
Lehner	hearth 2	hearth charcoal	A-30	8330±450	*107*	
Lehner	hearth 2	hearth charcoal	A-40a	10900±450	*107*	
Lehner	hearth 2	hearth charcoal	A-40b	12000±450	*107*	
Lindsay	late-Pleistocene loess	mammoth bone (HYP)	OxA-X-2736-15	12395±55	*88*	
Lindsay	late-Pleistocene loess	mammoth bone (XAD)	CAMS- 72348	12330±50	*159*	
Lindsay	late-Pleistocene loess	mammoth bone (XAD)	UCIAMS-12308	12300±35	*158*	
Lindsay	late-Pleistocene loess	mammoth bone (XAD)	UCIAMS-127316	12270±35	*158*	

Site name	Provenience	Sample material	Laboratory code	Date (BP or ka)	Source	Notes
Lubbock Lake	Stratum 1	clams (Sphaerium and Psidium), carbonate	I-246	12650±290	*128*	
Lubbock Lake	Stratum 1	clams (Sphaerium and Psidium), carbonate	SMU-295	12150±90	*128*	
Lubbock Lake	Stratum 1	wood	SMU-548	11100±100	*128*	
Lubbock Lake	Stratum 1	wood	SMU-263	11100±80	*128*	
Lubbock Lake	Stratum 1	bison bone apatite, same as SMU-367	SMU-317	8860±90	*128*	
Lubbock Lake	Stratum 1	bison bone collagen, same as SMU-317	SMU-367	7040±600	*128*	
Lubbock Lake	Stratum 2 (2ALB1)	snails (Helisoma trivolis, Lymnaea reflaxa), carbonate	SMU-292	10880±90	*128*	
Lubbock Lake	Stratum 2 (2ALB1)	organic mud, humin	SI-3202	10780±80	*128*	
Lubbock Lake	Stratum 2 (2ALB1)	diatomite, humic acid	SMU-285	10530±90	*128*	
Lubbock Lake	Stratum 2 (2ALB1)	snails, carbonate, solid carbon	L-283g	9700±450	*128*	
Lubbock Lake	Stratum 2 (2ALB2)	charcoal	SMU-547	10540±100	*128*	
Lubbock Lake	Stratum 2 (2ALB2)	cienaga, humin	SI-3200	10360±80	*128*	
Lubbock Lake	Stratum 2 (2ALB2)	diatomite, humic acid, same as SMU-247	SMU-251	10060±170	*128*	
Lubbock Lake	Stratum 2 (2ALB2)	diatomite, humin acid, same as SMU-251	SMU-247	7840±170	*128*	
Lubbock Lake	Stratum 2 (2A upper)	organic mud, humin	SI-3203	10015±75	*128*	
Lubbock Lake	Stratum 2 (2B base)	cienaga, humic acid	SMU-728	9990±100	*128*	
Lubbock Lake	Stratum 2 (2B base)	diatomite, humic acid	SMU-275	9960±80	*128*	
Lubbock Lake	Stratum 2 (2B middle)	charred bison bone, solid carbon	C-558	9883±350	*128*	
Lubbock Lake	Stratum 2 (2B middle)	charred bison bone, solid carbon	L-283H	7765±200	*128*	
Lubbock Lake	Stratum 2 (2B middle)	organic mud, humic acid	SMU-759	9330±70	*128*	
Lubbock Lake	Stratum 2 (2B upper)	organic mud, humin	SI-4177	8655±90	*128*	
Lubbock Lake	Stratum 2 (2B upper)	cienaga, humic acid	SMU-827	7980±180	*128*	
Lubbock Lake	Stratum 2 (2B upper)	cienaga, humic acid	SMU-830	8210±240	*128*	
Lubbock Lake	Stratum 2 (2B upper)	organic mud, humic acid	SI-302	7890±100	*128*	
Lubbock Lake	Stratum 2 (2B upper)	cienaga, humic acid	SMU-262	7970±70	*128*	

Site name	Provenience	Sample material	Laboratory code	Date (BP or ka)	Source	Notes
Lubbock Lake	Stratum 2 (2B upper)	organic mud, humin	SI-3204	7255±75	*128*	
Lubbock Lake	Stratum 2 (2B upper)	cienaga, humic acid	SMU-648	7100±80	*128*	
Lubbock Lake	Stratum 2 (2B upper)	cienaga, humin	SI-4178	6705±95	*128*	
Lubbock Lake	Stratum 2 (2B upper)	cienaga, humic acid	SMU-544	6400±80	*128*	
Lubbock Lake	Stratum 3 (3e)	humic acid	SMU-545	5770±80	*128*	
Lubbock Lake	Stratum 3 (3/)	buried A horizon, humin	SI-3197	6115±75	*128*	
Lubbock Lake	Stratum 3 (3/)	buried A horizon, humin, check on SI-3197	SI-4172	5475±75	*128*	
Lubbock Lake	Stratum 3 (3/)	buried A horizon, humic acid	SMU-531	4900±60	*128*	
Lubbock Lake	Stratum 4 (4/)	marsh, humin	SI-3205	5545±100	*128*	excluded from models (see site description for further information)
Lubbock Lake	Stratum 4 (4/)	marsh, humin, check on SI-3205	SI-4176	4355±80	*128*	excluded from models (see site description for further information)
Lubbock Lake	Stratum 4 (4/)	marsh, humin	SI-3206	3925±80	*128*	excluded from models (see site description for further information)
Lubbock Lake	Stratum 4 (4/)	marsh, humin, check on SI-3206	SI-4175	3175±85	*128*	excluded from models (see site description for further information)
Lubbock Lake	Stratum 4 (4/)	marsh, humic acid	SMU-697	2600±50	*128*	excluded from models (see site description for further information)
Lubbock Lake	Stratum 4 (4/)	marsh, humin	SI-4588	980±60	*128*	excluded from models (see site description for further information)
Lubbock Lake	Stratum 4 (4A)	bison bone collagen (average of several dates)	SMU-332/333	4910±50	*128*	excluded from models (see site description for further information)
Lubbock Lake	Stratum 4 (4A)	bison bone apatite, same as SMU-367	SMU-309	4470±50	*128*	excluded from models (see site description for further information)
Lubbock Lake	Stratum 4 (4B)	ash and humic acid, same as SI-4171	SMU-492	4960±50	*128*	excluded from models (see site description for further information)
Lubbock Lake	Stratum 4 (4B)	ash and humic acid, same as SMU-492	SI-4171	4700±65	*128*	excluded from models (see site description for further information)
Lubbock Lake	Stratum 4 (4B)	buried A horizon, humin	SI-4174	1955±75	*128*	excluded from models (see site description for further information)
Lubbock Lake	Stratum 4 (4B)	buried A horizon, humin	SI-3201	1215±65	*128*	excluded from models (see site description for further information)
Lubbock Lake	Stratum 4 (4B)	buried A horizon, humic acid	SMU-651	890±70	*128*	excluded from models (see site description for further information)
Lubbock Lake	Stratum 4 (4B)	buried A horizon, humin	SI-4169	880±70	*128*	excluded from models (see site description for further information)

Site name	Provenience	Sample material	Laboratory code	Date (BP or ka)	Source	Notes
Lubbock Lake	Stratum 4 (4B)	buried A horizon, humic acid	SMU-534	870±40	*128*	excluded from models (see site description for further information)
Lubbock Lake	Stratum 5 (5A/)	marsh, humic acid	SMU-698	600±50	*128*	excluded from models (see site description for further information)
Lubbock Lake	Stratum 5 (5A)	buried A horizon, humic acid	SMU-314	720±40	*128*	excluded from models (see site description for further information)
Lubbock Lake	Stratum 5 (5A)	buried A horizon, humin	SI-3208	640±75	*128*	excluded from models (see site description for further information)
Lubbock Lake	Stratum 5 (5A)	charcoal, lower FA8-6	SI-2701	505±55	*128*	excluded from models (see site description for further information)
Lubbock Lake	Stratum 5 (5A)	charcoal, upper FA8-6, same as SMU-345	SI-2700	380±40	*128*	excluded from models (see site description for further information)
Lubbock Lake	Stratum 5 (5A)	charcoal	SMU-546	320±60	*128*	excluded from models (see site description for further information)
Lubbock Lake	Stratum 5 (5A)	charcoal	SI-2704	315±50	*128*	excluded from models (see site description for further information)
Lubbock Lake	Stratum 5 (5A)	charcoal, upper FA8-6, same as SI-2700	SMU-345	300±60	*128*	excluded from models (see site description for further information)
Lubbock Lake	Stratum 5 (5A)	charcoal	SI-2703	285±60	*128*	excluded from models (see site description for further information)
Lubbock Lake	Stratum 5 (5A)	buried A horizon, humic acid	SMU-555	220±50	*128*	excluded from models (see site description for further information)
Lubbock Lake	Stratum 5 (5A)	modern A horizon, humic acid	SMU-343	160±60	*128*	excluded from models (see site description for further information)
Lubbock Lake	Stratum 5 (5A)	charred bison bone	I-208	160±90	*128*	excluded from models (see site description for further information)
Lubbock Lake	Stratum 5 (5A)	charred bison bone	I-140	70±70	*128*	excluded from models (see site description for further information)
Lubbock Lake	Stratum 5 (5B/)	wood	SMU-715	400±110	*128*	excluded from models (see site description for further information)
Lubbock Lake	Stratum 5 (5B/)	marsh, humic acid	SMU-831	390±50	*128*	excluded from models (see site description for further information)
Lubbock Lake	Stratum 5 (5B/)	wood	SI-716	210±40	*128*	excluded from models (see site description for further information)
Lubbock Lake	Stratum 5 (5B)	buried A horizon, humic acid	SMU-650	50±50	*128*	excluded from models (see site description for further information)
Manis	colluvium	mastodon tusk ivory sample no. 1 (XAD)	UCIAMS-11350	11975±35	*160*	
Manis	colluvium	mastodon tusk ivory sample no. 1 (XAD)	UCIAMS-12046	11975±35	*160*	

Site name	Provenience	Sample material	Laboratory code	Date (BP or ka)	Source	Notes
Manis	colluvium	mastodon tusk ivory sample no. 2 (XAD)	UCIAMS-11677	11890±35	*160*	
Manis	colluvium	mastodon rib bone (XAD)	UCIAMS-29113	11990±30	*160*	
Mead	CZ1	charcoal	Beta-312937	3780±30	*35*	
Mead	CZ1	charcoal	Beta-264529	4940±40	*34, 35*	
Mead	CZ2	charcoal	Beta-264525	4580±40	*35*	
Mead	CZ2	charcoal	Beta-264524	6050±40	*34, 35*	
Mead	CZ3	charcoal	Beta-264528	7790±50	*34, 35*	
Mead	CZ3	charcoal	Beta-264526	10140±50	*35*	
Mead	CZ3	charcoal	Beta-264527	10160±50	*35*	
Mead	CZ3	charcoal (Betula sp.)	Beta-337171	10220±40	*35*	
Mead	CZ3	charcoal (Populus sp.)	Beta-342449	10560±40	*35*	
Mead	CZ4	Wapiti antler tool	Beta-342930	11050±40	*17*	
Mead	CZ4	hearth charcoal (Betula sp.)	Beta-337174	11080±50	*35*	
Mead	CZ4	hearth charcoal (Populus/Salix)	Beta-337172	11100±50	*35*	
Mead	CZ4	hearth charcoal	Beta-264530	11210±60	*34, 35*	
Mead	CZ4	charcoal (Populus/Salix)	Beta-337181	11030±50	*17, 34*	
Mead	CZ4	charcoal (stratigraphic)	Beta-59121	11560±80	*17, 34*	
Mead	CZ4	charcoal (stratigraphic)	Beta-59120	11600±60	*17, 34*	
Mead	CZ5	bone collagen (Bison sp.)	Beta-264522	11460±50	*17, 34*	
Meadowcroft Rockshelter	Stratum IIa (F-46 lower)	charcoal	SI-2354"±16175±975	16175±975	*17, 34*	
Meadowcroft Rockshelter	Stratum IIa (F-46 lower)	charcoal	SI-1686	15120±165	*164*	
Meadowcroft Rockshelter	Stratum IIa (F-46 lower)	charcoal	SI-1872	14975±620	*164*	
Meadowcroft Rockshelter	Stratum IIa (F-46 lower)	charcoal	SI-2488	11320±340	*164*	
Meadowcroft Rockshelter	Stratum IIa (F-46 lower)	charcoal	SI-2065	13240±1010	*164*	
Meadowcroft Rockshelter	Stratum IIa (F-46 lower)	charcoal	SI-2489	12800±870	*164*	
Meadowcroft Rockshelter	Stratum IIa (F-46 lower)	charcoal	SI-2491	11300±700	*164*	
Meadowcroft Rockshelter	Stratum IIa (F-46 lower)	charcoal	SI-2061	9075±115	*164*	
Meadowcroft Rockshelter	Stratum IIa (F-46 lower)	charcoal	SI-2064	8010±110	*164*	

Site name	Provenience	Sample material	Laboratory code	Date (BP or ka)	Source	Notes
Meadowcroft Rockshelter	Stratum IIb	charcoal	SI-2056	5300±130	*164*	
Meadowcroft Rockshelter	Stratum IIb	charcoal	SI-2055	6670±140	*164*	
Meadowcroft Rockshelter	Stratum IIb	black walnut charcoal	Pitt-292	6630±70	*164*	
Meadowcroft Rockshelter	Stratum IIb	charcoal	SI-2358	6290±355	*164*	
Meadowcroft Rockshelter	Stratum IIb	charcoal	SI-1685	2870±85	*164*	
Meadowcroft Rockshelter	Stratum IIb	charcoal	SI-2356	4380±500	*164*	
Meadowcroft Rockshelter	Stratum IIb	charcoal	SI-2054	4005±85	*164*	
Meadowcroft Rockshelter	Stratum IIb	charcoal	SI-2058	3970±85	*164*	
Meadowcroft Rockshelter	Stratum IIb	charcoal	SI-2063	3950±240	*164*	
Meadowcroft Rockshelter	Stratum IIb	carbonized basketry fragments	SI-1680	3770±90	*164*	
Meadowcroft Rockshelter	Stratum IIb	charcoal	SI-1681	3210±95	*164*	
Meadowcroft Rockshelter	Stratum III	charcoal	SI-1679	3255±115	*164*	
Meadowcroft Rockshelter	Stratum III	charcoal	SI-2046	3115±70	*164*	
Meadowcroft Rockshelter	Stratum III	charcoal	SI-3030	3100±90	*164*	
Meadowcroft Rockshelter	Stratum III	charcoal	SI-2053	1140±115	*164*	
Meadowcroft Rockshelter	Stratum III	charcoal	SI-1664	3065±80	*164*	
Meadowcroft Rockshelter	Stratum III	charcoal	SI-2066	2930±75	*164*	
Meadowcroft Rockshelter	Stratum IV	charcoal	SI-2049	3050±85	*164*	
Meadowcroft Rockshelter	Stratum IV	charcoal	SI-1660	2860±80	*164*	
Meadowcroft Rockshelter	Stratum IV	charcoal	SI-1668	2820±75	*164*	

Site name	Provenience	Sample material	Laboratory code	Date (BP or ka)	Source	Notes
Meadowcroft Rockshelter	Stratum IV	charcoal	SI-1665	2815±80	*164*	
Meadowcroft Rockshelter	Stratum IV	charcoal	SI-3031	2655±120	*164*	
Meadowcroft Rockshelter	Stratum IV	charcoal	SI-2359	2485±350	*164*	
Meadowcroft Rockshelter	Stratum IV	charcoal	SI-1674	2325±75	*164*	
Meadowcroft Rockshelter	Stratum IV	charcoal	SI-2051	2290±90	*164*	
Meadowcroft Rockshelter	Stratum V	charcoal	SI-2487	2155±65	*164*	
Meadowcroft Rockshelter	Stratum V	charcoal	SI-2362	2075±125	*164*	
Meadowcroft Rockshelter	Stratum V	charcoal	SI-3022	1880±65	*164*	
Meadowcroft Rockshelter	Stratum V	charcoal	SI-3027	1790±60	*164*	
Meadowcroft Rockshelter	Stratum V	charcoal	SI-3024	1665±65	*164*	
Meay Channel I	Stratum X/XI	Pinus contorta wood	UCIAMS-163739	11440±25	*126*	
Meay Channel I	Stratum X	wood	UCIAMS-149779	11435±30	*126*	
Meay Channel I	Stratum X	Pinus contorta wood	UCIAMS-169402	11365±25	*126*	
Meay Channel I	Stratum X	wood	UCIAMS-142561	11295±30	*126*	
Meay Channel I	Stratum X	Pinus contorta wood	UCIAMS-163741	11260±25	*126*	
Meay Channel I	Stratum X	Pinus contorta wood	UCIAMS-163740	10720±60	*126*	
Meay Channel I	Stratum IX	Pinus contorta wood	UCIAMS-184916	10625±20	*126*	
Meay Channel I	Stratum IX	unidentified organic material	UCIAMS-169403	9820±80	*126*	
Meay Channel I	Stratum IX	Malus seed + wood	UCIAMS-179713	8410±20	*126*	
Meay Channel I	Stratum IX	unidentified organic material-root	UCIAMS-169401	4935±25	*126*	
Meay Channel I	Stratum VIII	Pinus contorta wood	UCIAMS-169399	10980±25	*126*	
Meay Channel I	Stratum VII	unidentified organic material-root	UCIAMS-169400	2855±15	*126*	
Meay Channel I	Stratum VII	charcoal	UCIAMS-179714	2650±15	*126*	

Site name	Provenience	Sample material	Laboratory code	Date (BP or ka)	Source	Notes
Meay Channel I	Stratum VII	unidentified plant material	UCIAMS-179712	2645±15	*126*	
Meay Channel I	Stratum VII	charcoal	UCIAMS-163742	2605±20	*126*	
Meay Channel I	Stratum VI	charcoal	UCIAMS-163743	2715±20	*126*	
Meay Channel I	Stratum II	charcoal	UCIAMS-186383	720±15	*126*	excluded from models (see site description for further information)
Mesa	"B"	hearth charcoal	DIC-1589	7620±95	*36*	
Mesa	"B"	hearth charcoal	Beta-55286	11660±80	*37*	
Mesa	"B"	hearth charcoal	Beta-57430/ CAMS-4147	11190±70	*37*	
Mesa	"Saddle"	hearth charcoal	Beta-50429	10980±280	*36*	
Mesa	"B"	hearth charcoal	Beta-55283/ CAMS-3569	10240±80	*37*	
Mesa	"A"	hearth charcoal	Beta50428/ ETH-9086	10090±85	*37*	
Mesa	"Saddle"	hearth charcoal	Beta-69898/ CAMS-11035	10070±60	*36*	
Mesa	"B"	hearth charcoal	Beta-52606/ CAMS-2688	10060±70	*37*	
Mesa	"B"	hearth charcoal	Beta-69900/ CAMS-11037	10050±90	*36*	
Mesa	"B"	hearth charcoal	Beta-55285/ CAMS-3571	10000±80	*37*	
Mesa	"B"	hearth charcoal	Beta-69899/ CAMS-11036	9900±80	*36*	
Mesa	"Saddle"	hearth charcoal	Beta-55282/ CAMS-3568	9990±80	*37*	
Mesa	"B"	hearth charcoal	Beta-57429/ CAMS-4146	9900±70	*37*	
Mesa	"Saddle"	hearth charcoal	Beta-50430/ ETH-9087	9945±75	*37*	
Mesa	"B"	hearth charcoal	Beta-55284/ CAMS-3570	9930±80	*37*	
Mesa	"Saddle"	soil charcoal	Beta-36805/ ETH-6570	9730±80	*37*	
Mesa	"B"	hearth charcoal	Beta-55284/ CAMS-3570	9930±80	*37*	
Moose Creek	Component I/lower paleosol complex/ Nenana	hearth charcoal	Beta-96627	11190±60	*41*	
Moose Creek	Transition between Component I and II (soil organics)	soil organics	GX-6281	11730±250	*43*	
Moose Creek	Transition between Component I and II (soil organics)	soil organics	I-11227	10640±280	*43*	
Moose Creek	Transition between Component I and II (soil organics)	soil organics	A-2144	8940±270	*43*	
Moose Creek	Transition between Component I and II (soil organics)	soil organics	A-2168	8160±260	*43*	
Moose Creek	Component II// Denali I	hearth charcoal	Beta-106040	10500±60	*41*	

Site name	Provenience	Sample material	Laboratory code	Date (BP or ka)	Source	Notes
Moose Creek	Component III/ Denali II	hearth charcoal	Beta-106041	5680±50	*41*	
Murray Springs	Graveyard Member (F1)	charcoal (Fraxinus sp.)	SMU-18	11190±180	*103*	
Murray Springs	Graveyard Member (F1)	charcoal	A-805	11150±450	*103*	
Murray Springs	Graveyard Member (F1)	charcoal	Tx-1413	11080±180	*103*	
Murray Springs	Graveyard Member (F1)	charcoal	Tx-1462	10930±170	*103*	
Murray Springs	Graveyard Member (F1)	charcoal	SMU-27	10890±180	*103*	
Murray Springs	Graveyard Member (F1)	charcoal	SMU-41	10840±70	*103*	
Murray Springs	Graveyard Member (F1)	charcoal	SMU-42	10840±140	*103*	
Murray Springs	Graveyard Member (F1)	charcoal	Tx-1459	10710±160	*103*	
Owl Ridge	Stratum 2/ Component 1/ Square N88E110	charcoal (*Salix* sp.)	AA-86969	11060±60	*46*	
Owl Ridge	Stratum 4/ Component 2/ Square N85E103	charcoal (*Salix* sp.)	UCIAMS-71261	10485±25	*46*	
Owl Ridge	Stratum 4/ Component 2/ Square N85E103	charcoal (*Salix* sp.)	AA-86968	10440±60	*46*	
Owl Ridge	Stratum 4/ Component 2/ Square N86E104	charcoal (*Salix* sp.)	AA-86964	10420±60	*46*	
Owl Ridge	Stratum 4/ Component 2/ Square N86E103	charcoal (*Salix* sp.)	AA-86960	10415±60	*46*	
Owl Ridge	Stratum 4/ Component 2/ Square N86E103	charcoal (*Salix* sp.)	AA-86962	10335±60	*46*	
Owl Ridge	Stratum 4/ Component 2/ Square N86E103	charcoal (*Salix* sp.)	AA-86963	10340±75	*46*	
Owl Ridge	Stratum 4/ Component 2/ Square N86E103	charcoal (*Salix* sp.)	AA-86961	10330±70	*46*	
Owl Ridge	Stratum 4/ Component 2/ Square N86E104	charcoal (*Salix* sp.)	AA-86965	10295±60	*46*	
Owl Ridge	Stratum 4/ Component 2/ Square N86E106	charcoal (*Salix* sp.)	AA-86966	10290±75	*46*	
Owl Ridge	Stratum 4/ Component 2/ Square N88E105	charcoal (*Salix* sp.)	UCIAMS-71260	10125±20	*46*	
Owl Ridge	Stratum 4/ Component 2/ Square N88E105	charcoal (*Salix* sp.)	AA-86967	10120±75	*46*	
Owl Ridge	Stratum 4/ Component 2/ Square N88E108	charcoal (*Salix* sp.)	Beta-289378	10020±40	*46*	
Owl Ridge	Stratum 4/ Component 2/ Square N95E98	charcoal (*Picea* sp.)	Beta-289382	80±40	*46*	

Site name	Provenience	Sample material	Laboratory code	Date (BP or ka)	Source	Notes
Owl Ridge	Strata 6/5/4/ Component 3/2/ Square N83E105	charcoal (*Salix* sp.)	Beta-289377	10080±40	*46*	
Owl Ridge	Strata 6/5/4/ Component 3/2/ Square N83E105	charcoal (*Salix* sp.)	Beta-289376	9550±40	*46*	
Owl Ridge	Stratum 5/ Component 3/ Square N92E110	charcoal (*Salix* sp.)	Beta-330172	9880±40	*46*	
Owl Ridge	Stratum 5/ Component 3/ Square N92E110	charcoal (*Salix* sp.)	Beta-289379	9790±40	*46*	
Page-Ladson	Stratum 3a	wood (Taxonium distichum)	UCIAMS-141961	13080±40	*171*	
Page-Ladson	Stratum 3a	wood (Taxonium distichum)	UCIAMS-141960	13945±50	*171*	
Page-Ladson	Stratum 3a	twig (Taxonium distichum)	UCIAMS-141959	12615±35	*171*	
Page-Ladson	Stratum 3a	twig (Taxonium distichum)	UCIAMS-141958	12495±35	*171*	
Page-Ladson	Stratum 3c	twig (Quercus sp.)	UCIAMS-141957	12420±30	*171*	
Page-Ladson	Stratum 3c	twig (Taxonium distichum)	UCIAMS-141956	12395±30	*171*	
Page-Ladson	Stratum 3c	wood (Taxonium distichum)	UCIAMS-141955	13585±35	*171*	
Page-Ladson	Stratum 3c	wood (Taxonium distichum)	UCIAMS-141954	13005±35	*171*	
Page-Ladson	Stratum 3c	wood (Taxonium distichum)	UCIAMS-141953	14510±40	*171*	
Page-Ladson	Stratum 3c	wood (Quercus-Leucobalanus group)	UCIAMS-141952	12385±35	*171*	
Page-Ladson	Stratum 3c	wood (Quercus-Leucobalanus group)	UCIAMS-141951	12415±30	*171*	
Page-Ladson	Stratum 3c	wood (Taxonium distichum)	UCIAMS-141950	13830±35	*171*	
Page-Ladson	Stratum 3c	wood (Fraxinus sp.)	UCIAMS-127303	12495±30	*171*	
Page-Ladson	Stratum 3c	bark (unknown peridem)	UCIAMS-127305	13015±30	*171*	
Page-Ladson	Stratum 3c	wood (Abies)	UCIAMS-127304	12420±30	*171*	
Page-Ladson	Stratum 3c	wood (Acer)	UCIAMS-127302	12425±30	*171*	
Page-Ladson	Stratum 3c	twig (Quercus sp.)	UCIAMS-141949	12385±35	*171*	
Page-Ladson	Stratum 3c	wood (Fraxinus sp.)	UCIAMS-141948	12430±30	*171*	
Page-Ladson	Stratum 3c	wood (Taxonium distichum)	UCIAMS-141947	13440±40	*171*	
Page-Ladson	Stratum 3c	twig (Fraxinus sp.)	UCIAMS-141946	12400±35	*171*	
Page-Ladson	Stratum 3c	twig (Taxonium distichum)	UCIAMS-141945	12400±35	*171*	
Page-Ladson	Stratum 3c	twig (Taxonium distichum)	UCIAMS-141944	12410±35	*171*	

Site name	Provenience	Sample material	Laboratory code	Date (BP or ka)	Source	Notes
Page-Ladson	Stratum 3c	twig (Quercus sp.)	UCIAMS-141943	12410±30	*171*	
Page-Ladson	Stratum 3c	twig (unidentified hardwood)	UCIAMS-141942	12440±30	*171*	
Page-Ladson	Stratum 3c	twig (unidentified hardwood)	UCIAMS-141941	12365±30	*171*	
Page-Ladson	Stratum 3c	twig (Fraxinus sp.)	UCIAMS-141940	12430±30	*171*	
Page-Ladson	Stratum 3c	twig (unidentified hardwood)	UCIAMS-141939	12430±35	*171*	
Page-Ladson	Stratum 4a	wood (unidentified hardwood)	UCIAMS-141938	12440±30	*171*	
Page-Ladson	Stratum 4b	wood (Morus rubra)	UCIAMS-141937	12380±35	*171*	
Page-Ladson	Stratum 4b	twig (unidentified hardwood)	UCIAMS-141935	12250±35	*171*	
Page-Ladson	Stratum 4b	wood (Fagus grandifolia)	UCIAMS-141934	12365±30	*171*	
Page-Ladson	Stratum 4b	wood (Taxonium distichum)	UCIAMS-141933	12295±35	*171*	
Page-Ladson	Stratum 4b	twig (Carya sp.)	UCIAMS-141932	12310±30	*171*	
Page-Ladson	Stratum 4b	wood (Fagus grandifolia)	UCIAMS-141931	12275±30	*171*	
Page-Ladson	Stratum 4b	twig (Carya sp. aquatic)	UCIAMS-141930	12370±30	*171*	
Page-Ladson	Stratum 4b	twig (unidentified hardwood, ring-porous)	UCIAMS-141929	12270±30	*171*	
Page-Ladson	Stratum 4b	twig (unidentified hardwood, diffuse-porous)	UCIAMS-141928	12335±35	*171*	
Page-Ladson	Stratum 4b	twig (unidentified hardwood)	UCIAMS-153343	12260±35	*171*	
Paisley Caves	Cave 5, LU 1b, excavation unit 5/5D	human coprolite (1961-P-5/5D-31)	Beta-2134244	12400±60	*175*	
Paisley Caves	Cave 5, LU 1b, excavation unit 5/5D	human coprolite (1961-P-5/5D-31)	OxA-16498	12275±55	*175*	
Paisley Caves	Cave 5, LU 1b, excavation unit 5/7C	human coprolite (1294-PC-5/7C-31)	OxA-16497	12345±55	*175*	
Paisley Caves	Cave 5, LU 1b, excavation unit 5/7C	human coprolite (1294-PC-5/7C-31)	Beta-2134263	12290±60	*175*	
Paisley Caves	Cave 5, LU 1a or b, excavation unit 5/6B	human coprolite (1294-PC-5/6B-50)	Beta-2164742	12260±60	*175*	
Paisley Caves	Cave 5, LU 1a or b, excavation unit 5/6B	human coprolite (1294-PC-5/6B-50)	OxA-16495	12140±70	*175*	
Paisley Caves	Cave 5, Profile III, LU 1; excavation unit 5/16A	Artemisa twig (geo stratigraphic)	UCIAMS-80384	12410±25	*9*	
Paisley Caves	Cave 5, Profile III, LU 1; excavation unit 5/16A	Artemisa twig (geo stratigraphic)	UCIAMS-80377	12405±25	*9*	

Site name	Provenience	Sample material	Laboratory code	Date (BP or ka)	Source	Notes
Paisley Caves	Cave 5, Profile III, LU 2; ; excavation unit 5/16A	Ericacaea twig (geo stratigraphic; 2010PC-224)	UCIAMS-80381	11500±30	*9*	entered as "Unit 2 (lower)" in the model
Paisley Caves	Cave 5, Profile III, LU 2; ; excavation unit 5/16A	Camelid coprolite (water soluble)	UCIAMS-90586	11315±25	*9*	entered as "Unit 2 (lower)" in the model
Paisley Caves	Cave 5, Profile III, LU 2; ; excavation unit 5/16A	Human coprolite (water soluble)	UCIAMS-90584	11250±25	*9*	entered as "Unit 2 (lower)" in the model
Paisley Caves	Cave 5, Profile III, LU 2; ; excavation unit 5/16A	Human coprolite (macro)	UCIAMS-90583	11205±25	*9*	entered as "Unit 2 (lower)" in the model
Paisley Caves	Cave 5, Profile III, LU 2, excavation unit 5/16A	Artemisa twig (water soluble proteins; 2010PC-223)	UCIAMS-80379	11295±25	*9*	entered as "ISL" in the model
Paisley Caves	Cave 5, Profile III, LU 2, excavation unit 5/16A	Artemisa twig (water soluble salts; 2010PC-223)	UCIAMS-80380	11165±25	*9*	entered as "ISL" in the model
Paisley Caves	Cave 5, Profile III, LU 2, excavation unit 5/16A	Artemisa twig (2010PC-223)	UCIAMS-80378	11070±25	*9*	entered as "ISL" in the model
Paisley Caves	Cave 5, Profile III, LU 2, excavation unit 5/18A	Unidentified macroflora in sediment	UCIAMS-98932	10855±30	*9*	entered as "Unit 2 (upper)" in the model
Schaefer	Paleoindian	mammoth bone (XAD)	CAMS-30171	12310±60	*153*	
Schaefer	Paleoindian	mammoth bone (XAD)	CAMS-61135	12320±50	*151*	
Schaefer	Paleoindian	mammoth bone (XAD)	CAMS-61143	12390±40	*151*	
Shawnee Minisink	hearth 2 (feature 9), sq. 4/4E (2006 excavations)	charred hawthorne seeds	OxA-17371	10970±50	*114*	incorrectly noted as "OxA-1731" in Gingerich , 2007, 2013
Shawnee Minisink	hearth 1 (feature 12), sq. 4/4E (2006 excavations)	hearth charcoal	UCIAMS-24866	11020±30	*5*	
Shawnee Minisink	hearth 1 (feature 12), sq. 4/4E (2006 excavations)	hearth charcoal	UCIAMS-24865	10915±25	*5*	
Shawnee Minisink	hearth 1 (feature 12), sq. 4/4E (2006 excavations)	hearth charcoal	Beta-203865	10820±50	*114*	
Shawnee Minisink	Zone 4 (1972 excavations)	hearth charcoal	Beta-127162	10900±40	*114*	
Shawnee Minisink	Zone 4 (1972 excavations)	hearth charcoal	Beta-101935	10940±90	*114*	
Shawnee Minisink	Zone 4 (1974 excavations)	charcoal (humates)	W-3391	11050±1000	*110*	
Shawnee Minisink	Zone 4 (1974 excavations)	charcoal	W-3388	9310±1000	*110*	
Shawnee Minisink	Zone 4 (1974 excavations)	hearth charcoal	W-3134	10750±600	*110*	
Shawnee Minisink	Zone 4 (1972 excavations)	hearth charcoal	W-2994	10590±300	*110*	
Sheriden Cave	Unit 5a	dentin collagen (C. scotti)	Beta-127908b	12840±100	*118*	
Sheriden Cave	Unit 5a	dentin collagen (C. scotti)	AA-127908a	12590±450	*118*	

Site name	Provenience	Sample material	Laboratory code	Date (BP or ka)	Source	Notes
Sheriden Cave	Unit 5a	dentin collagen (C. scotti)	AA-127907	12520±170	*118*	
Sheriden Cave	Unit 5a	bone collagen (M.nasutus)	Beta-139687	11860±40	*118*	
Sheriden Cave	Unit 5a	bone collagen (A. simus)	CAMS-12837	11480±60	*119*	
Sheriden Cave	Unit 5a	bone collagen (A. simus)	CAMS-12839	11570±70	*118*	
Sheriden Cave	Unit 5a	bone collagen (A. simus)	CAMS-33968	11570±50	*119*	
Sheriden Cave	Unit 5a	bone collagen (A. simus)	CAMS-12845	11610±90	*119*	
Sheriden Cave	Unit 5a	wood charcoal	Beta-127909	10840±80	*118*	
Sheriden Cave	Unit 5a	wood charcoal	Beta-127910	10960±60	*118*	
Sheriden Cave	Unit 5a	bone point (XAD)	UCIAMS-38249	10915±30	*117*	
Sheriden Cave	Unit 5b	wood charcoal	AA-21711	13210±80	*118*	
Sheriden Cave	Unit 5b	wood charcoal	PITT-0982	11710±220	*119*	
Sheriden Cave	Unit 5b	bone collagen (P. compressus)	CAMS-33970	11130±60	*118*	
Sheriden Cave	Unit 5b	bone collagen (P. compressus)	CAMS-10349	11060±60	*119*	
Sheriden Cave	Unit 5b	wood charcoal	AA-21712	10470±70	*118*	
Sheriden Cave	Unit 5c	wood charcoal	Beta-117607	10970±70	*118*	
Sheriden Cave	Unit 5c	wood charcoal	Beta-117601	10940±70	*118*	
Sheriden Cave	Unit 5c	bone collagen (C. ohioensis)	CAMS-26783	10850±60	*118*	
Sheriden Cave	Unit 5c	wood charcoal	Beta-117602	10850±70	*118*	
Sheriden Cave	Unit 5c	wood charcoal	AA-21710	10680±80	*118*	
Sheriden Cave	Unit 5c	wood charcoal	Beta-117606	10620±70	*118*	
Sheriden Cave	Unit 5c	wood charcoal	Beta-117603	10600±60	*118*	
Sheriden Cave	Unit 5c	wood charcoal	Beta-117605	10570±70	*118*	
Sheriden Cave	Unit 5c	wood charcoal	Beta-117604	10550±70	*118*	
Sheriden Cave	Unit 5c	bone collagen (R. tarandus)	Beta-139686	10440±40	*118*	
Sheriden Cave	Unit 6	wood charcoal	AA-21706	10020±115	*118*	
Sheriden Cave	Unit 6	wood charcoal	AA-21705	9775±70	*118*	
Sheriden Cave	Unit 6	wood charcoal	CAMS-24127	9190±60	*119*	
Sheriden Cave	Unit 6	wood charcoal	CAMS-24126	9170±60	*119*	
Swan Point	CZ4b	mammoth ivory tusk collagen	NSRL-2001/ CAMS-17045	12060±70	*50*	

Site name	Provenience	Sample material	Laboratory code	Date (BP or ka)	Source	Notes
Swan Point	CZ4b	mammoth ivory tusk collagen	AA-98488	12500±150	*17*	
Swan Point	CZ4b	mammoth ivory tusk collagen	Beta-365062	12170±50	*49*	
Swan Point	CZ4b	mammoth molar collagen	AA-74250	12110±120	*49*	
Swan Point	CZ4b	hearth charcoal (Populus/Salix)	Beta-209882	12290±40	*49*	
Swan Point	CZ4b	residue (carbonized fat/ grease)	Beta-209884	12220±40	*49*	
Swan Point	CZ4b	residue (carbonized fat/ grease)	Beta-209883	12100±40	*49*	
Swan Point	CZ4b	mammoth ivory tusk collagen	AA-74251	12050±120	*49*	
Swan Point	CZ4b	horse molar collagen	AA-74249	11950±100	*49*	
Swan Point	CZ4b	residue (carbonized fat/ grease)	Beta-170457	12360±60	*49*	
Swan Point	CZ4b	hearth charcoal (Populus/Salix)	Beta-QA-619	12040±40	*49*	
Swan Point	CZ4b	residue (carbonized fat/ grease)	Beta-175491	12110±50	*49*	
Swan Point	CZ4b	artifact residue	AA-19322	11770±140	*49*	
Swan Point	CZ4b	charcoal (Salix sp.)	Beta-71372/ CAMS-12389	11660±60	*50*	
Swan Point	CZ4b	charcoal (Populus/Salix)	Beta-56667/ CAMS-4252	11660±70	*50*	
Swan Point	CZ4a	burned bone collagen	Beta-175489 (KOH)	11360±50	*47*	
Swan Point	CZ4a	hearth	Beta-355852	11350±50	*47*	
Swan Point	CZ3b	Populus/Salix from hearth with burnt bone	Beta-401126	10620±40	*47*	
Swan Point	CZ3b	hearth charcoal	Beta-209885	10570±40	*48*	
Swan Point	CZ3b	charcoal	Beta-56666/ CAMS-4251	10230±80	*50*	
Swan Point	CZ3a	hearth bulk sample	Beta-355867	10160±50	*47*	
Swan Point	CZ3a	hearth stain	Beta-357816	10070±40	*47*	
Swan Point	CZ3a	hearth charcoal	Beta-170458	10050±60	*48*	
Swan Point	CZ3a	hearth charcoal	Beta-190578	10010±90	*48*	
Swan Point	CZ2	charcoal	WSU-4426	7400±80	*48*	
Swan Point	CZ2	charcoal	Beta-209886	6610±40	*48*	
Swan Point	CZ1b	cf. Larix from hearth?/reddish stain	Beta-401125	4480±30	*47*	
Swan Point	CZ1b	hearth charcoal	Beta-190580	4260±40	*48*	
Swan Point	CZ1b	Picea assoc. w/ calcined bone	Beta-401124	3060±30	*47*	
Swan Point	CZ1a	charcoal from hearth?/fcr	Beta-401123	1860±30	*47*	
Swan Point	CZ1a	charcoal/resin	WSU-4521	1750±80	*50*	

Site name	Provenience	Sample material	Laboratory code	Date (BP or ka)	Source	Notes
Swan Point	CZ1a	charcoal	WSU-4522	1670±60	*50*	
Swan Point	CZ1a	charcoal (Picea sp.)	WSU-4524	1570±70	*50*	
Swan Point	CZ1a	charcoal (Betula sp.)	WSU-4523	1220±70	*50*	
Swan Point	CZ1a	hearth charcoal	Beta-223302	860±40	*48*	
Swan Point	CZ1a	hearth bulk sample	Beta-340993	810±30	*47*	
Ushki	Below Component 7	charcoal	AA-45718	11820±100	*53*	
Ushki	Below Component 7	charcoal	AA-45712	11200±160	*53*	
Ushki	Below Component 7	charcoal	AA-45711	11870±90	*53*	
Ushki	Component 7	charcoal	AA-45716	11050±75	*53*	
Ushki	Component 7	charcoal	AA-45710	10675±75	*53*	
Ushki	Component 7	charcoal	AA-45708	10810±75	*53*	
Ushki	Component 7	charcoal	AA-45709	10850±320	*53*	
Ushki	Component 7	charcoal	SR-5810/ CAMS-74639	11330±50	*53*	
Ushki	Component 7	charcoal	AA-1388	11005±115	*53*	
Ushki	Component 7	humates	AA-41389	11050±75	*53*	
Ushki	Component 6	charcoal	AA-45720	10230±70	*53*	
Ushki	Component 6	charcoal	AA-45719	10385±90	*53*	
Ushki	Component 6	charcoal	AA-45717	11130±100	*53*	
Ushki	Component 6	charcoal	AA-45713	10040±130	*53*	
Ushki	Component 6	charcoal	AA-45715	10160±75	*53*	
Ushki	Component 6	charcoal	AA-45714	10800±175	*53*	
Ushki	Component 6	charcoal	SR-5811/ CAMS-74640	10460±80	*53*	
Ushki	Component 6	charcoal	AA-41386	10240±75	*53*	
Ushki	Component 6	humates	AA-41387	9485±275	*53*	
Walker Road	Loess 1 & 2	hearth charcoal	Beta-11254	11820±200	*54*	
Walker Road	Loess 1 & 2	hearth charcoal	AA-2264	11300±120	*54*	
Walker Road	Loess 1 & 2	hearth charcoal	AA-1681	11170±180	*54*	
Walker Road	Loess 1 & 2	hearth charcoal	AA-1683	11010±230	*54*	
Walker Road	Loess 4	charcoal	AA-1692	8720±250	*54*	
Walker Road	Loess 5	charcoal	GX-12875	4415±95	*54*	
Walker Road	Loess 5	charcoal	AA-1693	3816±79	*54*	
Wally's Beach	aeolian sand	camel bone (cat. no. 3610.1; XAD)	UCIAMS-116 400	11465±40	*134*	
Wally's Beach	aeolian sand	camel bone (cat. no. 3610.1; XAD)	UCIAMS-127 347	11425±30	*134*	
Wally's Beach	aeolian sand	camel bone (cat. no. 3610.1; HYP)	OxA-X-2736-8	11530±50	*88*	
Wally's Beach	aeolian sand	horse bone (1; cat no.3594; XAD)	UCIAMS-127 348	11470±35	*134*	
Wally's Beach	aeolian sand	horse bone (2; cat no. 2988.1; XAD)	UCIAMS-127 349	11410±30	*134*	

Site name	Provenience	Sample material	Laboratory code	Date (BP or ka)	Source	Notes
Wally's Beach	aeolian sand	horse bone (3; cat no. 944; XAD)	UCIAMS-127350	11460±30	*134*	
Wally's Beach	aeolian sand	horse bone (A; cat no. 315; XAD)	UCIAMS-127351	11440±30	*134*	
Wally's Beach	aeolian sand	horse bone (A; cat no. 315; XAD)	OxA-X-2736-10	11445±55	*88*	
Wally's Beach	aeolian sand	horse bone (B; cat. no. 164 XAD)	UCIAMS-127352	11475±30	*134*	
Wally's Beach	aeolian sand	horse bone (C; cat. no 683; XAD)	UCIAMS-127353	11440±30	*134*	
Wally's Beach	aeolian sand	horse bone (D, cat. no 77.1; XAD)	UCIAMS-127354	11430±30	*134*	
Wally's Beach	aeolian sand	muskox bone (cat no. 3293.1; XAD)	UCIAMS-127373	11320±30	*134*	
Wally's Beach	aeolian sand	muskox bone (cat no. 3293.1; HYP)	OxA-X-2736-9	11255±50	*88*	

Table S2. Age estimates obtained for archaeological components analyzed, at 95.4% and 68.2% confidence. These are represented by start Boundaries, Date functions, or calibrated dates. For more information on each site, see Supplementary Information, section 2.

Tradition or temporal category	**Archaeological site**	**Type of age estimate**	**cal BP (68.2% confidence)**	**cal BP (95.4% confidence)**
Beringian tradition	Berelekh	start `Boundary`	14190-13970	14315-13835
	Broken Mammoth	start `Boundary`	20655-13275	19270-13350
	Dry Creek	start `Boundary`	13525-13405	13700-13350
	Mead	start `Boundary`	13425-13310	13520-13010
	Mesa	`Date` within a `Phase`	13145-11135	13910-9355
	Moose Creek	start `Boundary`	13735-12980	15195-12865
	Owl Ridge	start `Boundary`	1338512820	14315-12745
	Swan Point	start `Boundary`	14450-14210	14680-14155
	Ushki	start `Boundary`	13290-13095	13435-12855
	Walker Road	start `Boundary`	13950-13220	14950-13075
Clovis	Anzick	`Date` within a `Phase`	12880-12710	13175-12485
	Aubrey	start `Boundary`	13760-13330	14750-13245
	Blackwater Locality No.1	start `Boundary`	13285-12855	13440-12675
	Cactus Hill	start `Boundary`	13140-12320	13595-11395
	Colby	`Date` within a `Phase`	12835-12650	13165-12350
	Debra L. Friedkin	start `Boundary`	14330-13465	14705-13070
	Dent	`Date` within a `Phase`	13125-12815	13545-12415
	Domebo	calibrated date (`R_Date`)	12825-12740	12910-12710
	El Fin del Mundo	start `Boundary`	14070-13705	14135-13470
	Gault	start `Boundary`	15180-13110	16895-12705
	Jake Bluff	`Date` within a `Phase`	12735-12690	12775-12645
	Lange/Ferguson	`Date` within a `Phase`	13270-12355	14285-11105
	Lehner	`Date` within a `Phase`	13130-12654	13579-9390
	Murray Springs	`Date` within a `Phase`	12840-12700	13015-12615

Tradition or temporal category	Archaeological site	Type of age estimate	cal BP (68.2% confidence)	cal BP (95.4% confidence)
	Shawnee-Minisink	`Date` within a `Phase`	12805-12720	12910-12650
	Sheriden Cave	start `Boundary`	14060-13600	14950-13555
Clovis-coeval	Arlington Springs	calibrated date (`R_Date`)	12915-12730	13015-12705
	Meay Channel I	start `Boundary`	13425-13255	13825-13205
	Lubbock Lake	start `Boundary`	15145-14035	16310-13830
	Wally's Beach	`Date` within a `Phase`	13305-13265	13340-13220
pre-Clovis	Bluefish Caves	calibrated date (`R_Date`)	23860-23505	24035-23310
	Cactus Hill	start `Boundary`	20470-19775	20585-18970
	Cooper's Ferry	start `Boundary`	16020-15445	16560-15285
	Debra L. Friedkin	start `Boundary`	15920-15060	16330-14690
	Gault	start `Boundary`	22835-18815	26435-17385
	Hebior	`Date within a Phase`	15055-14640	15615-13975
	Lindsay	`Date` within a `Phase`	14325-14130	14625-13945
	Manis	`Date` within a `Phase`	13820-13725	13795-13600
	Meadowcroft Rockshelter	start `Boundary`	22740-19485	24335-18620
	Page-Ladson	start `Boundary`	16835-14460	16985-14375
	Paisley Caves	`Date` within a `Phase`	14335-14105	14755-13780
	Schaefer	`Date within a Phase`	14495-14145	15020-13710
Western Stemmed tradition	Buhl	calibrated date (`R_Date`)	12705-12560	12740-12420
	Bonneville Estates	start `Boundary`	12715-12635	12760-12605
	Cooper's Ferry	calibrated date (`R_Date`)	13555-13385	13610-13275
	Paisley Caves	start `Boundary`	13090-13045	13110-13015

4. Archaeological sites excluded

4.1. Cerutti Mastodon site, San Diego (U.S.A.)

The Cerutti Mastodon site is reported as a 130,000 year-old archaeological site containing hammerstones and stone anvils, associated with the remains of a single mastodon[186]. The cultural aspect of the site and the methodology applied in the study have been questioned and criticized, however[187–192]. As such, pending future research, the site was excluded.

4.2. El Pit I, Quintana Roo (Mexico)

The El Pit I individual was found in a submerged sinkhole and directly dated to 11,332±64 BP (KIA-43524)[193]. Given the depositional environment and fraction dated (bone apatite; see ref[194]), this measurement is likely a minimum-age estimate. As such, this individual and site was excluded from the analysis pending future chronometric work.

4.3. Healy Lake, Alaska (U.S.A.)

Healy Lake Village is a stratified site containing three Cultural Stages—Chindadn (earliest), Transitional and Athapaskan—within ten stratigraphic levels[195]. The chronological dataset for Healy Lake is highly incongruent[195]. As such, the site was excluded.

4.4. La Prele, Wyoming (U.S.A.)

In 1986, the La Prele Mammoth locality (formerly known as Hinrichs or Fetterman) produced the remains of a mammoth and a small lithic assemblage. The association between the two, however, was deemed equivocal[196]. In 2014, the site was re-excavated and the discovery of new cultural material reported[197]. Given that the results of the most current efforts have yet to be published, La Prele was excluded from this analysis.

4.5. Miami, Texas (U.S.A.)

Miami (41RB1) is a Clovis, mammoth-butchering site with associated lithic tool technology[198]. There no direct bone dates for the site. Instead, the bone bed (loess layer), dated to 11,415±125 BP (AA-7086), is bracketed by four sediment dates (obtained from two separate samples) from under- and over-lying deposits. Considering that the limited number of dates do not warrant a model and the cultural event itself is not directly dated, this site was excluded.

4.6. Naharon individual, Quintana Roo (Mexico)

The Naharon individual, known as 'Naharon Woman', was found in a submerged sinkhole and directly dated to 11,670 ± 60 BP (UCR-4000A/CAMS-87301; total amino acid fraction)[193,199]. This measurement is regarded as problematic and preliminary, however, since biochemical examination of the bone determined organic carbon content to be extremely low[199]. As such, this site was excluded from the analysis pending future chronometric work.

4.7. Paleo Crossing, Ohio (U.S.A.)

Paleo Crossing (33ME274) is stratified site containing Clovis, Archaic, Woodland, and Late Prehistoric material[200–211]. Within the Clovis (lithic) assemblage layer, charcoal and organic fragments extracted from a cylindrical pit (containing a Clovis point base) and post molds were dated. The resulting dataset was conflicting, however, with ages ranging from 9,230±80 BP (AA-8252; above a cylindrical pit) to 13,100±100 BP (AA-8251; inside the cylindrical pit). Later efforts at dating two burned Clovis stone tools using luminescence methods resulted in a weighted average of 9.1±1.8 ka[211]. Considering that archaeological and chronometric investigations at the site are ongoing[211], this site was excluded.

4.8. Topper, South Carolina (U.S.A.)

Topper (38AL23) is a stratified site reported to contain a pre-Clovis and Clovis assemblage. Given that the human origin of the pre-Clovis component is equivocal[212], this site was excluded.

5. Sensitivity testing

To test the robustness of Clovis and Beringian tradition models presented in the main text (models 'A'; as applicable), Clovis and Beringian tradition models were run using start boundaries, instead of `Date` functions, for all single-phase, site-specific models (models 'B'). The output obtained shows that, within each tradition, the modeled boundaries are statistically indistinguishable (Table S3). Therefore, different approaches to site-specific model building (priors) had negligible impact on the output of tradition-level models (posteriors).

Table S3. Start boundaries yielded by models A and B, for Clovis and Beringian traditions, and χ^2 test results. Models A are those presented in the main text and models C include start boundaries for single-phase site-specific models (whereas for A, `Date` functions were used). The statistical analysis was done with OxCal 4.3[213], following Ward and Wilson[214], and the `Combine` command. The degrees of freedom are given by df and the χ^2 value calculated by T. Noted inside the brackets is the confidence level (at 5%) followed by the critical value of the χ^2 distribution. This value denotes the level above which T should not rise for the age estimates to be considered in good agreement. Results show that start boundaries for models A and B are highly comparable. Therefore, slight differences in site-specific model building had a negligible impact on the output of tradition-level models.

Tradition	**Model**	**cal BP (95.4% confidence)**	**χ^2 test result**
Clovis	A	14210-13495	df=1 T=0.026 (5% 3.841)
	B	14240-13505	
Beringian	A	14910-13395	df=1 T=0.239 (5% 3.841)
	B	14910-13450	

References

1. Smallwood, A. M. & Jennings, T. A. *Clovis: On the Edge of a New Understanding*. (Texas A&M University Press, 2014).
2. Haynes, C. V., Jr. Fluted Projectile Points: Their Age and Dispersion: Stratigraphically controlled radiocarbon dating provides new evidence on peopling of the New World. *Science* **145**, 1408–1413 (1964).
3. Haynes, G. *The Early Settlement of North America: The Clovis Era*. (Cambridge University Press, 2002).
4. Stanford, D., Bonnichsen, R., Meggers, B. & Steele, D. G. Paleoamerican origins: Models, evidence, and future directions. *Paleoamerican Origins: Beyond Clovis* 313–353 (2005).
5. Waters, M. R. & Stafford, T. W., Jr. Redefining the age of Clovis: implications for the peopling of the Americas. *Science* **315**, 1122–1126 (2007).
6. Howard, C. D. The Clovis Point: Characteristics and Type Description. *Plains Anthropol.* **35**, 255–262 (1990).
7. Goebel, T. Clovis culture update. *Clovis: On the edge of a new understanding* 325–352 (2015).
8. Goebel, T. & Keene, J. L. Are Great Basin stemmed points as old as Clovis in the Intermountain West? A review of the geochronological evidence. *Archaeology in the Great Basin and Southwest: Papers in Honor of Don D. Fowler* 35–60 (2014).
9. Jenkins, D. L. *et al.* Clovis age Western Stemmed projectile points and human coprolites at the Paisley Caves. *Science* **337**, 223–228 (2012).
10. Bryan, A. L. The stemmed point tradition: An early technological tradition in western North America. *Anthropological Papers in Memory of Earl H. Swanson, Jr* 77–107 (1980).
11. Beck, C. & Jones, G. T. Clovis and Western Stemmed: Population Migration and the Meeting of Two Technologies in the Intermountain West. *Am. Antiq.* **75**, 81–116 (2010).
12. Davis, L. G., Nyers, A. J. & Willis, S. C. Context, Provenance and Technology of a Western Stemmed Tradition Artifact Cache from the Cooper's Ferry Site, Idaho. *Am. Antiq.* **79**, 596–615 (2014).
13. Davis, L. G. *et al.* Late Upper Paleolithic occupation at Cooper's Ferry, Idaho, USA, ~16,000 years ago. *Science* **365**, 891–897 (2019).

14. Graf, K. E. & Buvit, I. Human Dispersal from Siberia to Beringia: Assessing a Beringian Standstill in Light of the Archaeological Evidence. *Curr. Anthropol.* **58**, S583–S603 (2017).
15. Agenbroad, L. D. *et al. American Beginnings: The Prehistory and Palaeoecology of Beringia*. (University of Chicago Press, 1996).
16. Holmes, C. E. Tanana River Valley Archaeology circa 14,000 to 9000 B.P. *Arctic Anthropol.* **38**, 154–170 (2001).
17. Potter, B. A., Holmes, C. E. & Yesner, D. R. Technology and economy among the earliest prehistoric foragers in interior eastern Beringia. in *Paleoamerican Odyssey* (eds. Graf, K. E., Ketron, C. V. & Waters, M. R.) 81–103 (Center for the Study of the First Americans, Texas A&M University College Station, 2014).
18. Pitulko, V. V. The Berelekh quest: A review of forty years of research in the mammoth graveyard in northeast Siberia. *Geoarchaeology* **26**, 5–32 (2011).
19. Pitulko, V. V., Basilyan, A. E. & Pavlova, E. Y. The Berelekh Mammoth 'Graveyard': New Chronological and Stratigraphical Data from the 2009 Field Season. *Geoarchaeology* **29**, 277–299 (2014).
20. Mocanov, Y. A. & Fedoseeva, S. A. Berelekh, Allakhovsk Region. in *American Beginnings: The Prehistory and Paleoecology of Beringia* (ed. West, F. H.) 218–221 (The University of Chicago Press, 1996).
21. Dilley, T. E. Late quaternary loess stratigraphy, soils, and environments of the Shaw Creek flats Paleoindian sites, Tanana Valley, Alaska. (1998).
22. Yesner, D. R., Holmes, C. E. & Crossen, K. J. Archaeology and paleoecology of the Broken Mammoth site, central Tanana Valley, interior Alaska, USA. *Current Research in the Pleistocene* **9**, 12 (1992).
23. Krasinski, K. E. & Yesner, D. R. Late Pleistocene/early Holocene site structure in Beringia: a case study from the Broken Mammoth site, interior Alaska. *Alaska Journal of Anthropology* **6**, 27–41 (2008).
24. Holmes, C. E. Broken Mammoth. in *American Beginnings: The Prehistory and Palaeoecology of Beringia* (ed. West, F. H.) 313–317 (University of Chicago Press, 1996).
25. Thorson, R. M. & Hamilton, T. D. Geology of the Dry Creek Site; a Stratified Early Man Site in Interior Alaska. *Quat. Res.* **7**, 149–176 (1977).

26. Goebel, T., Powers, R. & Bigelow, N. The Nenana Complex of Alaska and Clovis Origins. in *Clovis Origins and Adaptations* (eds. Bonnichsen, R. & Turnmire, K.) 49–79 (Center for the Study of the First Americans, 1991).
27. Powers, W. R. & Hamilton, T. D. *Dry Creek: A late Pleistocene human occupation in central Alaska*. (1978).
28. Powers, W. R. & Hoffecker, J. F. Late Pleistocene Settlement in the Nenana Valley, Central Alaska. *Am. Antiq.* **54**, 263–287 (1989).
29. Bigelow, N. H. & Powers, W. R. New AMS dates from the Dry Creek Paleoindian site, central Alaska. *Current Research in the Pleistocene* **11**, 114–116 (1994).
30. Bigelow, N. H. & Powers, W. R. Climate, Vegetation, and Archaeology 14,000–9000 Cal Yr B.P. in Central Alaska. *Arctic Anthropol.* **38**, 171–195 (2001).
31. Powers, W. R., Guthrie, R. D. & Hoffecker, J. F. *Dry Creek: Archaeology and paleoecology of a late Pleistocene Alaskan hunting camp*. (Texas A&M University Press, 2017).
32. Hoffecker, J. F., Powers, W. R. & Bigelow, N. H. Dry Creek. in *American Beginnings: The Prehistory and Paleoecology of Beringia* (ed. West, F. H.) 343–352 (The University of Chicago Press, 1996).
33. Graf, K. E. *et al.* Dry Creek Revisited: New Excavations, Radiocarbon Dates, and Site Formation Inform on the Peopling of Eastern Beringia. *Am. Antiq.* **80**, 671–694 (2015).
34. Potter, B. A., Gilbert, P. J., Holmes, C. E. & Crass, B. A. The Mead Site, a late Pleistocene - Holocene stratified site in Central Alaska. *Current Research in the Pleistocene* **28**, 73–75 (2011).
35. Little, A. A. Lithic Analysis at the Mead Site, Central Alaska. (University of Alaska Fairbanks, 2013).
36. Kunz, M. L. & Reanier, R. E. The Mesa Site: A Paleoindian Hunting Lookout in Arctic Alaska. *Arctic Anthropol.* **32**, 5–30 (1995).
37. Kunz, M. L. & Reanier, R. E. Paleoindians in beringia: evidence from arctic alaska. *Science* **263**, 660–662 (1994).
38. Reanier, R. E. The Antiquity of Paleoindian Materials in Northern Alaska. *Arctic Anthropol.* **32**, 31–50 (1995).
39. Bever, M. R. Stone Tool Technology and the Mesa Complex: Developing a Framework of Alaskan Paleoindian Prehistory. *Arctic Anthropol.* **38**, 98–118 (2001).

40. Bever, M. R. Distinguishing Holocene Microblades from a Paleoindian Component at the Mesa Site, Alaska. *J. Field Archaeol.* **33**, 133–150 (2008).
41. Pearson, G. A. Early Occupations and Cultural Sequence at Moose Creek: A Late Pleistocene Site in Central Alaska. *Arctic* **52**, 332–345 (1999).
42. Hoffecker, J. F. Moose Creek. in *American Beginnings: The Prehistory and Palaeoecology of Beringia* (ed. West, F. H.) 363–366 (University of Chicago Press, 1996).
43. Hoffecker, J. F. The Moose Creek site. *National Geographic Society Research Reports* **19**, 33–48 (1985).
44. Phippen, P. G. Archaeology at Owl Ridge: A Pleistocene-Holocene boundary age site in central Alaska. (University of Alaska Fairbanks, 1988).
45. Hoffecker, J. F., Powers, R. & Phippen, P. G. Owl Ridge. in *American Beginnings: The Prehistory and Palaeoecology of Beringia* (ed. West, F. H.) 353–356 (University of Chicago Press, 1996).
46. Graf, K. E. *et al.* Recent excavations at Owl Ridge, interior Alaska: Site stratigraphy, chronology, and site formation and implications for late Pleistocene archaeology and peopling of eastern Beringia. *Geoarchaeology* **35**, 3–26 (2019).
47. Hirasawa, Y. & Holmes, C. E. The relationship between microblade morphology and production technology in Alaska from the perspective of the Swan Point site. *Quat. Int.* **442**, 104–117 (2017).
48. Holmes, C. E. The Taiga period: Holocene archaeology of the northern boreal forest, Alaska. *Alaska Journal of Anthropology* **6**, 69–81 (2008).
49. Holmes, C. E. The Beringian and transitional periods in Alaska: technology of the east Beringian tradition as viewed from Swan point. in *From the Yenisei to the Yukon: Interpreting Lithic Assemblage Variability in Late Pleistocene/Early Holocene Beringia* (eds. Goebel, T. & Buvit, I.) 179–198 (Texas A&M University Press, 2011).
50. Holmes, C. E., VanderHoek, R. & Dilley, T. E. Swan Point. in *American Beginnings: The Prehistory and Palaeoecology of Beringia* (ed. West, F. H.) 319–323 (University of Chicago Press, 1996).
51. Coutouly, Y. A. G. & Holmes, C. E. The Microblade Industry from Swan Point Cultural Zone 4b: Technological and Cultural Implications from the Earliest Human Occupation in Alaska. *Am. Antiq.* **83**, 735–752 (2018).
52. Mochanov, Y. A. & Fedoseeva, S. A. Dyuktai Cave. in *American Beginnings: The Prehistory and Paleoecology of Beringia* (ed. West, F. H.) 164–174 (The University of Chicago Press, 1996).

53. Goebel, T., Waters, M. R. & Dikova, 2. Margarita. The Archaeology of Ushki Lake, Kamchatka, and the Pleistocene Peopling of the Americas. *Science* **301**, (2003).

54. Goebel, T., Powers, R., Bigelow, N. H. & Higgs, A. S. Walker Road. in *American Beginnings: The Prehistory and Palaeoecology of Beringia* (ed. West, F. H.) 356–363 (University of Chicago Press, 1996).

55. Morrow, J. E. & Fiedel, S. New radiocarbon dates for the Clovis component of the Anzick Site, Park County, Montana. in *Paleoindian archaeology: a hemispheric perspective* (eds. Morrow, J. E. & Gnecco, C.) 123–138 (University Press of Florida, 2006).

56. Rasmussen, M. *et al.* The genome of a Late Pleistocene human from a Clovis burial site in western Montana. *Nature* **506**, 225–229 (2014).

57. Stafford, T. W., Jull, A. J. T., Brendel, K., Duhamel, R. C. & Donahue, D. Study of Bone Radiocarbon Dating Accuracy at the University of Arizona NSF Accelerator Facility for Radioisotope Analysis. *Radiocarbon* **29**, 24–44 (1987).

58. Stafford, T. W., Hare, P. E., Currie, L., Jull, A. J. T. & Donahue, D. J. Accelerator radiocarbon dating at the molecular level. *J. Archaeol. Sci.* **18**, 35–72 (1991).

59. Lahren, L. & Bonnichsen, R. Bone Foreshafts From a Clovis Burial in Southwestern Montana. *Science* **186**, 147–150 (1974).

60. Wilke, P. J., Flenniken, J. J. & Ozbun, T. L. Clovis Technology at the Anzick Site, Montana. *J. Calif. Gt. Basin Anthropol.* **13**, 242–272 (1991).

61. Owsley, D. W., Hunt, D. R., Macintyre, I. G. & Logan, M. A. Clovis and Early Archaic Crania from the Anzick Site (24PA506), Park County, Montana. *Plains Anthropol.* **46**, 115–124 (2001).

62. Becerra-Valdivia, L. *et al.* Reassessing the chronology of the archaeological site of Anzick. *Proc. Natl. Acad. Sci. U. S. A.* **115**, 7000–7003 (2018).

63. Ferring, C. R. *The archaeology and paleoecology of the Aubrey Clovis site (41DN479) Denton County, Texas*. http://www.dtic.mil/docs/citations/ADA391588 (2001).

64. Ferring, C. R. The 1989 investigations at the Aubrey Clovis site, Texas. *Current Research in the Pleistocene* **7**, 0–12 (1990).

65. Haynes, C. V. & Agogino, G. A. Prehistoric Springs and Geochronology of the Clovis Site, New Mexico. *Am. Antiq.* **31**, 812–821 (1966).

66. Haynes, C. V. Geochronology of paleoenvironmental change, clovis type site, Blackwater draw, New Mexico. *Geoarchaeology* **10**, 317–388 (1995).

67. Howard, E. B. Association of artifacts with mammoth and bison in eastern New Mexico. *Science* **78**, 524 (1933).

68. Howard, E. B. The Occurrence of Flints and Extinct Animals in Pluvial Deposits near Clovis, New Mexico. Part I: Introduction. *Proceedings of the Academy of Natural Sciences of Philadelphia* **87**, 299–303 (1935).

69. Saunders, J. J., Agogino, G. A., Boldurian, A. T. & Haynes, C. V. A Mammoth-Ivory Burnisher-Billet from the Clovis Level, Blackwater Locality No. 1, New Mexico. *Plains Anthropol.* **36**, 359–363 (1991).

70. McAvoy, J. M. & McAvoy, L. D. *Archaeological Investigations of Site 44SX202, Cactus Hill, Sussex County, Virginia*. (Department of Historic Resources, 1997).

71. Feathers, J. K., Rhodes, E. J., Huot, S. & Mcavoy, J. M. Luminescence dating of sand deposits related to late Pleistocene human occupation at the Cactus Hill Site, Virginia, USA. *Quat. Geochronol.* **1**, 167–187 (2006/8).

72. Wagner, D. P. & McAvoy, J. M. Pedoarchaeology of Cactus Hill, a sandy Paleoindian site in southeastern Virginia, USA. *Geoarchaeology* **19**, 297–322 (2004).

73. Wagner, D. P. Cactus Hill, Virginia. in *Encyclopedia of Geoarchaeology* (ed. Gilbert, A. S.) 95–95 (Springer Netherlands, 2017).

74. Macphail, R. I. & McAvoy, J. M. A micromorphological analysis of stratigraphic integrity and site formation at Cactus Hill, an Early Paleoindian and hypothesized pre-Clovis occupation in south-central Virginia, USA. *Geoarchaeology* **23**, 675–694 (2008).

75. Goodyear, A. C. Evidence of Pre-Clovis Sites in the Eastern United States. in *Paleoamerican Origins: Beyond Clovis* (eds. Bonnichesen, R., Lepper, B. T., Standford, D. & Waters, M. R.) 103–112 (2005).

76. Frison, G. C. & Todd, L. C. *The Colby mammoth site: taphonomy and archaeology of a Clovis kill in northern Wyoming*. (University of New Mexico Press, 1986).

77. Walker, D. N. & Frison, G. C. The late Pleistocene mammalian fauna from the Colby Mammoth Kill site, Wyoming. *Rocky Mt Geol.* **19**, 69–79 (1980).

78. Morrow, J. E. *et al.* Pre-Clovis in Texas? A critical assessment of the 'Buttermilk Creek Complex'. *J. Archaeol. Sci.* **39**, 3677–3682 (2012).

79. Waters, M. R. *et al.* The Buttermilk Creek complex and the origins of Clovis at the Debra L. Friedkin site, Texas. *Science* **331**, 1599–1603 (2011).

80. Jennings, T. A. Clovis, Folsom, and Midland components at the Debra L. Friedkin site, Texas: context, chronology, and assemblages. *J. Archaeol. Sci.* **39**, 3239–3247 (2012).

81. Jennings, T. A. & Michael, R. Pre-Clovis Lithic Technology at the Debra L. Friedkin Site, Texas: Comparisons to Clovis Through Site-Level Behavior, Technological Trait-List, and Cladistic Analyses. *American Antiquity* **79**, 25–44 (2014).

82. Waters, M. R. *et al.* Pre-Clovis projectile points at the Debra L. Friedkin site, Texas—Implications for the Late Pleistocene peopling of the Americas. *Science Advances* **4**, eaat4505 (2018).

83. Haynes, C. V., Jr, McFaul, M., Brunswig, R. H. & Hopkins, K. D. Kersey--Kuner terrace investigations at the Dent and Bernhardt sites, Colorado. *Geoarchaeology: An International Journal* **13**, 201–218 (1998).

84. Brunswig, R. H. New interpretations of the Dent mammoth site. *Frontiers in Colorado Paleoindian archaeology* 87–121 (2007).

85. Saunders, J. J. Morphometrical analyses of Mammuthus columbi from the Dent site, Weld county, Colorado. *Deinsea* **6**, 55–78 (1999).

86. Agogino, G. Progress Report on the Chemical Removal of Preservative from Radiocarbon Samples. *La Conquista* **2**, (1963).

87. Agogino, G. An Early Attempt to Remove Preservatives from Bone. *Southwestern Lore* **63**, 42–43 (1997).

88. Devièse, T. *et al.* Increasing accuracy for the radiocarbon dating of sites occupied by the first Americans. *Quaternary Science Research* **198**, 171–180 (2018).

89. Leonhardy, F. C. *Domebo: A Paleo-Indian mammoth kill in the prairie-plains*. (Great Plains Historical Association, 1966).

90. Hofman, J. L. Dating the lower member of the Domebo Formation in western Oklahoma. *Current Research in the Pleistocene* **5**, 86–88 (1988).

91. Sanchez, G. *et al.* Human (Clovis)-gomphothere (Cuvieronius sp.) association ~ 13,390 calibrated yBP in Sonora, Mexico. *Proc. Natl. Acad. Sci. U. S. A.* **111**, 10972–10977 (2014).

92. Collins, M. B. The Gault Site, Texas, and Clovis research. *Athena Review* **3**, 31–42 (2002).

93. Vilsack, L. E. Investigations of Area 12: Gault Site. (Texas State University, San Marcos, 2016).

94. Gilmer, A. Geoarchaeological Investigations of Site Formation Processes in Area 15 at the Gault Site, Bell County, Texas. (Texas State University, San Marcos, 2013).

95. Gandy, J. L. Analysis of the lithic debitage from the older-than-Clovis stratigraphic layers of the Gault site, Texas. (Texas State University, San Marcos, 2013).

96. Williams, T. J. *et al.* Evidence of an early projectile point technology in North America at the Gault Site, Texas, USA. *Sci Adv* **4**, eaar5954 (2018).

97. Rodrigues, K. *et al.* OSL ages of the Clovis, Late Paleoindian, and Archaic components at Area 15 of the Gault Site, Central Texas, U.S.A. *Journal of Archaeological Science: Reports* **7**, 94–103 (2016).

98. Bement, L. C. & Carter, B. J. Clovis bison hunting at the Jake Bluff site, NW Oklahoma. *Current Research in the Pleistocene* **20**, 5–7 (2003).

99. Bement, L. C. & Carter, B. J. Jake Bluff: Clovis Bison Hunting on the Southern Plains of North America. *Am. Antiq.* **75**, 907–933 (2010).

100. Bement, L. C. & Carter, B. J. From Mammoth to bison: Changing Clovis Prey Availability at the End of the. *Clovis: On the Edge of a New Understanding* 263 (2014).

101. Hannus, L. A. The Lange/Ferguson Site: an event of Clovis mammoth butchery with the associated bone tool technology: the mammoth and its track. (Department of Anthropology, University of Utah, 1985).

102. Hannus, L. A. Flaked mammoth bone from the Lange/Ferguson site, White River badlands area, South Dakota. *Bone modification* 395–412 (1989).

103. Haynes, C. V. Contributions of Radiocarbon Dating to the Geochronology of the Peopling of the New World. in *Radiocarbon After Four Decades* 355–374 (Springer New York, 1992).

104. Taylor, R. E., Vance Haynes, C. & Stuiver, M. Clovis and Folsom age estimates: stratigraphic context and radiocarbon calibration. *Antiquity* **70**, 515–525 (1996).

105. Hannus, L. A. *Clovis Mammoth Butchery: The Lange/Ferguson Site and Associated Bone Tool Technology*. (Texas A&M University Press, 2018).

106. Haynes, C. V. Geochronology of the Lange/Ferguson Clovis Site. in *The Lange/Ferguson Site: An Event of Clovis Mammoth Butchery with an Associated Bone Tool Technology* (eds. Hannus, L. A. et al.) 29–59 (Texas A&M University Press, 2018).

107. Haury, E. W., Sayles, E. B. & Wasley, W. W. The Lehner Mammoth Site, Southeastern Arizona. *Am. Antiq.* **25**, 2–30 (1959).

108. Haynes, C. V. & Huckell, B. B. *Murray Springs: A Clovis Site with Multiple Activity Areas in the San Pedro Valley, Arizona*. (University of Arizona Press, 2007).

109. Haynes, C. V. & Hemmings, E. T. Mammoth-bone shaft wrench from murray springs, Arizona. *Science* **159**, 186–187 (1968).

110. McNett, C. W., McMillan, B. A. & Marshall, S. B. The Shawnee-Minisink Site. *Ann. N. Y. Acad. Sci.* **288**, 282–296 (1977).

111. McNett, C. W. *Shawnee Minisink: A Stratified Paleoindian–Archaic Site in the Upper Delaware Valley of Pennsylvania*. (Academic Press, 1985).

112. Gingerich, J. A. M. Revisiting Shawnee-Minisink. in *In the Eastern Fluted Point Tradition: Volume I* (ed. Gingerich, J. A. M.) vol. 1 218–256 (University of Utah Press, 2013).

113. Dent, R. J. Shawnee Minisink: new dates on the Paleoindian component. in *Poster presented at the 64th Annual Meeting of the Society for American Archaeology* (1999).

114. Gingerich, J. A. M. Shawnee-Minisink revisited: Re-evaluating the Paleoindian occupation. (University of Wyoming, 2007).

115. Gingerich, J. A. M. Down to Seeds and Stones: A New Look at the Subsistence Remains From Shawnee-Minisink. *Am. Antiq.* **76**, 127–144 (2011).

116. Gingerich, J. A. M., Whyte, T. R. & Whittaker, S. Misidentified Clovis-age fish bone at Shawnee-Minisink and the problem with single case studies in Late Pleistocene archaeology. *Journal of Archaeological Science: Reports* **25**, 94–99 (2019).

117. Waters, M. R., Stafford, T. W., Redmond, B. G. & Tankersley, K. B. The Age of the Paleoindian Assemblage at Sheriden Cave, Ohio. *Am. Antiq.* **74**, 107–111 (2009).

118. Redmond, B. G. & Tankersley, K. B. Evidence of Early Paleoindian Bone Modification and Use at the Sheriden Cave Site (33WY252), Wyandot County, Ohio. *Am. Antiq.* **70**, 503–526 (2005).

119. Tankersley, K. B. Sheriden: A Clovis cave site in eastern North America. *Geoarchaeology: An International Journal* **12**, 713–724 (1997).

120. Tankersley, K. B. & Landefeld, C. S. Geochronology of Sheriden Cave, Ohio: the 1997 field season. *Current Research in the Pleistocene* **15**, 136–138 (1998).

121. Tankersley, K. B. & Redmond, B. G. Radiocarbon dating of a Paleoindian projectile point from Sheriden Cave, Ohio. *Current Research in the Pleistocene* **16**, 76–77 (1999).

122. Tankersley, K. B., Ford, K. M., McDonald, H. G., Genheimer, R. A. & Hendricks, R. Late Pleistocene archaeology of Sheriden Cave, Wyandot County, Ohio. *Current Research in the Pleistocene* **14**, 81–83 (1997).

123. Tankersley, K. B., Redmond, B. G. & Grove, T. E. Radiocarbon dates associated with a single-beveled bone projectile point from Sheriden Cave, Ohio. *Current Research in the Pleistocene* **18**, 62–64 (2001).

124. Johnson, J. R., Stafford, T. W., Jr, Ajie, H. O. & Morris, D. P. Arlington springs revisited. in *Proceedings of the fifth California Islands symposium* vol. 23 541–545 (Santa Barbara, CA: Santa Barbara Museum of Natural History, 2002).

125. Orr, P. C. Arlington Springs man. *Science* **135**, 219 (1962).

126. McLaren, D. *et al.* Terminal Pleistocene epoch human footprints from the Pacific coast of Canada. *PLoS One* **13**, e0193522 (2018).

127. Johnson, E. & Holliday, V. T. Lubbock Lake: Late Quaternary cultural and environmental change on the Southern High Plains, USA. *J. Quat. Sci.* **4**, 145–165 (1989).

128. Holliday, V. T., Johnson, E., Haas, H. & Stuckenrath, R. Radiocarbon ages from the Lubbock Lake Site, 1950-1980: framework for cultural and ecological change on the Southern High Plains. *Plains Anthropologist* **28**, 165–182 (1983).

129. Knudson, R., Johnson, E. & Holliday, V. T. The 10,000-Year-Oid Lubbock Artifact Assemblage. *Plains Anthropol.* **43**, 239–256 (1998).

130. Johnson, E. & Holliday, V. T. Late Paleo-Indian Activity At The Lubbock Lake Site. *Plains Anthropol.* **26**, 173–193 (1981).

131. Johnson, E. & Holliday, V. T. A Plainview Kill/Butchering Locale On The Llano Est Acado-The Lubbock Lake Site. *Plains Anthropol.* **25**, 89–111 (1980).

132. Grayson, D. K. & Meltzer, D. J. Revisiting Paleoindian exploitation of extinct North American mammals. *J. Archaeol. Sci.* **56**, 177–193 (2015).

133. Grayson, D. K. & Meltzer, D. J. Clovis Hunting and Large Mammal Extinction: A Critical Review of the Evidence. *Journal of World Prehistory* **16**, 313–359 (2002).

134. Waters, M. R., Stafford, T. W., Jr, Kooyman, B. & Hills, L. V. Late Pleistocene horse and camel hunting at the southern margin of the ice-free corridor: reassessing the age of Wally's Beach, Canada. *Proc. Natl. Acad. Sci. U. S. A.* **112**, 4263–4267 (2015).

135. Kooyman, B., Hills, L. V., McNeil, P. & Tolman, S. Late Pleistocene Horse Hunting at the Wally's Beach Site (DhPg-8), Canada. *Am. Antiq.* **71**, 101–121 (2006).

136. McNeil, P., Hills, L. V., Kooyman, B. & Tolman, M. S. Late Pleistocene geology and fauna of the Wally's Beach Site (DhPg-8), Alberta, Canada. *Archaeology on the edge: new perspectives from the*

Northern Plains. Edited by B. Kooyman and J. Kelley. University of Calgary Press, Calgary, Alta. , Canadian Archaeological Association, Paper 79–94 (2004).

137. Kooyman, B., Hills, L. V., Tolman, S. & McNeil, P. Late Pleistocene Western Camel (Camelops Hesternus) Hunting in Southwestern Canada. *Am. Antiq.* **77**, 115–124 (2012).
138. Wheat, A. D. Survey of professional opinions regarding the peopling of the Americas. *The SAA Archaeological Record* **12**, 10–14 (2012).
139. Cinq-Mars, J. & Morlan, R. E. Bluefish Caves and Old Crow Basin: A New Rapport. in *Ice Age People of North America: Environments, Origins, and Adaptations* (eds. Bonnichsen, R. & Turnmire, K. L.) 200–212 (Oregon State University Press, 1999).
140. Bourgeon, L., Burke, A. & Higham, T. Earliest Human Presence in North America Dated to the Last Glacial Maximum: New Radiocarbon Dates from Bluefish Caves, Canada. *PLoS One* **12**, e0169486 (2017).
141. Potter, B. A. *et al.* Current evidence allows multiple models for the peopling of the Americas. *Sci Adv* **4**, eaat5473 (2018).
142. Davis, L. G. & Schweger, C. E. Geoarchaeological context of late Pleistocene and early Holocene occupation at the Cooper's Ferry site, western Idaho, USA. *Geoarchaeology* **19**, 685–704 (2004).
143. Goebel, T., Hockett, B., Adams, K. D., Rhode, D. & Graf, K. Climate, environment, and humans in North America's Great Basin during the Younger Dryas, 12,900–11,600 calendar years ago. *Quat. Int.* **242**, 479–501 (2011).
144. Davis, L. G., Macfarlan, S. J. & Henrickson, C. N. A PXRF-based chemostratigraphy and provenience system for the Cooper's Ferry site, Idaho. *J. Archaeol. Sci.* **39**, 663–671 (2012).
145. Davis, L. G. *et al.* Late Upper Paleolithic Occupation at Cooper's Ferry, Idaho, USA Shows Americas Settled Before ~16,000 Years Ago. *Science* (2019).
146. Overstreet, D. F. & Kolb, M. F. Geoarchaeological contexts for Late Pleistocene archaeological sites with human-modified woolly mammoth remains in southeastern Wisconsin, U.S.A. *Geoarchaeology* **18**, 91–114 (2003).
147. Johnson, E. Along the ice margin—The cultural taphonomy of Late Pleistocene mammoth in southeastern Wisconsin (USA). *Quat. Int.* **169-170**, 64–83 (2007).
148. Joyce, D. J. Chronology and new research on the Schaefer mammoth (?Mammuthus primigenius) site, Kenosha County, Wisconsin, USA. *Quat. Int.* **142**, 44–57 (2006).

149. Johnson, E. The taphonomy of mammoth localities in southeastern Wisconsin (USA). *Quat. Int.* **142**, 58–78 (2006).

150. Overstreet, D. F. Still more on cultural contexts of mammoth and mastodon in the southwestern Lake Michigan basin. *Current Research in the Pleistocene* **13**, 36–38 (1996).

151. Overstreet, D. F. Late Pleistocene geochronology and the Paleoindian penetration of the southwestern Lake Michigan Basin. *The Wisconsin Archeologist* **79**, 28–52 (1998).

152. Joyce, D. J. Pre-Clovis megafauna butchery sites in the western Great Lakes region, USA. in *Paleoamerican Oddysey* (eds. Graf, K. E., Ketron, C. V. & Waters, M. R.) 467–483 (Center for the Study of the First Americans, Texas A&M University College Station, 2014).

153. Overstreet, D. F. & Stafford, T. W., Jr. Additions to a revised chronology for cultural and non-cultural mammoth and mastodon fossils in the southwestern Lake Michigan Basin. *Current Research in the Pleistocene* **14**, (1997).

154. Dallman, J. E., Overstreet, D. F. & Stafford, T. W., Jr. A revised chronology for cultural and non-cultural mammoth and mastodon fossils in the southwestern Lake Michigan Basin. *Current Research in the Pleistocene* **13**, 10–13 (1996).

155. Davis, L. B. & Wilson, M. C. The late Pleistocene Lindsay mammoth (24DW501), eastern Montana: Possible man-mammoth association. *Current Research in the Pleistocene* **2**, 97–98 (1985).

156. Hill, C. L. & Davis, L. B. Stratigraphy, AMS radiocarbon age, and stable isotope biogeochemistry of the Lindsay Mammoth, eastern Montana. *Current Research in the Pleistocene* **15**, 109–112 (1998).

157. Krasinski, K. E. Broken bones and cutmarks: Taphonomic analyses and implications for the peopling of North America. (University of Nevada, Reno, 2010).

158. Waters, M. R. & Stafford, T. W. The first Americans: A review of the evidence for the Late-Pleistocene peopling of the Americas. *Paleoamerican odyssey* 543–562 (2013).

159. Huber, J. K. & Hill, C. L. Paleoecological inferences based on pollen and stable isotopes for mammoth-bearing deposits of the Oahe Formation (Aggie Brown Member), eastern Montana. *Current Research in the Pleistocene* **20**, 95–97 (2003).

160. Waters, M. R. *et al.* Pre-Clovis Mastodon Hunting 13,800 Years Ago at the Manis Site, Washington. *Science* **334**, 351–353 (2011).

161. Gustafson, C. E., Gilbow, D. W. & Daugherty, R. D. The Manis Mastodon Site: Early Man on the Olympic Peninsula. *Canadian Journal of Archaeology / Journal Canadien d'Archéologie* 157–164 (1979).

162. Petersen, K. L., Mehringer, P. J. & Gustafson, C. E. Late-Glacial Vegetation and Climate at the Manis Mastodon site, Olympic Peninsula, Washington. *Quat. Res.* **20**, 215–231 (1983).

163. Haynes, C. V. & Huckell, B. B. The Manis Mastodon: An Alternative Interpretation. *PaleoAmerica* **2**, 189–191 (2016).

164. Goldberg, P. & Arpin, T. L. Micromorphological Analysis of Sediments from Meadowcroft Rockshelter, Pennsylvania: Implications for Radiocarbon Dating. *J. Field Archaeol.* **26**, 325–342 (1999).

165. Adovasio, J. M., Pedler, D. R., Donahue, J. & Stuckenrath, R. Two Decades of Debate on Meadowcroft Rockshelter. *North American Archaeologist* **19**, 317–341 (1998).

166. Adovasio, J. M., Gunn, J. D., Donahue, J. & Stuckenrath, R. Excavations at Meadowcroft Rockshelter, 1973-1974: A Progress Report. *Pennsylvania Archaeologist* **45**, 1–30 (1975).

167. Adovasio, J. M., Donahue, J. & Stuckenrath, R. The Meadowcroft Rockshelter Radiocarbon Chronology 1975-1990. *Am. Antiq.* **55**, 348–354 (1990).

168. Adovasio, J. M., Gunn, J. D., Donahue, J. & Stuckenrath, R. Meadowcroft Rockshelter, 1977: An Overview. *Am. Antiq.* **43**, 632–651 (1978).

169. Haynes, C. V. Paleoindian Charcoal from Meadowcroft Rockshelter: Is Contamination a Problem? *Am. Antiq.* **45**, 582–587 (1980).

170. Kelly, R. L. A Comment on the Pre-Clovis Deposits at Meadowcroft Rockshelter. *Quat. Res.* **27**, 332–334 (1987).

171. Halligan, J. J. *et al.* Pre-Clovis occupation 14,550 years ago at the Page-Ladson site, Florida, and the peopling of the Americas. *Sci Adv* **2**, e1600375 (2016).

172. Webb, S. D. *First Floridians and Last Mastodons: The Page-Ladson Site in the Aucilla River*. (Springer Science & Business Media, 2006).

173. Jenkins, D. L. Distribution and dating of cultural and paleontological remains at the Paisley Five Mile Point Caves in the northern Great Basin. *Paleoindian or Paleoarchaic* 57e81 (2007).

174. Jenkins, D. L. *et al.* Geochronology, archaeological context, and DNA at the Paisley Caves. in *Paleoamerican Odyssey* (eds. Graf, K. E., Ketron, C. V. & Waters, M. R.) 485–510 (Center for the Study of the First Americans, Texas A&M University College Station, 2014).

175. Gilbert, M. T. P. *et al.* DNA from pre-Clovis human coprolites in Oregon, North America. *Science* **320**, 786–789 (2008).

176. Hockett, B. & Jenkins, D. L. Identifying Stone Tool Cut Marks and the Pre-Clovis Occupation of the Paisley Caves. *Am. Antiq.* **78**, 762–778 (2013).

177. Sistiaga, A., Berna, F., Laursen, R. & Goldberg, P. Steroidal biomarker analysis of a 14,000 years old putative human coprolite from Paisley Cave, Oregon. *J. Archaeol. Sci.* **41**, 813–817 (2014).

178. Shillito, L. M. *et al.* New Research at Paisley Caves: Applying New Integrated Analytical Approaches to Understanding Stratigraphy, Taphonomy, and Site Formation Processes. *PaleoAmerica* **4**, 82–86 (2018).

179. Goebel, T., Graf, K. & Rhode, D. The Paleoindian occupations at Bonneville Estates Rockshelter, Danger Cave, and Smith Creek Cave (eastern Great Basin, USA): Interpreting their radiocarbon chronologies. *British Archaeological Reports (BAR) International Series* **1655**, 147 (2007).

180. Graf, K. E. Stratigraphy and chronology of the Pleistocene to Holocene transition at Bonneville Estates Rockshelter, eastern Great Basin. in *Paleoindian or Archaic? Great Basin Human Ecology at the Pleistocene-Holocene Transition* (eds. Graf, K. E. & Schmitt, D. N.) 82–104 (The University of Utah Press, 2007).

181. Goebel, T., Graf, K. E., Hockett, B. & Rhode, D. Late-Pleistocene humans at Bonneville Estates Rockshelter, eastern Nevada. *Current Research in the Pleistocene* **20**, 3 (2003).

182. Goebel, T., Holmes, A., Keene, J. L. & Coe, M. M. Technological Change from the Terminal Pleistocene Through Early Holocene in the Eastern Great Basin, USA: The Record from Bonneville Estates Rockshelter. in *Lithic Technological Organization and Paleoenvironmental Change: Global and Diachronic Perspectives* (eds. Robinson, E. & Sellet, F.) 235–261 (Springer International Publishing, 2018).

183. Hockett, B. Nutritional ecology of late Pleistocene to middle Holocene subsistence in the Great Basin: zooarchaeological evidence from Bonneville Estates Rockshelter. *Paleoindian or paleoarchaic* 204–230 (2007).

184. Rhode, D. & Louderback, L. A. Dietary plant use in the Bonneville basin during the terminal Pleistocene/early Holocene transition. *Paleoindian or Paleoarchaic* 231–247 (2007).

185. Green, T. J. *et al.* The Buhl Burial: A Paleoindian Woman from Southern Idaho. *Am. Antiq.* **63**, 437–456 (1998).

186. Holen, S. R. *et al.* A 130,000-year-old archaeological site in southern California, USA. *Nature* **544**, 479–483 (2017).

187. Braje, T. J. *et al.* Were Hominins in California ~130,000 Years Ago? *PaleoAmerica* vol. 3 200–202 (2017).

188. Haynes, G. The Cerutti Mastodon. *PaleoAmerica* **3**, 196–199 (2017).

189. Ferraro, J. V. *et al.* Contesting early archaeology in California. *Nature* **554**, E1–E2 (2018).

190. Magnani, M. *et al.* Evaluating claims for an early peopling of the Americas: experimental design and the Cerutti Mastodon site. *Antiquity* **93**, 789–795 (2019).

191. Ferrell, P. M. The Cerutti Mastodon Site Reinterpreted with Reference to Freeway Construction Plans and Methods. *PaleoAmerica* **5**, 1–7 (2019).

192. Sutton, M. Q., Parkinson, J. & Rosen, M. D. Observations Regarding the Cerutti Mastodon. *PaleoAmerica* **5**, 8–15 (2019).

193. González, A. *et al.* The first human settlers on the Yucatán Peninsula: evidence from drowned caves in the state of Quintana Roo (South Mexico). in *Paleoamerican Odyssey* (eds. Graf, K. E., Ketron, C. V. & Waters, M. R.) 323–337 (Center for the Study of the First Americans, Texas A&M University College Station, 2014).

194. Zazzo, A. & Saliège, J.-F. Radiocarbon dating of biological apatites: A review. *Palaeogeogr. Palaeoclimatol. Palaeoecol.* **310**, 52–61 (2011).

195. Cook, J. P. Healy Lake. in *American Beginnings: The Prehistory and Palaeoecology of Beringia* (ed. West, F. H.) 323–327 (University of Chicago Press, 1996).

196. Byers, D. A. Taphonomic analysis, associational integrity, and depositional history of the Fetterman mammoth, eastern Wyoming, USA. *Geoarchaeology: An International Journal* **17**, 417–440 (2002).

197. Mackie, M. M., Surovell, T. A., Kelly, R. L. & O'Brien, M. J. New Excavations at the La Prele Mammoth Site, Converse County, Wyoming. (2017).

198. Holliday, V. T., Haynes, C. V., Jr, Hofman, J. L. & Meltzer, D. J. Geoarchaeology and geochronology of the Miami (Clovis) site, southern High Plains of Texas. *Quat. Res.* **41**, 234–244 (1994).

199. Taylor, R. E. Six Decades of Radiocarbon Dating in New World Archaeology 1. *Radiocarbon* **51**, 173–212 (2009).

200. Brose, D. S. Archaeological investigations at the Paleo Crossing site, a Paleoindian occupation in Medina County, Ohio. *The first discovery of America: Archaeological evidence of the early inhabitants of the Ohio area* 61–76 (1994).

201. Boulanger, M. T. *et al.* Neutron activation analysis of 12,900-year-old stone artifacts confirms 450–510+ km Clovis tool-stone acquisition at Paleo Crossing (33ME274), northeast Ohio, U.S.A. *J. Archaeol. Sci.* **53**, 550–558 (2015).

202. Eren, M. I. & Redmond, B. G. Clovis Blades at Paleo Crossing (33ME274), Ohio. *MidCont. J. Archaeol.* **36**, 173–194 (2011).

203. Eren, M. I. *et al.* Paleo Crossing (33ME274): a Clovis site in northeastern Ohio. in *In the Eastern Fluted Point Tradition: Volume II* (ed. Gingerich, J. A. M.) vol. 2 187–210 (University of Utah Press, 2018).

204. Miller, G. L. Illuminating activities at Paleo Crossing (33ME274) through microwear analysis. Lithic Technol 38 (2): 108--197. *Lithic Technology* **38**, 108–197 (2013).

205. Eren, M. I., Redmond, B. G. & Kollecker, M. A. Unifacial stone tool analyses from the Paleo Crossing site (33-ME-274), Ohio. *Current Research in the Pleistocene* **22**, 43–45 (2005).

206. Eren, M. I. The Paleo Crossing (33-ME-274) non-projectile point biface assemblage. *Current Research in the Pleistocene* **23**, 95–97 (2006).

207. Eren, M. I. Anvil Reduction at the Early-Paleoindian Site of Paleo Crossing (33ME274), Northeast Ohio. *Current Research in the Pleistocene* **27**, 75–77 (2010).

208. Eren, M. I., Redmond, B. G. & Kollecker, M. A. The Paleo Crossing (33-ME-274) fluted point assemblage. *Current Research in the Pleistocene* **21**, 38–39 (2004).

209. Tankersley, K. B. & Holland, J. D. Lithic Procurement Patterns at the Paleo Crossing Site, Medina County, Ohio. *Current Research in the Pleistocene* **11**, 61–63 (1994).

210. Eren, M. I. & Kollecker, M. A. Data on the post-Paleoindian projectile point assemblage from the Paleo Crossing Site (33-ME-274). *Ohio Archaeol* **54**, (2004).

211. Eren, M. I. *et al.* Thermoluminescence (TL) and Optically Stimulated Luminescence (OSL) Dating of Two Burned Clovis Wyandotte Chert Lithic Specimens from Paleo Crossing (33ME274), Ohio, USA. *Lithic Technology* **43**, 18–25 (2018).

212. Waters, M. R., Forman, S. L., Stafford, T. W., Jr. & Foss, J. Geoarchaeological investigations at the Topper and Big Pine Tree sites, Allendale County, South Carolina. *J. Archaeol. Sci.* **36**, 1300–1311 (2009/7).

213. Bronk Ramsey, C. Development of the radiocarbon program OxCal. *Radiocarbon* **43**, 355–363 (2001).

214. Ward, G. K. & Wilson, S. R. Procedures for Comparing and Combining Radiocarbon Age Determination: A Critique. *Archaeometry* **20**, 19–31 (1978).

V. Article 3: Challenges in sample processing within radiocarbon dating and their impact in ^{14}C-dates-as-data studies

Published as below.

Becerra-Valdivia, L., Leal-Cervantes, R., Wood, R. and Higham, T., 2020. Challenges in sample processing within radiocarbon dating and their impact in 14C-dates-as-data studies. *Journal of Archaeological Sciences*, 113:105043.

5.1. Main text

Challenges in sample processing within radiocarbon dating and their impact in ^{14}C-dates-as-data studies

Abstract

For decades, researchers have employed sets of radiocarbon dates to reconstruct trends in ancient human populations. The overarching assumption in this analysis is that the frequency of dates is proportional to the magnitude of past human activity. Thus, the distribution of summed or otherwise summarized dates is used to extrapolate population density and mobility patterns. There are, however, a number of underlying assumptions associated with this analysis that workers address to varying degrees and which, if false and not critically accounted for, will introduce bias, misrepresent the magnitude of activity, and ultimately prove misleading in archaeological interpretations. In this regard, research has so far mainly focused on correcting for the effects of time-dependent degradation of archaeological sites and constituent materials, calibration irregularities, and the efficacy of the statistical methods used. Assumptions directly related to sample processing in radiocarbon dating, however, are less discussed in '^{14}C-dates-as-data' analyses. It is, for example, assumed that all carbonaceous materials will yield sufficient, endogenous carbon for radiocarbon measurement. Yet sample failure in radiocarbon dating is common and contingent on, largely, deterministic factors such as post-depositional environment. Sets of radiocarbon dates analyzed, therefore, represent successful measurements independent of reliability. In this work, we discuss the biases introduced by challenges in radiocarbon processing and their impact on ^{14}C-dates-as-data studies.

1. Introduction

Within archaeological research, sets of radiocarbon dates are often used as a proxy to study the past (see Appendix). In this analysis, the overarching assumption is that the frequency of radiocarbon dates is proportional to the magnitude of past human activity and, in turn, the size of a population. As such, the distribution of summed or otherwise summarized radiocarbon dates is used to extrapolate population density, growth rate, mobility patterns, or occupational phases. There are, however, a number of underlying assumptions associated with this analysis:

1. The radiocarbon dataset used is a representative subsample of the archaeological record and this, in turn, adequately represents all past human activity.
2. Archaeological sites/features/items are uniformly preserved across time and space.
3. All archaeological sites, whether representative of ephemeral or long-lasting occupational events, carry the same importance in terms of population density.
4. All settlement patterns, modes of subsistence and cultural practices lead to the constant and equal deposition of material suitable for radiocarbon dating.
5. Population density events, e.g., booms and busts, as reflected by the archaeological record, are of sufficient duration and magnitude relative to the analytical uncertainties of the analysis for detection.
6. Research biases related to archaeological fieldwork and radiocarbon dating, e.g., interest, funding and access, have a negligible impact on the analysis.
7. All samples selected for radiocarbon dating directly relate to human activities and are a representative sample of the total occupational events at any given archaeological site.
8. All carbonaceous materials yield sufficient, endogenous radiocarbon for measurement.
9. The radiocarbon dating process, as performed in all laboratories, produces robust chronometric results.

10. Chronometric data used, as obtained from original sources and/or pre-existing databases, are reliable. Where applicable, this includes adequate treatment of non-atmospheric reservoir effects.

11. The sample size of any given dataset analyzed is adequate for the statistical methods used and provides meaningful results.

12. Statistical methods used in summarizing radiocarbon dates generate an estimate that reasonably conforms to the original underlying distribution of the data.

13. The irregularities and fluctuations in the calibration curve have no significant effect.

14. Environmental proxies used in conjunction are appropriate and reliable.

If assumptions are false, the effect of the biases they introduce should be reasonably quantified and, if significant, critically accounted for. Otherwise, a distribution will likely misrepresent the magnitude of human activity and misguide interpretation. In the literature, biases are considered to varying degrees and research has mainly focused on identifying and correcting for the time-dependent survival of archaeological sites/features/items (assumption 2; Davies et al., 2016; Rhode et al., 2014; Surovell et al., 2009), effects caused by the calibration curve (assumption 13; Armit et al., 2013; Bamforth and Grund, 2012; Chiverrell et al., 2011; Contreras and Meadows, 2014; Kerr and McCormick, 2014; Williams, 2012), appropriate sample size of datasets (assumption 11; Contreras and Meadows, 2014; Michczyńska and Pazdur, 2004; Timpson et al., 2014; Williams, 2012), and the efficacy of statistical methods used to summarize datasets (assumption 12; Blackwell and Buck, 2003; Blockley et al., 2000; Bronk Ramsey, 2017). Biases stemming from challenges in sample processing for radiocarbon dating, particularly in relation to assumptions 1, 8 and 9, have gone largely undiscussed (but see Bradtmöller et al., 2012; Housley et al., 1997; Jöris et al., 2003). As such, this work aims to identify these biases and consider their potential effect in ^{14}C-dates-as-data studies, using the database of the Oxford Radiocarbon Accelerator Unit (ORAU) as reference. The remaining eleven assumptions are not further reviewed as they lie outside the scope of this

work and are discussed at length already elsewhere in the literature (see Contreras and Meadows, 2014; van Andel et al., 2003; Williams, 2012).

2. Challenges in sample processing

The aim of radiocarbon dating is to obtain precise and accurate results for each sample measured. The main obstacles, prior to radiocarbon measurement and calibration, occur during laboratory processing[5] and include poor sample preservation and contamination. The former often results in insufficient yields of dateable material post-treatment and the latter introduces inaccuracy into the measurements obtained. Both are exacerbated when the true age of a sample nears the limit of radiocarbon dating, i.e., ~50 thousand radiocarbon years before present (ka BP), as diagenesis progresses and sensitivity to modern ^{14}C contamination increases exponentially.

2.1. Poor preservation

In radiocarbon dating, stable fractions of any given material type are targeted during chemical pretreatment as these are likely to better retain the original radiocarbon ratio signal of the sample (Table 1). For example, radiocarbon specialists often focus on bone collagen rather than bioapatite, because the latter exchanges carbon with dissolved carbonate and generally yields minimum-age estimates (but see Zazzo and Saliège, 2011). If samples are poorly preserved, however, the yield of the targeted fraction is often insufficient for radiocarbon measurement. This is often the case for bones with low collagen content and plant remains that completely dissolve during humic-acid removal[6]. Apart from antiquity, sample preservation is largely dependent on the interaction between material type and post-depositional conditions. High temperatures and tropical conditions, for

[5] Sequentially, this involves sampling, chemical pretreatment, freeze drying, combustion, and graphitization (see Brock et al., 2010a, for more information and ORAU protocols). At the ORAU, bones may undergo an additional prescreening step, prior to chemical pretreatment, to assess collagen preservation using nitrogen content as a proxy—nitrogen derives exclusively from the protein component in bone (see Brock et al., 2010b for technique details).

[6] Evidence suggests that humic acids removed during pretreatment are not necessarily exogenous contaminants, but are sometimes derived from degradation of the actual sample (Ascough et al., 2011; Wild et al., 2013).

example, are known to accelerate the degradation of bone collagen (Ortner et al., 1972; Pestle and Colvard, 2012; Von Endt and Ortner, 1984; see Holmes et al., 2006, 2005 for predictive models involving collagen degradation and site distribution) and charcoal (Bird et al., 2002; Higham et al., 2009). This is illustrated in (Wood et al., 2013), a research project designed to establish the chronologies of eleven Middle to Upper Palaeolithic (M-UP) sites in southern Iberia—a region of relatively high temperatures. Here, only ~12% of all prescreened bones analyzed were found suitable for collagen extraction and, consequently, only two sites yielded measurements (both sites found above 800 m.a.s.l.) In contrast, ~50% of prescreened bones from the cooler regions of northern Iberia—Asturias, Cantabria, the Basque Country and Catalonia—were found suitable for collagen extraction. Differences in soil pH can also drastically affect the preservation of archaeological materials. Generally, carbonates dissolve under low pH conditions (Berna et al., 2004), charred or carbonized organic remains readily degrade under high pH conditions (Braadbaart et al., 2009; Rebollo et al., 2008), and bone collagen deteriorates at pH extremes (Collins et al., 2002). In this sense, depending on the archaeological materials, regions with acidic soils often see a reduction in date frequency (see Bae, 2002; Berridge and Roberts, 1986). Unfortunately, sample failure due to poor preservation is quite common during laboratory processing, affecting samples from a wide range of locations (Fig. 1) and of different material types (Fig. 2). At the ORAU, 1,041 sites have remained undated due principally to insufficient carbon yield[7]. This constitutes approximately 10% of all sites recorded in the laboratory database for which samples were processed. Moreover, materials like tooth, bone, antler, charcoal, charred seeds, and plant remains—all common archaeological samples—show failure rates at around 21%, 16%, 15%, 15% and 11%, respectively (Fig. 2).

[7] Laboratory-processing error cannot be adequately disentangled from this estimate and is likely to be a contributing factor, albeit minor.

Table 1. Main stable molecular forms targeted in radiocarbon dating (adapted from Bronk Ramsey, 2008).

Material	**Molecular form**
Bone and teeth	Collagen (protein)
Charred or carbonized plant remains	Amorphous carbon (elemental carbon)
Wood and plant remains	Cellulose (polysaccharide)
Arthropod exoskeletons	Chitin (polysaccharide)
Hair, horn, nails, claws and beaks	Keratin (protein)
Animal fats and vegetable oils	Lipids (glyceride)
Mollusk shells, corals, speleothems	Aragonite or calcite (calcium carbonate)

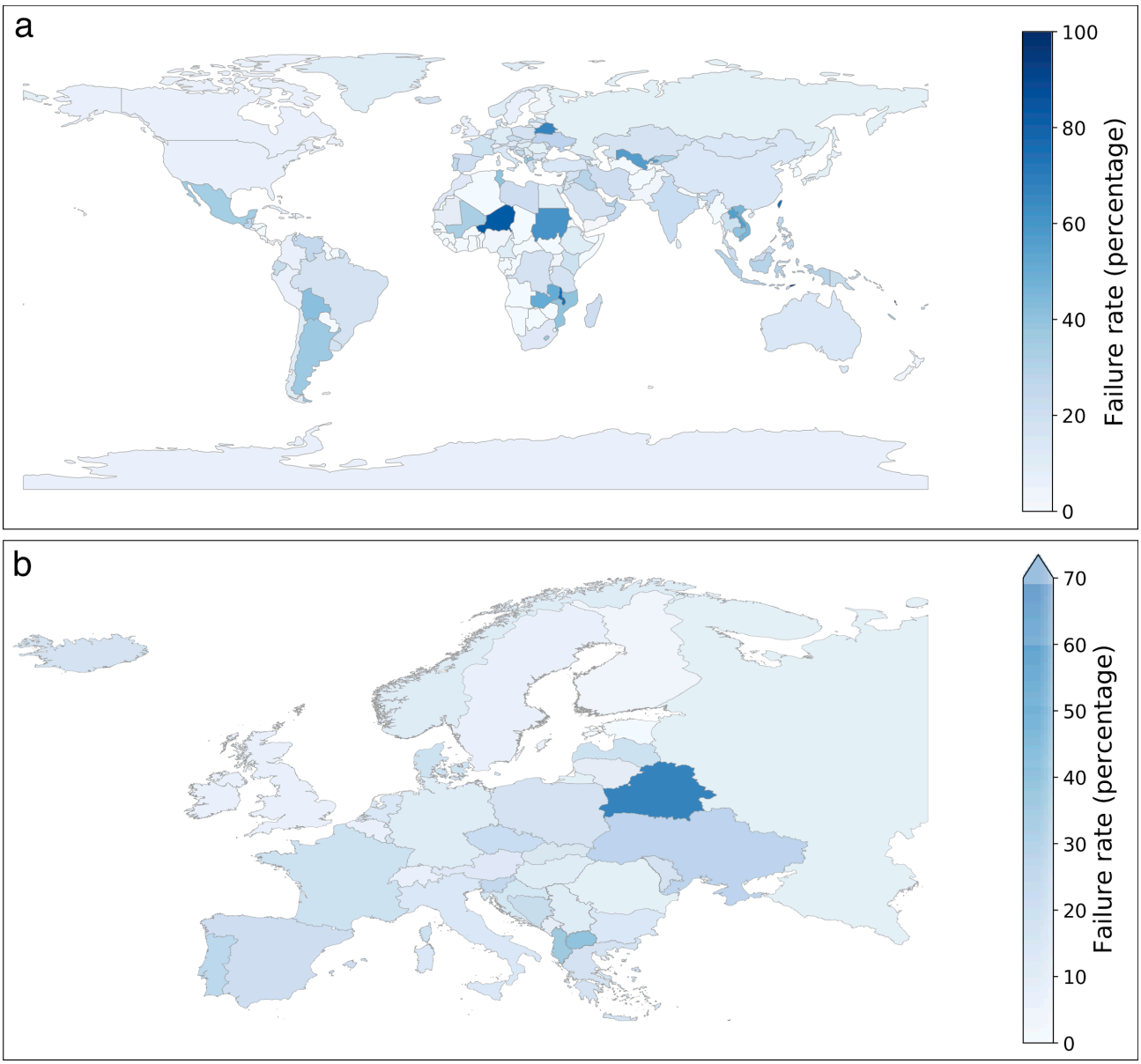


Fig. 1. (**a**) Map of countries from which samples have been submitted to the ORAU, between 1980 and 2019, and their individual failure rate. (**b**) subset of Europe. Factors like sample size and research focus vary for each country. As such, failure rates are not to be used comparatively but only serve to illustrate the ubiquity of sample failure due to, mainly, poor preservation. Failure rate = (total number of failed dates per country/total number of dates attempted per country)*100.



Fig. 2. Failure rate (%) of the top ten material types/categories (preset in the database) submitted to the ORAU between 1980 and 2019. "Other" is used as an editable database field by submitters and can represent a number of different material types not found within those preset. Factors like sample size and research focus vary for each material. As such, failure rates are not to be used comparatively but only serve to illustrate the ubiquity of sample failure due to, mainly, poor preservation. Failure rate = (total number of failed dates per material type/total number of dates attempted per material type)*100.

2.2. Contamination

For radiocarbon dating, sources of exogenous carbon include carbonates and humic acids from the sediment and consolidants applied during museum curation. The effects of contamination on a radiocarbon measurement largely depend on the age of the contaminant (from fully depleted to modern) and the "true" age of the sample. Modern contamination, for instance, has a more profound impact on older material (nearing 50 ka BP). For a sample dating to 40 ka BP, a 10% addition of modern carbon yields an age of 18 ka BP, and 40.8 ka BP if the sample contaminant is ^{14}C depleted. To remove contaminants, pretreatment protocols tailored to sample type, fragility, and age are employed (see Brock et al., 2010a for ORAU methods). In brief, carbonates are often leached in dilute acids to remove surface contamination, whilst non-carbonates, such as plant remains, often

undergo simple "ABA" (acid-base-acid) pretreatment. This involves sequential immersions in acid, base and acid solutions, which remove carbonates, humic contaminants, and dissolved atmospheric carbon dioxide, respectively. If consolidants are suspected to be present, chemical pretreatment is preceded by a series of solvent washes. For bone collagen[8], gelatinization (Longin, 1971) follows demineralization by ABA or acid-only treatment. Whereas these routine treatments normally remove sufficient contaminants from young samples to produce accurate dates, lengthier, more rigorous protocols are often required for Pleistocene-aged (>25-30 ka BP; Higham, 2011) or heavily contaminated samples (Deviese et al., 2017). These include acid-base-wet oxidation-stepped combustion for charcoal (ABOx-SC; Bird et al., 1999), and ultrafiltration (Brown et al., 1988) or hydroxyproline extraction (Deviese et al., 2017; Gillespie et al., 1984; Stafford et al., 1982) for bone. Discrepancies of several thousand radiocarbon years can exist between samples treated using routine and more stringent methods, with the latter yielding more reliable, often older results (Brock and Higham, 2009; Devièse et al., 2017; Douka et al., 2010b; Higham, 2011; Higham et al., 2009, 2006; Higham et al., 2009, 2006; Jacobi et al., 2006; Kosintsev et al., 2019; Marom et al., 2012; Wood et al., 2013, 2012).

Quality assurance parameters are often used to identify large amounts of contamination in many of the materials radiocarbon dated. For bone collagen, %C and C:N values, stable carbon isotopes and collagen yield might identify the presence of contaminants following pretreatment (van Klinken, 1999). For charcoal, %C values outside the expected yield of 50-70 (Braadbaart et al., 2009; Braadbaart and Poole, 2008) can denote contamination or diagenesis. With the exception of X-ray diffraction on aragonite shells, which can identify less than 1% of calcite contamination (Douka et al., 2010a; Sepulcre et al., 2009), these techniques are coarse, generally only identifying contaminants when they comprise a large percentage of the carbon in a sample. Although less

[8] We follow DeNiro and Weiner (1988) in their use of the term "collagen".

common than failure due to poor preservation, some grossly contaminated samples will go undated if measurement accuracy is expected to be seriously compromised following quality control assessment.

3. Discussion

Not all carbonaceous materials yield sufficient, endogenous carbon for radiocarbon measurement (assumption 8) due to poor preservation—the main reason for sample failure. This is due to factors that, depending on the spatio-temporal unit studied, may be deterministic. Therefore, large radiocarbon datasets of the type often used in ^{14}C-dates-as-data analyses are not necessarily representative of the archaeological record (assumption 1). For this reason, archaeological and chronometric records should be considered as separate; an ancient butchering site affected by repeated groundwater flooding may persist in the former, but will be removed from the latter if collagen fails to survive in that post-depositional environment (Hedges and Millard, 1995) and is solely targeted for dating. It is important to assess how well both records represent each other, and to what degree the complex and highly localized factors driving sample preservation can bias radiocarbon datasets. This last point is shared by (Torfing, 2015), who argues that the acid soils of Jutland, Denmark (Montanarella, 2010), have reduced the number of radiocarbon dates available from bone, skewing distributions produced (Hinz et al., 2012; Shennan et al., 2013) toward shell middens and periods of shell midden construction, and ultimately misrepresenting past human activity in the region.

Quantifying the effect of the preservation bias might prove impossible or, at the very least, challenging and time-consuming. This because poor preservation is best assessed on a site-by-site basis and, often, site reports only publish successful radiocarbon measurements, making no reference to the total number of samples submitted for dating or preservation issues. In addition, due

to slight differences in pretreatment protocols and quality assurance practices, sample failure rates almost certainly vary between laboratories. At the ORAU, for example, if the sample is near background (50 ka BP) and the amount of collagen extracted is <1% of the starting weight, it is usually failed and goes undated (Fiona Brock et al., 2010). In some instances, a minimum age is a useful measure of time and, under these circumstances, an "OxA-X-"[9] prefix is added to the result. If, however, the collagen yield is 0.5% and the sample yields a "greater than" age, e.g., >48 ka BP, the measurement is passed and receives a routine "OxA-" notation. On the other hand, due to the pronounced differences in contamination effects for material of a different age, a younger sample with a low collagen yield will not often be failed, but given an OxA-X- prefix and a caution comment. In many instances, pretreatment chemistry will be repeated using a larger starting weight in an attempt to improve yield or reassess the original measurement and its reproducibility. The same criteria might not be employed by all laboratories.

As for assumption 9, published chronometric data is not always accurate as contaminants may not be fully removed during pretreatment. In general, we would expect older, Pleistocene measurements to be underestimated, shifting the dataset toward younger ages. To preclude skewing caused by unreliable measurements, some ^{14}C-dates-as-data studies apply quality criteria to vet datasets. These vary in detail and depend greatly on the judgement of the authors. Other approaches intentionally avoid this practice to keep from biasing a dataset. Bias is a possibility, particularly if filters are applied without careful consideration of how contamination-derived inaccuracies might impact the spatio-temporal units studied and the archaeological sites therein. For example, if more stringent protocols are rated higher than routine methods—ABOx-SC vs. ABA—younger (<20 ka BP) measurements obtained using the latter might be unnecessarily excluded. This because, as

[9] Unlike the OxA prefix, OxA-X denotes samples that are research measurements using non-standard or experimental methods, or determinations that come with a caution based on the chemical parameters observed during pretreatment and measurement.

mentioned earlier, routine protocols like ABA are generally efficient in the decontamination of young material and the dates produced are no less reliable. Moreover, generalized screening treats dates as independent variables. In archaeology, however, dates are not separate from each other or their context and must be viewed and assessed according to the archaeological context from which they derive.

If unrecognized, unreliable dates have the potential to bias results in different ways. In Wood et al., (2013), for example, the application of improved ultrafiltration pretreatment methods identified a ~10,000-year age discrepancy in several archaeological samples in southern Iberia. This challenged the notion that the region served as a refugium for late-surviving Neanderthals (d'Errico et al., 1998; Guy Straus, 2005; Zilhao, 2006; Zilhão, 1993), which had been based on minimum-age estimates obtained from unreliable sample types, e.g., bulk sediment (Pessenda et al., 2001; Wang et al., 1996) and gentler, less robust pretreatment protocols (Wood et al., 2013). When combined with Bayesian age modelling (see Bronk Ramsey, 2009a), ultrafiltered measurements have contributed to a revised chronology for the M-UP transition in Iberia (Wood, 2011; Wood et al., 2013). Notably, this yields a distribution that is dissimilar to that derived from earlier chronometric analysis, prior to the routine use of ultrafiltration in the region (Wood, 2011), with a reduced peak at ~34 ka cal BP (Fig. 3). Both distributions can be reasonably expected to yield different archaeological interpretations. Given that it is estimated that as many as 70% of published dates for this period may be too young (Higham, 2011), this is likely to be echoed in other M-UP studies.

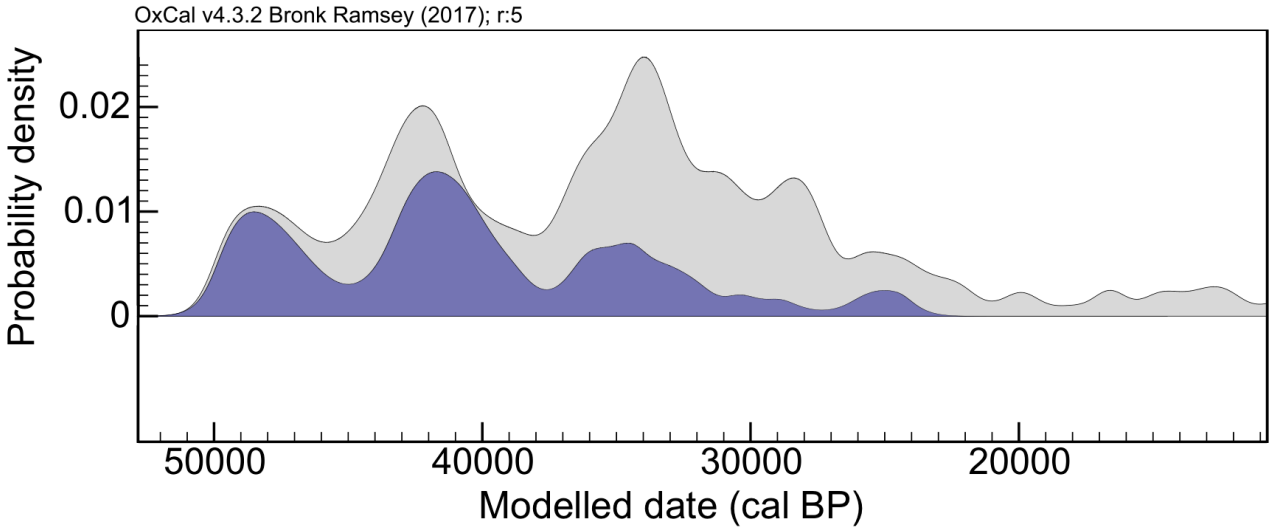


Fig. 3. Kernel density estimate (KDE) models for Middle-to-Upper Palaeolithic Iberia before (gray; n=365) and after (blue; n=141) the routine use of ultrafiltration and Bayesian age modelling. Data were compiled by Wood et al. (2011). All >50,000 BP and infinite ages were excluded (it is thus likely that the probability density around the limit of radiocarbon dating is artificially low). The density peak for the gray distribution centered at ~34 ka cal BP possibly represents minimum-age estimates obtained from unsuitable, i.e., less stringent than required given the antiquity of the samples, protocols and materials. The models were made using the `KDE_Model` function in the OxCal software (Bronk Ramsey, 2017, 2009a).

Confounding effects can also be observed at a smaller scale, when combining dates for single archaeological events. The site of Anzick, Montana, for example, contains the likely curated remains of a male infant (Anzick-1; sample SR-8151), from which a total of 17 radiocarbon dates—averaged[10] to 12650-12545 cal BP (95.4% confidence)—have been produced in an effort to obtain a contaminant-free measurement (Becerra-Valdivia et al., 2018). So far, only one (OxA-X-2739-54) has been found to be reliable[11] and in agreement with the stratigraphic context (Becerra-Valdivia et

[10] Calibration was undertaken using OxCal 4.3 (Bronk Ramsey, 2009a) and the IntCal13 calibration curve (Reimer et al., 2013). Averaging was done in the same platform, following Ward and Wilson (1978), using OxCal's "R_Combine" command.

[11] This reliability is based on the fact that it was obtained using a single amino-acid method (Deviese et al., 2017), thus removing all potential contaminants.

al., 2018), dating Anzick-1 to 12905-12695 cal BP (95.4% confidence). This is relevant to ^{14}C-dates-as-data studies because some researchers combine multiple dates from a single cultural feature, layer or phase, to offset data overrepresentation (in relation to assumption 7). In the case of Anzick-1, however, distributions for OxA-X-2739-54 and the seventeen-date average do not overlap at a 95.4% confidence level (Fig. 4). Therefore, depending on how overrepresentation is dealt with, the difference between inclusion and exclusion of unreliable estimates into calculations should be tested. To do this, a critical assessment of site-specific chronometric data is necessary.

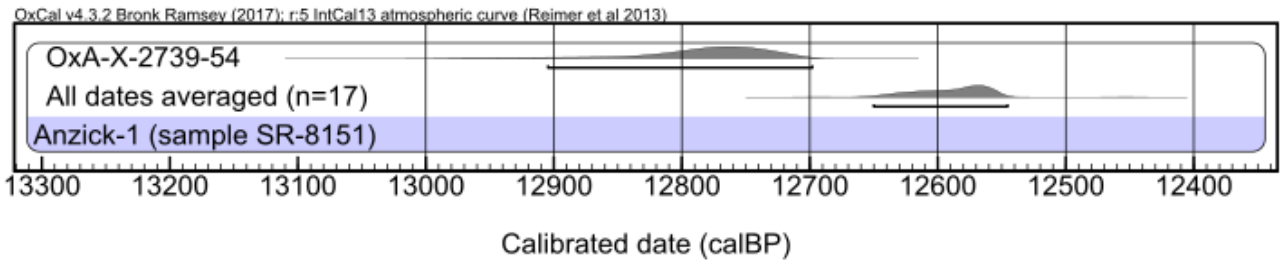


Fig. 4. Calibrated dates for sample SR-8151 (Anzick-1 individual from Anzick site, Montana; Becerra-Valdivia et al., 2018). At the top, the calibrated date for OxA-X-2739-54 (10.9 ka BP) at 12905-12695 cal BP (95.4% confidence). At the bottom, the average of 17 dates obtained for the same individual at 12650-12545 cal BP (95.4% confidence). At a 95.4% confidence level, both probability density functions fail to overlap. This illustrates the confounding effects that averaging, one approach used in ^{14}C-dates-as-data studies to offset data overrepresentation, can have at a small scale.

Conclusion

Challenges in radiocarbon sample processing have a direct impact on three of the fourteen underlying assumptions made in ^{14}C-dates-as-data studies, as identified earlier. For assumptions 1 and 8, we have shown that the radiocarbon dataset cannot always be considered an entirely representative subsample of the archaeological record, because not all carbonaceous materials yield

sufficient endogenous carbon for radiocarbon measurement. This is generally due to preservation issues influenced by sample antiquity and unique post-depositional conditions. These factors may be deterministic, depending on the spatio-temporal unit studied. Moreover, failure rates differ between radiocarbon laboratories, introducing further uncertainty. As for assumption 9, the radiocarbon dating process has long been known to produce unreliable results, primarily due to partial sample decontamination. Large discrepancies have become increasingly apparent over the years with the development of more rigorous pretreatment methods (that only a sub-section of radiocarbon laboratories employ) and the concomitant production of robust measurements in line with stratigraphic evidence—particularly for Pleistocene-aged and heavily contaminated samples. If unidentified, these inaccuracies have the potential to skew radiocarbon datasets and artificially alter a distribution. The critical assessment of site-specific chronometric data is, therefore, necessary and requires a basic understanding of the radiocarbon dating process and its complexities, as well as the spatio-temporal unit studied and each archaeological site.

We recommend that each study assesses the impact of sample preservation and contamination on a site-by-site basis. The success of identifying bias and offset results will inevitably vary according to each study, with those analyzing large spatial units spanning the spectrum of radiocarbon dating likely to encounter the greatest challenges. It might also prove informative to perform sensitivity testing by producing a number of distributions using different parameters and comparing the results. Assessing the impact of database vetting is one example. In case the effect of a single bias is unquantifiable or significant, the reliability of the method for the purpose of elucidating population dynamics should be questioned and not employed as the sole analytical tool; a number of ^{14}C-dates-as-data studies use the frequency of archaeological sites as a comparative proxy (see French and Collins, 2015; Schmidt et al., 2012; Tallavaara et al., 2010). Moreover, when studying human dispersals, we suggest the use of Bayesian site-based age modelling instead. The same has been

proposed by others in the past (Bayliss et al., 2007; Blackwell and Buck, 2003; Culleton, 2008). In contrast to the ^{14}C-dates-as-data approach, Bayesian age modelling allows the incorporation of relative information, e.g., stratigraphy, with dates, and can be employed to objectively identify and down-weight outlier dates (Bronk Ramsey, 2009b), obtain quantitative age estimates for archaeological events or calculate the commencement of individual archaeological sequences (Bronk Ramsey, 2009a). Given that human presence likely predates the archaeological record, the latter is key in the study of population dynamics. Literature on Bayesian age modelling is vast (see (Derek Hamilton and Krus, 2018, and references therein) and the analysis can be performed on the same platforms used for summarizing radiocarbon datasets, e.g., OxCal (Bronk Ramsey, 2009a, 2001).

Acknowledgments

Without implying their agreement with the content of this article, we thank Christopher Bronk Ramsey and Eileen Jacob (Oxford) for their assistance, as well as Jaime Swift (Oxford) and Katerina Douka (MPI-SHH, Jena) for enriching discussions on the topic. Funding was provided by the Clarendon Fund Scholarship, University of Oxford; the Natural Environment Research Council (NERC; NE/D014077/1); and the EPSRC Centre for Doctoral Training in Industrially Focused Mathematical Modelling (EP/L015803/1), University of Oxford.

Declarations of interest: none

References

Armit, I., Swindles, G.T., Becker, K., 2013. From dates to demography in later prehistoric Ireland? Experimental approaches to the meta-analysis of large 14C data-sets. J. Archaeol. Sci. 40, 433–

438.

Ascough, P.L., Bird, M.I., Francis, S.M., Lebl, T., 2011. Alkali extraction of archaeological and geological charcoal: evidence for diagenetic degradation and formation of humic acids. Journal of Archaeological Science 38, 69–78.

Bae, K., 2002. Radiocarbon Dates from Paleolithic Sites in Korea. Radiocarbon 44, 473–476.

Bamforth, D.B., Grund, B., 2012. Radiocarbon calibration curves, summed probability distributions, and early Paleoindian population trends in North America. J. Archaeol. Sci. 39, 1768–1774.

Bayliss, A., Bronk Ramsey, C., van der Plicht, J., Whittle, A., 2007. Bradshaw and Bayes: Towards a Timetable for the Neolithic. Cambridge Archaeological Journal 17, 1–28.

Becerra-Valdivia, L., Waters, M.R., Stafford, T.W., Jr, Anzick, S.L., Comeskey, D., Devièse, T., Higham, T., 2018. Reassessing the chronology of the archaeological site of Anzick. Proc. Natl. Acad. Sci. U. S. A. 115, 7000–7003.

Berna, F., Matthews, A., Weiner, S., 2004. Solubilities of bone mineral from archaeological sites: the recrystallization window. J. Archaeol. Sci. 31, 867–882.

Berridge, P., Roberts, A., 1986. The Mesolithic period in Cornwall. Cornish Archaeology 25, 7–34.

Bird, M.I., Ayliffe, L.K., Fifield, L.K., Turney, C.S.M., Cresswell, R.G., Barrows, T.T., David, B., 1999. Radiocarbon Dating of "Old" Charcoal Using a Wet Oxidation, Stepped-Combustion Procedure. Radiocarbon 41, 127–140.

Bird, M.I., Turney, C.S.M., Fifield, L.K., Jones, R., Ayliffe, L.K., Palmer, A., Cresswell, R., Robertson, S., 2002. Radiocarbon analysis of the early archaeological site of Nauwalabila I, Arnhem Land, Australia: implications for sample suitability and stratigraphic integrity. Quat. Sci. Rev. 21, 1061–1075.

Blackwell, P.G., Buck, C.E., 2003. The Late Glacial human reoccupation of north-western Europe: new approaches to space-time modelling. Antiquity 77, 232–240.

Blockley, S.P.E., Donahue, R.E., Pollard, A.M., 2000. Radiocarbon calibration and Late Glacial

occupation in northwest Europe. Antiquity 74, 112–119.

Braadbaart, F., Poole, I., 2008. Morphological, chemical and physical changes during charcoalification of wood and its relevance to archaeological contexts. J. Archaeol. Sci. 35, 2434–2445.

Braadbaart, F., Poole, I., van Brussel, A.A., 2009. Preservation potential of charcoal in alkaline environments: an experimental approach and implications for the archaeological record. J. Archaeol. Sci. 36, 1672–1679.

Bradtmöller, M., Pastoors, A., Weninger, B., Weniger, G.-C., 2012. The repeated replacement model--rapid climate change and population dynamics in Late Pleistocene Europe. Quat. Int. 247, 38–49.

Brock, F., Higham, T., Ditchfield, P., Bronk Ramsey, C., 2010a. Current Pretreatment Methods for AMS Radiocarbon Dating at the Oxford Radiocarbon Accelerator Unit (Orau). Radiocarbon 52, 103–112.

Brock, F., Higham, T., Christopher, R.B.R., 2010b. Pre-screening techniques for identification of samples suitable for radiocarbon dating of poorly preserved bones. J. Archaeol. Sci. 37, 855–865.

Brock, F., Higham, T.F.G., 2009. AMS Radiocarbon Dating of Paleolithic-Aged Charcoal from Europe and the Mediterranean Rim Using ABOx-SC. Radiocarbon 51, 839–846.

Bronk Ramsey, C., 2017. Methods for Summarizing Radiocarbon Datasets. Radiocarbon 59, 1809–1833.

Bronk Ramsey, C., 2009a. Bayesian Analysis of Radiocarbon Dates. Radiocarbon 51, 337–360.

Bronk Ramsey, C., 2009b. Dealing with Outliers and Offsets in Radiocarbon Dating. Radiocarbon 51, 1023–1045.

Bronk Ramsey, C., 2008. Radiocarbon dating: revolutions in understanding. Archaeometry.50, 249-275

Bronk Ramsey, C., 2001. Development of the Radiocarbon Calibration Program. Radiocarbon 43, 355–363.

Brown, T.A., Nelson, D.E., Vogel, J.S., Southon, J.R., 1988. Improved Collagen Extraction by Modified Longin Method. Radiocarbon 30, 171–177.

Chiverrell, R.C., Thorndycraft, V.R., Hoffmann, T.O., 2011. Cumulative probability functions and their role in evaluating the chronology of geomorphological events during the Holocene. J. Quat. Sci. 26, 76–85.

Collins, M.J., Nielsen-Marsh, C.M., Hiller, J., Smith, C.I., Roberts, J.P., Prigodich, R.V., Wess, T.J., Csapo, J., Millard, A.R., Turner-Walker, G., 2002. The survival of organic matter in bone: a review. Archaeometry 44, 383–394.

Contreras, D.A., Meadows, J., 2014. Summed radiocarbon calibrations as a population proxy: a critical evaluation using a realistic simulation approach. J. Archaeol. Sci. 52, 591–608.

Culleton, B.J., 2008. Crude demographic proxy reveals nothing about Paleoindian population. Proc. Natl. Acad. Sci. U. S. A. 105, E111.

Davies, B., Holdaway, S.J., Fanning, P.C., 2016. Modelling the palimpsest: An exploratory agent-based model of surface archaeological deposit formation in a fluvial arid Australian landscape. Holocene 26, 450–463.

DeNiro, M.J., Weiner, S., 1988. Chemical, enzymatic and spectroscopic characterization of “collagen” and other organic fractions from prehistoric bones. Geochim. Cosmochim. Acta 52, 2197–2206.

Derek Hamilton, W., Krus, A.M., 2018. The Myths and Realities of Bayesian Chronological Modeling Revealed. Am. Antiq. 83, 187–203.

d’Errico, F., Zilhão, J., Julien, M., Baffier, D., Pelegrin, J., 1998. Neanderthal Acculturation in Western Europe? A Critical Review of the Evidence and Its Interpretation. Curr. Anthropol. 39, S1–S44.

Deviese, T., Comeskey, D., McCullagh, J., Bronk Ramsey, C., Higham, T., 2017. New protocol for compound specific radiocarbon analysis of archaeological bones. Rapid Commun. Mass Spectrom. 32, 373–379.

Devièse, T., Karavanić, I., Comeskey, D., Kubiak, C., Korlević, P., Hajdinjak, M., Radović, S., Procopio, N., Buckley, M., Pääbo, S., Higham, T., 2017. Direct dating of Neanderthal remains from the site of Vindija Cave and implications for the Middle to Upper Paleolithic transition. Proc. Natl. Acad. Sci. U. S. A. 114, 10606–10611.

Douka, K., Hedges, R.E.M., Higham, T.F.G., 2010a. Improved AMS 14C Dating of Shell Carbonates Using High-Precision X-Ray Diffraction and a Novel Density Separation Protocol (Cards). Radiocarbon 52, 735–751.

Douka, K., Higham, T., Sinitsyn, A., 2010b. The Influence of Pretreatment Chemistry on the Radiocarbon Dating of Campanian Ignimbrite-Aged Charcoal from Kostenki 14 (Russia). Quat. Res. 73, 583–587.

French, J.C., Collins, C., 2015. Upper Palaeolithic population histories of Southwestern France: a comparison of the demographic signatures of 14C date distributions and archaeological site counts. J. Archaeol. Sci. 55, 122–134.

Gillespie, R., Hedges, R.E.M., Wand, J.O., 1984. Radiocarbon dating of bone by accelerator mass spectrometry. J. Archaeol. Sci. 11, 165–170.

Guy Straus, L., 2005. A mosaic of change: the Middle–Upper Paleolithic transition as viewed from New Mexico and Iberia. Quat. Int. 137, 47–67.

Hedges, R.E.M., Millard, A.R., 1995. Bones and Groundwater: Towards the Modelling of Diagenetic Processes. J. Archaeol. Sci. 22, 155–164.

Higham, T., 2011. European Middle and Upper Palaeolithic radiocarbon dates are often older than they look: problems with previous dates and some remedies. Antiquity 85, 235–249.

Higham, T., Brock, F., Peresani, M., Broglio, A., Wood, R., Douka, K., 2009. Problems with

radiocarbon dating the Middle to Upper Palaeolithic transition in Italy. Quaternary Science Reviews 28, 1257–1267.

Higham, T.F.G., Barton, H., Turney, C.S.M., Barker, G., Bronk Ramsey, C., Brock, F., 2009. Radiocarbon dating of charcoal from tropical sequences: results from the Niah Great Cave, Sarawak, and their broader implications. J. Quat. Sci. 24, 189–197.

Higham, T.F.G., Jacobi, R.M., Bronk Ramsey, C., 2006. AMS radiocarbon dating of ancient bone using ultrafiltration. Radiocarbon 48, 179–195.

Higham, T., Ramsey, C.B., Karavanić, I., Smith, F.H., Trinkaus, E., 2006. Revised direct radiocarbon dating of the Vindija G1 Upper Paleolithic Neandertals. Proc. Natl. Acad. Sci. U. S. A. 103, 553–557.

Hinz, M., Feeser, I., Sjögren, K.-G., Müller, J., 2012. Demography and the intensity of cultural activities: an evaluation of Funnel Beaker Societies (4200–2800 cal BC). J. Archaeol. Sci. 39, 3331–3340.

Holmes, K.M., Robson Brown, K.A., Oates, W.P., Collins, M.J., 2006. Assessing the distribution of Asian Palaeolithic sites: a predictive model of collagen degradation. J. Archaeol. Sci. 33, 971–986.

Holmes, K.M., Robson Brown, K.A., Oates, W.P., Collins, M.J., 2005. Assessing the distribution of African Palaeolithic sites: a predictive model of collagen degradation. Journal of Archaeological Science 32, 157–166.

Housley, R.A., Gamble, C.S., Street, M., Pettitt, P., 1997. Radiocarbon evidence for the Lateglacial Human Recolonisation of Northern Europe. Proceedings of the Prehistoric Society 63, 25–54.

Jacobi, R.M., Higham, T.F.G., Bronk Ramsey, C., 2006. AMS radiocarbon dating of Middle and Upper Palaeolithic bone in the British Isles: improved reliability using ultrafiltration. Journal of Quaternary Science 21, 557–573.

Jöris, O., ’Alvarez Fern’andez, E., Weninger, B., 2003. Radiocarbon evidence of the Middle to

Upper Palaeolithic transition in Southwestern Europe. Trabajos de Prehistoria 60, 15–38.

Kerr, T.R., McCormick, F., 2014. Statistics, sunspots and settlement: influences on sum of probability curves. J. Archaeol. Sci. 41, 493–501.

Kosintsev, P., Mitchell, K.J., Devièse, T., van der Plicht, J., Kuitems, M., Petrova, E., Tikhonov, A., Higham, T., Comeskey, D., Turney, C., Cooper, A., van Kolfschoten, T., Stuart, A.J., Lister, A.M., 2019. Evolution and extinction of the giant rhinoceros Elasmotherium sibiricum sheds light on late Quaternary megafaunal extinctions. Nat Ecol Evol 3, 31–38.

Longin, R., 1971. New method of collagen extraction for radiocarbon dating. Nature 230, 241–242.

Marom, A., McCullagh, J.S., Higham, T.F., Sinitsyn, A.A., Hedges, R.E., 2012. Single amino acid radiocarbon dating of Upper Paleolithic modern humans. Proc Natl Acad Sci USA 109, 6878–6881.

Michczyńska, D.J., Pazdur, A., 2004. Shape Analysis of Cumulative Probability Density Function of Radiocarbon Dates Set in the Study of Climate Change in the Late Glacial and Holocene. Radiocarbon 46, 733–744.

Montanarella, L., 2010. Map of Soil pH in Europe. Land Resources Management Unit, Institute for Environment & Sustainability, European Commission, Joint Research Centre. https://esdac.jrc.ec.europa.eu/content/soil-ph-europe

Ortner, D.J., vonEndt, D.W., Robinson, M.S., 1972. The Effect of Temperature on Protein Decay in Bone: Its Significance in Nitrogen Dating of Archaeological Specimens. Am. Antiq. 37, 514–520.

Pessenda, L.C.R., Gouveia, S.E.M., Aravena, R., 2001. Radiocarbon Dating of Total Soil Organic Matter and Humin Fraction and Its Comparison with 14C Ages of Fossil Charcoal. Radiocarbon 43, 595–601.

Pestle, W.J., Colvard, M., 2012. Bone collagen preservation in the tropics: a case study from ancient Puerto Rico. J. Archaeol. Sci. 39, 2079–2090.

Rebollo, N.R., Cohen-Ofri, I., Popovitz-Biro, R., Bar-Yosef, O., Meignen, L., Goldberg, P., Weiner, S., Boaretto, E., 2008. Structural characterization of charcoal exposed to high and low pH: implications for 14C sample preparation and charcoal preservation. Radiocarbon 50, 289–307.

Reimer, P.J., Bard, E., Bayliss, A., Warren Beck, J., Blackwell, P.G., Ramsey, C.B., Buck, C.E., Cheng, H., Lawrence Edwards, R., Friedrich, M., Grootes, P.M., Guilderson, T.P., Haflidason, H., Hajdas, I., Hatté, C., Heaton, T.J., Hoffmann, D.L., Hogg, A.G., Hughen, K.A., Felix Kaiser, K., Kromer, B., Manning, S.W., Niu, M., Reimer, R.W., Richards, D.A., Marian Scott, E., Southon, J.R., Staff, R.A., Turney, C.S.M., van der Plicht, J., 2013. IntCal13 and Marine13 Radiocarbon Age Calibration Curves 0–50,000 Years cal BP. Radiocarbon 55, 1869–1887.

Rhode, D., Brantingham, P.J., Perreault, C., Madsen, D.B., 2014. Mind the gaps: testing for hiatuses in regional radiocarbon date sequences. J. Archaeol. Sci. 52, 567–577.

Schmidt, I., Bradtmöller, M., Kehl, M., Pastoors, A., Tafelmaier, Y., Weninger, B., Weniger, G.-C., 2012. Rapid climate change and variability of settlement patterns in Iberia during the Late Pleistocene. Quat. Int. 274, 179–204.

Sepulcre, S., Durand, N., Bard, E., 2009. Mineralogical determination of reef and periplatform carbonates: Calibration and implications for paleoceanography and radiochronology. Glob. Planet. Change 66, 1–9.

Shennan, S., Downey, S.S., Timpson, A., Edinborough, K., Colledge, S., Kerig, T., Manning, K., Thomas, M.G., 2013. Regional population collapse followed initial agriculture booms in mid-Holocene Europe. Nat. Commun. 4, 2486.

Stafford, T.W., Jr, Duhamel, R.C., Haynes, C.V., Jr, Brendel, K., 1982. Isolation of proline and hydroxyproline from fossil bone. Life Sci. 31, 931–938.

Surovell, T.A., Finley, J.B., Smith, G.M., Jeffrey Brantingham, P., Kelly, R., 2009. Correcting temporal frequency distributions for taphonomic bias. Journal of Archaeological Science 36, 1715–1724.

Tallavaara, M., Pesonen, P., Oinonen, M., 2010. Prehistoric population history in eastern Fennoscandia. J. Archaeol. Sci. 37, 251–260.

Timpson, A., Colledge, S., Crema, E., Edinborough, K., Kerig, T., Manning, K., Thomas, M.G., Shennan, S., 2014. Reconstructing regional population fluctuations in the European Neolithic using radiocarbon dates: a new case-study using an improved method. J. Archaeol. Sci. 52, 549–557.

Torfing, T., 2015. Neolithic population and summed probability distribution of 14C-dates. J. Archaeol. Sci. 63, 193–198.

van Andel, T.H., Davies, W., Weninger, B., Jöris, O., 2003. Archaeological dates as proxies for the spatial and temporal human presence in Europe: a discourse on the method. Neanderthals and modern humans in the European landscape during the last glaciation 21–29.

van Klinken, G.J., 1999. Bone Collagen Quality Indicators for Palaeodietary and Radiocarbon Measurements. J. Archaeol. Sci. 26, 687–695.

Von Endt, D.W., Ortner, D.J., 1984. Experimental effects of bone size and temperature on bone diagenesis. J. Archaeol. Sci. 11, 247–253.

Wang, Y., Amundson, R., Trumbore, S., 1996. Radiocarbon Dating of Soil Organic Matter. Quat. Res. 45, 282–288.

Ward, G.K., Wilson, S.R., 1978. Procedures for Comparing and Combining Age Determinations: A Critique. Archaeometry 20, 19–31.

Wild, E.M., Steier, P., Fischer, P., Höflmayer, F., 2013. 14C Dating of Humic Acids from Bronze and Iron Age Plant Remains from the Eastern Mediterranean. Radiocarbon 55, 599–607.

Williams, A.N., 2012. The use of summed radiocarbon probability distributions in archaeology: a review of methods. J. Archaeol. Sci. 39, 578–589.

Wood, R.E., 2011. The contribution of new radiocarbon dating pre-treatment techniques to understanding the Middle to Upper Palaeolithic transition in Iberia (D.Phil.). University of

Oxford.

Wood, R.E., Barroso-Ruíz, C., Caparrós, M., Jordá Pardo, J.F., Galván Santos, B., Higham, T.F.G., 2013. Radiocarbon dating casts doubt on the late chronology of the Middle to Upper Palaeolithic transition in southern Iberia. Proc. Natl. Acad. Sci. U. S. A. 110, 2781–2786.

Wood, R.E., Douka, K., Boscato, P., Haesaerts, P., Sinitsyn, A., Higham, T.F.G., 2012. Testing the ABOx-SC method: Dating known-age charcoals associated with the Campanian Ignimbrite. Quat. Geochronol. 9, 16–26.

Zazzo, A., Saliège, J.-F., 2011. Radiocarbon dating of biological apatites: A review. Palaeogeogr. Palaeoclimatol. Palaeoecol. 310, 52–61.

Zilhao, J., 2006. Chronostratigraphy of the Middle-to-Upper Paleolithic Transition in the Iberian Peninsula. Pyrenae 7–84.

Zilhão, J., 1993. Le passage du Paléolithique moyen au Paléolithique supérieur dans le Portugal. El origen del hombre moderno en el Suroeste de Europa 127–145.

5.1. Supplementary Text

Appendix

This is a compilation of published sources reviewed, which utilize or discuss the ^{14}C-dates-as-data approach on the archaeological record.

Armit, I., Swindles, G.T., Becker, K., 2013. From dates to demography in later prehistoric Ireland? Experimental approaches to the meta-analysis of large 14C data-sets. J. Archaeol. Sci. 40, 433–438.

Bamforth, D.B., Grund, B., 2012. Radiocarbon calibration curves, summed probability distributions, and early Paleoindian population trends in North America. J. Archaeol. Sci. 39, 1768–1774.

Barton, L., Brantingham, P.J., Ji, D., 2007. Late Pleistocene climate change and Paleolithic cultural evolution in northern China: Implications from the Last Glacial Maximum, in: Developments in Quaternary Sciences. Elsevier, pp. 105–128.

Blackwell, P.G., Buck, C.E., 2003. The Late Glacial human reoccupation of north-western Europe: new approaches to space-time modelling. Antiquity 77, 232–240.

Blockley, S.P.E., Donahue, R.E., Pollard, A.M., 2000. Radiocarbon calibration and Late Glacial occupation in northwest Europe. Antiquity 74, 112–119.

Bocquet-Appel, J.-P., Demars, P.Y., 2000. Neanderthal contraction and modern human colonization of Europe. Antiquity 74, 544–552.

Bocquet-Appel, J.-P., Naji, S., Linden, M.V., Kozlowski, J.K., 2009. Detection of diffusion and contact zones of early farming in Europe from the space-time distribution of 14C dates. J. Archaeol. Sci. 36, 807–820.

Bradtmöller, M., Pastoors, A., Weninger, B., Weniger, G.-C., 2012. The repeated replacement model--rapid climate change and population dynamics in Late Pleistocene Europe. Quat. Int. 247, 38–49.

Brantingham, P.J., Kerry, K.W., Krivoshapkin, A.I., Kuzmin, Y.V., 2004. Time- space dynamics in the Early-Upper Paleolithic of northeast Asia, in: Madsen, D.B. (Ed.), Entering America: Northeast Asia and Beringia Before the Last Glacial Maximum. University of Utah Press, Salt Lake City, pp. 255–283.

Bright, J., Ugan, A., Hunsaker, L., 2002. The effect of handling time on subsistence technology. World Archaeol. 34, 164–181.

Bronk Ramsey, C., 2017. Methods for Summarizing Radiocarbon Datasets. Radiocarbon 59, 1809–1833.

Buchanan, B., Collard, M., Edinborough, K., 2008. Paleoindian demography and the extraterrestrial impact hypothesis. Proc. Natl. Acad. Sci. U. S. A. 105, 11651–11654.

Collard, M., Edinborough, K., Shennan, S., Thomas, M.G., 2010. Radiocarbon evidence indicates that migrants introduced farming to Britain. J. Archaeol. Sci. 37, 866–870.

Contreras, D.A., Meadows, J., 2014. Summed radiocarbon calibrations as a population proxy: a critical evaluation using a realistic simulation approach. J. Archaeol. Sci. 52, 591–608.

Crema, E.R., Habu, J., Kobayashi, K., Madella, M., 2016. Summed Probability Distribution of 14C Dates Suggests Regional Divergences in the Population Dynamics of the Jomon Period in Eastern Japan. PLoS One 11, e0154809.

Crombé, P., Robinson, E., 2014. 14C dates as demographic proxies in Neolithisation models of northwestern Europe: a critical assessment using Belgium and northeast France as a case-study. J. Archaeol. Sci. 52, 558–566.

Davies, B., Holdaway, S.J., Fanning, P.C., 2016. Modelling the palimpsest: An exploratory agent-based model of surface archaeological deposit formation in a fluvial arid Australian landscape. Holocene 26, 450–463.

Davies, W., 2001. A Very Model of a Modern Human Industry: New Perspectives on the Origins and Spread of the Aurignacian in Europe. Proceedings of the Prehistoric Society 67, 195–217.

Dolukhanov, P.M., Shukurov, A.M., Tarasov, P.E., Zaitseva, G.I., 2002. Colonization of Northern Eurasia by Modern Humans: Radiocarbon Chronology and Environment. J. Archaeol. Sci. 29, 593–606.

Dolukhanov, P., Sokoloff, D., Shukurov, A., 2001. Radiocarbon Chronology of Upper Palaeolithic Sites in Eastern Europe at Improved Resolution. J. Archaeol. Sci. 28, 699–712.

Faught, M.K., 2008. Archaeological Roots of Human Diversity in the New World: A Compilation of Accurate and Precise Radiocarbon Ages from Earliest Sites. Am. Antiq. 73, 670–698.

Fiedel, S.J., Kuzmin, Y.V., 2007. Radiocarbon Date Frequency as an Index of Intensity of Paleolithic Occupation of Siberia: Did Humans React Predictably to Climate Oscillations? Radiocarbon 49, 741–756.

French, J.C., Collins, C., 2015. Upper Palaeolithic population histories of Southwestern France: a comparison of the demographic signatures of 14C date distributions and archaeological site counts. J. Archaeol. Sci. 55, 122–134.

Gajewski, K., Munoz, S., Peros, M., Viau, A., Morlan, R., Betts, M., 2011. The Canadian Archaeological Radiocarbon Database (Card): Archaeological 14C Dates in North America and Their Paleoenvironmental Context. Radiocarbon 53, 371–394.

Gamble, C., Davies, W., Pettitt, P., Hazelwood, L., Richards, M., 2005. The archaeological and genetic foundations of the European population during the Late Glacial: implications for "agricultural thinking." Cambridge Archaeological Journal 15, 193–223.

Gamble, C., Davies, W., Pettitt, P., Richards, M., 2004. Climate change and evolving human diversity in Europe during the last glacial. Philos. Trans. R. Soc. Lond. B Biol. Sci. 359, 243–53; discussion 253–4.

Gayo, E.M., Latorre, C., Santoro, C.M., 2015. Timing of occupation and regional settlement patterns revealed by time-series analyses of an archaeological radiocarbon database for the South-Central Andes (16°–25°S). Quaternary International 356, 4–14.

Gkiasta, M., Russell, T., Shennan, S., Steele, J., 2003. Neolithic transition in Europe: the radiocarbon record revisited. Antiquity 77, 45–62.

Goldberg, A., Mychajliw, A.M., Hadly, E.A., 2016. Post-invasion demography of prehistoric humans in South America. Nature 532, 232–235.

González-Sampériz, P., Utrilla, P., Mazo, C., Valero-Garcés, B., Sopena, M.C., Morellón, M., Sebastián, M., Moreno, A., Martínez-Bea, M., 2009. Patterns of human occupation during the early Holocene in the Central Ebro Basin (NE Spain) in response to the 8.2 ka climatic event. Quat. Res. 71, 121–132.

Graf, K.E., 2005. Abandonment of the Siberian mammoth-steppe during the LGM: evidence from the calibration of 14C-dated archaeological occupations. Current Research in the Pleistocene 22, 2–5.

Haynes, C.V., Jr, 1969. The earliest americans. Science 166, 709–715.

Hinz, M., Feeser, I., Sjögren, K.-G., Müller, J., 2012. Demography and the intensity of cultural activities: an evaluation of Funnel Beaker Societies (4200–2800 cal BC). J. Archaeol. Sci. 39, 3331–3340.

Holdaway, S., Fanning, P., Rhodes, E., 2008. Challenging intensification: human—environment interactions in the Holocene geoarchaeological record from western New South Wales, Australia. Holocene 18, 403–412.

Holdaway, S.J., Fanning, P.C., Rhodes, E.J., Marx, S.K., Floyd, B., Douglass, M.J., 2010. Human response to Palaeoenvironmental change and the question of temporal scale. Palaeogeogr. Palaeoclimatol. Palaeoecol. 292, 192–200.

Holdaway, S., Porch, N., 1995. Cyclical patterns in the Pleistocene human occupation of Southwest Tasmania. Archaeology in Oceania 30, 74–82.

Housley, R.A., Gamble, C.S., Street, M., Pettitt, P., 1997. Radiocarbon evidence for the Lateglacial Human Recolonisation of Northern Europe. Proceedings of the Prehistoric Society 63, 25–54.

Johnson, C.N., Brook, B.W., 2011. Reconstructing the dynamics of ancient human populations from radiocarbon dates: 10 000 years of population growth in Australia. Proceedings of the Royal Society B: Biological Sciences 278, 3748–3754.

Jöris, O., Alvarez Fernandez, E., Weninger, B., 2003. Radiocarbon evidence of the Middle to Upper Palaeolithic transition in Southwestern Europe. Trabajos de Prehistoria 60, 15–38.

Kelly, R.L., Surovell, T.A., Shuman, B.N., Smith, G.M., 2013. A continuous climatic impact on Holocene human population in the Rocky Mountains. Proc. Natl. Acad. Sci. U. S. A. 110, 443–447.

Kerr, T.R., McCormick, F., 2014. Statistics, sunspots and settlement: influences on sum of probability curves. J. Archaeol. Sci. 41, 493–501.

Kuper, R., Kröpelin, S., 2006. Climate-controlled Holocene occupation in the Sahara: motor of Africa's evolution. Science 313, 803–807.

Kuzmin, Y.V., Keates, S.G., 2005. Dates Are Not Just Data: Paleolithic Settlement Patterns in Siberia Derived from Radiocarbon Records. Am. Antiq. 70, 773–789.

Louderback, L.A., Grayson, D.K., Llobera, M., 2011. Middle-Holocene climates and human population densities in the Great Basin, western USA. Holocene 21, 366–373.

Manning, K., Timpson, A., 2014. The demographic response to Holocene climate change in the Sahara. Quat. Sci. Rev. 101, 28–35.

Marquet, P.A., Santoro, C.M., Latorre, C., Standen, V.G., Abades, S.R., Rivadeneira, M.M., Arriaza, B., Hochberg, M.E., 2012. Emergence of social complexity among coastal hunter-gatherers in the Atacama Desert of northern Chile. Proc. Natl. Acad. Sci. U. S. A. 109, 14754–14760.

Martínez, G., Flensborg, G., Bayala, P.D., 2013. Chronology and human settlement in northeastern Patagonia (Argentina): Patterns of site destruction, intensity of archaeological signal, and population dynamics. Quat. Int. 301, 123–134.

Mulrooney, M.A., 2013. An island-wide assessment of the chronology of settlement and land use on

Rapa Nui (Easter Island) based on radiocarbon data. J. Archaeol. Sci. 40, 4377–4399.

Munoz, S.E., Gajewski, K., Peros, M.C., 2010. Synchronous environmental and cultural change in the prehistory of the northeastern United States. Proc. Natl. Acad. Sci. U. S. A. 107, 22008–22013.

Naudinot, N., Tomasso, A., Tozzi, C., Peresani, M., 2014. Changes in mobility patterns as a factor of 14C date density variation in the Late Epigravettian of Northern Italy and Southeastern France. J. Archaeol. Sci. 52, 578–590.

Oh, Y., Conte, M., Kang, S., Kim, J., Hwang, J., 2017. Population Fluctuation and the Adoption of Food Production in Prehistoric Korea: Using Radiocarbon Dates as a Proxy for Population Change. Radiocarbon 59, 1761–1770.

Oinonen, M., Pesonen, P., Tallavaara, M., 2010. Archaeological Radiocarbon Dates for Studying the Population History in Eastern Fennoscandia. Radiocarbon 52, 393–407.

Ozainne, S., Lespez, L., Garnier, A., Ballouche, A., Neumann, K., Pays, O., Huysecom, E., 2014. A question of timing: spatio-temporal structure and mechanisms of early agriculture expansion in West Africa. J. Archaeol. Sci. 50, 359–368.

Pablo, J.F.-L. de, de Pablo, J.F.-L., Gutiérrez-Roig, M., Gómez-Puche, M., McLaughlin, R., Silva, F., Lozano, S., 2019. Palaeodemographic modelling supports a population bottleneck during the Pleistocene-Holocene transition in Iberia. Nature Communications. https://doi.org/10.1038/s41467-019-09833-3

Peros, M.C., Munoz, S.E., Gajewski, K., Viau, A.E., 2010. Prehistoric demography of North America inferred from radiocarbon data. J. Archaeol. Sci. 37, 656–664.

Prates, L., Politis, G., Steele, J., 2013. Radiocarbon chronology of the early human occupation of Argentina. Quat. Int. 301, 104–122.

Rhode, D., Brantingham, P.J., Perreault, C., Madsen, D.B., 2014. Mind the gaps: testing for hiatuses in regional radiocarbon date sequences. J. Archaeol. Sci. 52, 567–577.

Rick, J.W., 1987. Dates as Data: An Examination of the Peruvian Preceramic Radiocarbon Record. Am. Antiq. 52, 55–73.

Riede, F., 2009. Climate and demography in early prehistory: using calibrated 14C dates as population proxies. Hum. Biol. 81, 309–338.

Riede, F., 2008. The Laacher See-eruption (12,920 BP) and material culture change at the end of the Allerød in Northern Europe. J. Archaeol. Sci. 35, 591–599.

Rieth, T.M., Hunt, T.L., Lipo, C., Wilmshurst, J.M., 2011. The 13th century polynesian colonization of Hawai'i Island. Journal of Archaeological Science 38, 2740–2749.

Schmidt, I., Bradtmöller, M., Kehl, M., Pastoors, A., Tafelmaier, Y., Weninger, B., Weniger, G.-C., 2012. Rapid climate change and variability of settlement patterns in Iberia during the Late Pleistocene. Quat. Int. 274, 179–204.

Shennan, S., Downey, S.S., Timpson, A., Edinborough, K., Colledge, S., Kerig, T., Manning, K., Thomas, M.G., 2013. Regional population collapse followed initial agriculture booms in mid-Holocene Europe. Nat. Commun. 4, 2486.

Shennan, S., Edinborough, K., 2007. Prehistoric population history: from the Late Glacial to the Late Neolithic in Central and Northern Europe. J. Archaeol. Sci. 34, 1339–1345.

Smith, M.A., Ross, J., 2008. What happened at 1500—1000 cal. BP in Central Australia? Timing, impact and archaeological signatures. Holocene 18, 379–388.

Smith, M.A., Williams, A.N., Turney, C.S.M., Cupper, M.L., 2008. Human—environment interactions in Australian drylands: exploratory time-series analysis of archaeological records. Holocene 18, 389–401.

Steele, J., 2010. Radiocarbon dates as data: quantitative strategies for estimating colonization front speeds and event densities. Journal of Archaeological Science 37, 2017–2030.

Story, D.A., Valastro, S., 1977. Radiocarbon Dating and the George C. Davis Site, Texas. J. Field Archaeol. 4, 63–89.

Surovell, T.A., Brantingham, P.J., 2007. A note on the use of temporal frequency distributions in studies of prehistoric demography. J. Archaeol. Sci. 34, 1868–1877.

Surovell, T.A., Finley, J.B., Smith, G.M., Jeffrey Brantingham, P., Kelly, R., 2009. Correcting temporal frequency distributions for taphonomic bias. Journal of Archaeological Science 36, 1715–1724.

Surovell, T., Waguespack, N., Brantingham, P.J., 2005. Global archaeological evidence for proboscidean overkill. Proc. Natl. Acad. Sci. U. S. A. 102, 6231–6236.

Tallavaara, M., Pesonen, P., Oinonen, M., 2010. Prehistoric population history in eastern Fennoscandia. J. Archaeol. Sci. 37, 251–260.

Tallavaara, M., Seppä, H., 2012. Did the mid-Holocene environmental changes cause the boom and bust of hunter-gatherer population size in eastern Fennoscandia? Holocene 22, 215–225.

Timpson, A., Colledge, S., Crema, E., Edinborough, K., Kerig, T., Manning, K., Thomas, M.G., Shennan, S., 2014. Reconstructing regional population fluctuations in the European Neolithic using radiocarbon dates: a new case-study using an improved method. J. Archaeol. Sci. 52, 549–557.

Timpson, A., Manning, K., Shennan, S., 2015. Inferential mistakes in population proxies: A response to Torfing's "Neolithic population and summed probability distribution of 14C-dates." J. Archaeol. Sci. 63, 199–202.

Torfing, T., 2015. Neolithic population and summed probability distribution of 14C-dates. J. Archaeol. Sci. 63, 193–198.

Turney, C.S.M., Hobbs, D., 2006. ENSO influence on Holocene Aboriginal populations in Queensland, Australia. Journal of Archaeological Science 33, 1744–1748.

van Andel, T.H., 1998. Middle and Upper Palaeolithic environments and the calibration of 14C dates beyond 10,000 BP. Antiquity 72, 26–33.

van Andel, T.H., Davies, W., Weninger, B., Jöris, O., 2003. Archaeological dates as proxies for the

spatial and temporal human presence in Europe: a discourse on the method. Neanderthals and modern humans in the European landscape during the last glaciation 21–29.

Wang, C., Lu, H., Zhang, J., Gu, Z., He, K., 2014. Prehistoric demographic fluctuations in China inferred from radiocarbon data and their linkage with climate change over the past 50,000 years. Quat. Sci. Rev. 98, 45–59.

Wendland, W.M., Bryson, R.A., 1974. Dating Climatic Episodes of the Holocene. Quat. Res. 4, 9–24.

Whitehouse, N.J., Schulting, R.J., McClatchie, M., Barratt, P., McLaughlin, T.R., Bogaard, A., Colledge, S., Marchant, R., Gaffrey, J., Bunting, M.J., 2014. Neolithic agriculture on the European western frontier: the boom and bust of early farming in Ireland. J. Archaeol. Sci. 51, 181–205.

Wicks, K., Mithen, S., 2014. The impact of the abrupt 8.2 ka cold event on the Mesolithic population of western Scotland: a Bayesian chronological analysis using “activity events” as a population proxy. J. Archaeol. Sci. 45, 240-269.

Williams, A.N., 2013. A new population curve for prehistoric Australia. Proc. Biol. Sci. 280, 20130486.

Williams, A.N., 2012. The use of summed radiocarbon probability distributions in archaeology: a review of methods. J. Archaeol. Sci. 39, 578–589.

Williams, A.N., Ulm, S., Goodwin, I.D., Smith, M., 2010. Hunter-gatherer response to late Holocene climatic variability in northern and central Australia. Journal of Quaternary Science 25, 831–838.

Williams, A., Santoro, C.M., Smith, M.A., Latorre, C., 2008. El impacto de ENSO en el desierto de Atacama y la zona árida de Australia: análisis exploratorios de series temporales arqueológicas. chungara 245–259.

Zahid, H.J., Robinson, E., Kelly, R.L., 2016. Agriculture, population growth, and statistical analysis

of the radiocarbon record. Proc. Natl. Acad. Sci. U. S. A. 113, 931–935.

Zilhão, J., d'Errico, F., 1999. The Chronology and Taphonomy of the Earliest Aurignacian and Its Implications for the Understanding of Neandertal Extinction. Journal of World Prehistory 13, 1–68.

VI. Discussion and conclusion

Considering the variable of *time* to be fundamental in the study of human dispersals, this thesis has built a robust chronological framework using radiocarbon dating and Bayesian age modelling methods. This has enabled the elucidation of broad spatio-temporal patterns in the initial dispersal of humans into America, and the framing of current bio-cultural and climatic evidence. As outlined in Chapter I, the first underlying objective (a),

> *obtaining new radiocarbon measurements for Clovis, Clovis-coeval and/or pre-Clovis archaeological sites across the continent, and resolving the chronological uncertainty of key archaeological sites by producing reliable radiocarbon measurements using rigorous pretreatment methods,*

was accomplished by processing material from a total of 18 archaeological sites (Chapter III; Appendix A), from which a total of 143 bone samples were prescreened for collagen preservation, 203 samples were processed for radiocarbon dating, and 133 dates were obtained (Table 1). All sites and dates gave important insights into the research question, with the results of three already published in either first- (Anzick; Chapter III) or co-authored publications (Spirit Cave and Cooper's Ferry, Appendix B and C, respectively). Dating discrepancies at archaeological sites attesting to cultural activity and/or human predation on extinct fauna, were resolved using the single-amino-acid dating method described in Chapter II (Methods) and reference (158). This involved material from North American kill/butchery sites—Wally's Beach (222–225), Dent (1, 226–232), La Prele (233, 234), and Lindsay (235, 236)—and Anzick. I should note here that whereas I processed the Anzick material, the dating of the kill/butchery sites was part of a collaborative effort (Appendix D) and samples were processed by my co-authors at the ORAU. Hence, these data are not included in Table 1.

Table 1. Archaeological sites processed in this thesis, with the number of bone samples prescreened for collagen preservation, samples processed for radiocarbon dating, and radiocarbon dates obtained. Site descriptions, including materials, results and implications, are included Chapter III and Appendix A. Success rate (%), where multiple dates obtained for the same sample = 1 (in the case of Anzick and Hartley Mammoth). Arranged in alphabetical order.

Archaeological site	**Samples prescreened for collagen preservation**	**Samples processed for ^{14}C dating**	**Radiocarbon dates obtained**	**Success rate (%)**
Alexon Bison	0	1	0	0
Anzick	0	4	16	100
Blackwater Draw, Locality no. 1	20	3	0	0
Catalán Seco	0	2	2	100
Chiquihuite Cave, X-12 & -16	0	50	37	74
Cooper's Ferry	0	53	20	38
Cuchipuy	0	16	14	88
Eagle Cave	5	34	12	35
East Wenatchee	0	1	0	0
Gault	91	0	0	-
Guest Mammoth	0	1	0	0
Hartley Mammoth	0	1	3	100
Nials	6	6	6	100
PAIC-88	0	5	5	100
PAIC-91	0	11	11	100
Powars II	21	6	6	100
Spirit Cave	0	1	1	100
Tagua Tagua 1 & 2	0	8	0	0
Totals	**143**	**203**	**133**	**59**

For Anzick, the resolution of temporal discrepancies between Anzick-1 and the associated Clovis artifacts showed that both were coeval, keeping in line with the archaeological evidence and confirming the site' status as the only known Clovis burial. This has important implications for First Americans research, as the findings imply that the makers of Clovis were not the initial

arrivals to North America; aDNA research suggests the ancestral Native American lineage was already structured by the time Anzick-1 lived, having undergone likely in situ (129–131) divergence around 17.5-14.6 ka (129–134). This is consistent with the conclusions reached in Chapter IV, where it is suggested that the earliest dispersals into North America predate the geological age of Anzick-1 (12,905-12,695 cal BP at 95.4% confidence) and the estimated start of Clovis itself (14,210-13,495 cal BP at 95.4% confidence).

Along with Anzick, results from the redating of vertebrate fossils from kill/butchery sites (Appendix D) contributed toward the reliability of the chronological framework created (Chapter IV) and serve to highlight the importance of pretreatment methodology in the production of reliable results. In First Americans research, given the 'young' age of the period and the consequent diminished impact of modern contamination (the correlation is discussed in Chapter V), this tends to assume importance in the dating of heavily contaminated bone samples. In brief, this study found that out of seven bone samples processed using hydroxyproline (HYP) isolation and bulk collagen protocols, four showed discrepancies. This suggested that the latter had failed in removing modern-carbon contaminants cross-linked to the collagen. The new, more accurate HYP results generally coincided with previously-reported XAD-derived ages for these sites [see references (228, 237) for details on this method), with the exception of a sample (SR-6606) from Dent. In this case, the HYP protocol was either more efficient or dead carbon had contaminated the chromatography column during processing. Given the results for Anzick, where the XAD protocol underestimated the geological age of sample SR-8151 (Anzick-1), the former is most likely. The high-accuracy results provided reliable age estimates for these sites and confirmed their placement within (Wally's Beach, Dent, and La Prele) or before (Lindsay) the Clovis period [at the traditional span of 11,500 to 10,900 BP (32, 33)].

The second underlying objective (b),

> *using Bayesian age modelling to statistically integrate and assess archaeological and chronometric data (previously published and newly obtained) by building site-specific and large-scale models,*

was accomplished in Chapter IV through the compilation of chronometric data (n=705) from 39 Clovis, Clovis-coeval and pre-Clovis archaeological sites found across North America and Beringia; their statistical treatment through site-specific Bayesian modelling; and the creation of large-scale models centred on technological traditions and the spatial distribution of sites. The chronometric data was comprised of previously published measurements, as noted in the literature, and newly obtained radiocarbon measurements obtained through objective (a).

The third and final underlying objective (c),

> *assessing the reliability of the '^{14}C-dates-as-data' approach in the study of population dynamics in contrast to Bayesian age modelling,*

was addressed in Chapter V, where the ^{14}C-dates-as-data approach, the only other analysis that integrates quantitative methods and the radiocarbon record in the study of population dynamics, is assessed through a radiocarbon dating perspective. Here, potentially confounding biases introduced by challenges in laboratory processing—poor sample preservation and contamination—were considered, being the first instance of such discussion in the literature. Through this analysis, it is argued that if the assumptions on which the ^{14}C-dates-as-data method relies are untested or untestable, the reliability of the method itself should be questioned and other population proxies jointly used. Moreover, in case of questions pertaining directly to human dispersals, the use of Bayesian age modelling is advocated instead. This is because although summarizing radiocarbon dates to quantify and visualise their distribution is in itself a useful exercise (done here in Chapter IV, Figs. 2 and 3), the ^{14}C-dates-as-data approach removes

radiocarbon dates from their archaeological context and, in doing so, provides little insight into the archaeological record or human dispersal patterns. After all, a radiocarbon date on its own is a minimum-age estimate for an archaeological event and this, in turn, postdates human presence. Instead, Bayesian age modelling allows for the joint assessment of chronometric and archaeological evidence, can be employed to obtain quantitative age estimates of archaeological events and the commencement of single or multiple sequences, and, if including outlier analysis (217), assesses archaeological sites individually, objectively identifying and down-weighting outlier dates (see Chapters II, IV). Accordingly, the Bayesian approach is used in this thesis.

In summary, the work accomplished through objectives (a) and (b) enabled the creation of a chronological framework which, in tandem with current climatic and genetic evidence, allowed for the elucidation of broad spatio-temporal patterns and the proposal of a new peopling model. This, outlined in Chapter IV, suggests that the earliest arrivals to mid-latitude North America were probably maritime-adapted humans from eastern Asia, who most likely crossed near the end of the LGM, and is based on evidence indicating that although widespread occupation began during GI-1, humans were already present during or immediately after the LGM. Notably, this overturns the notion that North America was first penetrated only after 16-15,000 years ago (238). Moreover, for the first time, the synchronous commencement of Beringian, Clovis and Western Stemmed cultural traditions across North America was identified. Given that this coincides with last appearance dates for 18 extinct mammal genera, the possibility that human *expansion* was strongly correlated with the extinctions of North American Pleistocene fauna is raised.

6.1. Future research

6.1.1. South and Central America

Although this investigation has provided a chronological foundation with which to study the peopling of the Americas, the continued integration of new archaeo-chronometric evidence should strengthen the models and yield more reliable, meaningful results. In the future, research should be focused on Central and South America, where data are comparatively limited (13, 99–105) and require systematic attention (98). Improving our knowledge of early human presence in these regions is key to better understanding the settlement of America. After all, it was an archaeological site in Chile, South America, which effectively refuted the Clovis-first model and caused a shift in First Americans research. To this end, there are a number of archaeological sites with immediate potential for chronometric research—Taima Taima, Venezuela (239–242); Toca do Garrincho, Brazil (243–245), Lapa Vermelha IV, Brazil (246, 247); and Santana do Riacho, Brazil (248, 249). Taima Taima contains the remains of a butchered mastodon with associated lithic artifacts, dated in the 1970s to the late Pleistocene. The human-modified bone samples, however, have yet to be radiocarbon dated. In Toca do Garrincho, two human teeth were excavated from below a stalagmite dated to 10,020±290 (GIF-9335). The teeth were reported to have low collagen preservation and produced a date of 12,210 ± 40 BP (Beta-13604). This was obtained, however, on (as noted) carbon from the acid washes (243) and should be viewed as a minimum age. The same fraction was dated for the Lapa Vermelha skeleton, known as ‘Luzia’, yielding an age of 9,330 ± 60 BP (Beta-84439). In Santana do Riacho, a human skeleton and a possible hearth were dated to 11,960 ± 250 BP (GIF 5089) and 12,760 ± 70 (Beta 96759; bone collagen), correspondingly. The latter, however, is noted as being older than expected (248). Given the importance of these ancient individuals and their current chronological uncertainty, renewed attempts at collagen extraction and dating would be worthwhile. This is further emphasized by the Australasian genetic signal present in the region by 10.4 ka (129), which requires further testing (135).

6.1.2. Chiquihuite Cave

As described in Appendix A, Chiquihuite Cave (excavation areas X-12 and X-16), Zacatecas, is a high-altitude (2,740 m.a.s.l.) site with lithic artifacts located in pre- and post-LGM deposits (Appendix A, section 4). In X-12, radiocarbon and OSL measurements were obtained on samples closely related to artefacts found along the sequence (Appendix A, section 4, Fig. 7). These were included in a Bayesian age model that estimates the start of the sequence to 32,950-31,430 years cal BP (95.4% confidence level), and the end to 13,250-10,830 years cal BP (95.4% confidence level; Appendix A, section 4, Fig. 8). These results were incorporated into a co-authored manuscript submitted to *Nature* in August, 2018, which is currently under review and undergoing improvement. For this reason, Chiquihuite Cave was excluded from the Bayesian analysis in Chapter IV. However, as it stands, the antiquity and location of Chiquihuite Cave—around 5,500 km from eastern Beringia—suggest that humans first arrived in North America during MIS 3 [estimated to end at 29 ka (250)]. This departs from current genetic timelines that place the split between ancestral Native Americans and Siberian/East Asian populations at 25 ± 1.1 ka (130, 131), suggesting the existence of a yet unsampled human population. Given that, recently, an unknown group that likely diverged from Native Americans 30-22 ka was found (129), this is not beyond the realm of possibility. Only further investigations will be able to elucidate the connection between Chiquihuite ancestors and the ancestral Native American lineage. If unrelated, this implies a minimum of two separate human arrivals to North America during the Pleistocene, and the model presented in this thesis for the initial peopling of the Americas would require amending.

6.1.3. Changes in calibration

Updated calibration curves should be released some time in 2020. Although it is likely that the most drastic changes will occur in the older sections, age estimates exceeding the tree-ring

archive (>13,900 cal BP) (170) might also be affected. For the purpose of this study, this concerns the pre-Clovis period. The magnitude of this potential shift, however, is yet unknown. Its impact on the models here presented would have to be tested in the future and the conclusions duly amended.

6.2. Conclusion

Through the use of radiocarbon dating and Bayesian age modelling, this thesis has created a chronological framework for the initial dispersal of modern humans into America. This represents the first use of Bayesian age modeling to discern large-scale spatio-temporal patterns in the Americas, and provides a new, chronometry-centered model with which to study the peopling process and frame current genetic, cultural and climatic evidence. In the future, continued research in the First Americans field should test and improve the conclusions here drawn, adding to the chronological framework created. This, in itself, suggests exciting and interesting possibilities for what likely was a complex and dynamic peopling process. The key, moving forward, is to assess the data critically, yet equitably, with an emphasis placed on interdisciplinary collaboration. Ultimately, only time will further unfold the prehistoric landscape of America and tell the story of the first humans to enter it.

Bibliography

1. M. R. Waters, T. W. Stafford Jr, Redefining the age of Clovis: implications for the peopling of the Americas. *Science* **315**, 1122–1126 (2007).

2. G. Haynes, The Millennium before Clovis. *PaleoAmerica* **1**, 134–162 (2015).

3. T. D. Dillehay, *Monte Verde, a Late Pleistocene Settlement in Chile: The archaeological context and interpretation* (Smithsonian Institution Press, 1997).

4. T. J. Williams, D. B. Madsen, The Upper Paleolithic of the Americas. *PaleoAmerica*, 1–19 (2019).

5. D. H. Sandweiss, *et al.*, Quebrada jaguay: early south american maritime adaptations. *Science* **281**, 1830–1832 (1998).

6. T. Goebel, J. L. Keene, Are Great Basin stemmed points as old as Clovis in the Intermountain West? A review of the geochronological evidence. *Archaeology in the Great Basin and Southwest: Papers in Honor of Don D. Fowler*, 35–60 (2014).

7. R. Suárez, The Paleoamerican Occupation of the Plains of Uruguay: Technology, Adaptations, and Mobility. *PaleoAmerica* **1**, 88–104 (2015).

8. R. Suárez, J. M. López, Archaeology of the Pleistocene–Holocene transition in Uruguay: an overview. *Quat. Int.* **109–110**, 65–76 (2003).

9. C. Méndez, D. Jackson, R. Seguel, A. N. Delaunay, Early high-quality lithic procurement in the semiarid north of Chile. *Current Research in the Pleistocene* **27**, 19–21 (2010).

10. C. Méndez, D. Jackson, Terminal Pleistocene lithic technology and use of space in Central Chile. *Chungara, Revista de Antropología Chilena* (2015).

11. K. B. Jones, G. W. L. Hodgins, D. H. Sandweiss, Radiocarbon Chronometry of Site QJ-280, Quebrada Jaguay, a Terminal Pleistocene to Early Holocene Fishing Site in Southern Peru. *The Journal of Island and Coastal Archaeology*, 1–19 (2017).

12. E. J. Reitz, H. E. McInnis, D. H. Sandweiss, Others, Terminal Pleistocene and Early Holocene fishing strategies at Quebrada Jaguay and the Ring Site, southern Peru. *Journal of Archaeological Science: Reports* **8**, 447–453 (2016).

13. L. Bueno, A. S. Dias, J. Steele, The Late Pleistocene/Early Holocene archaeological record in Brazil: A geo-referenced database. *Quat. Int.* **301**, 74–93 (2013).

14. A. C. Roosevelt, *et al.*, Paleoindian Cave Dwellers in the Amazon: The Peopling of the Americas. *Science* **272**, 373–384 (1996).

15. D. J. Meltzer, *First Peoples in a New World: Colonizing Ice Age America* (University of California Press, 2009).

16. D. J. Meltzer, *The Great Paleolithic War: How Science Forged an Understanding of America's Ice Age Past* (University of Chicago Press, Chicago, 2015).

17. E. Sapir, "Time perspective in aboriginal American culture: a study in method" (Canada Department of Mines, 1916).

18. A. Hrdlička, "The origin and antiquity of the American Indian" in *Annual Report of the Board of Regents of the Smithsonian Institution Showing the Operations, Expenditures, and Condition of the Institution for the Year Ending June 30 1923*, Board of Regents of The Smithsonian Institution, Ed. (Washinton Government Printing Office, 1925), pp. 481–494.

19. B. G. Trigger, *A History of Archaeological Thought*, 2nd Ed. (Cambridge University Press, 2006).

20. H. J. Cook, New geological and paleontological evidence bearing on the antiquity of mankind in America. *Nat. Hist.* **27**, 240–247 (1927).

21. J. D. Figgins, H. J. Cook, *The antiquity of man in America* (American Museum of Natural History, 1927).

22. E. B. Howard, Association of artifacts with mammoth and bison in eastern New Mexico. *Science* **78**, 524 (1933).

23. E. B. Howard, The Occurrence of Flints and Extinct Animals in Pluvial Deposits near Clovis, New Mexico. Part I: Introduction. *Proceedings of the Academy of Natural Sciences of Philadelphia* **87**, 299–303 (1935).

24. C. D. Howard, The Clovis Point: Characteristics and Type Description. *Plains Anthropol.* **35**, 255–262 (1990).

25. D. Stanford, R. Bonnichsen, B. Meggers, D. G. Steele, "Paleoamerican origins: Models, evidence, and future directions" in *Paleoamerican Origins: Beyond Clovis*, R. Bonnichsen, B. T. Lepper, D. Stanford, M. R. Waters, Eds. (The Center for the Study of First Americans, Texas A&M, College Station, 2005), pp. 313–353.

26. A. M. Smallwood, T. A. Jennings, *Clovis: On the Edge of a New Understanding* (Texas A&M University Press, 2014).

27. E. Antevs, The Spread of Aboriginal Man to North America. *Geogr. Rev.* **25**, 302–309 (1935).

28. P. S. Martin, Pleistocene ecology and biogeography of North America. *U. Of Arizona. Program in Geochronology. Contrib* **9**, 375–420 (1958).

29. P. S. Martin, The discovery of America. *Science* **179**, 969–974 (1973).

30. D. K. Grayson, D. J. Meltzer, A requiem for North American overkill. *J. Archaeol. Sci.* **30**, 585–593 (2003).

31. G. Haynes, Extinctions in North America's Late Glacial landscapes. *Quat. Int.* **285**, 89–98 (2013).

32. C. V. Haynes, Contributions of Radiocarbon Dating to the Geochronology of the Peopling of the New World in *Radiocarbon After Four Decades*, (Springer New York, 1992), pp. 355–374.

33. C. V. Haynes, D. J. Donahue, A. J. T. Jull, T. H. Zabel, Application of accelerator dating to fluted points in Paleoindian sites. *Archaeology of Eastern North America* **12**, 184–191 (1984).

34. M. M. Prasciunas, T. A. Surovell, Reevaluating the duration of Clovis: The problem of non-representative radiocarbon. *Clovis: on the edge of a new understanding*, 21–35 (2015).

35. D. J. Meltzer, *et al.*, On the Pleistocene Antiquity of Monte Verde, Southern Chile. *Am. Antiq.* **62**, 659–663 (1997).

36. J. Chappell, J. Head, J. Magee, Beyond the radiocarbon limit in Australian archaeology and Quaternary research. *Antiquity* **70**, 543–552 (1996).

37. T. Higham, European Middle and Upper Palaeolithic radiocarbon dates are often older than they look: problems with previous dates and some remedies. *Antiquity* **85**, 235–249 (2011).

38. A. D. Krieger, Early man in the New World. *Prehistoric man in the New World*, 23–81 (1964).

39. J. M. Adovasio, J. D. Gunn, J. Donahue, R. Stuckenrath, Meadowcroft Rockshelter, 1977: An Overview. *Am. Antiq.* **43**, 632–651 (1978).

40. J. M. Adovasio, J. D. Gunn, J. Donahue, R. Stuckenrath, Excavations at Meadowcroft Rockshelter, 1973-1974: A Progress Report. *Pennsylvania Archaeologist* **45**, 1–30 (1975).

41. J. M. Adovasio, J. Donahue, R. Stuckenrath, The Meadowcroft Rockshelter Radiocarbon Chronology 1975-1990. *Am. Antiq.* **55**, 348–354 (1990).

42. J. M. Adovasio, D. R. Pedler, J. Donahue, R. Stuckenrath, Two Decades of Debate on Meadowcroft Rockshelter. *North American Archaeologist* **19**, 317–341 (1998).

43. C. V. Haynes, Paleoindian Charcoal from Meadowcroft Rockshelter: Is Contamination a Problem? *Am. Antiq.* **45**, 582–587 (1980).

44. P. Goldberg, T. L. Arpin, Micromorphological Analysis of Sediments from Meadowcroft Rockshelter, Pennsylvania: Implications for Radiocarbon Dating. *J. Field Archaeol.* **26**, 325–342 (1999).

45. S. J. Fiedel, The Anzick genome proves Clovis is first, after all. *Quat. Int.* **444**, 4–9 (2017).

46. R. L. Kelly, Maybe we do know when people first came to North America; and what does it mean if we do? *Quat. Int.* **109–110**, 133–145 (2003).

47. L. E. Lisiecki, M. E. Raymo, A Pliocene-Pleistocene stack of 57 globally distributed benthic δ18O records. *Paleoceanography* **20** (2005).

48. V. V. Pitulko, *et al.*, The Yana RHS site: humans in the Arctic before the last glacial maximum. *Science* **303**, 52–56 (2004).

49. A. E. Basilyan, M. A. Anisimov, P. A. Nikolskiy, V. V. Pitulko, Wooly mammoth mass accumulation next to the Paleolithic Yana RHS site, Arctic Siberia: its geology, age, and relation to past human activity. *J. Archaeol. Sci.* **38**, 2461–2474 (2011).

50. P. Nikolskiy, V. Pitulko, Evidence from the Yana Palaeolithic site, Arctic Siberia, yields clues to the riddle of mammoth hunting. *J. Archaeol. Sci.* **40**, 4189–4197 (2013).

51. V. V. Pitulko, *et al.*, Paleoanthropology. Early human presence in the Arctic: Evidence from 45,000-year-old mammoth remains. *Science* **351**, 260–263 (2016).

52. T. Goebel, M. R. Waters, 2. Margarita Dikova, The Archaeology of Ushki Lake, Kamchatka, and the Pleistocene Peopling of the Americas. *Science* **301** (2003).

53. L. Bourgeon, A. Burke, T. Higham, Earliest Human Presence in North America Dated to the Last Glacial Maximum: New Radiocarbon Dates from Bluefish Caves, Canada. *PLoS One* **12**, e0169486 (2017).

54. J. Cinq-Mars, R. E. Morlan, "Bluefish Caves and Old Crow Basin: A New Rapport" in *Ice Age People of North America: Environments, Origins, and Adaptations*, R. Bonnichsen, K. L. Turnmire, Eds. (Oregon State University Press, 1999), pp. 200–212.

55. R. E. Morlan, D. E. Nelson, T. A. Brown, J. S. Vogel, J. R. Southon, Accelerator Mass Spectrometry Dates on Bones from Old Crow Basin, Northern Yukon Territory. *Canadian Journal of Archaeology / Journal Canadien d'Archéologie* **14**, 75–92 (1990).

56. R. E. Morlan, Current perspectives on the Pleistocene archaeology of eastern Beringia. *Quat. Res.* **60**, 123–132 (2003).

57. T. Goebel, M. R. Waters, D. H. O'Rourke, The late Pleistocene dispersal of modern humans in the Americas. *Science* **319**, 1497–1502 (2008).

58. W. R. Powers, J. F. Hoffecker, Late Pleistocene Settlement in the Nenana Valley, Central Alaska. *Am. Antiq.* **54**, 263–287 (1989).

59. J. F. Hoffecker, Late Pleistocene and Early Holocene Sites in the Nenana River Valley, Central Alaska. *Arctic Anthropol.* **38**, 139–153 (2001).

60. C. E. Holmes, Tanana River Valley Archaeology circa 14,000 to 9000 B.P. *Arctic Anthropol.* **38**, 154–170 (2001).

61. T. Goebel, R. Powers, N. Bigelow, "The Nenana Complex of Alaska and Clovis Origins" in *Clovis Origins and Adaptations*, R. Bonnichsen, K. Turnmire, Eds. (Center for the Study of the First Americans, 1991), pp. 49–79.

62. M. L. Kunz, R. E. Reanier, The Mesa Site: A Paleoindian Hunting Lookout in Arctic Alaska. *Arctic Anthropol.* **32**, 5–30 (1995).

63. R. E. Reanier, The Antiquity of Paleoindian Materials in Northern Alaska. *Arctic Anthropol.* **32**, 31–50 (1995).

64. J. F. Hoffecker, S. A. Elias, *Human Ecology of Beringia* (Columbia University Press, 2007).

65. P. U. Clark, *et al.*, The Last Glacial Maximum. *Science* **325**, 710–714 (2009).

66. A. C. Mix, E. Bard, R. Schneider, Environmental processes of the ice age: land, oceans, glaciers (EPILOG). *Quat. Sci. Rev.* **20**, 627–657 (2001).

67. A. S. Dyke, An outline of North American deglaciation with emphasis on central and northern Canada. *Developments in Quaternary Sciences* **2**, 373–424 (2004).

68. M. W. Pedersen, *et al.*, Postglacial viability and colonization in North America's ice-free corridor. *Nature* **537**, 45–49 (2016).

69. P. D. Heintzman, *et al.*, Bison phylogeography constrains dispersal and viability of the Ice Free Corridor in western Canada. *Proc. Natl. Acad. Sci. U. S. A.* **113**, 8057–8063 (2016).

70. J. K. Feathers, E. J. Rhodes, S. Huot, J. M. Mcavoy, Luminescence dating of sand deposits related to late Pleistocene human occupation at the Cactus Hill Site, Virginia, USA. *Quat. Geochronol.* **1**, 167–187 (2006/8).

71. J. M. McAvoy, L. D. McAvoy, *Archaeological Investigations of Site 44SX202, Cactus Hill, Sussex County, Virginia* (Department of Historic Resources, 1997).

72. M. T. P. Gilbert, *et al.*, DNA from pre-Clovis human coprolites in Oregon, North America. *Science* **320**, 786–789 (2008).

73. D. L. Jenkins, *et al.*, Clovis age Western Stemmed projectile points and human coprolites at the Paisley Caves. *Science* **337**, 223–228 (2012).

74. M. R. Waters, *et al.*, Pre-Clovis Mastodon Hunting 13,800 Years Ago at the Manis Site, Washington. *Science* **334**, 351–353 (2011).

75. M. R. Waters, S. L. Forman, T. W. Stafford Jr., J. Foss, Geoarchaeological investigations at the Topper and Big Pine Tree sites, Allendale County, South Carolina. *J. Archaeol. Sci.* **36**, 1300–1311 (2009/7).

76. J. J. Halligan, *et al.*, Pre-Clovis occupation 14,550 years ago at the Page-Ladson site, Florida, and the peopling of the Americas. *Sci Adv* **2**, e1600375 (2016).

77. M. R. Waters, *et al.*, The Buttermilk Creek complex and the origins of Clovis at the Debra L. Friedkin site, Texas. *Science* **331**, 1599–1603 (2011).

78. K. Rodrigues, *et al.*, OSL ages of the Clovis, Late Paleoindian, and Archaic components at Area 15 of the Gault Site, Central Texas, U.S.A. *Journal of Archaeological Science: Reports* **7**, 94–103 (2016).

79. L. E. Vilsack, "Investigations of Area 12: Gault Site," Texas State University, San Marcos. (2016).

80. J. L. Gandy, "Analysis of the lithic debitage from the older-than-Clovis stratigraphic layers of the Gault site, Texas," Texas State University, San Marcos. (2013).

81. M. Collins, NSF Technical Report: "ProtoClovis" or "PreClovis"? Investigating Cultural Antecedents of Clovis at the Gault Site, Texas (2015).

82. M. B. Collins, The Gault Site, Texas, and Clovis research. *Athena Review* **3**, 31–42 (2002).

83. D. J. Joyce, “Pre-Clovis megafauna butchery sites in the western Great Lakes region, USA” in *Paleoamerican Odyssey*, K. E. Graf, C. V. Ketron, M. R. Waters, Eds. (Center for the Study of the First Americans, Texas A&M University, College Station, 2013), pp. 467–483.

84. D. F. Overstreet, M. F. Kolb, Geoarchaeological contexts for Late Pleistocene archaeological sites with human-modified woolly mammoth remains in southeastern Wisconsin, U.S.A. *Geoarchaeology* **18**, 91–114 (2003).

85. D. J. Joyce, Chronology and new research on the Schaefer mammoth (?Mammuthus primigenius) site, Kenosha County, Wisconsin, USA. *Quat. Int.* **142**, 44–57 (2006).

86. J. M. Erlandson, *et al.*, The Kelp Highway Hypothesis: Marine Ecology, the Coastal Migration Theory, and the Peopling of the Americas. *The Journal of Island and Coastal Archaeology* **2**, 161–174 (2007).

87. J. M. Erlandson, T. J. Braje, From Asia to the Americas by boat? Paleogeography, paleoecology, and stemmed points of the northwest Pacific. *Quat. Int.* **239**, 28–37 (2011).

88. K. R. Fladmark, The feasibility of the northwest coast as a migration route for early man. *Early man in America from a circum-Pacific perspective*, 119–128 (1978).

89. K. R. Fladmark, Routes: Alternate Migration Corridors for Early Man in North America. *Am. Antiq.* **44**, 55–69 (1979).

90. C. Beck, G. T. Jones, Clovis and Western Stemmed: Population Migration and the Meeting of Two Technologies in the Intermountain West. *Am. Antiq.* **75**, 81–116 (2010).

91. E. James Dixon, F. J. Dixon, *Bones, Boats & Bison: Archeology and the First Colonization of Western North America* (UNM Press, 1999).

92. E. James Dixon, Human colonization of the Americas: timing, technology and process. *Quat. Sci. Rev.* **20**, 277–299 (2001).

93. N. A. Easton, Mal de Mer above Terra Incognita, or, “What Ails the Coastal Migration Theory?” *Arctic Anthropol.* **29**, 28–41 (1992).

94. C. A. S. Mandryk, H. Josenhans, D. W. Fedje, R. W. Mathewes, Late Quaternary paleoenvironments of Northwestern North America: implications for inland versus coastal migration routes. *Quat. Sci. Rev.* **20**, 301–314 (2001).

95. R. Gruhn, The Pacific Coast route of initial entry: an overview. *Method and Theory for Investigating the Peopling of the Americas*, 249–256 (1994).

96. L. G. Davis, *et al.*, Late Upper Paleolithic Occupation at Cooper's Ferry, Idaho, USA Shows Americas Settled Before ~16,000 Years Ago. *Science* (2019).

97. G. Politis, L. Prates, S. I. Perez, "Early Asiatic Migration to the Americas: A View from South America" in *Mobility and Ancient Society in Asia and the Americas*, M. D. Frachetti, R. N. Spengler III, Eds. (Springer International Publishing, 2015), pp. 89–102.

98. L. A. Borrero, Ambiguity and Debates on the Early Peopling of South America. *PaleoAmerica* **2**, 11–21 (2016).

99. L. Bueno, L. Prates, G. G. Politis, J. Steele, A Late Pleistocene/early Holocene archaeological 14C database for South America and the Isthmus of Panama: Palaeoenvironmental contexts and demographic interpretations. *Quat. Int.*, 1–2 (2013).

100. R. Cooke, A. Ranere, G. Pearson, R. Dickau, Radiocarbon chronology of early human settlement on the Isthmus of Panama (13,000–7000 BP) with comments on cultural affinities, environments, subsistence, and technological change. *Quat. Int.* **301**, 3–22 (2013).

101. K. Rademaker, G. R. M. Bromley, D. H. Sandweiss, Peru archaeological radiocarbon database, 13,000–7000 14C B.P. *Quat. Int.* **301**, 34–45 (2013).

102. J. M. Capriles, J. Albarracin-Jordan, The earliest human occupations in Bolivia: A review of the archaeological evidence. *Quat. Int.* **301**, 46–59 (2013).

103. C. Méndez Melgar, Terminal Pleistocene/early Holocene 14C dates form archaeological sites in Chile: Critical chronological issues for the initial peopling of the region. *Quat. Int.* **301**, 60–73 (2013).

104. J. M. López Mazz, Early human occupation of Uruguay: Radiocarbon database and archaeological implications. *Quat. Int.* **301**, 94–103 (2013).

105. L. Prates, G. Politis, J. Steele, Radiocarbon chronology of the early human occupation of Argentina. *Quat. Int.* **301**, 104–122 (2013).

106. D. J. Meltzer, J. M. Adovasio, T. D. Dillehay, On a Pleistocene human occupation at Pedra Furada, Brazil. *Antiquity* **68**, 695–714 (1994).

107. T. D. Dillehay, *et al.*, New Archaeological Evidence for an Early Human Presence at Monte Verde, Chile. *PLoS One* **10**, e0141923 (2015).

108. F. J. Aceituno, N. Loaiza, M. E. Delgado-Burbano, G. Barrientos, The initial human settlement of Northwest South America during the Pleistocene/Holocene transition: Synthesis and perspectives. *Quat. Int.* **301**, 23–33 (2013).

109. R. A. Farina, *et al.*, Arroyo del Vizcaino, Uruguay: a fossil-rich 30-ka-old megafaunal locality with cut-marked bones. *Proceedings of the Royal Society B: Biological Sciences* **281**, 20132211–20132211 (2013).

110. C. Lahaye, *et al.*, Another site, same old song: The Pleistocene-Holocene archaeological sequence of Toca da Janela da Barra do Antonião-North, Piauí, Brazil. *Quat. Geochronol.* **49**, 223–229 (2019).

111. C. Bayón, T. Manera, G. Politis, S. Aramayo, Following the Tracks of the First South Americans. *Evolution: Education and Outreach* **4**, 205–217 (2011).

112. L. Núñez, J. Varela, R. Casamiquela, C. Villagrán, Reconstruccion Multidisciplinaria de la Ocupacion Prehistorica de Quereo, Centro de Chile. *Latin American Antiquity* **5**, 99–118 (1994).

113. T. D. Dillehay, *et al.*, A late pleistocene human presence at Huaca Prieta, Peru, and early Pacific Coastal adaptations. *Quat. Res.* **77**, 418–423 (2012).

114. T. D. Dillehay, *et al.*, Simple technologies and diverse food strategies of the Late Pleistocene and Early Holocene at Huaca Prieta, Coastal Peru. *Sci Adv* **3**, e1602778 (2017).

115. R. Casamiquela, J. Montané, R. Santana, Convivencia del hombre con el mastodonte en Chile central. *Noticiario Mensual del Museo Nacional de Historia Natural* **11**, 1–6 (1967).

116. J. Montané, Paleo-Indian remains from laguna de tagua tagua, central chile. *Science* **161**, 1137–1138 (1968).

117. L. Nuñez, *et al.*, Cuenca de Taguatagua en Chile: el ambiente del Pleistoceno superior y ocupaciones humanas. *Revista Chilena de Historia Natural* **67**, 503–519 (1994).

118. D. Jackson, C. Méndez, L. Núñez, D. Jackson, Procesamiento de fauna extinta durante la transición Pleistoceno-Holoceno en el centro-norte de Chile. *Boletín de Arqueología PUCP*, 315–336 (2011).

119. J. Montane, Primera fecha radiocarbónica de Tagua-Tagua. *Not. Mens. Mus. Nac. Hist. Nat.* **139** (1968).

120. D. Jackson, C. Méndez, R. Seguel, A. Maldonado, G. Vargas, Initial Occupation of the Pacific Coast of Chile during Late Pleistocene Times. *Curr. Anthropol.* **48**, 725–731 (2007).

121. A. C. Roosevelt, Relatório preliminar sobre o levantamento e escavações na Caverna da Pedra Pintada, Monte Alegre, Pará, Brasil. *Segunda etapa de campo do projeto arqueológico Santarém* (1991).

122. M. Michab, *et al.*, Luminescence dates for the Paleoindian site of Pedra Pintada, Brazil. *Quat. Sci. Rev.* **17**, 1041–1046 (1998).

123. R. Suárez, High resolution AMS 14C dates for late Pleistocene Fishtail technology from the Tigre site, Uruguay river basin, South America. *Quat. Sci. Rev.* **213**, 155–161 (2019).

124. K. E. Stothert, D. R. Piperno, T. C. Andres, Terminal Pleistocene/Early Holocene human adaptation in coastal Ecuador: the Las Vegas evidence. *Quat. Int.* **109–110**, 23–43 (2003).

125. M. R. Waters, T. Amorosi, T. W. Stafford, Redating Fell's Cave, Chile and the Chronological Placement of the Fishtail Projectile Point. *Am. Antiq.* **80**, 376–386 (2015).

126. T. D. Dillehay, J. Rossen, G. Maggard, K. Stackelbeck, P. Netherly, Localization and possible social aggregation in the Late Pleistocene and Early Holocene on the north coast of Perú. *Quat. Int.* **109–110**, 3–11 (2003).

127. C. Weitzel, N. Mazzia, N. Flegenheimer, Assessing Fishtail points distribution in the southern Cone. *Quat. Int.* **473**, 161–172 (2018).

128. A. Lourdeau, Lithic Technology and Prehistoric Settlement in Central and Northeast Brazil: Definition and Spatial Distribution of the Itaparica Technocomplex. *PaleoAmerica* **1**, 52–67 (2015).

129. J. V. Moreno-Mayar, *et al.*, Early human dispersals within the Americas. *Science* **362**, eaav2621 (2018).

130. M. Raghavan, *et al.*, Genomic evidence for the Pleistocene and recent population history of Native Americans. *Science* **349**, aab3884 (2015).

131. J. V. Moreno-Mayar, *et al.*, Terminal Pleistocene Alaskan genome reveals first founding population of Native Americans. *Nature* **553**, 203–207 (2018).

132. M. Rasmussen, *et al.*, The genome of a Late Pleistocene human from a Clovis burial site in western Montana. *Nature* **506**, 225–229 (2014).

133. D. Reich, *et al.*, Reconstructing Native American population history. *Nature* **488**, 370–374 (2012).

134. C. L. Scheib, *et al.*, Ancient human parallel lineages within North America contributed to a coastal expansion. *Science* **360**, 1024–1027 (2018).

135. C. Posth, *et al.*, Reconstructing the Deep Population History of Central and South America. *Cell* **175**, 1185–1197.e22 (2018).

136. B. Llamas, *et al.*, Ancient mitochondrial DNA provides high-resolution time scale of the peopling of the Americas. *Sci Adv* **2**, e1501385 (2016).

137. S. L. Bonatto, F. M. Salzano, A single and early migration for the peopling of the Americas supported by mitochondrial DNA sequence data. *Proc. Natl. Acad. Sci. U. S. A.* **94**, 1866–1871 (1997).

138. E. Tamm, *et al.*, Beringian standstill and spread of Native American founders. *PLoS One* **2**, e829 (2007).

139. P. Skoglund, D. Reich, A genomic view of the peopling of the Americas. *Current Opinion in Genetics & Development* **41**, 27–35 (2016).

140. S. de Azevedo, M. Quinto-Sánchez, C. Paschetta, R. González-José, The first human settlement of the New World: A closer look at craniofacial variation and evolution of early and late Holocene Native American groups. *Quat. Int.* **431, Part B**, 152–167 (2017).

141. M. A. Taylor, I. L. Hendy, D. K. Pak, Deglacial ocean warming and marine margin retreat of the Cordilleran Ice Sheet in the North Pacific Ocean. *Earth Planet. Sci. Lett.* **403**, 89–98 (2014).

142. P. Skoglund, *et al.*, Genetic evidence for two founding populations of the Americas. *Nature* **525**, 104–108 (2015).

143. V. Battaglia, *et al.*, The first peopling of South America: new evidence from Y-chromosome haplogroup Q. *PLoS One* **8**, e71390 (2013).

144. M. Sikora, *et al.*, The population history of northeastern Siberia since the Pleistocene. *Nature* **570**, 182–188 (2019).

145. M. Raghavan, *et al.*, Upper Palaeolithic Siberian genome reveals dual ancestry of Native Americans. *Nature* **505**, 87–91 (2014).

146. S. González, *et al.*, Earliest humans in the Americas: new evidence from Mexico. *J. Hum. Evol.* **44**, 379–388 (2003).

147. A. González, *et al.*, The first human settlers on the Yucatán Peninsula: evidence from drowned caves in the state of Quintana Roo (South Mexico). *PaleoAmerican Odyssey. Center for the Study of the First Americans, Orono*, 323–337 (2013).

148. W. A. Neves, *et al.*, "Early human occupation of Lagoa Santa, eastern central Brazil: craniometric variation of the initial settlers of south america" in *Paleoamerican Odyssey*, K. E. Graf, C. V. Ketron, M. R. Waters, Eds. (Center for the Study of the First Americans, Texas A&M University, College Station, 2013), pp. 397–414.

149. A. Marangoni, D. Caramelli, G. Manzi, Homo sapiens in the Americas. Overview of the earliest human expansion in the New World. *J. Anthropol. Sci.* **92**, 79–97 (2014).

150. D. Jackson, C. Méndez, M. de Saint Pierre, E. Aspillaga, G. G. Politis, Direct Dates and mtDNA of Late Pleistocene Human Skeletons from South America: A Comment on Chatters et al. (2014). *PaleoAmerica* **1**, 213–216 (2015).

151. W. A. Neves, M. Hubbe, G. Correal, Human skeletal remains from Sabana de Bogotá, Colombia: A case of Paleoamerican morphology late survival in South America? *Am. J. Phys. Anthropol.* **133**, 1080–1098 (2007).

152. W. A. Neves, H. M. Pucciarelli, Morphological affinities of the first Americans: an exploratory analysis based on early South American human remains. *J. Hum. Evol.* **21**, 261–273 (1991).

153. W. A. Neves, M. Hubbe, Cranial morphology of early Americans from Lagoa Santa, Brazil: implications for the settlement of the New World. *Proc. Natl. Acad. Sci. U. S. A.* **102**, 18309–18314 (2005).

154. D. G. Steele, J. F. Powell, Paleobiology of the first Americans. *Evol. Anthropol.* **2**, 138–146 (1993).

155. N. von Cramon-Taubadel, A. Strauss, M. Hubbe, Evolutionary population history of early Paleoamerican cranial morphology. *Sci Adv* **3**, e1602289 (2017).

156. R. González-José, M. C. Bortolini, F. R. Santos, S. L. Bonatto, The peopling of America: craniofacial shape variation on a continental scale and its interpretation from an interdisciplinary view. *Am. J. Phys. Anthropol.* **137**, 175–187 (2008).

157. S. de Azevedo, *et al.*, Evaluating microevolutionary models for the early settlement of the New World: the importance of recurrent gene flow with Asia. *Am. J. Phys. Anthropol.* **146**, 539–552 (2011).

158. T. Deviese, D. Comeskey, J. McCullagh, C. Bronk Ramsey, T. Higham, New protocol for compound specific radiocarbon analysis of archaeological bones. *Rapid Commun. Mass Spectrom.* **32**, 373–379 (2017).

159. T. Devièse, *et al.*, Direct dating of Neanderthal remains from the site of Vindija Cave and implications for the Middle to Upper Paleolithic transition. *Proc. Natl. Acad. Sci. U. S. A.* **114**, 10606–10611 (2017).

160. A. Marom, J. S. O. McCullagh, T. F. G. Higham, A. A. Sinitsyn, R. E. M. Hedges, Single amino acid radiocarbon dating of Upper Paleolithic modern humans. *Proc. Natl. Acad. Sci. U. S. A.* **109**, 6878–6881 (2012).

161. S. Nalawade-Chavan, *et al.*, New single amino acid hydroxyproline radiocarbon dates for two problematic American Mastodon fossils from Alaska. *Quat. Geochronol.* **20**, 23–28 (2014).

162. N. Reynolds, R. Dinnis, A. A. Bessudnov, T. Devièse, T. Higham, The Kostënki 18 child burial and the cultural and funerary landscape of Mid Upper Palaeolithic European Russia. *Antiquity* **91**, 1435–1450 (2017).

163. M. Sikora, A. Seguin-Orlando, V. C. Sousa, Ancient genomes show social and reproductive behavior of early Upper Paleolithic foragers (2017).

164. T. Higham, *et al.*, The timing and spatiotemporal patterning of Neanderthal disappearance. *Nature* **512**, 306–309 (2014).

165. J. R. Arnold, W. F. Libby, Age determinations by radiocarbon content; checks with samples of known age. *Science* **110**, 678–680 (1949).

166. W. F. Libby, E. C. Anderson, J. R. Arnold, Age Determination by Radiocarbon Content: World-Wide Assay of Natural Radiocarbon. *Science* **109**, 227–228 (1949).

167. H. Godwin, Half-life of Radiocarbon. *Nature* **195**, 984–984 (1962).

168. D. E. Vries, H, Variation in concentration of radiocarbon with time and location on earth. *Proc. K. Ned. Akad. Wet. C* **61**, 1–9 (1958).

169. M. Stuiver, H. E. Suess, On the Relationship Between Radiocarbon Dates and True Sample Ages. *Radiocarbon* **8**, 534–540 (1966).

170. P. J. Reimer, *et al.*, IntCal13 and Marine13 Radiocarbon Age Calibration Curves 0–50,000 Years cal BP. *Radiocarbon* **55**, 1869–1887 (2013).

171. A. G. Hogg, *et al.*, SHCal13 Southern Hemisphere Calibration, 0–50,000 Years cal BP. *Radiocarbon* **55**, 1889–1903 (2013).

172. E. Q. Alves, K. Macario, P. Ascough, The worldwide marine radiocarbon reservoir effect: definitions, mechanisms, and prospects. *Reviews of* (2018).

173. F. Brock, T. Higham, P. Ditchfield, C. Bronk Ramsey, Current Pretreatment Methods for AMS Radiocarbon Dating at the Oxford Radiocarbon Accelerator Unit (Orau). *Radiocarbon* **52**, 103–112 (2010).

174. C. B. Ramsey, T. Higham, P. Leach, Towards High-Precision AMS: Progress and Limitations. *Radiocarbon* **46**, 17–24 (2004).

175. A. Sillen, J. Parkington, Diagenesis of Bones from Eland's Bay Cave. *J. Archaeol. Sci.* **23**, 535–542 (1996).

176. F. Brock, T. Higham, C. Bronk Ramsey, Pre-screening techniques for identification of samples suitable for radiocarbon dating of poorly preserved bones. *J. Archaeol. Sci.* **37**, 855–865 (2010).

177. F. Brock, *et al.*, Reliability of Nitrogen Content (%N) and Carbon:Nitrogen Atomic Ratios (C:N) as Indicators of Collagen Preservation Suitable for Radiocarbon Dating. *Radiocarbon* **54**, 879–886 (2012).

178. M. J. DeNiro, S. Weiner, Chemical, enzymatic and spectroscopic characterization of "collagen" and other organic fractions from prehistoric bones. *Geochim. Cosmochim. Acta* **52**, 2197–2206 (1988).

179. G. J. van Klinken, Bone Collagen Quality Indicators for Palaeodietary and Radiocarbon Measurements. *J. Archaeol. Sci.* **26**, 687–695 (1999).

180. R. E. M. Hedges, G. J. Van Klinken, A Review of Current Approaches in the Pretreatment of Bone for Radiocarbon Dating by AMS. *Radiocarbon* **34**, 279–291 (1992).

181. R. Longin, New method of collagen extraction for radiocarbon dating. *Nature* **230**, 241–242 (1971).

182. T. A. Brown, D. E. Nelson, J. S. Vogel, J. R. Southon, Improved Collagen Extraction by Modified Longin Method. *Radiocarbon* **30**, 171–177 (1988).

183. M. Dee, C. Bronk Ramsey, Refinement of graphite target production at ORAU. *Nuclear Instruments and Methods in Physics Research Section B: Beam Interactions with Materials and Atoms* **172**, 449–453 (2000).

184. R. E. Wood, C. Bronk Ramsey, T. F. G. Higham, Refining Background Corrections for Radiocarbon Dating of Bone Collagen at Orau. *Radiocarbon* **52**, 600–611 (2010).

185. C. Bronk Ramsey, Development of the radiocarbon program OxCal. *Radiocarbon* **43**, 355–363 (2001).

186. S. O. Rasmussen, *et al.*, A new Greenland ice core chronology for the last glacial termination. *J. Geophys. Res.* **111**, 527 (2006).

187. S. O. Rasmussen, *et al.*, A stratigraphic framework for abrupt climatic changes during the Last Glacial period based on three synchronized Greenland ice-core records: refining and extending the INTIMATE event stratigraphy. *Quat. Sci. Rev.* **106**, 14–28 (2014).

188. J. van der Plicht, E. Jansma, H. Kars, The "Amsterdam Castle": A Case Study of Wiggle Matching and the Proper Calibration Curve. *Radiocarbon* **37**, 965–968 (1995).

189. F. G. McCormac, A. Bayliss, D. M. Brown, P. J. Reimer, M. M. Thompson, Extended Radiocarbon Calibration in the Anglo-Saxon Period, AD 395–485 and AD 735–805. *Radiocarbon* **50**, 11–17 (2008).

190. A. Hogg, J. Palmer, G. Boswijk, P. Reimer, D. Brown, Investigating the Interhemispheric 14C Offset in the 1st Millennium AD and Assessment of Laboratory Bias and Calibration Errors. *Radiocarbon* **51**, 1177–1186 (2009).

191. R. E. Taylor, J. Southon, Reviewing the Mid-First Millennium BC 14C "warp" using 14C/ bristlecone pine data. *Nucl. Instrum. Methods Phys. Res. B* **294**, 440–443 (2013).

192. J. W. Beck, *et al.*, Extremely large variations of atmospheric 14C concentration during the last glacial period. *Science* **292**, 2453–2458 (2001).

193. D. L. Hoffmann, *et al.*, Towards radiocarbon calibration beyond 28ka using speleothems from the Bahamas. *Earth Planet. Sci. Lett.* **289**, 1–10 (2010).

194. J. Southon, A. L. Noronha, H. Cheng, R. L. Edwards, Y. Wang, A high-resolution record of atmospheric 14C based on Hulu Cave speleothem H82. *Quat. Sci. Rev.* **33**, 32–41 (2012).

195. R. G. Fairbanks, *et al.*, Radiocarbon calibration curve spanning 0 to 50,000 years BP based on paired 230Th/234U/238U and 14C dates on pristine corals. *Quat. Sci. Rev.* **24**, 1781–1796 (2005).

196. N. Durand, *et al.*, Comparison of 14C and U-Th Ages in Corals from IODP #310 Cores Offshore Tahiti. *Radiocarbon* **55**, 1947–1974 (2013).

197. E. Bard, M. Arnold, B. Hamelin, N. Tisnerat-Laborde, G. Cabioch, Radiocarbon Calibration by Means of Mass Spectrometric 230Th/234U and 14C Ages of Corals: An Updated Database Including Samples from Barbados, Mururoa and Tahiti. *Radiocarbon* **40**, 1085–1092 (1998).

198. H. Kitagawa, J. Van Der Plicht, A 40,000-Year Varve Chronology from Lake Suigetsu, Japan: Extension of the 14C Calibration Curve. *Radiocarbon* **40**, 505–515 (1997).

199. H. Kitagawa, J. van der Plicht, Atmospheric Radiocarbon Calibration Beyond 11,900 cal BP from Lake Suigetsu Laminated Sediments. *Radiocarbon* **42**, 370–381 (2000).

200. C. B. Ramsey, *et al.*, A Complete Terrestrial Radiocarbon Record for 11.2 to 52.8 kyr B.P. *Science* **338**, 370–374 (2012).

201. B. Kromer, S. W. Manning, M. Friedrich, S. Talamo, N. Trano, 14C Calibration in the 2nd and 1st Millennia BC—Eastern Mediterranean Radiocarbon Comparison Project (EMRCP). *Radiocarbon* **52**, 875–886 (2010).

202. Q. Hua, *et al.*, Atmospheric 14C variations derived from tree rings during the early Younger Dryas. *Quat. Sci. Rev.* **28**, 2982–2990 (2009).

203. M. Schaub, *et al.*, Lateglacial environmental variability from Swiss tree rings. *Quat. Sci. Rev.* **27**, 29–41 (2008).

204. K. A. Hughen, *et al.*, Marine04 Marine Radiocarbon Age Calibration, 0–26 Cal Kyr Bp. *Radiocarbon* **46**, 1059–1086 (2004).

205. E. Bard, Correction of accelerator mass spectrometry 14C ages measured in planktonic foraminifera: paleoceanographic implications. *Paleoceanography* **3**, 635–645 (1988).

206. E. Bard, F. Rostek, G. Ménot-Combes, Radiocarbon calibration beyond 20,000 14C yr B.P. by means of planktonic foraminifera of the Iberian Margin. *Quat. Res.* **61**, 204–214 (2004).

207. K. A. Hughen, J. R. Southon, S. J. Lehman, J. T. Overpeck, Synchronous radiocarbon and climate shifts during the last deglaciation. *Science* **290**, 1951–1955 (2000).

208. K. Hughen, J. Southon, S. Lehman, C. Bertrand, J. Turnbull, Marine-derived 14C calibration and activity record for the past 50,000 years updated from the Cariaco Basin. *Quat. Sci. Rev.* **25**, 3216–3227 (2006).

209. E. Bard, *et al.*, Radiocarbon Calibration/Comparison Records Based on Marine Sediments from the Pakistan and Iberian Margins. *Radiocarbon* **55**, 1999–2019 (2013).

210. H. Oeschger, U. Siegenthaler, U. Schotterer, A. Gugelmann, A box diffusion model to study the carbon dioxide exchange in nature. *Tell'Us* **27**, 168–192 (1975).

211. M. Stuiver, T. F. Braziunas, Modeling Atmospheric 14C Influences and 14C Ages of Marine Samples to 10,000 BC. *Radiocarbon* **35**, 137–189 (1993).

212. M. Stuiver, G. W. Pearson, T. Braziunas, Radiocarbon Age Calibration of Marine Samples Back to 9000 Cal Yr BP. *Radiocarbon* **28**, 980–1021 (1986).

213. M. Niu, T. J. Heaton, P. G. Blackwell, C. E. Buck, The Bayesian Approach to Radiocarbon Calibration Curve Estimation: The IntCal13, Marine13, and SHCal13 Methodologies. *Radiocarbon* **55**, 1905–1922 (2013).

214. C. Bronk Ramsey, Bayesian Analysis of Radiocarbon Dates. *Radiocarbon* **51**, 337–360 (2009).

215. T. Bayes, LII. An essay towards solving a problem in the doctrine of chances. By the late Rev. Mr. Bayes, FRS communicated by Mr. Price, in a letter to John Canton, AMFR S. *Philosophical transactions of the Royal Society of London*, 370–418 (1763).

216. E. C. Harris, *Principles of Archaeological Stratigraphy* (Elsevier, 2014).

217. C. Bronk Ramsey, Dealing with Outliers and Offsets in Radiocarbon Dating. *Radiocarbon* **51**, 1023–1045 (2009).

218. M. Rosenblatt, Remarks on Some Nonparametric Estimates of a Density Function. *Ann. Math. Stat.* **27**, 832–837 (1956).

219. E. Parzen, On Estimation of a Probability Density Function and Mode. *Ann. Math. Stat.* **33**, 1065–1076 (1962).

220. C. Bronk Ramsey, Methods for Summarizing Radiocarbon Datasets. *Radiocarbon* **59**, 1809–1833 (2017).

221. B. W. Silverman, *Density Estimation for Statistics and Data Analysis* (Chapman and Hall, 1986).

222. M. R. Waters, T. W. Stafford Jr, B. Kooyman, L. V. Hills, Late Pleistocene horse and camel hunting at the southern margin of the ice-free corridor: reassessing the age of Wally's Beach, Canada. *Proc. Natl. Acad. Sci. U. S. A.* **112**, 4263–4267 (2015).

223. B. Kooyman, L. V. Hills, P. McNeil, S. Tolman, Late Pleistocene Horse Hunting at the Wally's Beach Site (DhPg-8), Canada. *Am. Antiq.* **71**, 101–121 (2006).

224. P. McNeil, L. V. Hills, B. Kooyman, M. S. Tolman, Late Pleistocene geology and fauna of the Wally's Beach Site (DhPg-8), Alberta, Canada. *Archaeology on the edge: new perspectives from the Northern Plains. Edited by B. Kooyman and J. Kelley. University of Calgary Press, Calgary, Alta. , Canadian Archaeological Association, Paper*, 79–94 (2004).

225. B. Kooyman, L. V. Hills, S. Tolman, P. McNeil, Late Pleistocene Western Camel (Camelops Hesternus) Hunting in Southwestern Canada. *Am. Antiq.* **77**, 115–124 (2012).

226. C. V. Haynes Jr, M. McFaul, R. H. Brunswig, K. D. Hopkins, Kersey--Kuner terrace investigations at the Dent and Bernhardt sites, Colorado. *Geoarchaeology: An International Journal* **13**, 201–218 (1998).

227. T. W. Stafford, P. E. Hare, L. Currie, A. J. T. Jull, D. J. Donahue, Accelerator radiocarbon dating at the molecular level. *J. Archaeol. Sci.* **18**, 35–72 (1991).

228. T. W. Stafford, A. J. T. Jull, K. Brendel, R. C. Duhamel, D. Donahue, Study of Bone Radiocarbon Dating Accuracy at the University of Arizona NSF Accelerator Facility for Radioisotope Analysis. *Radiocarbon* **29**, 24–44 (1987).

229. R. H. Brunswig, New interpretations of the Dent mammoth site. *Frontiers in Colorado Paleoindian archaeology*, 87–121 (2007).

230. J. J. Saunders, Morphometrical analyses of Mammuthus columbi from the Dent site, Weld county, Colorado. *Deinsea* **6**, 55–78 (1999).

231. G. Agogino, Progress Report on the Chemical Removal of Preservative from Radiocarbon Samples. *La Conquista* **2** (1963).

232. G. Agogino, An Early Attempt to Remove Preservatives from Bone. *Southwestern Lore* **63**, 42–43 (1997).

233. M. M. Mackie, T. A. Surovell, R. L. Kelly, M. J. O'Brien, New Excavations at the La Prele Mammoth Site, Converse County, Wyoming (2017).

234. D. A. Byers, Taphonomic analysis, associational integrity, and depositional history of the Fetterman mammoth, eastern Wyoming, USA. *Geoarchaeology: An International Journal* **17**, 417–440 (2002).

235. L. B. Davis, M. C. Wilson, The late Pleistocene Lindsay mammoth (24DW501), eastern Montana: Possible man-mammoth association. *Current Research in the Pleistocene* **2**, 97–98 (1985).

236. C. L. Hill, L. B. Davis, Stratigraphy, AMS radiocarbon age, and stable isotope biogeochemistry of the Lindsay Mammoth, eastern Montana. *Current Research in the Pleistocene* **15**, 109–112 (1998).

237. T. W. Stafford, K. Brendel, R. C. Duhamel, Radiocarbon, 13C and 15N analysis of fossil bone: Removal of humates with XAD-2 resin. *Geochim. Cosmochim. Acta* **52**, 2257–2267 (1988).

238. B. A. Potter, *et al.*, Current evidence allows multiple models for the peopling of the Americas. *Sci Adv* **4**, eaat5473 (2018).

239. R. Gruhn, A. L. Bryan, The record of Pleistocene megafaunal extinction at Taima-Taima, northern Venezuela. *Pleistocene extinctions: A prehistoric revolution. University of Arizona Press, Tucson*, 128–137 (1984).

240. A. L. Bryan, R. Gruhn, The radiocarbon dates of Taima-Taima. *Taima Taima: A late Pleistocene Paleoindian kill site in northernmost South America. Final Report of*, 53–58 (1976).

241. A. L. Bryan, R. M. Casamiquela, J. M. Cruxent, R. Gruhn, C. Ochsenius, An El Jobo Mastodon Kill at Taima-taima, Venezuela. *Science* **200**, 1275–1277 (1978).

242. C. Ochsenius, R. Gruhn, *Taima-Taima: A Late Pleistocene Paleo-Indian Kill Site in Northernmost South America: Final Reports of 1976 Excavations* (Center for the Study of First, 1979).

243. N. Guidon, E. Peyre, C. Guérin, Y. Coppens, Resultados da datação de dentes humanos da Toca do Garrincho, Piauí, Brasil. *Clio* **14**, 75–86 (2000).

244. A. Peyre, J. Granat, N. Guidon, Dents et crânes humains fossiles du Garrincho (Brésil) et peuplements anciens de l'Amérique. *Actes Societe francaise d'histoire de l'art dentaire* **14**, 32–37 (2009).

245. E. Peyre, C. Guérin, N. Guidon, Y. Coppens, Des restes humains pléistocènes dans la grotte du Garrincho, Piauí, Brésil. *Comptes Rendus de l'Académie des Sciences-Series IIA-Earth and Planetary Science* **327**, 355–360 (1998).

246. J. Feathers, R. Kipnis, L. Piló, M. Arroyo-Kalin, D. Coblentz, How old is Luzia? Luminescence dating and stratigraphic integrity at Lapa Vermelha, Lagoa Santa, Brazil. *Geoarchaeology* **25**, 395–436 (2010).

247. W. A. Neves, J. F. Powell, A. Prous, E. G. Ozolins, M. Blum, Lapa vermelha IV Hominid 1: morphological affinities of the earliest known American. *Genet. Mol. Biol.* **22**, 461–469 (1999).

248. W. A. Neves, A. Prous, R. González-José, R. Kipnis, J. Powell, Early Holocene human skeletal remains from Santana do Riacho, Brazil: implications for the settlement of the New World. *J. Hum. Evol.* **45**, 19–42 (2003).

249. A. G. M. Araujo, W. A. Neves, L. B. Piló, J. P. V. Atui, Holocene Dryness and Human Occupation in Brazil During the "Archaic Gap." *Quat. Res.* **64**, 298–307 (2005).

250. L. E. Lisiecki, M. E. Raymo, A Pliocene−Pleistocene stack of 57 globally distributed benthic δ18O records. *Paleoceanography* (2005).

Appendices

Appendix A: Chronometric work apart from the articles presented

Chronometric data not part of the articles presented were obtained for 17 additional archaeological sites as part of this research (Fig. 1). This section provides a brief description of each site, the purpose of the work that was undertaken, and any results obtained.

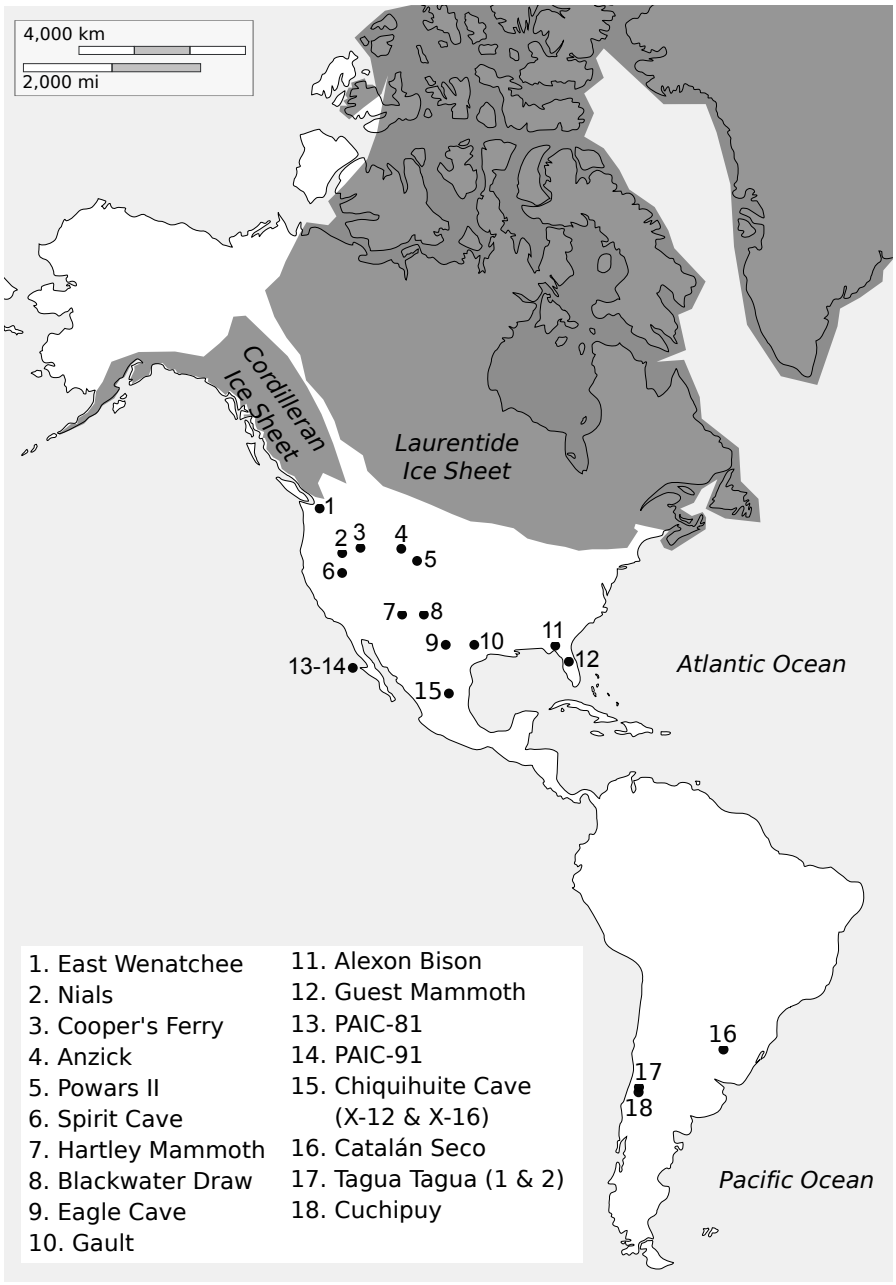


Fig. 1. Map with the location of all archaeological sites from which archaeological material was analysed in this thesis.

1. Alexon Bison Kill Site, Florida, U.S.A.

The Alexon Bison Kill Site contains the partial skeletal remains of a bison, with a chert point fragment embedded in the skull (1). Unpublished dates on unpurified collagen suggested that the specimen dated to the early Holocene (2). Therefore, collagen extraction following AG protocol was attempted on a petrosal fragment for a HYP measurement. The sample (~1,000 mg of bone powder), however, yielded no collagen, suggesting poor collagen preservation. Hence, no further chronometric work was attempted.

2. Blackwater Draw (Locality no. 1), New Mexico, U.S.A.

Blackwater Draw, Locality no. 1 (henceforth BWD), is the archaeological type-site for Clovis points and the eponymously-named culture and period. The site was initially discovered by a road construction crew who, whilst mining for gravel, uncovered large quantities of bison and mammoth skeletal remains (3). Alerted to the find, E.B. Howard excavated the site in the spring of 1933, finding bones in association with fluted points (3, 4). Since then, the chronology at the site has been defined through the efforts of V. Haynes and G. Agogino (5, 6). Geological units were assigned alphabetic determinations (A-G, starting at the bedrock), with Unit C, the 'brown sand wedge', corresponding to the Clovis level. Over 50 radiocarbon determinations have been published for BWD. Most of these, however, were obtained from geological samples, with very few extracted from Unit C (5, 6). Moreover, although human-modified faunal bones were recovered (7), none have been successfully dated so far.

With the aim of obtaining direct radiocarbon measurements from human-modified bone material, Dr. Eileen Johnson (Museum of Texas Tech University) and Prof. David Meltzer (Southern Methodist University, SMU) were contacted—both in charge of portions of the BWD collection. At

SMU, no human-modified bones were identified and sampling was unsuccessful. Human-modified material was present at the other university but, due to a reluctance to allow destructive analyses on these important samples, 20 unmodified fragments from the same layer were, as a first step, prescreened to test the assemblage's preservation. Sample TTU-A50515, a human-modified radial segment showing helical fractures and hack marks (7) (Fig. 2), was later sent to the ORAU in case prescreening results proved positive.



Fig. 2. Sample TTU-A50515 from Blackwater Draw, Locality no. 1, a human-modified radial segment showing helical fractures and hack marks (marked in red). Photographs provided by Dr. Eileen Johnson.

The 20 samples prescreened for bone collagen preservation showed consistently low values (Table 1). Three of the samples, however, showed slightly increased values as compared to the total assemblage and these were chemically pretreated following AG. The collagen yield thereby obtained was low, with only one sample (TTU-A50291) producing enough for radiocarbon dating at

1.77% (Table 2). Based on these results, a Texas Tech University committee deemed the destruction of a human-modified faunal sample for radiocarbon dating too risky and did not allow further sampling. Hence, sample TTU-A50515 was returned and no further chronometric work was attempted.

Table 1. %N values for 20 faunal bone samples from Blackwater Draw, Locality no. 1. Subsamples are denoted as ‘a’ or ‘b’. Results suggest low collagen preservation, with none reaching the cut-off value of 0.76 %N.

Sample	Weight (mg)	N (ug)	%N
50291a	3.03	9.33	0.31
50291b	2.9	10.14	0.35
50298	2.92	5.80	0.20
50301a	3.08	5.81	0.19
50301b	2.92	5.78	0.20
50305a	3.06	5.01	0.16
50305b	3.15	4.92	0.16
50315	2.92	6.10	0.21
50332	3.08	4.86	0.16
50333	3.27	5.41	0.17
50355	2.92	5.31	0.18
50362	3.04	4.53	0.15
116001a	2.99	4.33	0.14
116001b	3.09	4.42	0.14
116002	3.21	4.90	0.15
116003	3.01	5.14	0.17
116004	3.04	4.85	0.16
116005	2.93	5.19	0.18
116006	2.96	4.53	0.15
116007	2.9	4.60	0.16
116008	3.11	4.94	0.16
116009	3.11	5.28	0.17
116010	3.02	5.38	0.18
116011	3.13	5.28	0.17

Table 2. Chemical pretreatment (AG) data for three samples from Blackwater Draw, Locality no. 1, that showed slightly higher %N values than the rest of the material prescreened.

Sample	P code	Starting weight (mg)	Collagen yield (mg)	Yield (%)
TTU-A50291	AG	620	10.98	1.77
TTU-50301	AG	620	2.22	0.36
TTU-A50315	AG	710	0	0

3. Catalán Seco 7, Artigas, Uruguay

Catalán Seco 7 (CS-7) is a lithic workshop and quarry with bifacial technology on silicified sandstone (8), excavated in 2017 by Dr. Rafael Suárez (Universidad de la República, Montevideo). CS-7 was found near Catalán Seco 1 (CS-1), an archaeological site of similar characteristics (8). Given that there was no chronological control on the site or the Catalán Seco locality, this project sought to date two charcoal samples found in association with lithic artefacts within a test unit (Fig. 3). Results—12,530-12,100 and 12,710-12,530 cal BP (95.4% confidence)—suggest a likely Paleoindian occupation of CS-7 (Table 3). Given that archaeological work at the site has halted, however, no further chronometric work has been carried out.

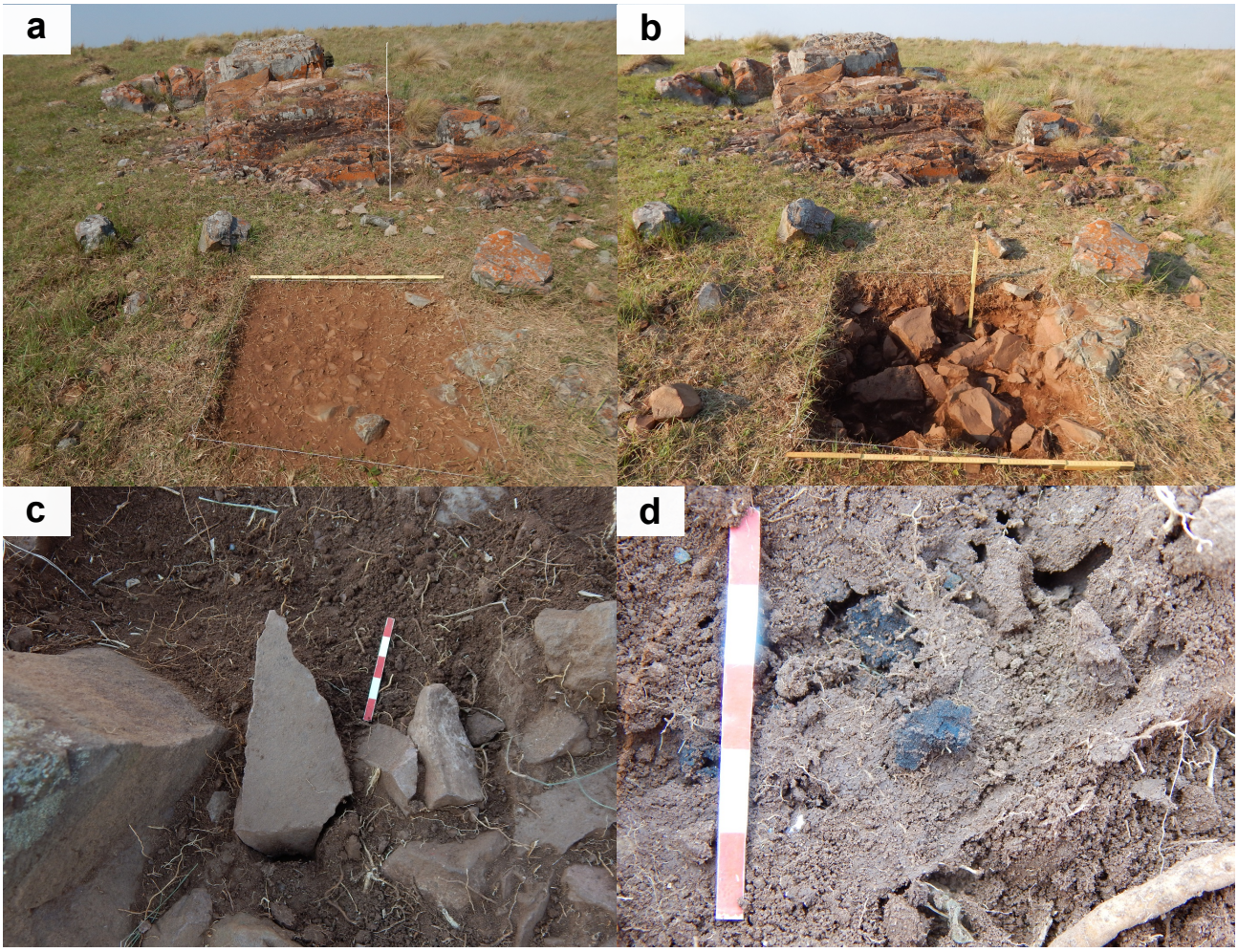


Fig. 3. Photographs of excavations at Catalan Seco 7 (**a-b**), a lithic artefact found in situ (**c**), and charcoal fragments processed for dating (**d**). Photographs provided by Dr. Rafael Suárez.

Table 3. Radiocarbon dating results for Catalan Seco 7. 'P', pretreatment. %C is the percentage of carbon in the combusted sample. Stable isotope ratios of C are expressed in per mil (‰) relative to Vienna Pee Dee belemnite. Calibration was done using the OxCal 4.3 software (9) and the SHCal13 calibration curve (10).

P no.	Sample no.	Material	P code	%C	$\delta^{13}C$ (‰)	Laboratory no.	Date (BP)	±	cal. BP (95.4% confidence)
44246	M1 OX	charcoal	ZR	64.8	-26.4	OxA-36638	10430	45	12529-12102
44247	M1OX	charcoal	ZR	66.2	-25.5	OxA-36639	10630	45	12709-12535

4. Chiquihuite Cave (X-12 & -16), Zacatecas, Mexico

Chiquihuite Cave is a high-altitude (2,740 m.a.s.l.), archaeological site located in an arid region in the northeast of Zacatecas state, at the base of the highest peak of the Astillero Mountains. The cave has two galleries measuring ~50x50 m, and up to 15 m in height. After initial field surveys in 2010 and 2011, a 3x2 m test pit was excavated next to the northern wall of the front chamber by Dr. C. F. Ardelean, University of Zacatecas, and his team (11). This small trench produced the first evidence of human presence at more than 3m of depth; a concentration of small-animal bones, a bear baculum, and three limestone flakes. The baculum was directly dated to 27,830 ± 150 BP (Beta-345055), while sediment near the feature yielded an optically stimulated luminescence (OSL) age of 29,180 ± 2,570 ya (X-4135). Due to the significance of these initial findings, two new field seasons undertaken during 2016 and 2017, extended the initial test pit to a 16x5 m excavation area (X-12; Fig. 4). Along the sequence, evidence for human occupation was found within three occupational components, labelled Stratigraphic Components (SC-) A, B, and C (12). SC-A is the youngest, showing evidence of Colonial and late pre-Columbian materials. SC-B is separated from the next component, SC-C, by a well-defined, thick clay layer that extends uniformly throughout the sequence and dates to the LGM. Lithic artefacts (n=1930; Fig. 5) made from limestone were found in all strata, with increased frequency in the upper stratigraphic component [SC-B; (12)]. Notably, a large laurel-leaf flaked biface was extracted from the deepest layers uncovered (square I5-6; western profile), between samples LEMA-576 and LEMA-577, dating to 20,896±80 and 21,401±95 years BP, correspondingly (Fig. 6). The entire lithic assemblage reflects a previously unknown and largely unchanged technological tradition; no relevant technological mutations are currently apparent (12). However, further lithic analysis is needed to better understand this industry.

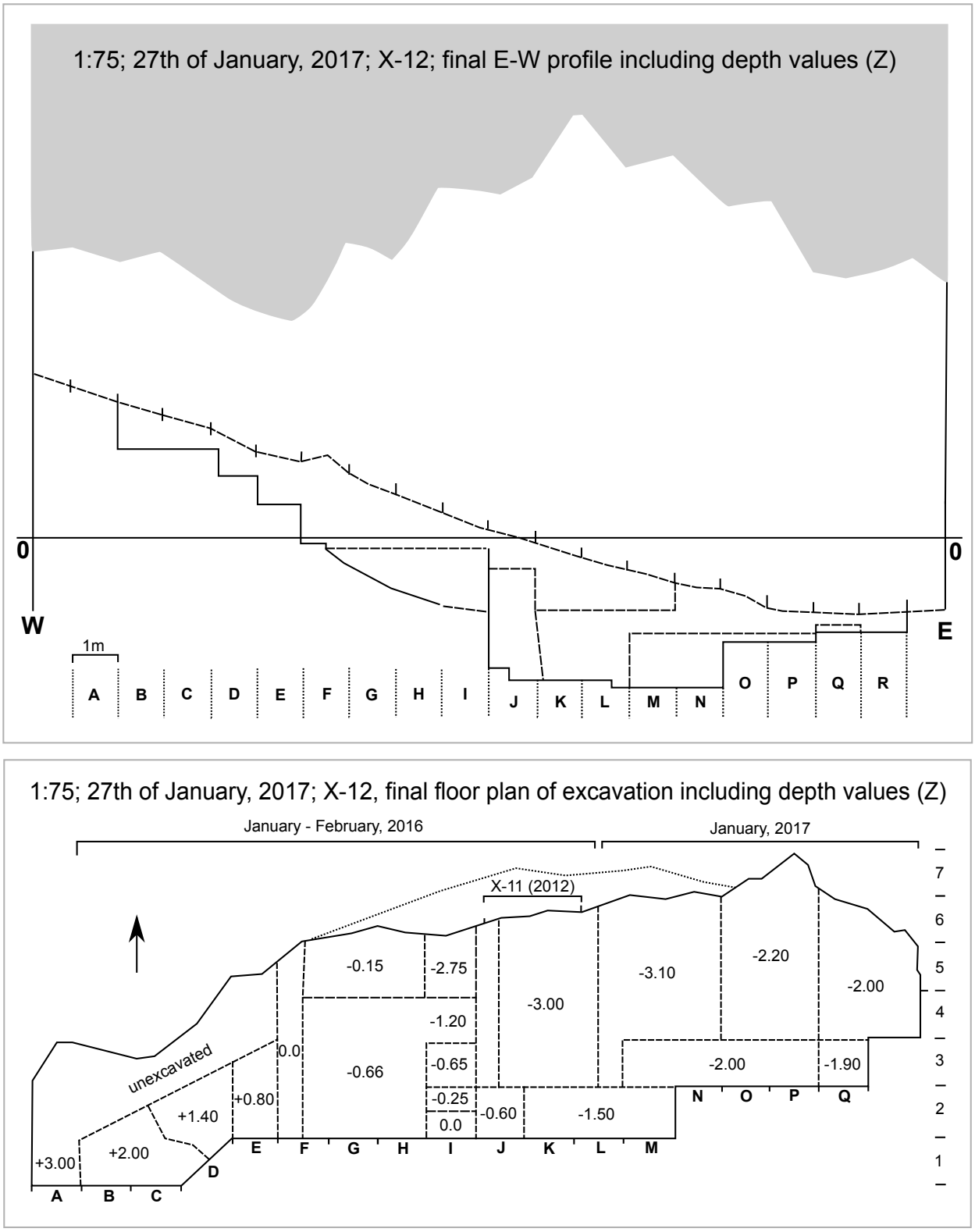


Fig. 4. Profile and floor plan schematics for Chiquihuite Cave, X-12.



Fig. 5. Lithic artefacts at Chiquihuite Cave, X-12. Every item has a 1 cm scale bar. **a, b,** Cores. **c-i,** Flakes with platforms. **j,** Macro-blade. **k-p,** Micro-blades. **q-s,** Microliths (blade medial fragments). **t,** Scraper on flake. **u,** Burin. **v-h',** Points and point-like shapes. **i',** Adze. Most items are from SC-B. Artefacts **f**, **w**, **f'** and **h'** belong to SC-C. Bifacial point **w** was associated to a charcoal dating to 27,929±82 BP (PRI-5414). Figure provided by Dr. Ciprian Ardelean.

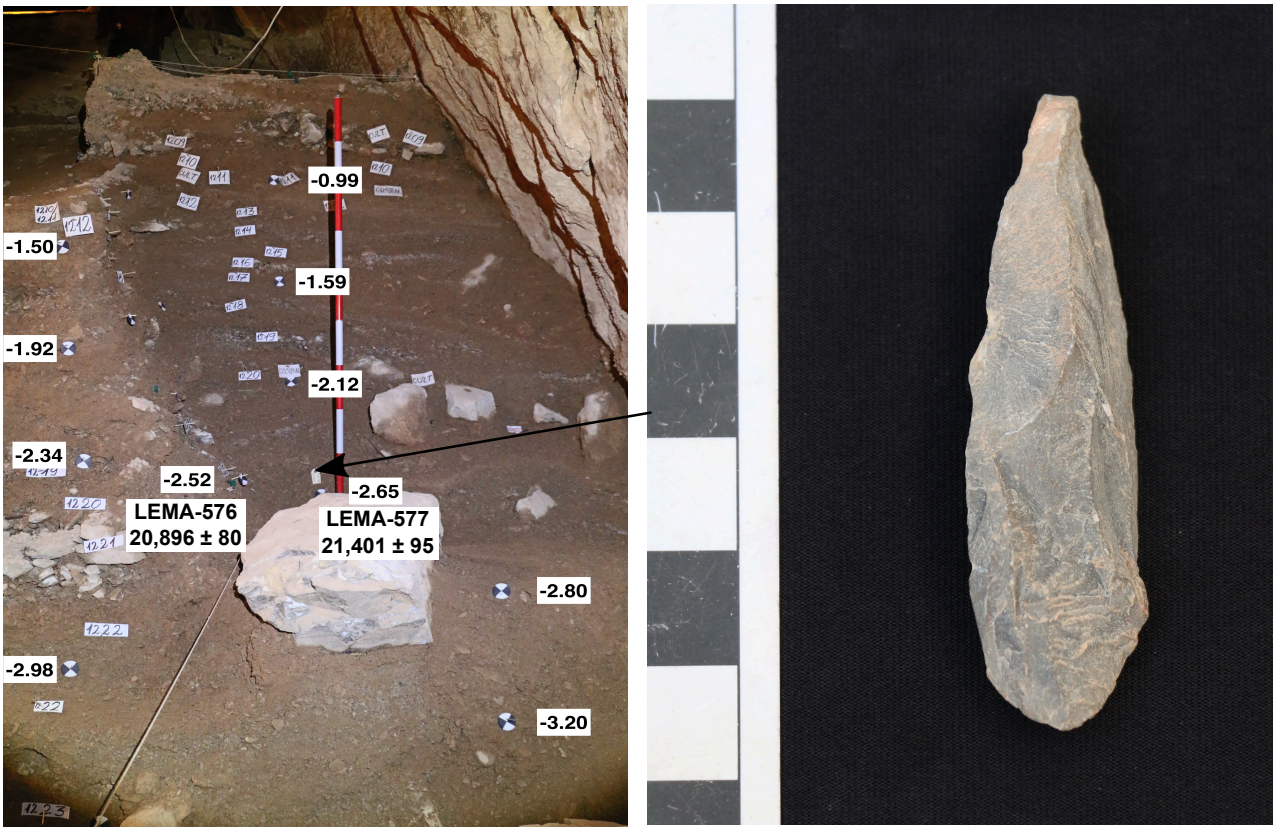


Fig. 6. Photograph of the western profile at squares I5 and I6, Chiquihuite Cave (X-12) and a photograph of a large laurel-leaf flaked biface obtained from the same sequence (the arrow points to its location when discovered). Note that the biface was located between samples LEMA-576 (at -2.52m in depth) and LEMA-577 (at -2.65m in depth), dating to 20,896 ± 80 and 21,401 ± 95 BP, correspondingly.

Given the potential of Chiquihuite Cave as a pre-Clovis site, 33 charcoal and faunal bone samples were processed for radiocarbon dating (Table 4). Sample selection was aimed at maintaining a close spatial relationship with lithic artefacts found along the sequence (Fig. 7). Of these, 25 were successfully measured. Along with previously-obtained radiocarbon and OSL measurements (Table 5), these were incorporated into a Bayesian age model for SC-B and -C. Modelled output estimates the start of the sequence to 32,950-31,430 years cal. BP (pre-LGM; 95.4% confidence level), and

the end to 13,250-10,830 years cal. BP [around the Younger Dryas (YD; ~12,900-11,700 years ago) (13)] (95.4% confidence level) (Fig. 8). Five dates—ICA-16OS 0510 (bulk sediment; ^{14}C), LEMA-577.1.1 (charcoal; ^{14}C), LEMA-576.1.1 (charcoal; ^{14}C), Oxford X-7227 (sediment; OSL), and Beta-436709 (bulk sediment; ^{14}C)—were identified as outliers (likelihood ≥60%) by the outlier model. For ICA-16OS 0510, LEMA-577.1.1 and LEMA-576.1.1, the inconsistency is largely caused by a temporal gap between strata 1223 and 1220-1222, which likely reflects a real taphonomic event or an artefact of sampling/dating bias. The same applies for Oxford X-7227 and strata 1218-1219 and 1217. It is also possible that ICA-16OS 0510 is a minimum-age estimate due to the quality of the dated fraction (bulk sediment) (14, 15). Overall, however, the chronological sequence for Chiquihuite Cave shows good agreement. These results have been incorporated into a co-authored manuscript that is currently being reviewed in *Nature*.

Table 4 here placeholder

Table 4 here placeholder

Table 4 here placeholder

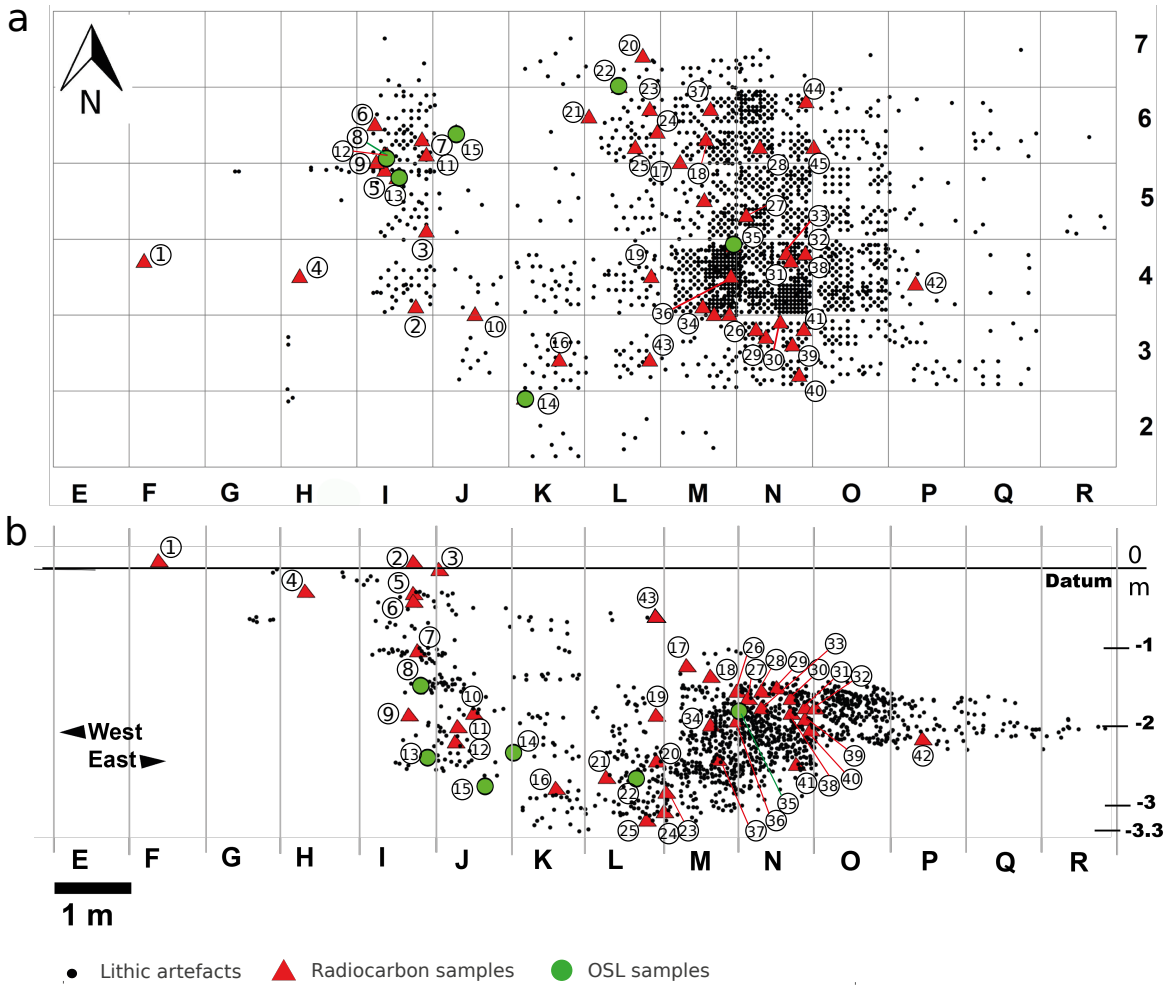


Fig. 7. Horizontal (floor plan; **a**) and vertical (side view; **b**) spatial distribution of lithic artefacts and dated samples at Chiquihuite Cave, X-12. Illustrated samples: 1) LEMA-635.1.1 & -635.1.2; 2) OxA-36608 & LEMA-978.1.1; 3) OxA-36610; 4) LEMA-574.1.1; 5) LEMA-640.1.1; 6) OxA-36496; 7) OxA-36613; 8) X-7227; 9) OxA-36614; 10) LEMA-636.1.1 & -636.1.2; 11) LEMA-576.1.1; 12) LEMA-577.1.1; 13) X-7228; 14) X-7231 & 7232; 15) X-7229; 16) OxA-36530; 17) OxA-36633; 18) OxA-36609; 19) OxA-36612; 20) OxA-36360; 21) BETA-345055; 22) X-4135; 23) OxA-34965; 24) ICA-16OS/0510; 25) PRI-5414; 26) OxA-36616; 27) OxA-36620; 28) OxA-36618; 29) OxA-36615; 30) OxA-36617; 31) OxA-36621; 32) OxA-36619; 33) OxA-36753; 34) OxA-36611; 35) X-7233; 36) LEMA-573.1.1; 37) OxA-36359; 38) LEMA-892.1.2; 39) OxA-36622; 40) OxA-36623; 41) OxA-36634; 42) LEMA-893.1.1; 43) LEMA-977.1.1; 44) OxA-36624; 45) OxA-36625. Modified from a figure provided by Dr. Ciprian Ardelean.

Table 5 place holder

Table 5 place holder

Table 5 place holder

Table 5 place holder

Table 5 place holder

Table 5 place holder

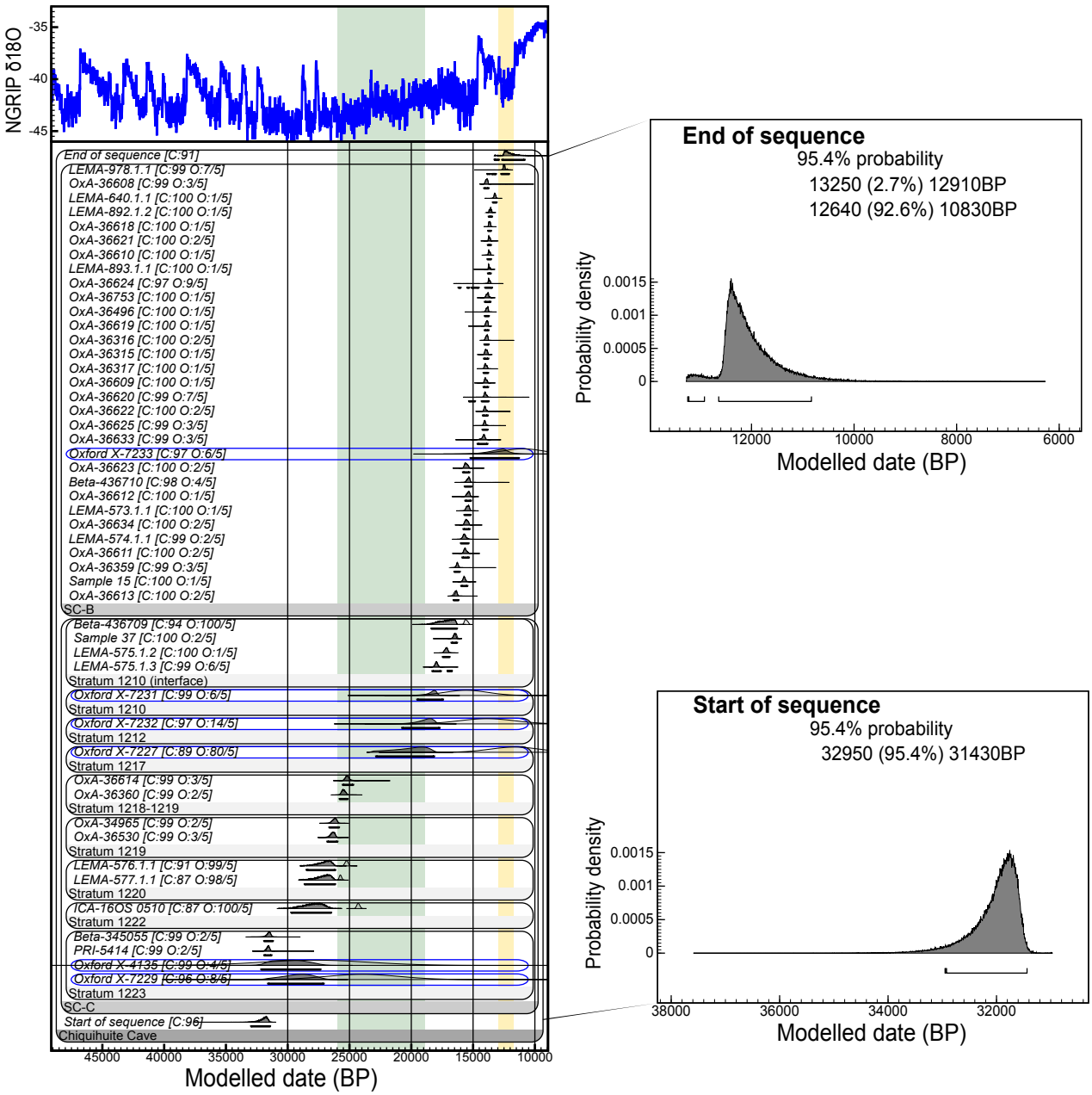


Fig. 8. Bayesian age model of Chiquihuite Cave. OSL dates are outlined in blue. The green band represents the span of the LGM (per (17)), whilst the yellow indicates the Younger Dryas (per reference 13). 'C', convergence values. Outlier analysis output is noted as 'O:posterior probability/ prior probability'. δ18O data according to the Greenland ice core timescale (GICC05) (18). Modelled output estimates the start of the cultural occupation at Chiquihuite Cave to 32,950-31,430 years cal. BP (pre-LGM; 95.4% confidence level), and the end to 13,250-10,830 years cal. BP [around the Younger Dryas, ~12,900-11,700 years ago (13)] (95.4% confidence level).

In early 2019, a new area located at the original entrance of the cave was excavated (X-16). This was sealed by flowstone and, below, the same lithic industry as in X-12 was found (12). From this excavation, seventeen bone and charcoal samples were submitted for dating, with five failing due to insufficient yield for measurement (Table 6). Radiocarbon dating results show the deposits date to the Pleistocene, congruent with the chronology at X-12. These results will be included in a second manuscript, after the X-12 evidence is published.

Table 6.

Table 6.

Table 6.

5. Cooper's Ferry, Idaho, U.S.A.

Cooper's Ferry, Oregon, is a multi-cluster, stratified [lithostratigraphic units (LU) 1-9] site containing Western Stemmed Tradition (WST) lithics, faunal remains, and pit features (19–24). Concentrated on the Great Basin, U.S.A., the antiquity of the WST is not yet clear, with some believing it predates Clovis (23). Given that only three sites date the tradition (25–27), obtaining a reliable chronology at Cooper's Ferry was crucial. To this end, fourteen bone samples were first prescreened for collagen preservation. Of these, only four contained enough collagen for measurement. The low success rate (~29%) suggested poor preservation at the site. To obtain more data, a further 39 samples (bone and charcoal) collected in 2018 were obtained for processing. Of these, 16 were successfully measured (Table 7).

Table 7.

Table 7.

Table 7.

Table 7.

Table 7.

Along with previously obtained OSL and radiocarbon dates, data were incorporated into a Bayesian age model for the earliest components at Area A (LU5-3). This work was included in a *Science* publication, where the site is argued to provide evidence for a coastal entry into mid-latitude North America, and a cultural connection with northeastern Asian Upper Palaeolithic archaeological traditions (24) (Appendix B).

6. Cuchipuy, O'Higgins, Chile

Cuchipuy is an ancient cemetery also located within the Laguna de Tagua Tagua area, 8 km east of the Tagua Tagua 1 and 2 archaeological sites. Cuchipuy is located at the base of a hill and was cut, to the east, by the construction of a road that first exposed the human burials. Initial excavations occurred in 1978 and 1979 under J. Kaltwasser, and were part of a salvage operation (28–32). Then, archaeologists identified four distinct geocultural strata within different excavation units across a 30x40 m area (Fig. 9). Stratum 1 corresponds to a top layer containing multiple isolated human burials with associated ceramic artefacts. Stratum 2 is gravelly, lacking in ceramics, and with stone structures containing multiple human burials. Stratum 3 is a layer of earth, fine sand, and calcium carbonate, devoid of burials and with very few human bones and cultural materials. Stratum 4, at a starting depth of 1.80-2 m and thickness of 1 m, is the deepest, final layer and contains human burials associated with lithic points and ornaments (32). In between 1980-1982, Beta Analytic, Inc., produced eleven charcoal, bone, and sediment dates for Strata 2-4 (33). The dataset obtained was highly incongruent, however, with paired skeleton and charcoal samples in Stratum 4 (Unit 2) dating to 6,105±145 (Beta-1454) and 8,070±100 BP (Beta-1453), respectively. Notwithstanding, archaeologists believed the deepest layer to be older than ~8,000 BP due to the apparent correspondence between Stratum 4 and lithostratigraphic unit 5 at Tagua Tagua 1 and 2 (see section 16) (32, 34). To test the hypothesis, this project secured samples from 16 human skeletons extracted

from the lowest level (Stratum 4). These were selected by Prof. E. Aspillaga (Universidad de Chile), who first excavated the site and performed morphometric analysis of the human remains. Of the 16 samples, fourteen were successfully measured (Table 8). Results showed the individuals to date to the Middle Archaic, in line with previously-obtained data and outside the time range of this thesis.



Fig. 9. Photograph of stratigraphy at Cuchipuy (Unit 2, embankment, 0-4.65 m north; from reference 29). Layers a, b, c, and d correspond to Strata 1, 2, 3, and 4, respectively.

Table 8.

Table 8.

7. Eagle Cave, Texas, U.S.A.

Eagle Cave (41VV167) is a stratified (zones 1-10) site that has been intermittently excavated since the 1930s (35, 36). Previous excavations, focused on recovering display artefacts, stopped at a limestone dust layer showing no signs of human occupation. In 2014-2017, the Ancient Southwest Texas (ASWT) project conducted controlled excavations and broke through this layer, exposing bison and mammoth bones, lithic tool technology, hearths, and decomposed organics in Zones 9/10 (37) (Fig. 10). Of the >300 point-provenienced bison bone fragments found, 30% showed evidence of human modification via cut marks (38) (Fig. 11). The lowest cultural feature at the site is 14 (Zone 10) and contains human-modified bison bones. The chronology at the site has so far been established by 27 radiocarbon dates ranging from 11,180 ± 40 BP (Beta-445876) to 2,038 ± 22 BP (D-AMS-18138) (38). None of the bones, modified or otherwise, have been processed for radiocarbon dating.

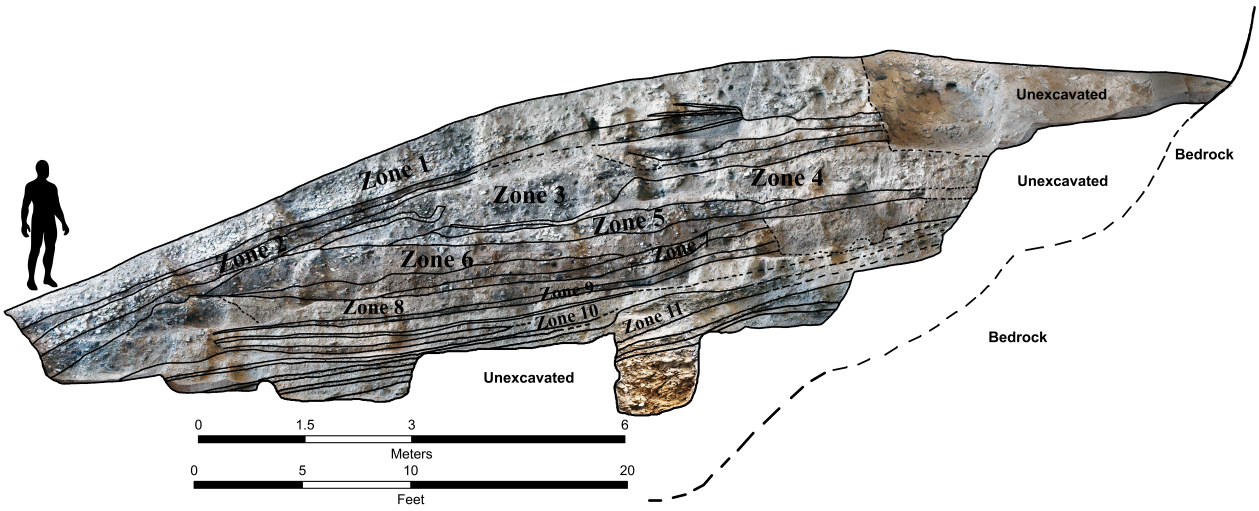


Fig. 10. Profile of Eagle Cave. Zones 10 and 9 contains Paleoindian material. Figure provided by the Ancient Southwest Texas Project, Texas State University.



Fig. 11. A cut-marked (red circle) bison bone fragment (FN35837) from Eagle Cave. Photograph provided by the Ancient Southwest Texas Project, Texas State University.

With the aim of obtaining direct radiocarbon measurements from human-modified bone material, five unmodified bone samples from Zone 10 were first secured for prescreening (Table 9). Given that results showed good collagen preservation (>0.91%), five (unmodified) mammoth and (cut-marked) bison bone fragments from the same level were processed for radiocarbon dating. An additional 19 charcoal, macro-botanics and sediment samples were included to increase the chronological resolution of the entire archaeological sequence. Of the five bone samples, none yielded enough collagen for measurement (the %N results previously obtained proved to be false positives). In a last attempt, nine further human-modified bison bone samples were processed, along with a wood fragment found in direct association with one of the bones (Fig. 12). Again, however, none of the bone samples contained enough collagen for dating (Table 10). The wood sample was processed using the RR protocol (without sonication) and thus yielded a minimum-age estimate of 10,548±32 BP (OxA-38601). In summary, of 34 samples processed for dating, only twelve were

successfully measured (35% success rate; Table 10; see Fig. 13 for their location in the stratigraphy).

Table 9. %N values for five faunal bone samples from Eagle Cave. Results suggest good collagen preservation, with all samples passing the cut-off value of 0.76 %N.

Sample	Weight (mg)	N (ug)	%N
34171/34171	0.98	13.1	1.34
34308	0.99	9.98	1.01
35863	1.14	17.28	1.52
35864	1.11	11.68	1.05
34171/34177	1.2	11.62	0.97



Fig. 12. Sample FN35834, a wood fragment found in direct association with cut-marked bison bones. Photograph provided by the Ancient Southwest Texas Project, Texas State University.

Table 10.

Table 10.

Table 10.

Table 10.

Table 10.

Table 10.

Table 10.

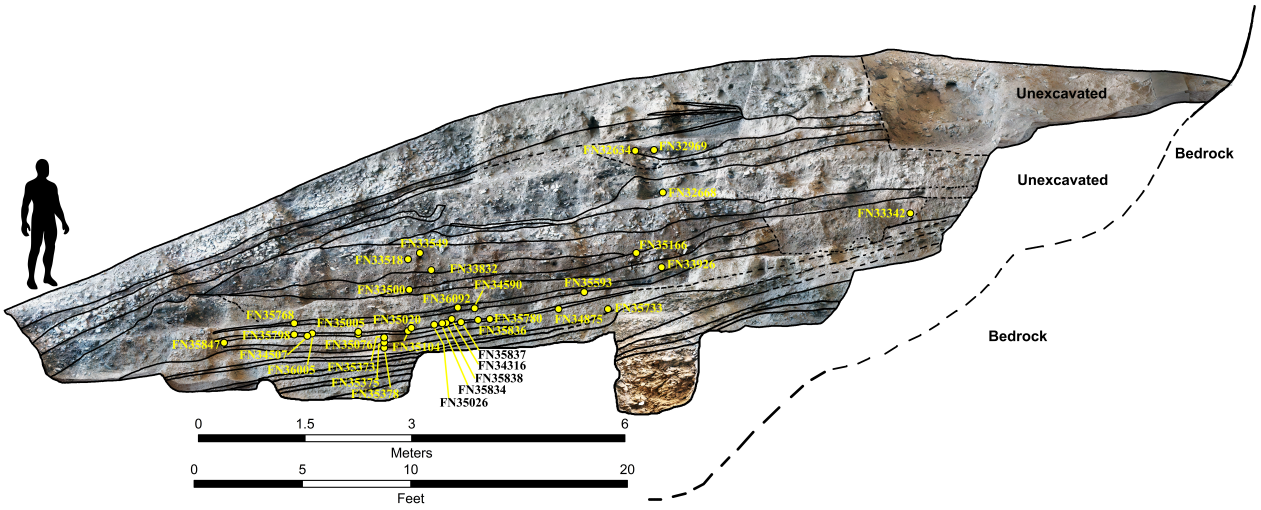


Fig. 13. Stratigraphic location of processed samples for Eagle Cave. Figure provided by the Ancient Southwest Texas Project, Texas State University.

Together with previously-obtained dates, data were incorporated into two Bayesian models—one for Zones 6-1 (Fig. 14), and another for 10-8 (Fig. 15). A single model containing all zones failed due to a large temporal gap between Zones 8, 7 and 6. This is likely the product of sampling and/or measurement success bias. Evaluated separately, the upper sequence (Zones 6-1) contains three outliers—DAMS-13536, -27494 and -13537. These are best explained by a number of intrusive pits and cultural reworking of older deposits. The second sequence (Zones 10-8; basal) shows four outliers—Beta-445875, DAMS-18143, -18139 and -DAMS-18140. DAMS-18140 and -18139, in Zone 10, are likely due to bioturbation—although efforts were made to avoid sampling from burrows or questionable contexts (38). DAMS-18143 is most likely an outlier due to a clear temporal gap between Zones 10 and 9. The last outlier, Beta-445875, was sampled from an intrusive pit and is a clear underestimate given the stratigraphic context. Zone 10 is estimated to start at 14130-12560 cal BP, with the oldest feature falling into the Folsom period—outside the time range for this thesis.

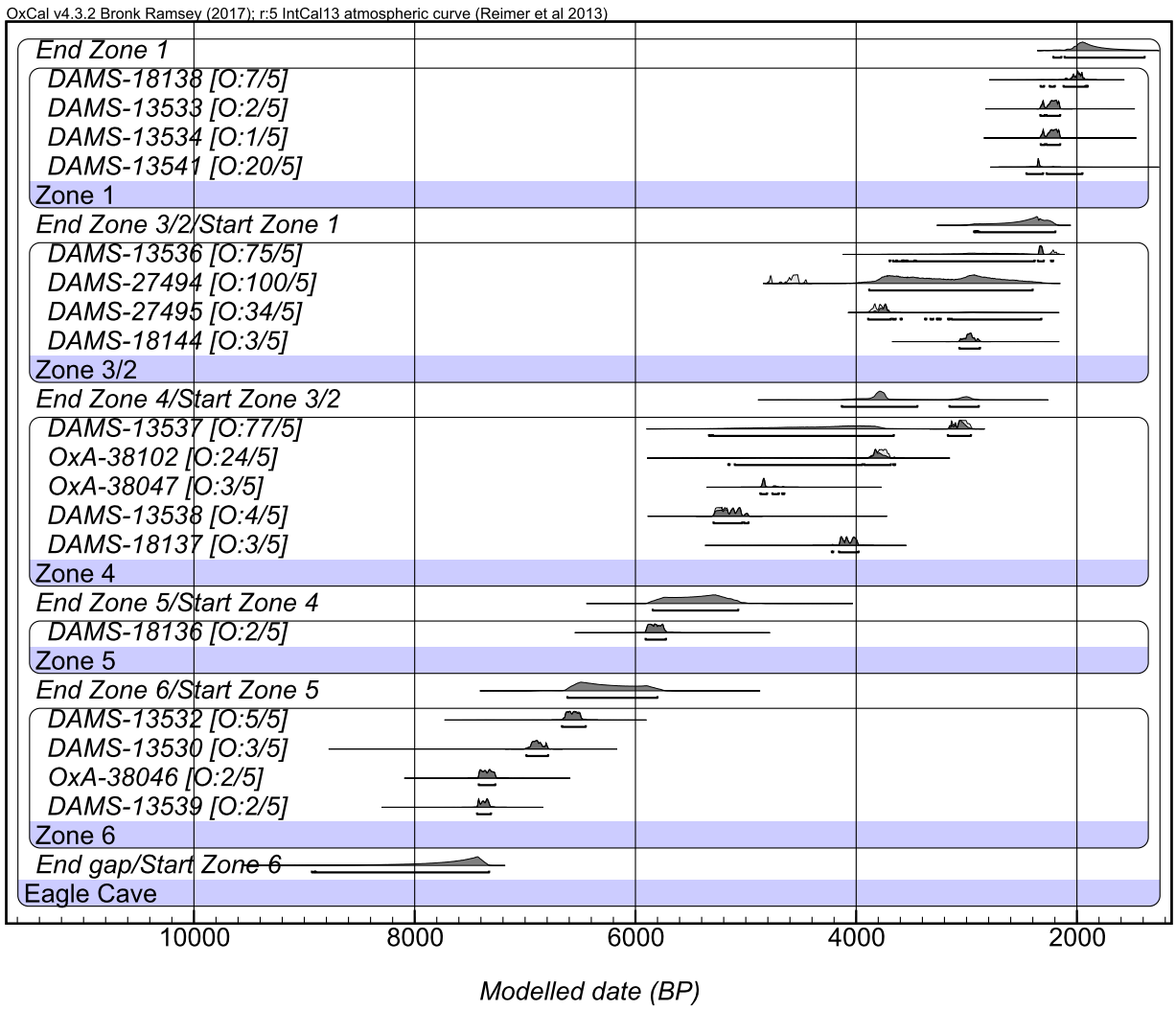


Fig. 14. Bayesian age model of Eagle Cave, zones 6-1. Outlier analysis output is noted as 'O:posterior probability/prior probability'. δ18O data according to the Greenland ice core timescale (GICC05) (18).

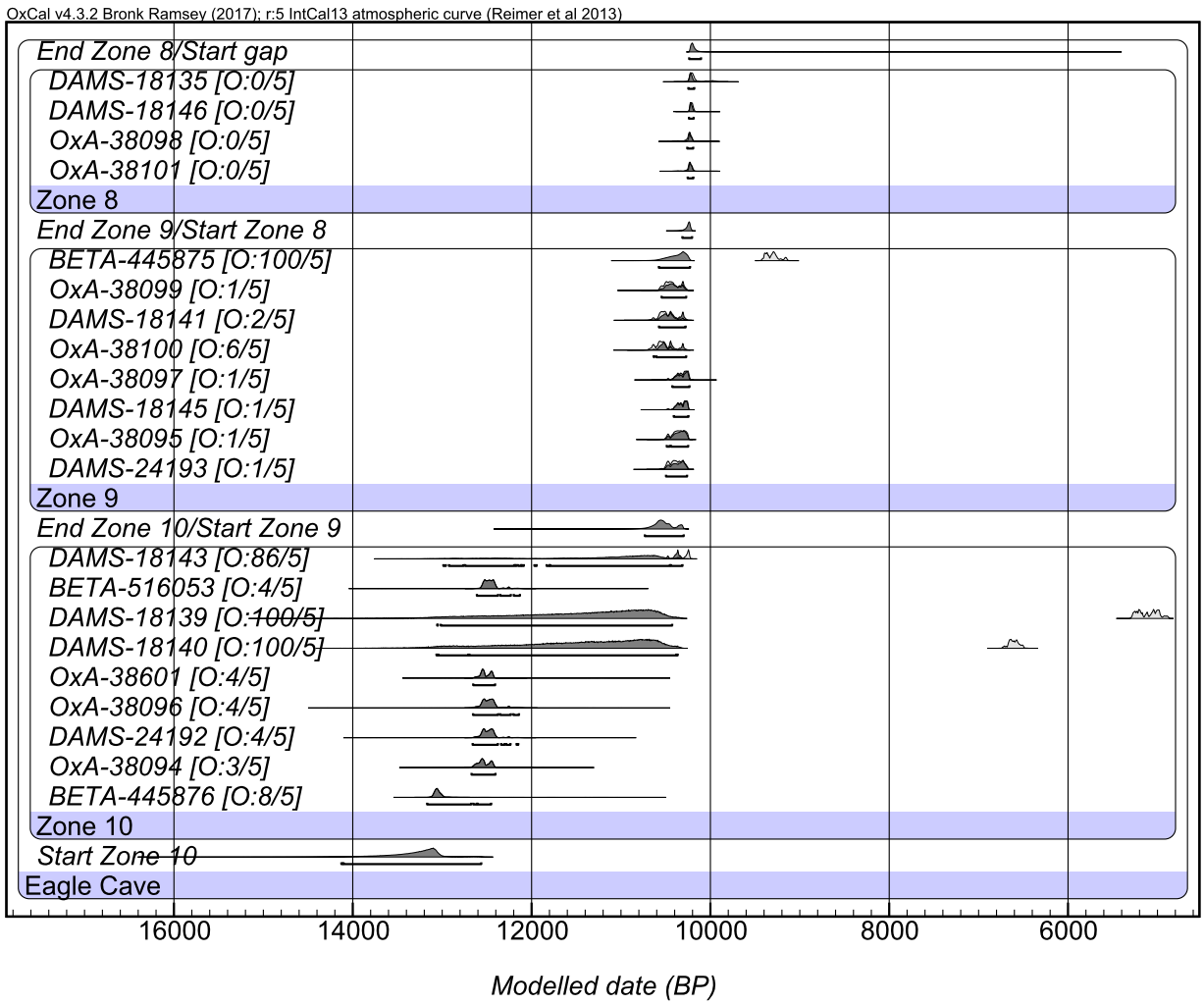


Fig. 15. Bayesian age model of Eagle Cave, zones 10-8. Outlier analysis output is noted as 'O:posterior probability/prior probability'. δ18O data according to the Greenland ice core timescale (GICC05) (18).

8. East Wenatchee, Washington, U.S.A.

Originally discovered in 1987, East Wenatchee contains an important Clovis cache with traces of Glacier Peak Ash (dated to 11,600±50 BP) (39) cemented to the undersides of some of the lithic points (40, 41). Given the temporal discrepancy between the minimum age provided by the ash and a previously-obtained measurement of 5,215±90 BP (Beta-43663) on a bone artefact (sample CN1990.6.) (2), dating via HPLC was attempted on the same sample. This (~1,000 mg of bone powder), however, yielded no collagen following AG protocol, suggesting poor collagen

preservation. Results imply that the previous measurement was not likely obtained from collagen and should be viewed with caution.

9. Gault, Texas, U.S.A.

Gault (41BL323) is a large (800x200 m) stratified, multi-component archaeological site in the head of Buttermilk Creek Valley, Bell County, Texas, containing Late Prehistoric, Archaic, and Paleoindian sequences (42–48). Known to archaeologists since 1929, the site has been intermittently excavated since 1991 by Prof. M. Collins (Texas State University, San Marcos) and colleagues. The excavation area is divided into fifteen excavation blocks (Fig. 16), with nine showing early Palaeolithic lithic evidence. Most Late Prehistoric and Archaic deposits have been heavily disturbed due to looting. Within the Paleoindian layer, Clovis is represented by thousands of stone and osseous artefacts (42). Pre-Clovis evidence is present in Areas 12 and 15 (43, 44, 46).

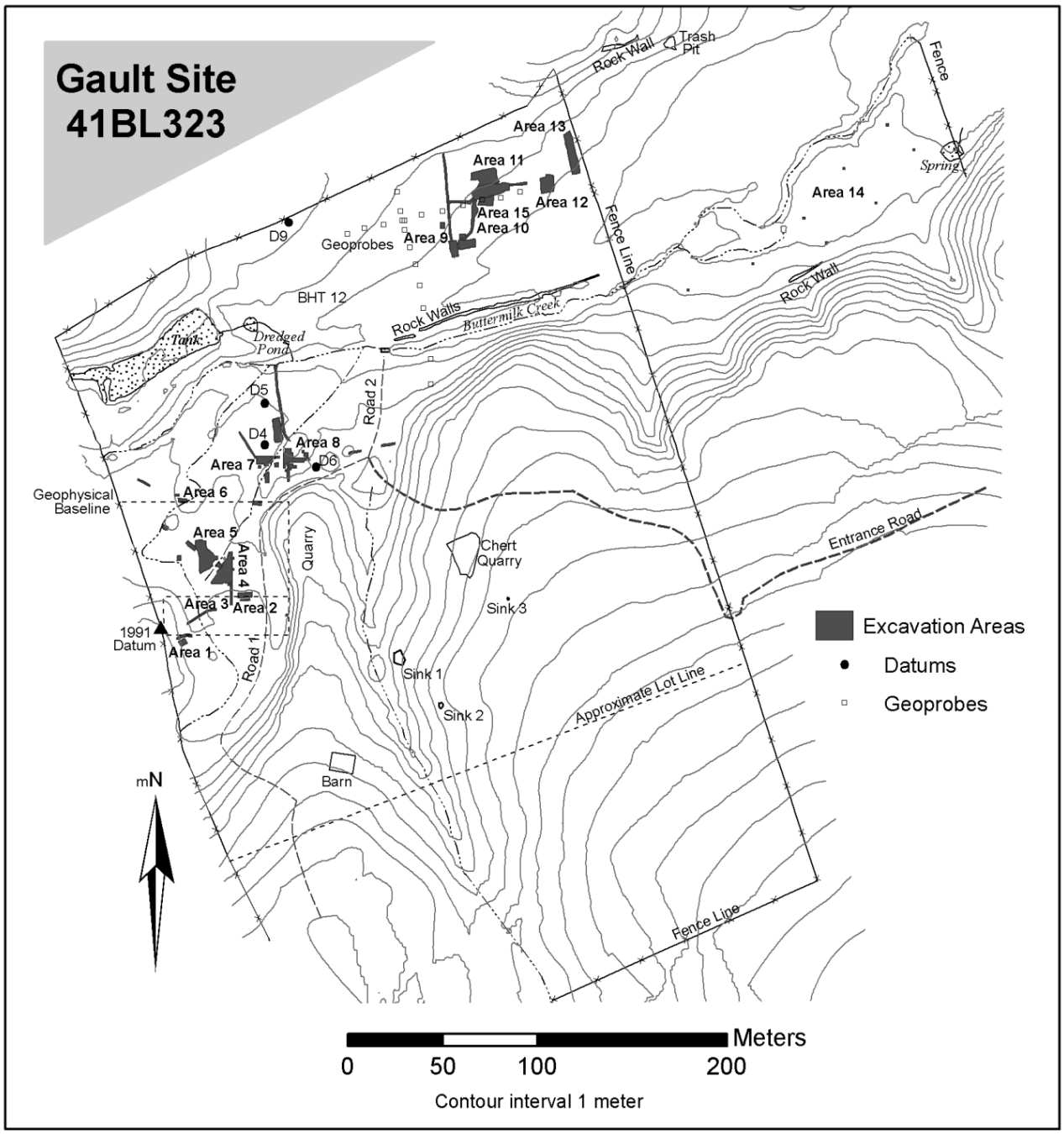


Fig. 16. Excavation area at Gault (from reference 48).

The chronology at the site has been established thorough OSL dating (45, 47), as radiocarbon dating of faunal remains proved unsuccessful due to insufficient collagen yields (49). In an effort to test previous results, this project secured ninety-one samples of whole bone powder for prescreening (Table 11). A mammoth mandible (UT number 3120) was subsampled four times in different

locations. Results showed a consistently poor level of preservation, with %N values barely reaching 0.08. Thus, no radiocarbon dating was attempted.

Table 11. %N values for 91 faunal bone samples from Gault. Results suggest very poor collagen preservation, with none of the samples passing the cut-off value of 0.76 %N.

Sample	Weight (mg)	N (µg)	%N	Sample	Weight (mg)	N (µg)	%N
UT no. 1066; Gault no. 38; Oxford subsample 1	2.67	1.40	0.05	UT no. 1048; Gault no. 15; Oxford subsample 2	2.43	1.09	0.04
UT no. 1066; Gault no. 38; Oxford subsample 2	2.50	1.44	0.06	UT no. 1048; Gault no. 15; Oxford subsample 3	2.51	1.71	0.07
UT no. 1066; Gault no. 38; Oxford subsample 3	2.41	1.19	0.05	UT no. 1048; Gault no. 15; Oxford subsample 4	2.61	1.15	0.04
UT no. 1066; Gault no. 38; Oxford subsample 4	2.43	1.36	0.06	UT no. 1048; Gault no. 15; Oxford subsample 5	2.88	1.38	0.05
UT no. 1066; Gault no. 38; Oxford subsample 5	2.37	0.93	0.04	UT no. 1048; Gault no. 15; Oxford subsample 6	2.96	0.98	0.03
UT no. 1066; Gault no. 38; Oxford subsample 6	2.37	0.98	0.04	UT no. 1048; Gault no. 15; Oxford subsample 7	2.54	0.75	0.03
UT no. 1066; Gault no. 38; Oxford subsample 7	2.62	1.10	0.04	UT no. 1048; Gault no. 15; Oxford subsample 8	2.77	1.52	0.05
UT no. 1066; Gault no. 38; Oxford subsample 8	2.83	1.53	0.05	UT no. 1048; Gault no. 15; Oxford subsample 9	2.77	1.52	0.05
UT no. 1066; Gault no. 38; Oxford subsample 9	2.41	1.15	0.05	UT no. 1048; Gault no. 15; Oxford subsample 10	3.02	1.51	0.05
UT no. 1066; Gault no. 38; Oxford subsample 10	2.38	0.95	0.04	UT no. 1048; Gault no. 15; Oxford subsample 11	2.88	1.27	0.04
UT no. 1066; Gault no. 38; Oxford subsample 11	2.78	1.20	0.04	UT no. 1048; Gault no. 15; Oxford subsample 12	2.30	1.06	0.05
UT no. 1066; Gault no. 38; Oxford subsample 12	2.34	0.89	0.04	UT no. 4367-1; Gault no. 1; Oxford subsample 1	2.39	0.90	0.04
UT no. 1066; Gault no. 38; Oxford subsample 13	2.30	0.95	0.04	UT no. 4115; Gault no. 12; Oxford subsample 1	2.48	2.26	0.09
UT no. 1066; Gault no. 38; Oxford subsample 14	2.96	1.11	0.04	UT no. 1048; Oxford subsample 1	2.33	0.87	0.04
UT no. 1066; Gault no. 38; Oxford subsample 15	2.85	0.98	0.03	UT no. 1241; Gault no. 27; Oxford subsample 1	2.55	0.85	0.03
UT no. 1066; Gault no. 38; Oxford subsample 16	2.65	1.43	0.05	UT no. 1241; Gault no. 27; Oxford subsample 2	2.34	0.80	0.03
UT no. 1066; Gault no. 38; Oxford subsample 17	2.55	1.04	0.04	UT no. 4636-3; Gault no. 1; Oxford subsample 1	2.53	1.13	0.04
UT no. 1066; Gault no. 38; Oxford subsample 18	2.60	1.66	0.06	UT no. 2746; Gault no. 3; Oxford subsample 1	2.41	0.54	0.02
UT no. 1066; Gault no. 38; Oxford subsample 19	2.88	1.25	0.04	UT no. 2746; Gault no. 3; Oxford subsample 2	2.95	0.81	0.03
UT no. 1066; Gault no. 38; Oxford subsample 20	2.56	1.71	0.07	UT no. 4256-14; Gault no. 1; Oxford subsample 1	2.63	0.71	0.03
UT no. 1066; Gault no. 38; Oxford subsample 21	2.39	1.15	0.05	UT no. 3054-4; Gault no. 2; Oxford subsample 1	2.70	0.70	0.03
UT no. 1066; Gault no. 38; Oxford subsample 22	2.75	1.29	0.05	UT no. 3054-4; Gault no. 2; Oxford subsample 2	2.40	0.66	0.03
UT no. 1066; Gault no. 38; Oxford subsample 23	2.72	1.35	0.05	UT no. 2947-7; Gault no. 1; Oxford subsample 1	2.70	0.84	0.03

Sample	Weight (mg)	N (µg)	%N	Sample	Weight (mg)	N (µg)	%N
UT no. 1066; Gault no. 38; Oxford subsample 24	2.91	1.32	0.05	UT no. 2947-11; Oxford subsample 1	2.42	0.74	0.03
UT no. 1066; Gault no. 38; Oxford subsample 25	2.43	1.04	0.04	UT no. 2947-11; Oxford subsample 2	3.04	0.89	0.03
UT no. 1066; Gault no. 1; Oxford subsample 1	2.66	1.42	0.05	UT no. 2875-14; Gault no. 1; Oxford subsample 1	2.59	0.82	0.03
UT no. 1066; Gault no. 5; Oxford subsample 1	2.41	0.78	0.03	UT no. 2875-14; Gault no. 1; Oxford subsample 2	2.41	1.08	0.05
UT no. 1066; Gault no. 5; Oxford subsample 2	2.39	1.35	0.06	UT no. A1B8-1; Oxford subsample 1	2.52	1.20	0.05
UT no. 1066; Gault no. 5; Oxford subsample 3	2.30	1.25	0.05	UT no. A1B8-1; Oxford subsample 2	2.46	0.86	0.04
UT no. 1066; Gault no. 5; Oxford subsample 4	2.41	0.85	0.04	UT no. 1048-2; Gault no. 1; Oxford subsample 1	2.47	0.66	0.03
UT no. 1066; Gault no. 5; Oxford subsample 5	2.67	1.27	0.05	UT no. 4317-87; Gault no. 1; Oxford subsample 1	3.10	0.71	0.02
UT no. 1066; Gault no. 1; Oxford subsample 1; glenoid rim	2.75	1.10	0.04	UT no. 256-11039; Gault no. 1; Oxford subsample 1	2.72	0.79	0.03
UT no. 1066; Gault no. 1; Oxford subsample 1; glenoid fossa	2.45	1.14	0.05	UT no. 256-11039; Gault no. 2; Oxford subsample 1	2.36	0.59	0.02
UT no. 1066; Gault no. 1; Oxford subsample 1; possible astragalus	2.68	1.45	0.05	UT no. 1048; Gault no. 5; Oxford subsample 1	2.74	0.63	0.02
UT no. 6348-8; Oxford subsample 1	2.86	0.95	0.03	UT no. 1048; Gault no. 5; Oxford subsample 2	2.59	1.10	0.04
UT no. 6348-8; Oxford subsample 2	3.07	1.35	0.04	UT no. 2541-2; Gault no. 1; Oxford subsample 1	2.39	0.64	0.03
UT no. 6348-6; Oxford subsample 1	2.55	0.93	0.04	UT no. 2541-2; Gault no. 1; Oxford subsample 2	2.49	0.87	0.03
UT no. 6348-6; Oxford subsample 2	2.42	0.80	0.03	UT no. 4773-1; Gault no. 28; Oxford subsample 1	2.52	0.77	0.03
UT no. 6348-7; Oxford subsample 1	2.38	0.87	0.04	UT no. 4773-1; Gault no. 28; Oxford subsample 2	2.44	0.84	0.03
UT no. 6224-5; Oxford subsample 1	2.58	0.60	0.02	UT no. 4292-12; Gault no. 6; Oxford subsample 1	2.42	0.78	0.03
UT no. 4636-7; Oxford subsample 1	2.52	1.02	0.04	UT no. 4292-12; Gault no. 6; Oxford subsample 2	2.34	0.83	0.04
UT no. 4636-7; Oxford subsample 2	2.65	1.06	0.04	UT no. 3120; Oxford subsample 1	2.41	0.66	0.03
UT Lindsey Pit; Oxford subsample 1	2.45	0.70	0.03	UT no. 3120; Oxford subsample 2	2.87	0.03	0.00
UT no. 3479; Oxford subsample 1	2.76	0.93	0.03	UT no. 3120; Oxford subsample 3	2.56	0.71	0.03
UT no. 4369; Gault no. 7; Oxford subsample 1	2.63	0.89	0.03	UT no. 3120; Oxford subsample 4	2.85	0.82	0.03
UT no. 1048; Gault no. 15; Oxford subsample 1	3.01	2.20	0.07				

10. Guest Mammoth, Florida, U.S.A.

Originally discovered in 1973, the Guest Mammoth site contains the remains of two mammoths in association with lithic technology, dated to 9,840±190 BP (GaK-4215; bone collagen) (50, 51). In

an effort to obtain a HYP measurement, ~1,200 mg of bone powder were processed following AG protocol. This yielded no collagen, however, suggesting poor collagen preservation. Results imply that the previous measurement, albeit likely on different element (there are no published details on the sample submitted to Gakushuin University) (50, 51), should be viewed with caution.

11. Hartley Mammoth, New Mexico, U.S.A.

The Hartley Mammoth site contains the remains of two mammoths, a female adult and a young calf. Processed at the same time as Anzick-1 (52), a bone sample (SR-9067) from this site was used for comparative purposes following AF, AG, and HYP protocols. Results show that AG and AF dates are in good agreement with each other, whilst the HYP measurement is comparatively older (Table 12). Given that the HYP protocol is more efficient in the removal of exogenous carbon (52–59), 32,750±430 BP (OxA-X-2737-65) is considered to be the most robust age estimate for sample SR-9067. This site is considered to be paleontological in nature, however, and is thus excluded from Chapter 5.

Table 12. Radiocarbon dating results for Hartley Mammoth. 'P', pretreatment. The percent collagen is the yield of extracted collagen as a function of the starting weight of bone samples. C:N is the atomic weight ratio of carbon to nitrogen. %C is the percentage of carbon in the combusted sample. Stable isotope ratios of C and N are expressed in per mil (‰) relative to Vienna Pee Dee belemnite and ambient inhalable reservoir. Calibration was done using the OxCal 4.3 software (9) and the IntCal13 calibration curve (16). For the HYP date, the background carbon derived from the HPLC separation has been subtracted using a correction calculation described in reference 56.

P no.	Sample no.	P code	%C	C:N	δ^{13}C‰	δ^{15}N‰	Lab no.	Date (BP)	±	cal. BP (95.4% confidence)
43905	SR-9067	AG	36.5	3.4	-19.4	8.3	OxA-36,306	28,100	350	38233-35881
43905	SR-9067	AF	40.7	3.2	-19.2	8.5	OxA-36,358	29,520	340	34305-32939

P no.	Sample no.	P code	%C	C:N	δ^{13}C‰	δ^{15}N‰	Lab no.	Date (BP)	±	cal. BP (95.4% confidence)
43905	SR-9067	HYP	43.2	5.8	-25.5	5.0	OxA-X-2737-56	32,750	430	32967-31251

12. Nials, Oregon, U.S.A.

Nials is an archaeological site first excavated in the late 1990s, containing stemmed projectile point technology and faunal remains, tentatively dated to the Holocene (60). Given the need to clarify the chronology at the site, J. Pratt (Texas A&M University) recently carried out fieldwork and secured bone samples for radiocarbon dating. Interested in obtaining chronometric data for the Paleoindian layer, six of these samples were prescreened for collagen preservation and, following positive results, radiocarbon dated (Tables 13-14). With the exception of OxA-X-2772-27, which had a C:N value of 3.5, the dataset showed good agreement with the stratigraphic evidence and suggests the human occupation is older than previously hypothesised (61). More chronometric work is required, however, pending future archaeological work.

Table 13. %N values for six faunal bone samples from Nials. Results suggest good to marginal collagen preservation, with all but one sample passing the cut-off value of 0.76 %N.

Sample	Weight (mg)	N (ug)	%N
FS 51 Artifact 18	1.03	18.03	1.75
FS 63 Artifact 37	1.05	10.68	1.02
FS 59 Artifact 1	1.01	14.57	1.44
FS 88 Artifact 1	1.01	12.31	1.22
FS 62 Artifact 10	0.98	8.92	0.91
FS 51 Artifact 23	1.08	7.25	0.67

Table 14.

Table 14.

13. PAIC-88 & -91, Baja California, Mexico

Between 2016 and 2017, an archaeological team led Profs. L. Davis (Oregon State University) and M. Des Lauriers (California State University) conducted a series of surveys on Cedros Island, Mexico (~20 km away from the Baja California peninsula), and discovered several new coastal sites with surface materials dating to 13-12,000 cal BP (62). Their eroded margins suggested that at least 1-2 m of undisturbed, stratified deposits were still preserved, likely containing older cultural material. Previous work at Cedros has identified ancient shell middens containing marine and terrestrial fauna, lithic tools of varying technological traditions, and shell hooks dating to between 11,300 and 10,700 cal BP (63, 64). These finds suggest that early occupants of North America were maritime adapted (64). In January, 2019, a second series of test excavations of late Pleistocene sites was conducted to i) establish a chronostratigraphic framework for the earliest occupations at the island, ii) identify sites with stratigraphic integrity and long depositional histories for future excavations, and iii) quantify the effect of marine ^{14}C reservoir changes through the period of interest by measuring paired terrestrial and marine samples. Through this work, sites PAIC-88 and -91 were found.

Site PAIC-88 is an ancient shell midden site discovered next to an ancient sprint deposit. Surface shells yielded a series of ^{14}C dates ranging between 12,614 and 12,744 cal BP (62). The presence of buried marine shells at more than a meter below surface suggested the presence of older cultural deposits. In January, 2019, a 5x1 m test unit was excavated (Fig. 17). Charcoal, lithics, and shell were recovered in LU-2 and -1. For this project, five charcoals were sampled for radiocarbon dating. Their location within the stratigraphy is noted in Fig. 17.

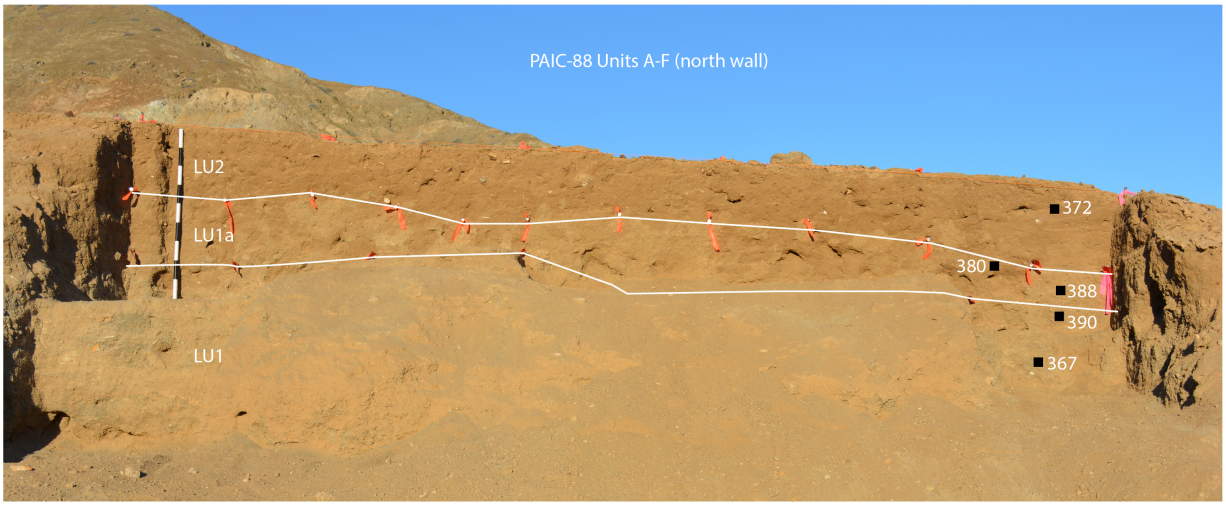


Fig. 17. Photograph of PAIC-88, Units A-F (north wall). The location of samples extracted for radiocarbon dating within Unit A is noted with black squares. Photograph provided by Dr. Loren Davis.

Site PAIC-91 is a remnant deposit at the highest elevation of any of the early sites found, with a surface date of ~11,000 BP on shell (uncorrected) (62). Due to its potential, a single 1.5x1 m test unit was excavated in 2019, encountering an intact, stratified deposit containing cultural materials to a depth of at least 1.5 meters (Fig. 18). Charcoal, lithics, shell, and smaller amounts of bone were recovered in LU-4, -2, and -1, with a sterile, indurated layer in the middle (LU3). For this project, eleven charcoal and shell samples (three of them paired) were selected for radiocarbon dating. Their location within the stratigraphy is noted in Fig. 18.

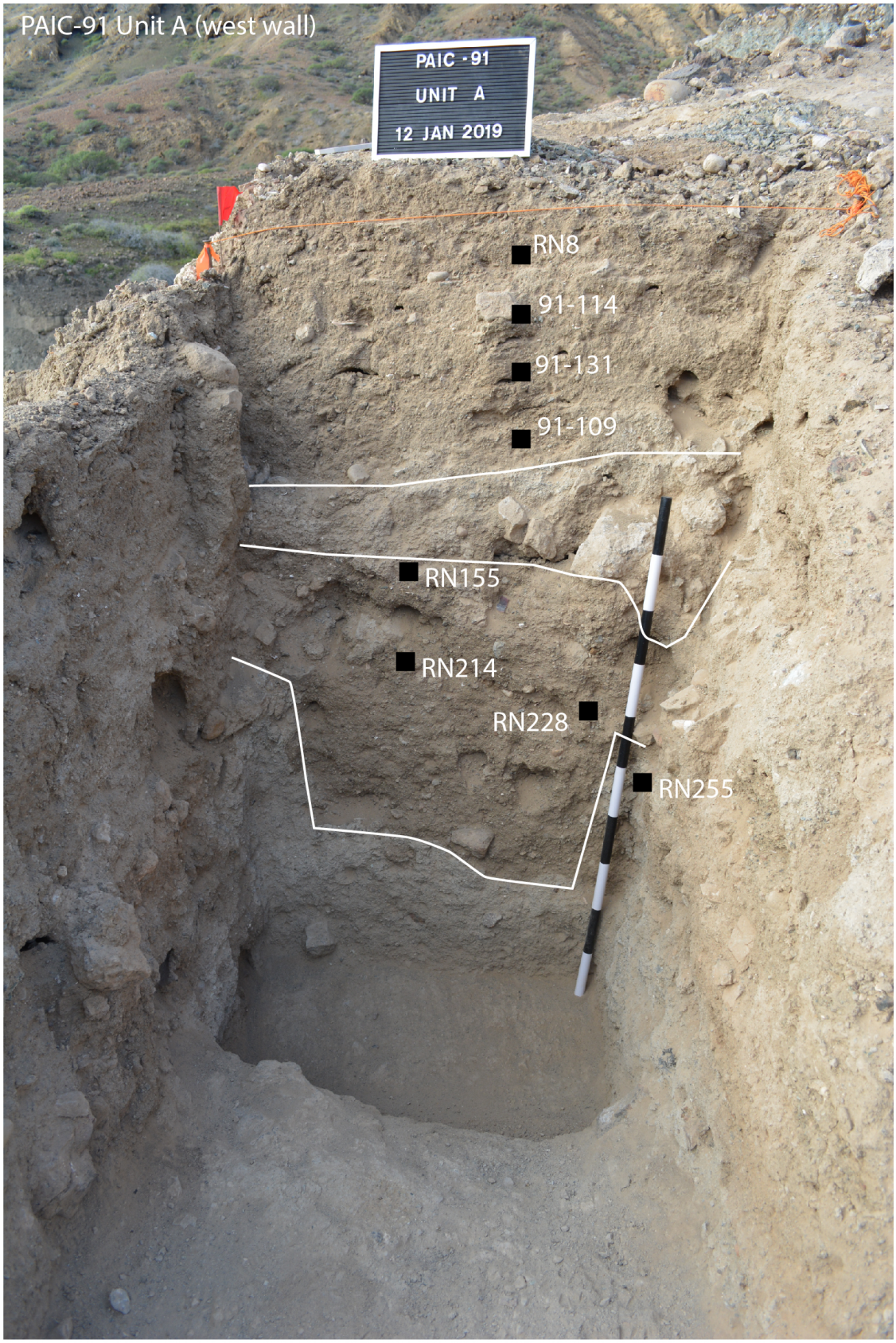


Fig. 18. Photograph of PAIC-91, Unit A (west wall). The location of samples extracted for radiocarbon dating is noted with black squares. Photograph provided by Dr. Loren Davis.

All samples processed obtained measurements (Table 15). For PAIC-88 and -91, results showed poor agreement with the stratigraphic evidence, suggesting continued erosion and redeposition within the deposits (particularly for the latter). Given the data, the association between paired samples from PAIC-91 is uncertain and ΔR calculations were not performed. Chronometric data obtained has, however, informed archaeological investigations and should guide future fieldwork.

Table 15.

Table 15.

Table 15.

14. Powars II, Wyoming, U.S.A.

Powars II (48PL330) is a red-ochre quarry containing Clovis, Goshen, Folsom, Hell Gap, and other late Paleoindian technology (67, 68). This site is important as ochre was a material known to have been used by Clovis people in funerary rituals, e.g., Anzick-1 (69–73). Currently, Powars II is dated by two unprovenienced, Clovis bone rods obtained during 2014-2016 salvage excavations (67). Both were dated by Beta Analytic, Inc. The first, noted as void of collagen, was suggested by the laboratory to have been cremated and a carbonate fraction was dated (Beta-442511; 9,250±20 BP). The second received a collagen date of 8,920±30 BP (Beta-445766). Archaeologists were doubtful, however, as the dates seemed to underestimate the age of the artifacts. In 2017, a controlled excavation began and point-provenienced bone samples were extracted for dating (74) (Fig. 19, black dots). These were found in close association with lithic material from different cultural traditions (with Clovis at the bottom). The site has future potential as bedrock as not yet been reached, and there are indications of lithic technology below Clovis (74). Archaeological fieldwork is pending.

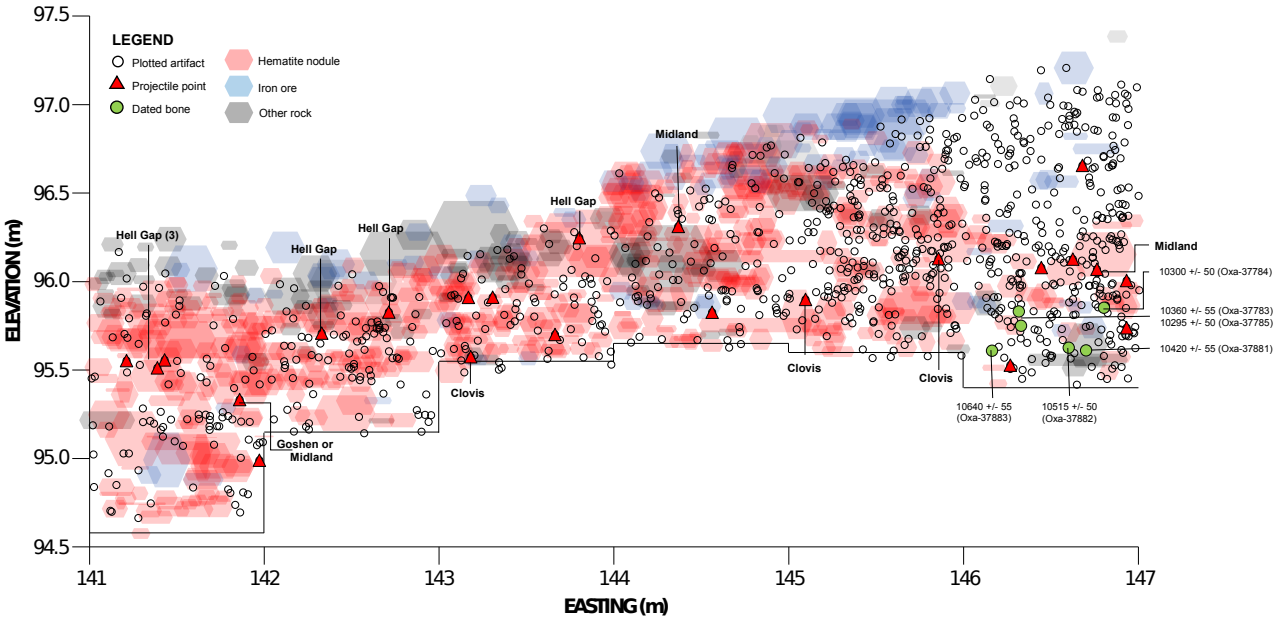


Fig. 19. Backplot of artefacts and rocks mapped in the intact portion of the Powars II site as of November, 2019. Units 141E and 146 E completed to bedrock. Plotted artefacts comprised of mapped chipped stone and faunal remains > 2cm max length. Plotted rocks comprised of hematite, iron, and other rocks > 10 cm max length. Rock depicted in schematic relative to the upper and lower elevations (y-axis) and max length (x-axis). Figure and caption provided by Spencer R. Pelton.

With the aim of obtaining a reliable chronological sequence for Powars II, 21 bone samples were prescreened to determine the degree of collagen preservation at the site. Results showed varied %N values, ranging from 0.14 to 0.83 (Table 16). The six samples with values ≥0.50 were chosen for dating and processed following the AG protocol. All were extracted from below Clovis artefacts, as shown in Fig. 19). Dates obtained (Table 17) proved to be inconsistent with the stratigraphic context. Indeed, the oldest date obtained was OxA-37883, at 10640±55 BP, which postdates Clovis (if taking 10,900 BP to be the end of the period). To the archaeologist, this evidence, coupled with the location of ochre nodules/bone samples and the increased preservation of bone samples at the eastern-most unit, suggested that this area was a wash during the site's occupation. Future

archaeological fieldwork and OSL dating will serve to better elucidate taphonomic processes at Powars II. Chronometric work is thus ongoing.

Table 16. %N values for 21 samples from Powars II. Results are varied, with some passing the cut-off value of 0.76 %N.

Sample	Weight (mg)	N (ug)	%N
827	2.04	8.43	0.41
887	2.13	6.09	0.29
889	2.04	10.20	0.50
787	2	2.83	0.14
782	2.15	6.10	0.28
971	2.14	8.82	0.41
1079	2.19	18.11	0.83
1005	2.2	5.37	0.24
1022	2.1	5.30	0.25
917	2.15	9.30	0.43
962	2.2	13.41	0.61
443	1.98	4.72	0.24
837	2	3.07	0.15
639	2.01	6.85	0.34
938	2.12	6.24	0.29
897	1.98	13.38	0.68
981	2.18	7.27	0.33
1058	2.12	6.68	0.32
1070	2.07	12.19	0.59
976	2.11	4.68	0.22
1072	1.99	11.24	0.56

Table 17.

Table 17.

Table 17.

15. Spirit Cave, Nevada, U.S.A.

Originally investigated in 1940, Spirit Cave is a rockshelter containing two bundle burials ('Spirit Cave 2' and 'Spirit Cave Mummy') wrapped in twined mats and laid one one top of the other (75–80). The skeleton of the lower individual (Spirit Cave Mummy) was virtually complete and partially mummified. In the 1990s, previous radiocarbon dating efforts on hair, bone and mat fragments from the Spirit Cave Mummy yielded ages ranging from 9350±40 (UCR-3261-2/CAMS 12353) to 9460±60 BP (UCR-3324-2/CAMS 24197) (81). To obtain newer measurements on samples that were genetically sequenced, this project focused on obtaining HYP dates for the two individuals (samples CGG2_17374 and CGG2_17378), plus a geologically younger skeleton (Spirit Cave 3; CGG2_17379). AF measurements from the same samples had been previously obtained at the ORAU commercially.

Results obtained showed relatively good agreement between previous AF and new dates (Table 18). For the Spirit Cave Mummy, the ORAU measurements slightly predated those obtained in the 1990s. This work was published in *Science*, 2018, as part of a collaboration designed to elucidate the genetic background of the earliest human dispersals into the continent (82) (Appendix C). In it, the Spirit Cave Mummy was found to be part of the Southern Native American branch, and closely linked to Anzick-1.

Table 18. Radiocarbon dating results for Spirit Cave. 'P', pretreatment. The percent collagen is the yield of extracted collagen as a function of the starting weight of bone samples. C:N is the atomic weight ratio of carbon to nitrogen. %C is the percentage of carbon in the combusted sample. Stable isotope ratios of C and N are expressed in per mil (‰) relative to Vienna Pee Dee belemnite and ambient inhalable reservoir. Calibration was done using the OxCal 4.3 software (9) and the IntCal13

calibration curve (16). For HYP dates, the background carbon derived from the HPLC separation has been subtracted using a correction calculation described in reference 56.

P no.	Sample no.	P code	% collagen yield	C:N	%C	$\delta^{13}C$ (‰)	$\delta^{15}N$ (‰)	Laboratory no.	Date (BP)	±	cal. BP (95.4% confidence)
43584	CGG2_17374	AF*	8.6	3.2	44.1	-15.3	16.3	OxA-36200	9615	50	11170-10771
		HYP	/	5.0	39.4	-20.1	18.8	OxA-X-2772-8	9600	55	11165-10751
43585	CGG2_17378	AF*	8.6	3.5	46.0	-15.3	15.9	OxA-36201	9645	65	11199-10772
		HYP	/	5.1	43.3	-21.3	18.3	OxA-X-2767-11	9540	50	11097-10697
43586	CGG2_17379	AF*	9.1	3.5	47.2	-18.3	12.7	OxA-36202	4682	35	5576-5317
		HYP	14.3	5.1	38,1	-22.6	15.5	OxA-X-2767-12	4750	36	5587-5329

16. Tagua Tagua 1 & 2, O'Higgins, Chile

The archaeological sites of Tagua Tagua 1 (TT-1) and Tagua Tagua 2 (TT-2) were excavated by Julio Montané in 1967 (TT-1) (83, 84), and by Lautaro Núñez in the 1990s (TT-1 was expanded and TT-2 first excavated; Fig. 20) (85). Within lithostratigraphic units 5 and 6, at a depth range of 1.04-2.5 m, both sites contain the remains of extinct fauna—predominantly mastodon (*Stegomaston humboldti*), horse (*Equus*), and deer (*Antifer*)—found in close association with lithic and osseous artefacts. In total, the Tagua Tagua sites contain 319 skeletal elements distributed in fourteen different loci, as well as 22 lithic tools (including three Fell-style points extracted from TT-2) and four bone artefacts. Coupled with this evidence, the lack of anatomical arrangement of single individuals and the presence of cut marks in bone fragments suggest that TT-1 and -2 were prehistoric butchering sites (86). In 1968, the chronology at TT-1 was established by a single charcoal date of 11,380±320 BP (GX-1205) (84, 87). Following the Núñez excavations, charcoal dates 9,900±100 BP (Beta-45519) and 10,120±30 BP (Beta-45520) were obtained for TT-2. Direct dating of the human-modified bone fragments had not been attempted since the 1960s when, according to Montané (87), the age of a mastodon bone could not be determined due to low collagen yield.

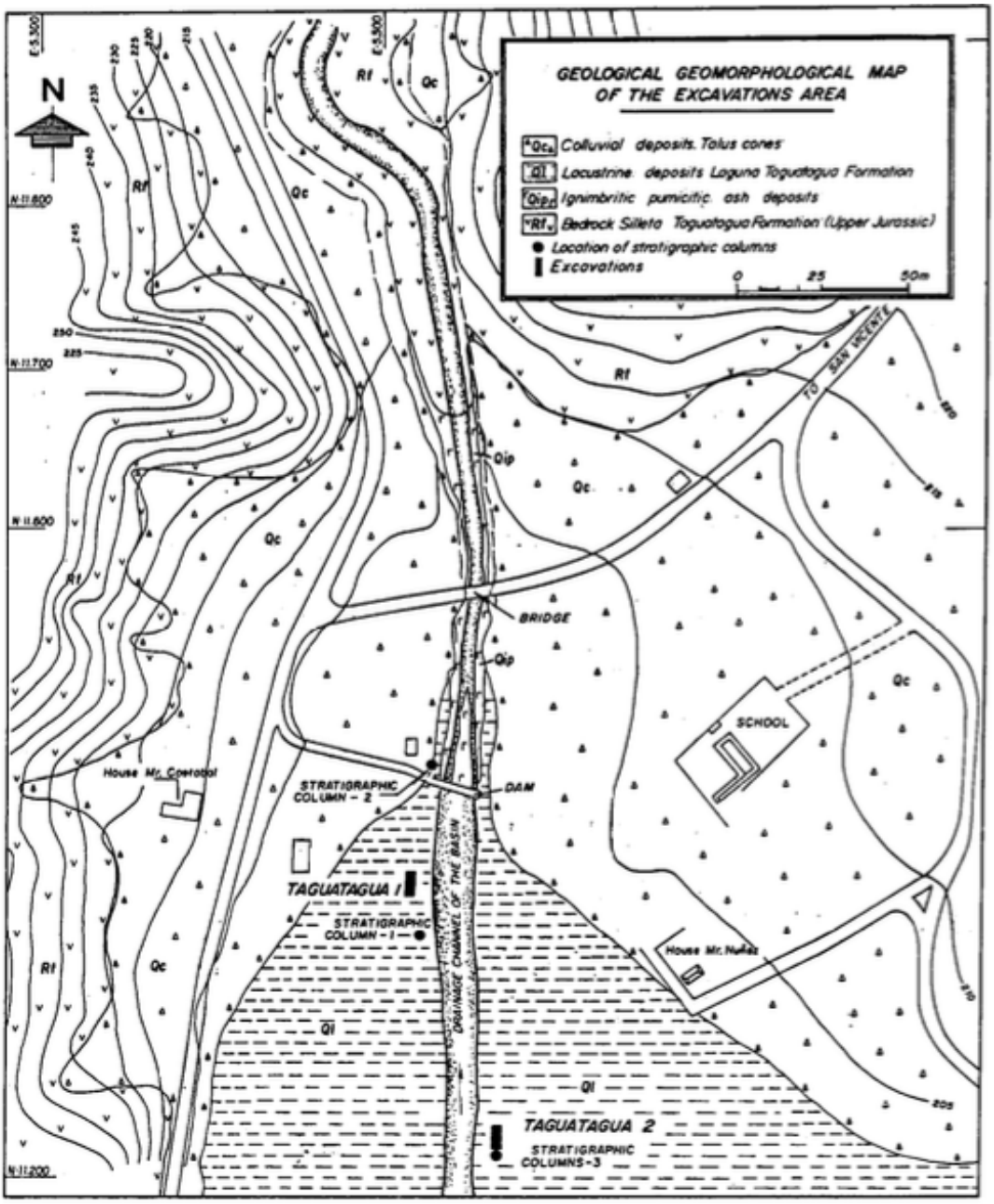


Fig. 20. Map of Tagua Tagua excavations (from reference 85).

With the aim of directly dating the faunal remains, sampling for TT-1 and -2 focused on obtaining, as prioritised, i) human-modified samples from extinct fauna, ii) human-modified elements from extant fauna, or iii) non-modified elements from extinct fauna within the palaeoindial level (lithostratigraphic units 5 and 6). According to this criteria, a total number of eight samples were secured (Table 19). These include samples of *Stegomaston platensis* and *Equus* found by Montané in TT-1; a cut-marked *Stegomaston platensis* vertebra from TT-2 (Figure 21); a fragment of a

Stegomaston platensis mandible corresponding to a second, infant individual from TT-2; and cut-marked bird bone fragments from both sites. Unfortunately, after processing as AG, none of the samples yielded collagen. This was consistent with previous findings (87) and suggests poor collagen preservation at both sites. No further chronometric work was attempted.

Table 19. Faunal bone samples obtained from the archaeological sites of Tagua Tagua 1 (TT-1) and 2 (TT-2). Some samples lacked specific site information, but, according to the documentation, were extracted from one of the two Tagua Tagua excavations.

Site	**Sample no.**	**Context**	**Sample obtained for ^{14}C dating**	**Observations**	**Weight of sample (g)**
TT-2	TT-2 C1 H13	Núñez excavation; Palaeoindian level	*Stegomastodon humboldti;* vertebra fragment	cut marked	1.9
TT-2	TT-2 C3 H40	Núñez excavation; Palaeoindian level	infant *Stegomastodon humboldti*; mandible fragment	-	2.5
TT-1	SGO PV-244	Montané's excavation; Palaeoindial level	S*tegomastodon humboldti;* tibia fragment	-	2.1
TT-1	SGO PV-246	Montané's excavation; Palaeoindial level	*Hippidion;* metatarsal fragment	-	1.4
-	SGO PV-23695	Palaeoindian level	bird; long bone fragment	cut marked	0.4
-	SGO PV-23248	Palaeoindian level	bird; long bone fragment	cut marked	0.7
TT-1	SGO PV-23242	Palaeoindian level	bird; long bone fragment	cut marked	1.1
-	SGO PV-23413	Palaeoindian level	bird; long bone fragment	cut marked	0.6



Fig. 21. Photographs of sample TT-2 C1 H13 (Tagua Tagua 2), showing cut marks in different locations (parallel lines; encircled in red).

References

1. S. David Webb, J. T. Milanich, R. Alexon, J. S. Dunbar, A Bison Antiquus Kill Site, Wacissa River, Jefferson County, Florida. *Am. Antiq.* **49**, 384–392 (1984).

2. M. Waters (2018). Personal communication. E-mail received by Lorena Becerra-Valdivia.

3. E. B. Howard, The Occurrence of Flints and Extinct Animals in Pluvial Deposits near Clovis, New Mexico. Part I: Introduction. *Proceedings of the Academy of Natural Sciences of Philadelphia* **87**, 299–303 (1935).

4. E. B. Howard, Association of artifacts with mammoth and bison in eastern New Mexico. *Science* **78**, 524 (1933).

5. C. V. Haynes, G. A. Agogino, Prehistoric Springs and Geochronology of the Clovis Site, New Mexico. *Am. Antiq.* **31**, 812–821 (1966).

6. C. V. Haynes, Geochronology of paleoenvironmental change, clovis type site, Blackwater draw, New Mexico. *Geoarchaeology* **10**, 317–388 (1995).

7. E. Johnson, "Human modified bones from early southern Plains Sites" in *Bone Modification*, R. Bonnichsen, M. H. Sorg, Eds. (Centre for the Study of First Americans, Orono, 1989), pp. 431–471.

8. R. Suárez (2017). Personal communication. E-mail received by Lorena Becerra-Valdivia.

9. C. Bronk Ramsey, Development of the radiocarbon program OxCal. *Radiocarbon* **43**, 355–363 (2001).

10. A. G. Hogg, *et al.*, SHCal13 Southern Hemisphere Calibration, 0–50,000 Years cal BP. *Radiocarbon* **55**, 1889–1903 (2013).

11. C. F. Ardelean, "Archaeology of Early Human Occupations and the Pleistocene-Holocene Transition in the Zacatecas Desert, Northern Mexico," University of Exeter. (2013) (October 15, 2017).

12. C. Ardelean (2019). Personal communication. E-mail received by Lorena Becerra-Valdivia.

13. S. O. Rasmussen, *et al.*, A stratigraphic framework for abrupt climatic changes during the Last Glacial period based on three synchronized Greenland ice-core records: refining and extending the INTIMATE event stratigraphy. *Quat. Sci. Rev.* **106**, 14–28 (2014).

14. Y. Wang, R. Amundson, S. Trumbore, Radiocarbon Dating of Soil Organic Matter. *Quat. Res.* **45**, 282–288 (1996).

15. L. C. R. Pessenda, S. E. M. Gouveia, R. Aravena, Radiocarbon Dating of Total Soil Organic Matter and Humin Fraction and Its Comparison with 14C Ages of Fossil Charcoal. *Radiocarbon* **43**, 595–601 (2001).

16. P. J. Reimer, *et al.*, IntCal13 and Marine13 Radiocarbon Age Calibration Curves 0–50,000 Years cal BP. *Radiocarbon* **55**, 1869–1887 (2013).

17. P. U. Clark, *et al.*, The Last Glacial Maximum. *Science* **325**, 710–714 (2009).

18. S. O. Rasmussen, *et al.*, A new Greenland ice core chronology for the last glacial termination. *J. Geophys. Res.* **111**, 527 (2006).

19. L. G. Davis, C. E. Schweger, Geoarchaeological context of late Pleistocene and early Holocene occupation at the Cooper's Ferry site, western Idaho, USA. *Geoarchaeology* **19**, 685–704 (2004).

20. T. Goebel, B. Hockett, K. D. Adams, D. Rhode, K. Graf, Climate, environment, and humans in North America's Great Basin during the Younger Dryas, 12,900–11,600 calendar years ago. *Quat. Int.* **242**, 479–501 (2011).

21. L. G. Davis, S. J. Macfarlan, C. N. Henrickson, A PXRF-based chemostratigraphy and provenience system for the Cooper's Ferry site, Idaho. *J. Archaeol. Sci.* **39**, 663–671 (2012).

22. L. G. Davis, A. J. Nyers, S. C. Willis, Context, Provenance and Technology of a Western Stemmed Tradition Artifact Cache from the Cooper's Ferry Site, Idaho. *Am. Antiq.* **79**, 596–615 (2014).

23. T. Goebel, J. L. Keene, Are Great Basin stemmed points as old as Clovis in the Intermountain West? A review of the geochronological evidence. *Archaeology in the Great Basin and Southwest: Papers in Honor of Don D. Fowler*, 35–60 (2014).

24. L. G. Davis, *et al.*, Late Upper Paleolithic Occupation at Cooper's Ferry, Idaho, USA Shows Americas Settled Before ~16,000 Years Ago. *Science* (2019).

25. T. J. Green, *et al.*, The Buhl Burial: A Paleoindian Woman from Southern Idaho. *Am. Antiq.* **63**, 437–456 (1998).

26. K. E. Graf, "Stratigraphy and chronology of the Pleistocene to Holocene transition at Bonneville Estates Rockshelter, eastern Great Basin" in *Paleoindian or Archaic? Great Basin Human Ecology at the Pleistocene-Holocene Transition*, K. E. Graf, D. N. Schmitt, Eds. (The University of Utah Press, 2007), pp. 82–104.

27. D. L. Jenkins, *et al.*, Clovis age Western Stemmed projectile points and human coprolites at the Paisley Caves. *Science* **337**, 223–228 (2012).

28. J. Kaltwasser, A. Medina, J. Munizaga, Cementerio de periodo Arcaico en Cuchipuy in *Actas Del VIII Congreso de Arqueología Chilena*, (Sociedad Chilena de Arqueología, Universidad Austral de Chile, 1979), pp. 275–280.

29. J. Kaltwasser, A. Medina, J. Munizaga, Cementerio del periodo arcaico en Cuchipuy. *Revista Chilena de Antropología* **3** (1980).

30. J. Kaltwasser, A. Medina, J. Munizaga, El hombre de Cuchipuy (Prehistoria de Chile Central).

Revista Chilena de Humanidades **1**, ág–87 (1982).

31. J. Kaltwasser, A. Medina, J. Munizaga, El hombre de Cuchipuy. *Revista Chilena de Antropología*, 43–48 (1984).

32. J. Kaltwasser, A. M. Rojas, E. A. Fontaine, C. P. Diaz, El hombre de Cuchipuy, Prehistoria de Chile Central en el Período Arcaico. *Chungara: Revista de Antropología Chilena*, 99–105 (1986).

33. J. Kaltwasser, A. Medina, J. Munizaga, Estudio de once fechas de RC 14 relacionadas con el hombre de Cuchipuy. *Boletín de prehistoria de Chile* **9**, e14 (1983).

34. E. Aspillaga (2017).

35. J. W. Davenport, *Archaeological Exploration of Eagle Cave, Langtry, Texas* (Witte Memorial Museum, 1938).

36. R. E. Ross, M. L. Parsons, *The Archeology of Eagle Cave* (Texas Archeological Salvage Project, 1965).

37. C. W. Koenig, C. J. Jurgens, J. K. Hanselka, S. L. Black, C. D. Frederick, Multidisciplinary Investigations of a Late Paleoindian Bison Butchery Event from a Southwest Texas Rockshelter (2018).

38. C. Koenig (2018). Personal communication. E-mail received by Lorena Becerra-Valdivia.

39. S. C. Kuehn, *et al.*, The latest Pleistocene Glacier Peak tephra set revisited and revised: Major- and trace-element characterization, distribution, and a new chronology in western North America. *Quat. Res.* **71**, 201–216 (2009).

40. P. J. Mehringer, F. F. Foit, Volcanic ash dating of the Clovis cache at East Wenatchee,

Washington. *Natl. Geogr. Res.* **6**, 495–503 (1990).

41. R. B. Waitt, Megafloods and Clovis cache at Wenatchee, Washington. *Quat. Res.* **85**, 430–444 (2016).

42. M. B. Collins, The Gault Site, Texas, and Clovis research. *Athena Review* **3**, 31–42 (2002).

43. J. L. Gandy, "Analysis of the lithic debitage from the older-than-Clovis stratigraphic layers of the Gault site, Texas," Texas State University, San Marcos. (2013).

44. M. Collins, NSF Technical Report: "ProtoClovis" or "PreClovis"? Investigating Cultural Antecedents of Clovis at the Gault Site, Texas (2015).

45. K. Rodrigues, *et al.*, OSL ages of the Clovis, Late Paleoindian, and Archaic components at Area 15 of the Gault Site, Central Texas, U.S.A. *Journal of Archaeological Science: Reports* **7**, 94–103 (2016).

46. L. E. Vilsack, "Investigations of Area 12: Gault Site," Texas State University, San Marcos. (2016).

47. T. J. Williams, *et al.*, Evidence of an early projectile point technology in North America at the Gault Site, Texas, USA. *Sci Adv* **4**, eaar5954 (2018).

48. A. Gilmer, Geoarchaeological Investigations of Site Formation Processes in Area 15 at the Gault Site, Bell County, Texas (2013).

49. M. Collins (2017). Personal communication. E-mail received by Lorena Becerra-Valdivia.

50. S. L. Rayl, "A paleo-Indian mammoth kill site near Silver Springs, Florida," Northern Arizona University. (1974).

51. C. A. Hoffman, A mammoth kill site in the Silver Springs Run. *The Florida Anthropologist* **36**,

83–87 (1983).

52. L. Becerra-Valdivia, *et al.*, Reassessing the chronology of the archaeological site of Anzick. *Proc. Natl. Acad. Sci. U. S. A.* **115**, 7000–7003 (2018).

53. S. Nalawade-Chavan, *et al.*, New single amino acid hydroxyproline radiocarbon dates for two problematic American Mastodon fossils from Alaska. *Quat. Geochronol.* **20**, 23–28 (2014).

54. A. Marom, J. S. McCullagh, T. F. Higham, A. A. Sinitsyn, R. E. Hedges, Single amino acid radiocarbon dating of Upper Paleolithic modern humans. *Proc Natl Acad Sci USA* **109**, 6878–6881 (2012).

55. R. Bourrillon, R. White, E. Tartar, L. Chiotti, A new Aurignacian engraving from Abri Blanchard, France: Implications for understanding Aurignacian graphic expression in Western and Central Europe. *Quaternary* **491**, 46–64 (2017).

56. T. Deviese, D. Comeskey, J. McCullagh, C. B. Ramsey, T. Higham, New protocol for compound specific radiocarbon analysis of archaeological bones. *Rapid Commun. Mass Spectrom.* **32**, 373–379 (2017).

57. T. Devièse, *et al.*, Direct dating of Neanderthal remains from the site of Vindija Cave and implications for the Middle to Upper Paleolithic transition. *Proc Natl Acad Sci USA* **114**, 10606–10611 (2017).

58. N. Reynolds, R. Dinnis, A. A. Bessudnov, T. Devièse, T. Higham, The Kostënki 18 child burial and the cultural and funerary landscape of Mid Upper Palaeolithic European Russia. *Antiquity* **91**, 1435–1450 (2017).

59. M. Sikora, A. Seguin-Orlando, V. C. Sousa, Ancient genomes show social and reproductive behavior of early Upper Paleolithic foragers. *Science* **eaao1807** (2017).

60. L. M. Bonstead, The Nials Site: An early Holocene occupation in the Harney Basin, Oregon (2001).

61. J. Pratt (2018). Personal communication. E-mail received by Lorena Becerra-Valdivia.

62. L. Davis (2018). Personal communication. E-mail received by Lorena Becerra-Valdivia.

63. M. R. Des Lauriers, *Island of Fogs: Archaeological and Ethnohistorical Investigations of Isla Cedros, Baja California* (University of Utah Press, 2010) (March 22, 2019).

64. M. R. Des Lauriers, L. G. Davis, J. Turnbull, J. R. Southon, R. E. Taylor, The earliest shell fishhooks from the Americas reveal fishing technology of Pleistocene maritime foragers. *Am. Antiq.* **82**, 498–516 (2017).

65. R. Berger, R. E. Taylor, W. F. Libby, Radiocarbon content of marine shells from the california and mexican west coast. *Science* **153**, 864–866 (1966).

66. R. E. Taylor, J. Southon, M. R. Des Lauriers, Holocene Marine Reservoir Time Series ΔR Values from Cedros Island, Baja California. *Radiocarbon* **49**, 899–904 (2007).

67. G. C. Frison, *et al.*, Further insights into Paleoindian use of the Powars II red ocher quarry (48PL330), Wyoming. *Am. Antiq.* **83**, 485–504 (2018).

68. M. D. Stafford, G. C. Frison, D. Stanford, G. Zeimans, Digging for the color of life: Paleoindian red ochre mining at the Powars II site, Platte County, Wyoming, USA. *Geoarchaeology: An International Journal* **18**, 71–90 (2003).

69. L. Lahren, R. Bonnichsen, Bone Foreshafts From a Clovis Burial in Southwestern Montana. *Science* **186**, 147–150 (1974).

70. P. J. Wilke, J. J. Flenniken, T. L. Ozbun, Clovis Technology at the Anzick Site, Montana. *J.*

Calif. Gt. Basin Anthropol. **13**, 242–272 (1991).

71. D. W. Owsley, D. R. Hunt, I. G. Macintyre, M. A. Logan, Clovis and Early Archaic Crania from the Anzick Site (24PA506), Park County, Montana. *Plains Anthropol.* **46**, 115–124 (2001).

72. M. Rasmussen, *et al.*, The genome of a Late Pleistocene human from a Clovis burial site in western Montana. *Nature* **506**, 225–229 (2014).

73. L. Becerra-Valdivia, *et al.*, Reassessing the chronology of the archaeological site of Anzick. *Proc. Natl. Acad. Sci. U. S. A.* **115**, 7000–7003 (2018).

74. S. Pelton (2018). Personal communication. E-mail received by Lorena Becerra-Valdivia.

75. A. Dansie, Early Holocene burials in Nevada: Overview of localities, research, and legal issues. *Nevada Hist. Soc. Qtly* **40**, 4–14 (1997).

76. R. L. Jantz, D. W. Owsley, Pathology, taphonomy, and cranial morphometrics of the Spirit Cave Mummy. *Nev. Hist. Soc. Q.* **40**, 62–84 (1997).

77. D. L. Kirner, *et al.*, Dating the Spirit Cave mummy: the value of reexamination. *Nev. Hist. Soc. Q.* **40**, 54–56 (1997).

78. L. K. Napton, The Spirit Cave mummy: coprolite investigations. *Nev. Hist. Soc. Q.* **40**, 97–104 (1997).

79. J. P. Barker, C. Ellis, S. Damadio, *Determination of cultural affiliation of ancient human remains from Spirit Cave, Nevada* (US Bureau of Land Management, 2000).

80. B. Hockett, E. Palus, A Brief History and Perspective on Spirit Cave, Nevada. *PaleoAmerica* **4**, 1–7 (2018).

81. D. R. Tuohy, A. Dansie, New information regarding early Holocene manifestations in the

western Great Basin. *Nev. Hist. Soc. Q.* **40**, 24–53 (1997).

82. J. V. Moreno-Mayar, *et al.*, Early human dispersals within the Americas. *Science* **362**, eaav2621 (2018).

83. R. Casamiquela, J. Montané, R. Santana, Convivencia del hombre con el mastodonte en Chile central. *Noticiario Mensual del Museo Nacional de Historia Natural* **11**, 1–6 (1967).

84. J. Montané, Paleo-Indian remains from laguna de tagua tagua, central chile. *Science* **161**, 1137–1138 (1968).

85. L. Nuñez, *et al.*, Cuenca de Taguatagua en Chile: el ambiente del Pleistoceno superior y ocupaciones humanas. *Revista Chilena de Historia Natural* **67**, 503–519 (1994).

86. D. Jackson, C. Méndez, L. Núñez, D. Jackson, Procesamiento de fauna extinta durante la transición Pleistoceno-Holoceno en el centro-norte de Chile. *Boletín de Arqueología PUCP*, 315–336 (2011).

87. J. Montane, Primera fecha radiocarbónica de Tagua-Tagua. *Not. Mens. Mus. Nac. Hist. Nat.* **139** (1968).

Appendix B: Co-authored publication including work on Spirit Cave, Nevada

Published as per below.

Moreno-Mayar, J. Víctor; Vinner, Lasse; de Barros Damgaard, Peter; de la Fuente, Constanza; Chan, Jeffrey; Spence, Jeffrey P.; Allentoft, Morten E.; Vimala, Tharsika; Racimo, Fernando; Pinotti, Thomaz; Rasmussen, Simon; Pedersen, Mikkel W.; Margaryan, Ashot; Orbegozo, Miren Iraeta; Milopotamitaki, Dorothea; Wooller, Matthew; Bataille, Clement; Becerra-Valdivia, Lorena; Chivall, David; Comeskey, Daniel; Devièse, Thibaut; Grayson, Donald K.; George, Len; Harry, Harold; Alexandersen, Verner; Primeau, Charlotte; Connolly, Thomas J.; Endzweig, Pamela; Erlandson, Jon; Jenkins, Dennis; Stafford, Thomas; Cybulski, Jerome; Vullo, Carlos; Morello, Flavia; Vilar, Miguel; Wells, Spencer; Gregersen, Kristian; Hansen, Kasper Lykke; Lynnerup, Niels; Mirazón Lahr, Marta; Kjær, Kurt; Strauss, André; Alfonso-Durruty, Antonio Salas; Schroeder, Hannes, Thomas, Higham, Ripan S. Malhi, Jeffrey T. Rasic, Luiz Souza, Marta; Santos, Fabricio R.; Malaspinas, Anna-Sapfo; Sikora, Martin; Nielsen, Rasmus; Song, Yun S.; Meltzer, David J.; Willerslev, Eske (2018). Early human dispersals within the Americas. *Science*, eaav2621. DOI: 10.1126/science.aav2621

Place holder

Place holder

Place holder

Place holder

Place holder

Place holder

Place holder

Place holder

Place holder

Place holder

Place holder

Place holder

Appendix C: Co-authored publication including work on Cooper's Ferry, Idaho

Published as per below.

Davis, L.G., Madsen, D.B., Becerra-Valdivia, L., Higham, T., Sisson, D.A., Skinner, S.M., Stueber, D., Nyers, A.J., Keen-Zebert, A., Neudorf, C. and Cheyney, M., 2019. Late Upper Paleolithic occupation at Cooper's Ferry, Idaho, USA,~ 16,000 years ago. *Science*, 365(6456), pp.891-897.

Place holder

Place holder

Place holder

Place holder

Place holder

Place holder

Place holder

Appendix D: Co-authored publication on the redating of heavily contaminated bones from kill/butchery sites in North America

Published as per below.

Devièse, T., Stafford Jr, T.W., Waters, M.R., Wathen, C., Comeskey, D., Becerra-Valdivia, L. and Higham, T., 2018. Increasing accuracy for the radiocarbon dating of sites occupied by the first Americans. *Quaternary Science Reviews*, 198, pp.171-180.

Place holder

Place holder

Place holder

Place holder

Place holder

Place holder

Place holder

Place holder

Place holder

Author contribution statements

Place holder

Place holder

Place holder